THE BUCKLING AND POST-BUCKLING BEHAVIOUR OF SIMPLY SUPPORTED RECTANGULAR PLATES WITH CENTRALLY LOCATED CIRCULAR HOLES

by

DAVID RITCHIE

A Thesis presented to the University of Strathclyde for the Degree of Doctor of Philosophy

Department of Mechanics of Materials
The University of Strathclyde

August 1975

ABSTRACT

This thesis describes an investigation into the buckling, post-buckling behaviour and collapse of simply supported square and rectangular plates with centrally located circular holes.

The review of the current literature is preceded by a brief description of the approximate methods of plate buckling and post-buckling analysis. The basic equations of compatibility, equilibrium and strain energy are described.

Theoretical analyses of the pre-buckling, buckling and post-buckling behaviour are presented. The pre-buckling analysis is by the finite element method and the buckling and post-buckling analyses use the minimisation of total potential energy. The buckling analysis uses the pre-buckling stress distribution with an approximate out-of-plane deflection function with arbitrary coefficients. The post-buckling analysis uses finite element and analytical stress distributions to ensure internal equilibrium and assumes that the out-of-plane deflected shape is the buckling mode. A simple collapse analysis was also presented.

An experimental programme is described which was carried out to determine buckling loads, post-buckling deflections and collapse loads. The experimental investigation of the distribution of strains along the plate centre lines is also described.

Comparison of the theoretical results is made with the results of the experimental investigation and, in addition, with the theoretical and experimental results of other

investigators. These results are all fully discussed and the conclusions drawn from the discussion are presented.

The thesis is ended by three appendices, the first of which describes and discusses the derivation of the finite element plane stress stiffness matrix, and the second describes the method of determining the smallest eigenvalue. The third appendix describes the material properties of the plate specimens, and their derivation.

This Thesis is dedicated to

Mr. Robert F. Ritchie

and

Mrs. Janet M. Ritchie

the author's parents.

CONTENTS

Abstract		i
Dedication		iii
Contents		iv
Notation		
Chapter 1	Introduction and Review of Literature	1
1.1	Introduction	1
1.2	Plates with Holes	7
1.3	Summary	15
Chapter 2	Basic Equations of Thin Plates	25
2.1	Basic Equations	25
2.2	Strain Energy Equations	29
Chapter 3	Theoretical Analysis	32
3.1	Pre-Buckling Analysis	33
3.2	Initial Instability	35
3.2.1	Description of Stability Analysis	35
3.2.2	Application of the Stability Analysis	40
3.3	Post Buckling Analysis	41
3.3.1	Description of the Post-Buckling Analysis	41
3.3.2	Application of the Post-Buckling Analysis	50
3.4	A Simplified Failure Analysis	58
Chapter 4	Experimental Investigation	84
4.1	The Test Program	85

4.2 Test Equipment 86

4.2.1 The Plate Test Rig 86

4.2.2 The Loading Machine 89

4.2.3 Strain Measuring Equipment 89

4.3 The Plate Specimens 90

4.4 Test Procedure 91

4.4.1 Test Series A 91

4.4.2 Test Series B
The Strain Investigation 94

Chapter 5 Theoretical and Experimental Results 98

5.1 Initial Instability 98

5.1.1 Comparison of Experimental and Theoretical Results 100

5.1.2 Comparison of the Theoretical Results with the Results of Other Investigators 101

5.2 Theoretical and Experimental Load-Deflection Behaviour 101

5.2.1 Out-of-Plane Deflections 102

5.2.2 Load - Edge Displacement Behaviour 103

5.3 Ultimate Loads 104

5.4 The Internal Stress Distributions 105

5.4.1 Rectangular Plates 106

5.4.2 Square Plates 108

Chapter 6 Discussion of the Theoretical and Experimental Results 180

6.1 Buckling 180

6.2 Post-Buckling Behaviour 182

6.2 Post-Buckling Behaviour

6.2.1 Out-of-plane Deflections 182

6.2.2 End Compression 183

6.2.3 Post-Buckling Stresses 184

6.3 Collapse 186

Chapter 7 General Discussion on the Buckling and Post-Buckling Behaviour of Plates with Holes 190

7.1 Buckling 190

7.2 Post-Buckling Behaviour and Collapse 193

Chapter 8 Conclusions 197

8.1 Suggestions for Future Work 197

8.2 Conclusions 197

Bibliography 199

Acknowledgements 205

Appendix I 206

Appendix 2 214

Appendix 3 216

NOTATION

The following list of symbols have been used throughout the text. Additional symbols are explained where they first appear.

A_n	Arbitrary coefficients of the deflection function.
$\bar{A}_n$	Deflection function coefficients at buckling normalised with respect to the largest term.
A_r	Post-buckling deflection coefficient.
$\{A\},\{\bar{A}\}$	Column vectors of the coefficients A_n and $\bar{A}_n$ respectively.
a	The length of the plate in the loaded direction.
B_1, B_2	Coefficients of the stress function F_2.
b	Half width of the plate across the direction of loading.
b_e	Effective width of an unperforated plate.
b_{ec}	Approximate effective width of a plate with a hole.
C_{1nm}, C_{4nm}	Coefficients of stress function F_2.
c	Radius of the hole
D	Plate flexural rigidity $\frac{Et^3}{12(1-\nu^2)}$
E	Young's Modulus of Elasticity.
F	Airey Stress Function.
F_2, F_3	Post-buckling stress functions arising from the out-of-plane deflections.

F_{2A}, F_{2B}	Components of stress function F_2
$f(x)$	The deflection in the x-direction.
G	The shear modulus.
$g_n(y)$	The deflection function in the y-direction.
$h_{nm}(x,y)$	A function representing the function of x and y in stress function F_2 , i.e. $F_2 = \sum_{n=1} \sum_{m=1} A_n A_m h_{nm}(x,y)$ $n=1,3,5$ etc.
J_{2nm}, J_{3nm}	Coefficients of stress function F_2 .
$J_o(x)$	Bessel function of x
$K_{1nm}, K_2,$ K_{3nm}, K_{4nm}	Components of the strain energy equation written as terms of $A_n . A_m$
$[K_{1nm}], [K_{1nm}],$ $[K_{4nm}]$	The coefficients K_{1nm} , K_{3nm} and K_{4nm} written in matrix form.
$\bar{K}_1, \bar{K}_2, \bar{K}_3, \bar{K}_4$	Components of the total strain energy calculated from the deflection function coefficients $\bar{A}_n$
k	The number of half-wavelengths in the direction of loading.
M_x, M_y	Bending moments per unit width of a plate normal to the x and y directions respectively.
M_{xy}	Twisting moment per unit width of a plate.
N_x, N_y	Normal mid-plane forces per unit length perpendicular to the x and y directions respectively.
N_{xy}	Shearing force in the direction of the y-axis per unit length along the y-axis.
N_e	Number of elements in the finite element analysis.

N — Number of terms of the deflection function used in the solution.

n_{xr}, n_{yr}, n_{xyr} — Components of the stress resultants N_x, N_y and N_{xy} due to stress system r.

$^{p}n_{xr}, ^{p}n_{yr}, ^{p}n_{xyr}$ — Components of the stress resultants N_x, N_y and N_{xy} in element p due to stress system r

$\bar{n}_{xr}, \bar{n}_{yr}, \bar{n}_{xyr}$ — The stress resultants n_{xr}, n_{yr}, n_{xyr} referred to their appropriate characterising load or deflection parameter, e.g.

$$^{p}n_{x1} = \phi . {}^{p}\bar{n}_{x1}$$
$$n_{x2} = A_r^2 . \bar{n}_{x2}$$
$$^{p}n_{x3} = A_r^2 . {}^{p}\bar{n}_{x3}$$

n — Number of half-waves across the direction of loading.

P — Total applied end load.

P_1, P_2, P_3 — Components of the applied end load arising from the pre-buckling stress system, and the post-buckling F_2 and F_3 stress functions respectively.

$\bar{P}_1, \bar{P}_2, \bar{P}_3$ — Components of the end load referred to their appropriate characterising parameter, i.e.

$$P_1 = \phi \bar{P}_1 \quad , \quad P_2 = A_r^2 \bar{P}_2 \quad , \quad P_3 = A_r^2 \bar{P}_3$$

P_c — Critical load of a plate with a hole.

P_{cu} — Critical load of an unperforated plate.

P_i — The load on node i on the hole edge calculated from stress function F_2 for the calculation of stresses $^{p}n_{x3}$, $^{p}n_{y3}$ and $^{p}n_{xy3}$.

P_{ult} — The ultimate load of a plate.

r_x, r_y — Radii of curvature in x and y directions.

S_p	The surface area of finite element p .
t	The plate thickness.
u	Mid-surface deformation in the x-direction.
V	Total Strain Energy.
V_1, V_2	Strain energy due to mid-surface deformations and bending respectively.
v	Mid-surface deformation in the y-direction.
w	Out-of-plane deflection in the middle surface.
x, y	Rectangular Cartesian co-ordinates.
σ_Y	The yield stress of the material.
σ_{xmax}	The maximum stress in the plate parallel to the x-axis.
ϕ	The applied edge displacement (or load) parameter.
ν	Poisson's Ratio.
$\varepsilon_x, \varepsilon_y$	Direct strains in the x and y directions.
$\varepsilon_{xr}, \varepsilon_{yr}$	Direct strains in the x and y directions arising from stress system r .
${}_p\varepsilon_{xr}, {}_p\varepsilon_{yr}$	Components of the direct strains ε_x and ε_y arising from stress system r in element p .
${}_p\bar{\varepsilon}_{xr}, {}_p\bar{\varepsilon}_{yr}$	The direct strains ${}_p\varepsilon_{xr}$ and ${}_p\varepsilon_{yr}$ related to the relevant characterising load or deflection parameter, e.g. $${}_p\varepsilon_{x1} = \phi \cdot {}_p\bar{\varepsilon}_{x1}$$ $$\varepsilon_{x2} = A_r^1 \cdot \bar{\varepsilon}_{x2}$$ $${}_p\varepsilon_{x3} = A_r^1 \cdot {}_p\bar{\varepsilon}_{x3}$$

γ_{xy} Shear strain in the x-y plane.

γ_{xyr} Shear strain γ_{xy} arising from stress system r .

$p\gamma_{xyr}$ Shear strain γ_{xy} arising from stress system r in element p .

$p\bar{\gamma}_{xyr}$ Shear strain $p\gamma_{xyr}$ related to the appropriate characterising load or deflection parameter.

F_2^{II} $\frac{\partial^2 F_2}{\partial y^2}$

CHAPTER ONE

Introduction and Review of Literature

1.1 Introduction

Thin plates are among the most commonly used types of load-bearing members throughout a wide range of engineering structures. The trend in shipbuilding, aircraft and vehicle body manufacture has been from stressed skin structures, where the coverings and panelling over the load-bearing frames were allowed to carry a small part of that load, to monocoque structures, which are built fully from thin plating and shells.

Openings have to be cut in some thin plate structural members in order to allow access, or to lighten the structure. For efficient and safe design it is necessary to have some knowledge of the stability and of the post-buckling and ultimate strengths of plates containing such perforations.

1.3. The behaviour of thin plates under in-plane loading is of particular importance, as it is one of the principal types of loading encountered. Thin flat plates have three phases of behaviour under compressive loading. The first phase occurs while the plate is compressed without any out-of-plane deformation. At a certain load this flat shape becomes unstable and beyond this lies the second phase, during which buckles, or waves, grow elastically. The second phase ends when the material begins to yield. The third phase of behaviour starts with the growth of plasticity and ends when the plate is incapable of

supporting further loading and collapses.

The division between the first and second phases of behaviour of a compressed flat plate is called initial instability or buckling. This point occurs when the energy of the load is more easily absorbed by the plate bulging or buckling than solely by middle surface deformations in the plane of the plate. 1

A large amount of work has been done on the subject for various plate shapes and boundary conditions. This work has been adequately reviewed by Timoshenko and Gere (1), Bleich (2) and Bulson (3) and therefore it is only necessary to give a brief outline of the principal methods of analysis of this problem as background information to the literature on the buckling of plates with holes. Most of the methods of analysis reviewed can also be applied to the post-buckling behaviour of thin plates.

Bending can be regarded as being initiated at the point of initial instability of a thin flat plate. At this point, the out-of-plane displacements are only on the point of growing. Hence, it may be assumed that stretching caused by out-of-plane bending has no effect on the level of direct stresses in the plate. This simplifies the differential equations which describe the equilibrium and compatibility of the stresses and deformations in the plate and also simplifies the equations of strain energy. Even this simplification of the governing equations only allows a few cases of rectangular uniform plates with regular boundary conditions to be solved exactly. Approximate energy and numerical methods must be used for irregular

or complex shapes or boundary conditions. The most successful of these approximate energy methods are the Rayleigh-Ritz, Galerkin and Lagrangian Multiplier methods.

In the Rayleigh-Ritz method the total potential energy is written in terms of approximate displacement functions, containing arbitrary coefficients, and is minimised with respect to these coefficients. The method is described at greater length and discussed in detail by Oden (4) and by Argyris and Kelsey (5). Each term of the approximate displacement functions must at least satisfy the kinematic boundary conditions. Overall static equilibrium is approximately produced by minimising the total potential energy. In the particular case of plate buckling, only the out-of-plane deflections need be represented by an approximate function, if a two-dimensional plane stress pre-buckling solution for the plate geometry and boundary conditions is known.

Alfutov and Balabukh (36) rewrote the strain energy equations of a plate into a form which did not require the exact prebuckling stress distribution, but required a stress distribution which could be separated into a statically determinate stress distribution which satisfied the stress boundary conditions, and another which satisfied the compatibility equations for the out-of-plane deflection function with zero stress on the boundaries. Khan and Walker (37) used this method of analysis for the buckling load of plates under localised edge loads, and related the deflection function to an approximate solution for the compatibility equation by Galerkin's method.

This method is useful if a reasonably accurate statically determinate approximation for the pre-buckling stress distribution is known, and a solution for the compatibility equation can be found. However, if the pre-buckling stress distribution is readily available, or too complex to be represented by a simple statically determinate stress distribution, then it is obviously more advantageous to use the actual pre-buckling solution.

If the virtual displacements specified by the deflection function are considered not to disturb the deformed boundaries of the compressed undeflected plate, then no external work is done during these deflections. It therefore follows from reference (4) that only the strain energy requires to be minimised. As an alternative, Timoshenko (1) approached the problem of stability by ignoring the stretching of the plate during bending, and equated the change in bending strain energy caused by a variation of the deflection function from the undeflected state, to the external work done by that same variation. Due to the origin of Timoshenko's equations, both methods are equivalent.

The Lagrangian Multiplier method requires displacements to be represented by approximate series functions, but does not require these functions to satisfy either the kinematic or static equilibrium boundary conditions. The additional constraint equations necessary for the displacement functions to satisfy the boundary conditions are added to the equation for total potential energy, after being multiplied by constants known as Lagrangian multipliers.

The modified energy equation is then minimised with respect to the displacement function coefficients and the further equations required for a solution come from the equations of additional restraint. This method has been used successfully by Budiansky and Hu (6) to provide both upper and lower bounds to various problems of rectangular plates.

It may be possible to apply this method to boundaries of irregular shape by using Langrangian multipliers to satisfy boundary conditions at discrete points on these boundaries where the displacement functions do not satisfy the appropriate conditions. The idealisation of continuous boundaries as discrete points has been successfully carried out by Conway and Leissa (7) in order to satisfy solutions for the differential equations of plate equilibrium for bending and buckling. However, the solution of the equilibrium equation was mathematically exact and Lagrangian multipliers were not used.

The Galerkin method requires the deflection functions chosen to satisfy all the boundary conditions. This method is fully explained in reference (5), but it is obvious that the method is extremely difficult to apply to plates with highly irregular boundaries or complex loading conditions.

The two most widely employed numerical methods are the Finite Element and Finite Difference methods. It is not considered necessary to describe these methods in detail, as they are fully discussed in references (8) and (26).

Geometrically non-linear finite elements are discussed by Zienkiewicz (8) and Argyris, Kelsey and Kamel (9). Finite element subdivisions can reproduce highly irregular boundaries and the buckling of square plates with central

circular holes has been studied for shear loading by Rockey, Anderson and Cheung (10)in this way. The finite element displacement method is basically a minimisation of the total potential energy of a structure, in which the structure is idealised by the displacements of a limited number of points, which are the corners or nodes of 'finite elements' of the structure. The load-displacement characteristics, or stiffnesses of each of these elements can be determined, thus allowing the strain energy of the structure to be written in terms of the nodal displacements as the sum of the strain energy of the individual elements. Hence the method depends on how accurately the elements themselves can reproduce the behaviour of the plate. Many elements have been proposed or developed, and references (11), (12) and (13) are included in the bibliography as being typical of the range of these elements. However, the type of problem studied by the use of these elements for large deflection behaviour has been limited to simple regular structures.

Finite differences have a limited application if highly irregular boundary conditions are to be applied. The conventional triangular or rectangular grid is very difficult to apply to irregular boundaries and high orders of derivatives. Series Functions with arbitrary coefficients could be used to approximate local deformation surfaces, but this added complexity begins to erode the advantage of relative simplicity which the finite difference method has over finite elements.

There are other methods which idealise plates into

discrete points or regions. Yettram and Awadalla (14) wrote the energy equations in terms of displacements at the corners of regions of a plate, and used Castigliano's first theorem to produce a relationship between the corresponding loads and displacements. Walker (15) considered the overall behaviour of a plate as being the sum of localised displacements. The strain energy was written in terms of the governing parameter or coefficient of each local perturbation and the equilibrium conditions were determined by minimising the total potential energy.

The main disadvantage of the numerical methods is that they produce very large eigenvalue problems for initial instability, which have to be examined for the lowest eigenvalue and its corresponding eigenvector, and non-linear analysis produces large systems of simultaneous non-linear equations.

1.2 Plates with Holes

The buckling of plates with circular holes has been studied under various conditions of edge loading and restraint, and much of this work has been summarised by Bulson (3). However, little work has been done on post-buckling behaviour and collapse.

The earliest work on the stability of rectangular plates with holes was carried out by Levy, Woolley and Kroll (16). This was applied to square plates with a ring stiffener around the edge of the hole, but the plate without any stiffening was considered as a special case. Initial instability was calculated by the Rayleigh-Ritz

method. The pre-buckling stress distribution came from work by Gurney (17) on an infinite sheet with a constant uniaxial stress applied at infinity and containing a stiffened circular hole. An approximate deflection function of the form

$$w = \sum_{n=1}^{N} \sum_{m=1}^{M} a_{nm} \cos\frac{n\pi x}{a} \cdot \cos\frac{m\pi y}{b}$$

was used, selecting only the terms which gave the most rapid convergence. Instability was related to a parameter S in the stress distribution, which corresponded to the uniform applied stress at infinity. The critical applied stress was calculated from the average of the mean stress on the loaded edge and the mean stress across the minimum section for the critical value of S. The critical stress thus calculated decreased with increasing hole size. The investigation was carried out for plates with hole sizes ranging from 0.125 to 0.5 times the plate width. The results of Levy et al. are illustrated in Figure 1.1. The stress distribution was only an approximation to the stresses in a finite plate, hence these results corresponded to plates with some additional restraint or loading applied at the nominally unloaded edges. This approximation excluded these results from any discussion on the effects of in-plane restraint on critical loads.

Kumai (18) used the Rayleigh-Ritz method to study simply supported and clamped square plates. An infinite plate stress distribution in curvilinear co-ordinates was used to represent the pre-buckling stress distribution. The deflected shapes were of simple sine/cosine relationships

with an exponential function, and were of the form

$$w = w_0 \left[\cos \pi x . \cos \pi y + b e^{-c(x^2+y^2)} \right]$$

for a simply supported square plate of sides having unit length and the origin of the co-ordinates in the centre of the plate. In radial co-ordinates this was approximated by

$$w = w_0 \left[J_0(2\pi r) + b e^{-cr^2} \right]$$

By substituting the equation for w in radial co-ordinates into the expression for zero radial moment and Kirchoff's free edge boundary conditions at the edge of the hole, values of b and c were obtained.

The theoretical analysis showed the critical stress to decrease with increasing hole size for simply supported plates, and also showed a change to occur in the buckling mode of clamped plates beyond a certain hole size. Kumai carried out an experimental investigation which confirmed the theoretical predictions. These tests were conducted on perspex plates, whose holes were progressively enlarged. The loads were applied through a system of levers in order to approximate a uniform stress loading. The slope of the plate at a point was measured from the reflections of a light source from a mirror attached to the plate at that point. The slopes were used in the Southwell-Donnel method to estimate the buckling load. The results are summarised in Figure 1.2.

Kumai's theoretical results show better agreement with his experimental results than do those of Levy. This is attributed to his use of the exponential function in attempting to approximately satisfy the hole free edge

boundary conditions. However, for large hole sizes, the addition of this term means that none of the boundary conditions are satisfied. The plane stress distribution is for an infinite plate, and therefore also limited in accuracy to small hole sizes. No information was given on how the buckling loads were estimated from the critical infinite applied stress.

The stability of square plates with uniform edge displacements and straight unloaded edges was studied by Schlack (19). The Rayleigh-Ritz energy method was used, with all the displacements represented by functions containing arbitrary coefficients, i.e.

$$u = Bx + t\left(1 - \frac{x^2}{a^2}\right)\frac{x}{a}\sum_{n=1}^{N}\sum_{m=1}^{M} B_{nm}\left(\frac{x}{a}\right)^m\left(\frac{y}{b}\right)^n$$

$$v = Cy + t\left(1 - \frac{y^2}{b^2}\right)\frac{y}{b}\sum_{n=1}^{N}\sum_{m=1}^{M} C_{nm}\left(\frac{x}{a}\right)^m\left(\frac{y}{b}\right)^n$$

$$w = t\left(1 - \frac{x^2}{a^2}\right)\left(1 - \frac{y^2}{b^2}\right)\sum_{n=1}^{N}\sum_{m=1}^{M} A_{nm}\left(\frac{x}{a}\right)^m\left(\frac{y}{b}\right)^n$$

The effect of adding a term, which was singular at the centre of the hole, was assessed, but was not used in later work (20). The critical load was calculated from the critical displacement, as being the average load in the compressed direction along the length of the plate. The theoretical analysis showed that the critical stress decreased with increase in hole size, and this was verified by experimental work carried out by Schlack. The experimental work was performed on aluminium square plates whose holes were widened progressively from a diameter of 0.1 to 0.3 times the plate width (19) and to 0.7 times the plate width (20). The critical load was estimated as

being the point of inflection of the load deflection curve, and was determined by numerically analysing the load-deflection data. The point of inflection of the load-deflection curve was recommended by Coan (21) and Yamaki (22) as corresponding closely to the buckling load of a flat plate. Schlack's results are summarised in Figure 1.3.

The effect of the position of a circular hole on the critical load of a square plate was examined theoretically and experimentally by Yoshiki et al. (23). The same method of theoretical analysis was used as in reference (18), with modification to the exponential term in order that the singular point occurred at the centre of the hole. The applied critical load was calculated from the average stress in the direction of loading across the minimum section and at the loaded edge for the critical value of the stress at infinity. There is a discrepancy between Yoshiki's and Kumai's theoretical results, which suggests that Kumai used another method of evaluating a critical load from the critical stress at infinity.

Tests were carried out on 600 mm x 600 mm x 6.6 mm steel plates. No details were given of the test rig, except that it had a rigid loading head. The loading was therefore expected to be of the constant displacement type. The nature of the in-plane restraint on the uncompressed edges was not mentioned. Critical loads were estimated from the plot of load against the square of the out-of-plane deflection. The experimental critical loads showed good agreement with theory and with the experimental and theoretical results of

Kumai. The experimental results of Yoshiki and Kumai for plates without a hole indicate that the uncompressed edges were probably free to move in their own plane. The theoretical and experimental results of Yoshiki are summarised in Figure 1.4.

Some discussion was made by Yoshiki et al. on the difference between constant stress and constant displacement loaded edges, and their representation by infinite plate and strip stress distributions. The conclusion was that infinite plate or strip stress distributions could be used for plates compressed by a uniform edge displacement, but that exact or finite element stress distributions should be used for constant applied stress loading of plates with large holes. A finite plate stress distribution from an unspecified source was applied to a particular case. However, this theoretical result did not show any better agreement with the experimental results than the other theoretical results based on infinite plate stress distributions.

The use of finite element stress distributions in the Rayleigh-Ritz method was proposed by Kawai and Ohtsubo (24) for the solution of plate stability problems. In order to demonstrate this method, the problem of the simply supported square plate with a central circular hole was studied. The out-of-plane deflection was represented by a polynomial series, and Green's theorem was used to simplify integration of the energy equations over the finite element areas.

Kawai and Ohtsubo studied plates with the same boundary conditions as Schlack (19), Kumai (18) and Fujita (23)

and their theoretical results showed good agreement with the experimental work of these previous authors. Comparison is made between Kawai and Ohtsubo's results and those of Kumai in Figure 1.5.

Kawai and Ohtsubo were first to compare the effects of restraint in the plane of the plate at the unloaded edges. They were also able to show theoretically the distinct differences in buckling strengths of plates loaded by constant stress, and those loaded by uniform displacements.

The buckling and ultimate strengths of perforated compression flanges of thin walled members were studied by Yu and Davis (31) for various boundary and loading conditions. Flanges, fully supported or with one edge free, with single centrally located holes were investigated experimentally for initial instability and, in addition, fully supported shear webs were also investigated experimentally for buckling. The experimental results were compared with the theoretical results of other investigators (16), (18), (19), (23), (24) in order to find those which most closely predicted the experimental results. The ultimate strengths of fully supported flanges under direct compression were also measured.

The tests on the fully supported flanges were carried out on beam and column specimens. The ratio of hole sizes investigated was for diameter/width ratios 0 - 0.722 and width to thickness ratio 36.6 - 78.2. The aspect ratio of the perforated compression flanges was 2.6. The experimental variation of the buckling loads against hole size is

shown in comparison with the theoretical results of Kawai and Ohtsubo (24) for simply supported square plates in Figure 1.6. Yu and Davis recommended that the theoretical curve for the buckling loads of constant stress loaded plates in Figure 1.6 be used for the prediction of local buckling of fully supported compression flanges. The ultimate strengths of these flanges were comparable to the ultimate strength of solid flanges.

The post buckling strength was defined in terms of modifications to Winter's 'effective width' formulae (33). The results of the local buckling investigation indicated to Yu and Davis that the fully supported perforated flange with a hole of diameter/width ratio greater than 0.7 could be replaced by two strips, each with one edge free and width ½(total width-diameter). Two coefficients dependent on the hole diameter/plate width ratio were introduced into Winter's design formula, and the resulting expression was equated to the expression for the effective width of a flange with one edge free at the transitional value of hole diameter/plate width ratio of 0.7. This enabled the values of these coefficients to be found, which gave a continuous relationship for the effective width relative to the hole diameter.

For fully supported flanges, this was:-

$$b_e = 1.9t\sqrt{\frac{E}{\sigma_{max}}}\left(1-\frac{Ad}{\omega}\right)\left[1-0.415\left(\frac{t}{\omega-d}\right)\sqrt{\frac{E}{\sigma_{max}}}\left(1-B\frac{d}{\omega}\right)\right]$$

d = hole diameter

b_e = effective breadth

ω = plate width

A = 0.226

B = 0.0379

Comparison was made between the design formula and experimental results derived from the ultimate loads of the columns. These are reproduced in Figure 1.7.

No comments were made on the mode of buckling or on the modes of failure.

1.3 Summary

The discussion of the methods of analysis of stability and post-buckling behaviour of plates, subjected to compressive edge loads, has indicated that the most suitable line of approach to the analysis of the buckling and post-buckling behaviour of plates with holes lies with approximate energy methods.

Despite the large body of work on the buckling strength of perforated plates under direct compression, there is relatively little knowledge of the behaviour of rectangular plates, and no attempt has previously been made to analytically describe the post-buckling behaviour of perforated plates under edge compression. The modes of failure of square and rectangular plates have not been investigated, and apart from the empirical equations drawn up by Yu and Davis for the compression flanges of cold rolled thin compression members, no method of predicting the ultimate strength has been devised.

The work described in this thesis was an investigation into the initial buckling, post-buckling load deflection behaviour, internal stresses and collapse of simply supported square and rectangular plates with single centrally located holes. The boundary conditions chosen

to be applied were:-

(i) All edges simply supported.

(ii) Constant displacement along the loaded edge.

(iii) The unloaded edges are allowed to move freely in the plane of the plate, i.e. no direct stress normal to the edges.

(iv) All edges free of shear stress.

These boundary conditions were selected as being those which could be produced experimentally with the greatest degree of accuracy and reliability, so that valid comparisons can be made between experimental and theoretical results.

The investigation took the form of experimental tests on square and rectangular plates of aspect ratio 2:1 in order to determine buckling loads, post-buckling load deflection behaviour, collapse loads and the stress distribution in certain areas of the plates. Square and rectangular plates of aspect ratio 2:1 buckle into square waves, i.e. where the half wavelength equals the plate width. Thus the square plates enabled the effect of a hole at the centre of a square wave to be studied and rectangular plates enabled the effect of a hole between two square waves to be assessed. The investigation also included the development of an analytical method of predicting the elastic buckling and subsequent non-linear behaviour of perforated square and rectangular plates. The method of analysis was applied to plates with the previously described boundary conditions, but its application to other boundary conditions including rotational and

in-plane restraint and constant stress applied loading is indicated. A simple analysis for the determination of collapse loads is proposed.

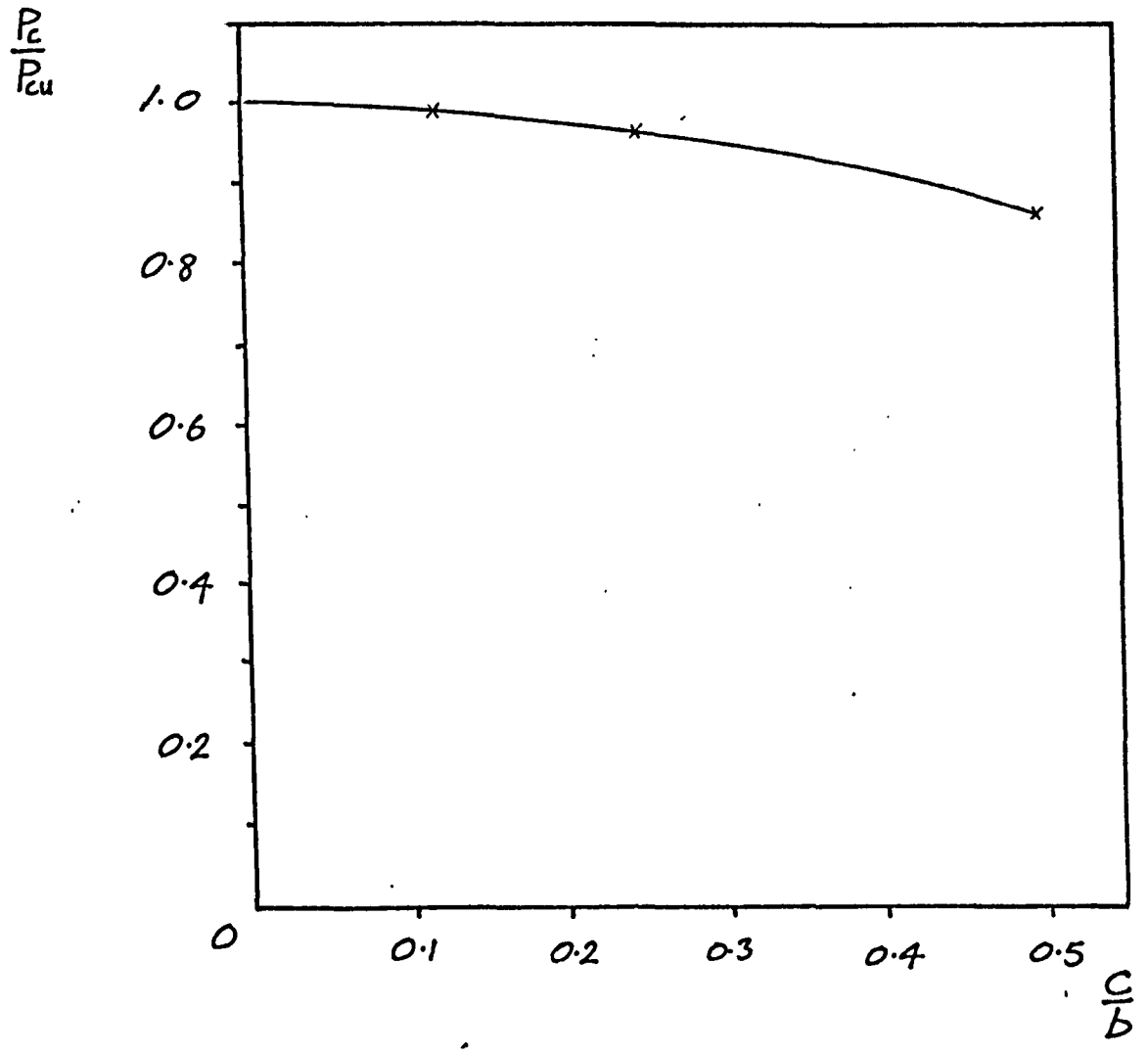

FIGURE 1.1 THEORETICAL VARIATION OF BUCKLING LOAD WITH HOLE RADIUS DERIVED BY LEVY ET AL (16)

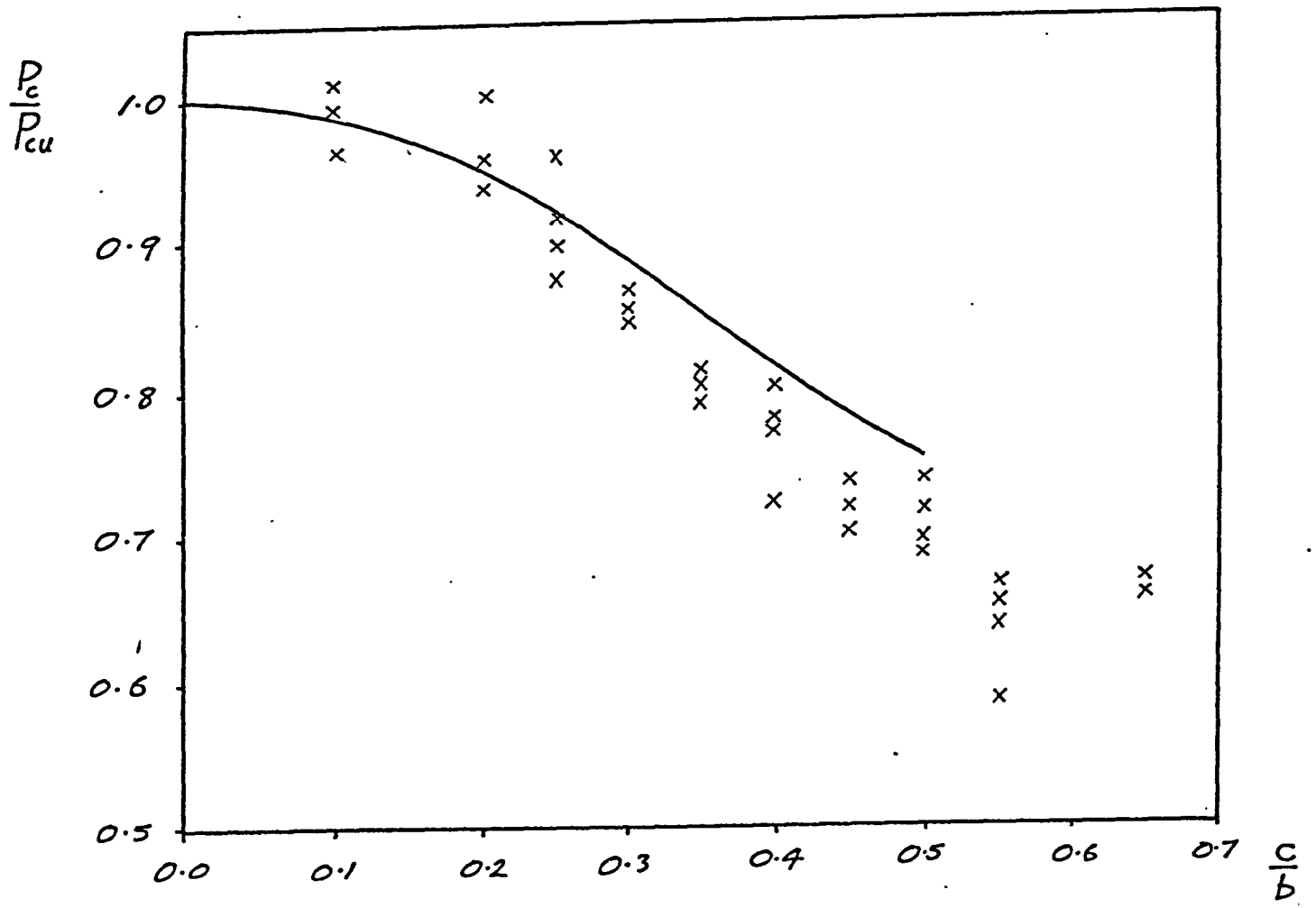

FIGURE 1·2 COMPARISON BETWEEN THEORETICAL AND EXPERIMENTAL VARIATION OF BUCKLING LOAD WITH HOLE RADIUS DERIVED BY KUMAI (18)

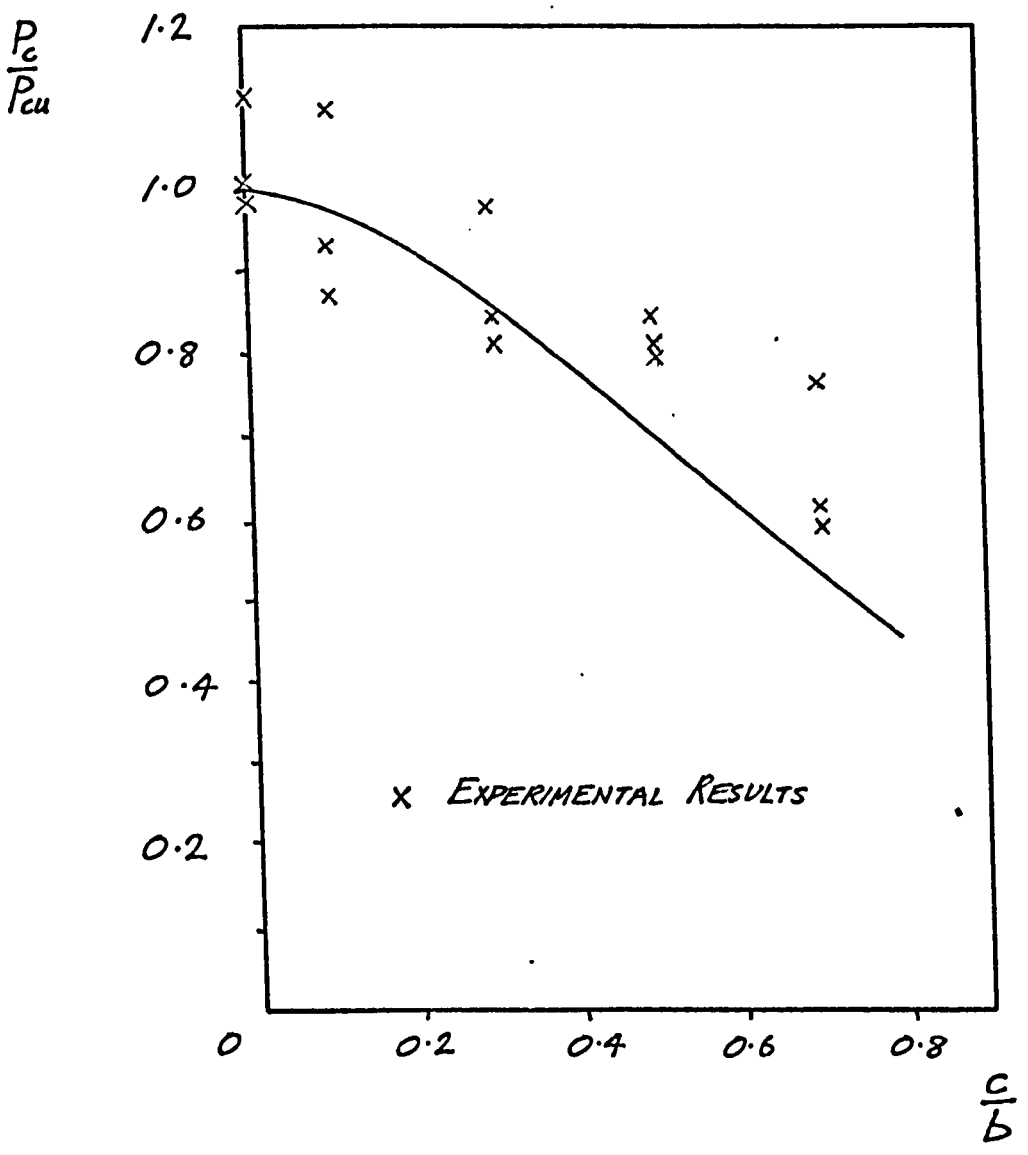

FIGURE 1.3 THE THEORETICAL AND EXPERIMENTAL VARIATION OF BUCKLING LOAD WITH HOLE RADIUS DERIVED BY SCHLACK (19) (20)

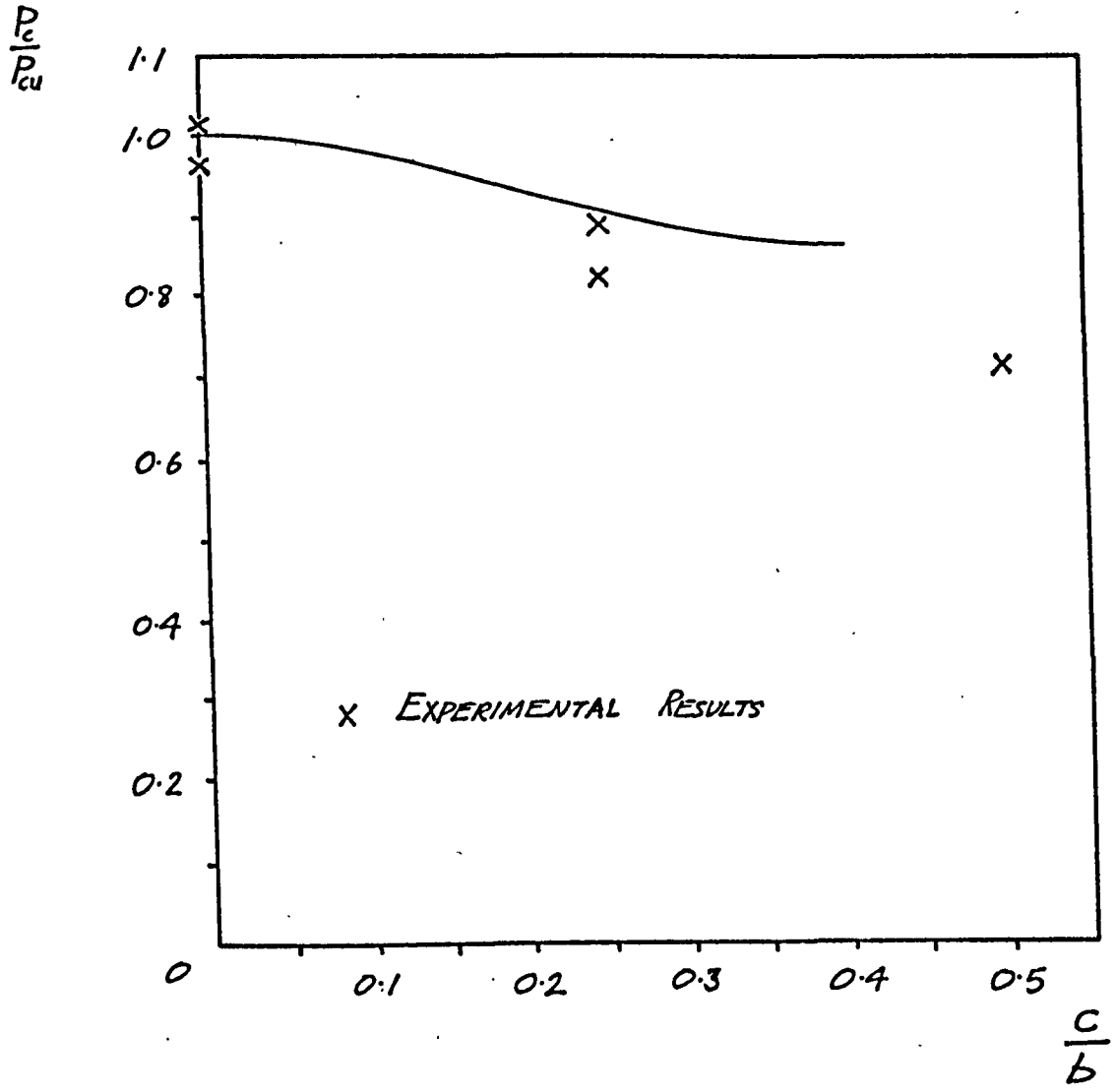

FIGURE 1.4 THE THEORETICAL AND EXPERIMENTAL VARIATION OF BUCKLING LOAD WITH HOLE RADIUS DERIVED BY YOSHIKI ET AL (23)

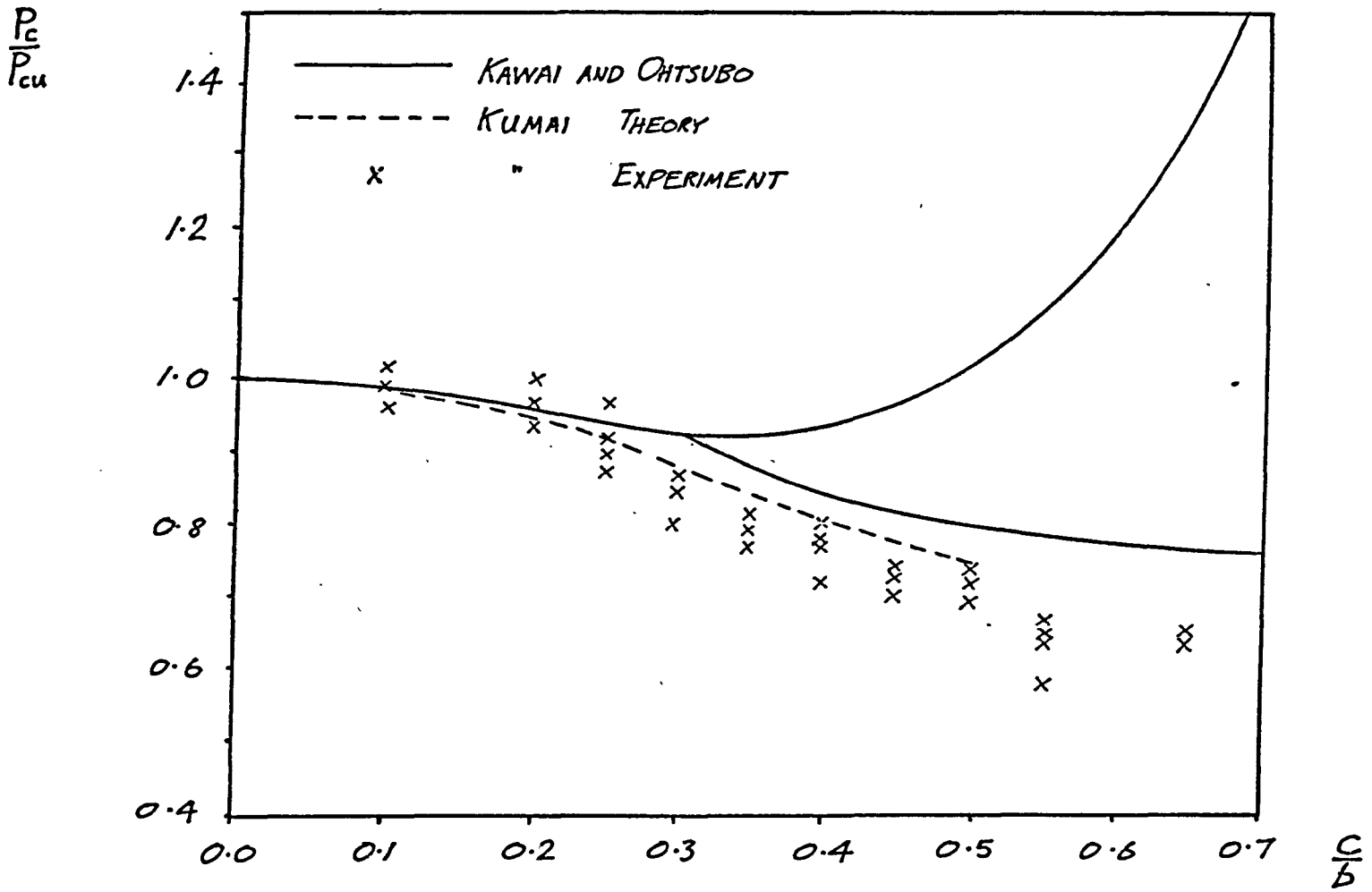

FIGURE 1.5 THE THEORETICAL RESULTS OF KAWAI AND OHTSUBO (24) AND THE RESULTS OF KUMAI (18)

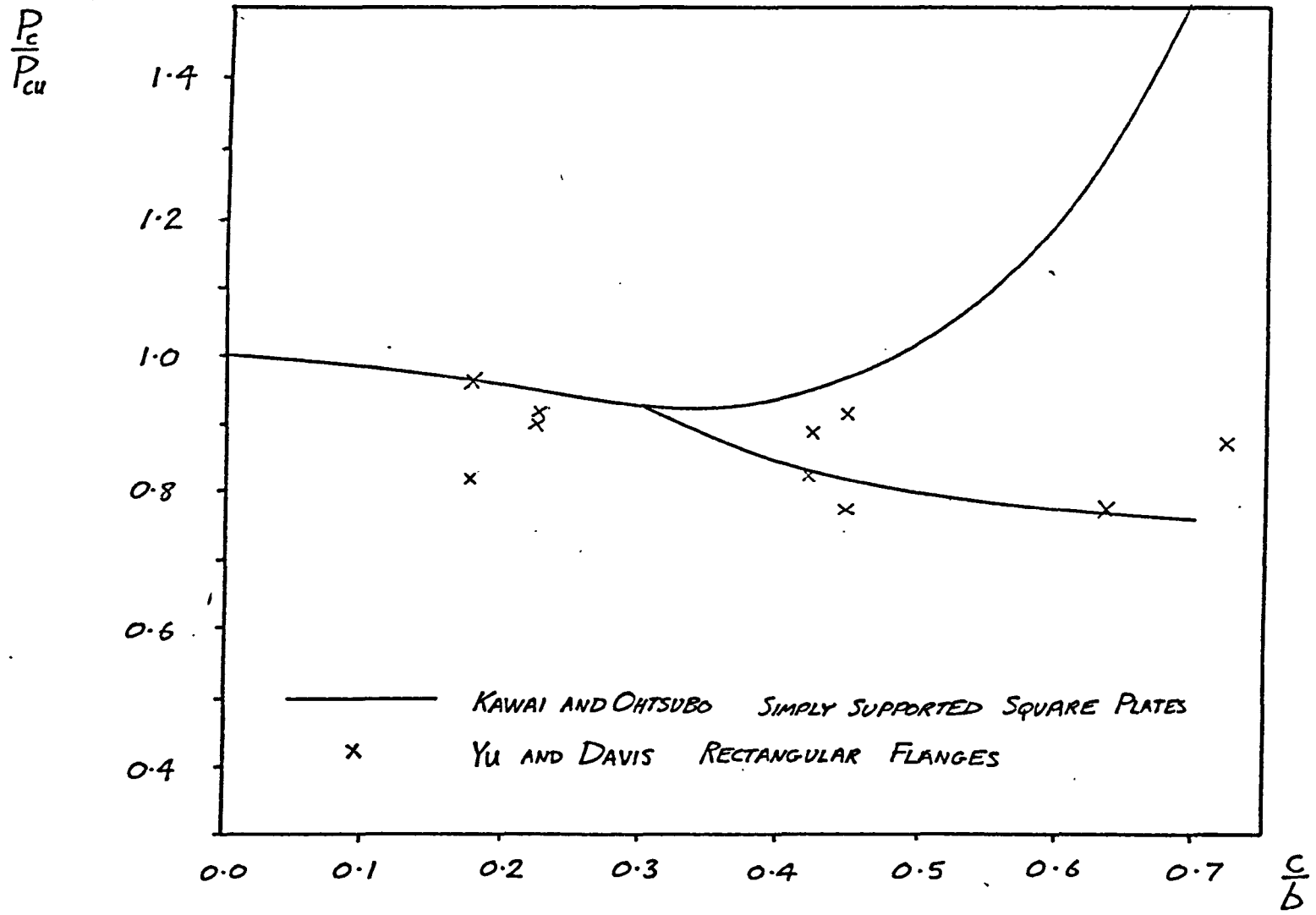

FIGURE 1.6 COMPARISON BETWEEN THE EXPERIMENTAL RESULTS OF YU AND DAVIS (31) AND THEORETICAL RESULTS OF KAWAI AND OHTSUBO FOR SIMPLY SUPPORTED SQUARE PLATES

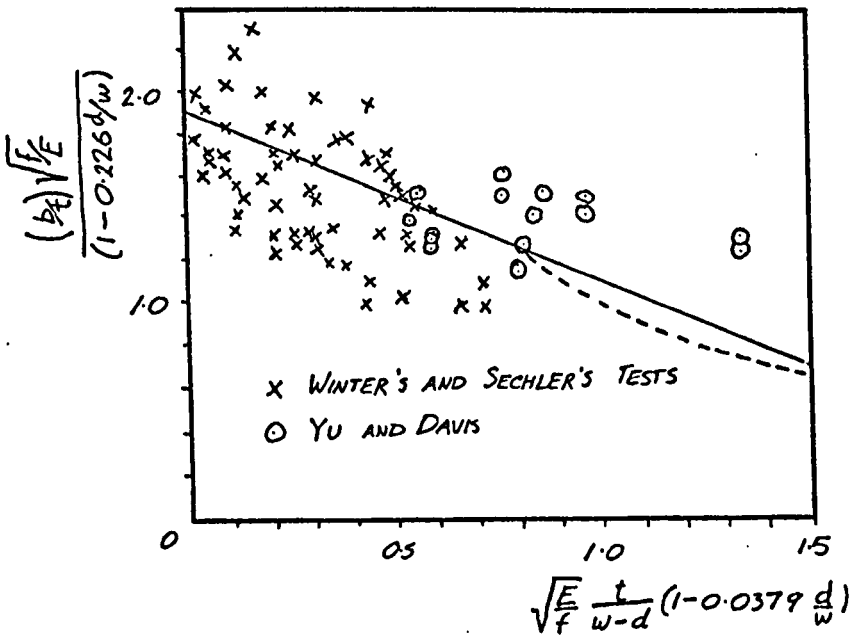

FIGURE 1.7 COMPARISON OF EFFECTIVE WIDTHS

d HOLE DIAMETER
f MAXIMUM STRESS
b EFFECTIVE WIDTH
w FLANGE WIDTH

CHAPTER TWO

Basic Equations

2.1 Basic Equations of Equilibrium and Compatability

The deformation of a thin plate under compressive loading, in which the out-of-plane deflections are of the order of two to three times the plate thickness, can be treated as being produced by interdependent stress systems whose individual actions can be analysed separately. The distribution of stress in a plate is due to the bending of the plate itself, stretching of the plate during bending, and to the in-plane applied loads. By making the following assumptions, the actions of the stresses in the plate may be regarded as being due to 'small deflection' bending, and to the superposition of the stretching of a constant thickness membrane on the stresses in a loaded plate with no out-of-plane deformation.

(i) Plane sections remain plane during bending.

(ii) Deformations in the plane of the plate are small in relation to the overall plate dimensions, therefore the products of the derivatives of the in-plane displacements may be neglected.

(iii) Deformations in the plane of the plate may be represented by u and v, the middle surface movements.

(iv) The out-of-plane deflection of the plate can be represented by the deflection w of the middle surface of the plate.

Assumption (i) allows bending moments to be related to out-of-plane deflections by 'small deflection' theory (reference 25). For an element of a plate loaded as in Figure 2.1, the expressions for the bending moments are as follows:-

$$M_x = -D\left(\frac{\partial^2 w}{\partial x^2} - \nu \frac{\partial^2 w}{\partial y^2}\right)$$

$$M_y = -D\left(\frac{\partial^2 w}{\partial y^2} - \nu \frac{\partial^2 w}{\partial x^2}\right)$$

$$M_{xy} = D(1-\nu)\frac{\partial^2 w}{\partial x \partial y} \qquad 2.1\,a,b,c$$

The stress resultants in the plane of the plate are related to the strains by the conditions of plane stress, i.e.

$$\varepsilon_x = \frac{1}{tE}(N_x - \nu N_y)$$

$$\varepsilon_y = \frac{1}{tE}(N_y - \nu N_x)$$

$$\gamma_{xy} = \frac{1}{tG} \cdot N_{xy} \qquad 2.2\,a,b,c$$

The actions of N_x, N_y and N_{xy} on a plate element are shown in Figure 2.2. Manipulation of the stress resultants can be simplified by introducing an Airey stress function which inter-relates the stress resultants thus:-

$$N_x = t.\frac{\partial^2 F}{\partial y^2}$$

$$N_y = t.\frac{\partial^2 F}{\partial x^2}$$

$$N_{xy} = -t.\frac{\partial^2 F}{\partial x \partial y} \qquad 2.3\,a, b, c$$

By substituting equations 2.3 a, b and c into equations 2.2 a,b,c, ε_x , ε_y and γ_{xy} become

$$\varepsilon_x = \frac{1}{E}\left(\frac{\partial^2 F}{\partial y^2} - \nu\frac{\partial^2 F}{\partial x^2}\right)$$

$$\varepsilon_y = \frac{1}{E}\left(\frac{\partial^2 F}{\partial x^2} - \nu\frac{\partial^2 F}{\partial y^2}\right)$$

$$\gamma_{xy} = -\frac{2(1+\nu)}{E}\frac{\partial^2 F}{\partial x \partial y} \qquad 2.4\,a, b, c$$

The strain components ε_x , ε_y and γ_{xy} were derived in reference (4) from variational calculus, as being:-

$$\varepsilon_x = \frac{\partial u}{\partial x} + \frac{1}{2}\left[\left(\frac{\partial u}{\partial x}\right)^2 + \left(\frac{\partial v}{\partial x}\right)^2 + \left(\frac{\partial w}{\partial x}\right)^2\right]$$

$$\varepsilon_y = \frac{\partial v}{\partial y} + \frac{1}{2}\left[\left(\frac{\partial u}{\partial y}\right)^2 + \left(\frac{\partial v}{\partial y}\right)^2 + \left(\frac{\partial w}{\partial y}\right)^2\right]$$

$$\gamma_{xy} = \frac{\partial v}{\partial x} + \frac{\partial u}{\partial y} + \frac{\partial u}{\partial x}.\frac{\partial u}{\partial y} + \frac{\partial v}{\partial x}.\frac{\partial v}{\partial y} + \frac{\partial w}{\partial x}.\frac{\partial w}{\partial y}$$

$$2.5\,a, b, c$$

The application of assumption (ii) to equations 2.5a, b and c reduces them to

$$\varepsilon_x = \frac{\partial u}{\partial x} + \frac{1}{2}\left(\frac{\partial w}{\partial x}\right)^2$$

$$\varepsilon_y = \frac{\partial v}{\partial y} + \frac{1}{2}\left(\frac{\partial w}{\partial y}\right)^2$$

$$\gamma_{xy} = \frac{\partial v}{\partial x} + \frac{\partial u}{\partial y} + \frac{\partial w}{\partial x} \cdot \frac{\partial w}{\partial y}$$

2.6 a, b, c

In order to express the strain components in terms of w, as a step to relating F and w, the second derivatives of equations 2.6 a, b and c can be collected together to give

$$\frac{\partial^2 \varepsilon_x}{\partial y^2} + \frac{\partial^2 \varepsilon_y}{\partial x^2} - \frac{\partial^2 \gamma_{xy}}{\partial x \partial y} = \left[\left(\frac{\partial^2 w}{\partial x \partial y}\right)^2 - \frac{\partial^2 w}{\partial x^2} \cdot \frac{\partial^2 w}{\partial y^2}\right] \qquad 2.7$$

Substituting equations 2.4a, 2.4b and 2.4c into the left hand side of equation 2.7 gives

$$\frac{\partial^4 F}{\partial x^4} + 2 \cdot \frac{\partial^4 F}{\partial x^2 \partial y^2} + \frac{\partial^4 F}{\partial y^4} = E \cdot \left[\left(\frac{\partial^2 w}{\partial x \partial y}\right)^2 - \frac{\partial^2 w}{\partial x^2} \cdot \frac{\partial^2 w}{\partial y^2}\right] \qquad 2.8$$

A second equation, relating F and w can be found by considering the equilibrium of forces in a direction normal to the plane of the plate. For a plate with no transverse loading, this equation is

$$\frac{\partial^4 w}{\partial x^4} + 2 \cdot \frac{\partial^4 w}{\partial x^2 \partial y^2} + \frac{\partial^4 w}{\partial y^4} = \frac{t}{D}\left[\frac{\partial^2 F}{\partial y^2} \cdot \frac{\partial^2 w}{\partial x^2} + \frac{\partial^2 F}{\partial x^2} \cdot \frac{\partial^2 w}{\partial y^2} - 2 \cdot \frac{\partial^2 F}{\partial x \partial y} \cdot \frac{\partial^2 w}{\partial x \partial y}\right] \qquad 2.9$$

This equation is not used in the analysis, as equilibrium is approximately satisfied by minimising the potential

energy of the plate, and for this reason its derivation has not been more fully explained.

2.2 Strain Energy Equations

The strain energy of a plate due to the stretching of its middle surface may be calculated from the in-plane stress resultants and the corresponding strains. For a linear elastic plate, the equation of this membrane strain energy is:-

$$V_1 = \frac{1}{2}\iint \left(N_x . \varepsilon_x + N_y . \varepsilon_y + N_{xy} . \gamma_{xy} \right) dx\, dy \qquad 2.10$$

This equation can be rewritten by substituting equations 2.2a, 2.2b and 2.2c into equation 2.10.

$$V_1 = \frac{1}{2Et}\iint \left(N_x^2 + N_y^2 - 2\nu N_x N_y + 2(1+\nu) N_{xy}^2 \right) dx\, dy \qquad 2.11$$

Equation 2.11 may be further rewritten in terms of a stress function F , by substitution of equations 2.3a, 2.3b and 2.3c.

$$V_1 = \frac{t}{2E}\iint \left\{ \left(\frac{\partial^2 F}{\partial x^2} + \frac{\partial^2 F}{\partial y^2} \right)^2 - 2(1+\nu)\left[\frac{\partial^2 F}{\partial x^2} \cdot \frac{\partial^2 F}{\partial y^2} - \left(\frac{\partial^2 F}{\partial x \partial y} \right)^2 \right] \right\} dx\, dy \qquad 2.12$$

Because plane sections are assumed to remain plane, the strain energy of bending is simply the work done by the rotation of internal moments in the plate during bending. The rotation of a plane normal to the mid surface of the plate is simply the change in radius of curvature, the curvature being directly related to the deflection function w , by

$$\frac{1}{r_x} = -\frac{\partial^2 w}{\partial x^2} \qquad \frac{1}{r_y} = -\frac{\partial^2 w}{\partial y^2} \qquad \frac{1}{r_{xy}} = \frac{\partial^2 w}{\partial x \partial y}$$

The strain energy of bending is thus:-

$$V_2 = \frac{1}{2}\iint\left[M_x\left(\frac{\partial^2 w}{\partial x^2}\right) + M_y\left(\frac{\partial^2 w}{\partial y^2}\right) + M_{xy}\left(\frac{\partial^2 w}{\partial x\,\partial y}\right)\right] dx\,dy \qquad 2.13$$

This can be written in terms of w by substituting equations 2.1a - 2.1c for M_x, M_y and M_{xy}.

$$V_2 = \frac{D}{2}\iint\left\{\left(\frac{\partial^2 w}{\partial x^2} + \frac{\partial^2 w}{\partial y^2}\right)^2 - 2(1-\nu)\left[\frac{\partial^2 w}{\partial x^2}\cdot\frac{\partial^2 w}{\partial y^2} - \left(\frac{\partial^2 w}{\partial x\,\partial y}\right)^2\right]\right\} dx\,dy \qquad 2.14$$

The total strain energy V of the plate is the sum of the bending strain energy V_2 and the membrane strain energy V_1, i.e.

$$V = V_1 + V_2 \qquad 2.15$$

The equilibrium equation 2.9 can be derived, as previously outlined, from the equilibrium of a small element as shown in Figure 2.2, but it can also be derived from the strain energy equation 2.15. Cox, in reference 27, showed that by equating the variation of V caused by a small variation in w, to zero, the equilibrium equation 2.9 could be derived. This is equivalent to the minimisation of the strain energy with respect to the out-of-plane deflection w, which is a statement of the equilibrium in the direction of w, i.e. perpendicular to the plane of the plate.

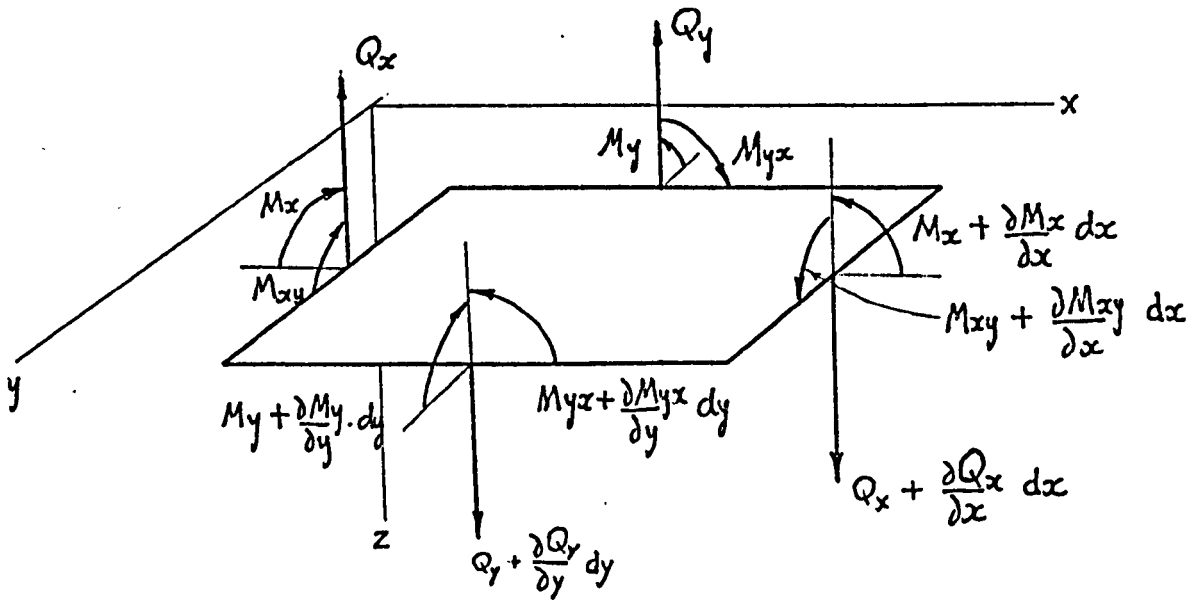

FIGURE 2.1

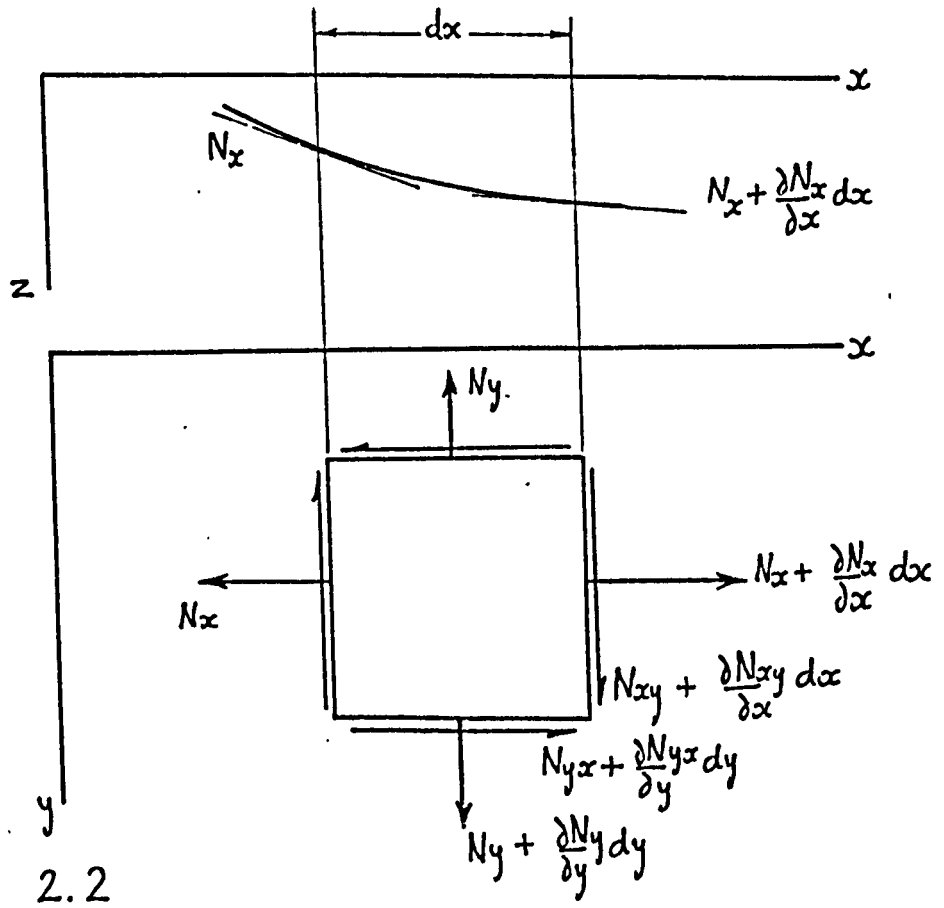

FIGURE 2.2

CHAPTER THREE

Theoretical Analysis

The theoretical analysis of the behaviour of a flat plate with a centrally located circular hole under edge compression is described in this chapter under the following headings:

3.1 Pre-Buckling Analysis.

3.2 Initial Instability.

3.3 Post-Buckling Analysis.

3.4 A Simplified Failure Analysis.

The co-ordinate system chosen to represent the plate is shown in Figure 3.1. The boundary conditions described in Chapter One can be stated, using these co-ordinates, as follows:-

(1) The plate is loaded in the direction of the x-axis in a manner such that the sides x=a and x=o are uniformly displaced and have zero shearing stress resultants i.e.

$u|_{x=0}$ = a constant $\quad u|_{x=a}$ = a constant

(2) The unloaded edges $y=\pm b$ are free from restraint in the plane of the plate. This means that the normal direct stress and shearing stress resultants are zero, i.e. $N_{xy}|_{y=\pm b} = N_y|_{y=\pm b} = 0$

(3) The edges of the plate are simply supported, i.e. no out-of-plane deflections and no rotational restraint at the edges of the plate.

$$\omega|_{x=0} = \omega|_{x=a} = \omega|_{y=\pm b} = 0$$

$$M_x|_{x=0} = M_x|_{x=a} = M_y|_{y=\pm b} = 0$$

The analysis is described specifically for these boundary conditions in each section. However, the analysis can be applied to plates with different boundary conditions and geometries, and this has been indicated, where appropriate, in each section with any necessary differences in the method of analysis.

3.1 Pre-Buckling Analysis

The pre-buckling analysis was accomplished using constant strain plane stress finite element analysis, as in reference (8). The use of finite element analysis is well established and its derivation is fully described in reference (8).

The development of the finite element meshes illustrated in Figures 3.2 and 3.3 was based on the comparison of results from various finite element meshes for rectangular plates, with the theoretical stress distributions around a circular hole in a strip under tension derived by Howland (28). Various subdivisions for a rectangular plate with a hole of diameter 0.3 times the plate width were devised, and the solutions for these with a uniform edge displacement were compared with the stresses in the loaded direction across the minimum section. The mesh shown in Figure 3.2 was the optimum solution for mesh size and element arrangement. Comparison between finite element and theoretical results is shown in Figure 3.4 for a hole

diameter of 0.3 times plate width, and agreement is within ten per cent. The average element stress around each node was plotted with the centroidal value of the stress in Figure 3.4. The presentation of finite element results is subsequently made as a line passing through the average nodal values, which is also a line of best fit to the centroidal values.

The mesh subdivision of the rectangular plate with a hole of diameter 0.3 times the plate width was used as a basis for the subdivisions of plates with other hole sizes. The co-ordinates of the nodal points were scaled radially between the hole centre and the plate edges to produce holes of differing sizes. The effect of this distortion of the mesh on the accuracy of the results was slight, and the Finite Element distribution of stresses in the loaded direction across the minimum section, for plates with hole diameters of 0.1 and 0.5 times the plate width, is shown in Figure 3.4 in comparison to the theoretical solutions.

The mesh for square plates was based on the rectangular mesh, by using a similar number of elements and a similar geometrical arrangement. The square plate meshes were distorted in the same manner as the rectangular meshes in order to obtain different hole sizes.

The derivation of the stiffness matrix of a constant strain triangular finite element is fully described in Appendix One.

The analyses were carried out for square plates and for rectangular plates with an aspect ratio of 2:1 for the range of hole diameters of 0.0 to 0.7 times the plate width. The results are described and compared with the

experimental results in Chapter Five. However, the stress distributions of a square and a rectangular plate with uniformly displaced loaded edges and holes of diameters 0.2 and 0.4 times the plate width are illustrated in Figures 3.5 and 3.6 as examples. In Figure 3.6 the relative magnitudes of the stresses in each direction along the axis can be seen. The stresses in the direction of loading across the minimum section are the largest.

The variation of axial stiffness of the square and rectangular plates with hole size is illustrated in Figures 3.7 and 3.8 respectively.

3.2 Initial Instability

3.2.1 Description of the Stability Analysis

The Rayleigh-Ritz energy method and its application to stability problems was discussed in Chapter One. In order to determine the initial buckling load, an approximate deflection function w , containing arbitrary coefficients was chosen. The approximation was made that the buckled shape in the loaded direction was fixed and the deflection took the form

$$w = f(x) \sum_{n=1}^{N} A_n g_n(y) \qquad 3.1$$

The strain energy V is composed of two parts, the bending energy V_2 and the energy due to membrane stresses V_1 . V_1 and V_2 are given by equations 2.11 and 2.14. Substitution of equation 3.1 for w , into equation 2.14 gave an expression for V_2 of the form

$$V_2 = \sum_{n=1}^{N}\sum_{m=1}^{N} A_n . A_m . K_{1nm} \qquad 3.2$$

where

$$K_{lnm} = \frac{D}{2}\int^{A}\left\{\left[f''(x).g_n(y) + f(x)g_m''(y)\right]\left[f''(x)g_m(y) + f(x).g_n''(y)\right]\right.$$
$$\left.-2(1-\nu)\left[f''(x)f(x).g_n(y)g_m''(y) - f'(x)^2 g_n'(y).g_m'(y)\right]\right\}dxdy$$

The integral $\int^{A} dxdy$ is the integral of the function over the surface area of the plate, excluding the area of the hole, i.e.

$$\int^{A} dxdy = 4\int_0^{\frac{a}{2}-c}\int_0^{b} dydx + 4\int_{\frac{a}{2}-c}^{\frac{a}{2}}\int_{\sqrt{c^2-(x-\frac{a}{2})^2}}^{b} dydx$$

The strain energy due to in-plane stresses was calculated using the results of the finite element analysis with the strains caused by stretching during bending. Equation 2.10 was re-written in a more convenient form as

$$V_1 = \frac{1}{2}\sum_{p=1}^{Ne}\left\{{}^{p}n_x\iint_{Sp}\varepsilon_x dxdy + {}^{p}n_y\iint_{Sp}\varepsilon_y dxdy + {}^{p}n_{xy}\iint_{Sp}\gamma_{xy}\,dxdy\right\} \qquad 3.3$$

where ${}^{p}n_x$ = the stress resultant in the x-direction in element no. p

${}^{p}n_y$ = the stress resultant in the y-direction in element no. p

${}^{p}n_{xy}$ = the shear stress resultant in element p 3.4

The finite element stress distribution was calculated for some unit loading parameter and was related to the actual loading by the multiplier, ϕ. The stress resultants can be re-written in terms of the loading parameter ϕ and the stress resultants calculated from the unit value of this

parameter i.e.

$$
\begin{aligned}
{}_{p}n_{x} &= \phi\, {}_{p}\bar{n}_{x} \\
{}_{p}n_{y} &= \phi\, {}_{p}\bar{n}_{y} \\
{}_{p}n_{xy} &= \phi\, {}_{p}\bar{n}_{xy}
\end{aligned}
\qquad 3.5a, b, c
$$

The strain components ε_x, ε_y and γ_{xy} came from equations 2.6a, 2.6b and 2.6c respectively. These were again rewritten to accommodate that component of each, which came from the finite element analysis.

$$
\begin{aligned}
\varepsilon_x &= {}_{p}\varepsilon_x + \frac{1}{2}\left(\frac{\partial w}{\partial x}\right)^2 \\
\varepsilon_y &= {}_{p}\varepsilon_y + \frac{1}{2}\left(\frac{\partial w}{\partial y}\right)^2 \\
\gamma_{xy} &= {}_{p}\gamma_{xy} + \left(\frac{\partial w}{\partial x}\right)\left(\frac{\partial w}{\partial y}\right)
\end{aligned}
\qquad 3.6a, b, c
$$

Where ${}_{p}\varepsilon_x$ = strain component in x-direction in element p

${}_{p}\varepsilon_y$ = strain component in y-direction in element p

${}_{p}\gamma_{xy}$ = shear strain component in element p

These strain components can be written in terms of the applied loading parameter ϕ in a similar manner to the stress resultants, i.e.

$$
\begin{aligned}
{}_{p}\varepsilon_x &= \phi\, {}_{p}\bar{\varepsilon}_x \\
{}_{p}\varepsilon_y &= \phi\, {}_{p}\bar{\varepsilon}_y \\
{}_{p}\gamma_{xy} &= \phi\, {}_{p}\bar{\gamma}_{xy}
\end{aligned}
$$

Substituting equations 3.6a, 3.6b and 3.6c into equation 3.3 gave the following equation for the strain energy V_1,

$$
V_1 = \frac{1}{2}\sum_{p=1}^{Ne}\Big\{ {}_{p}n_x \cdot {}_{p}\varepsilon_x \cdot S_p + {}_{p}n_y \cdot {}_{p}\varepsilon_y \cdot S_p + {}_{p}n_{xy} \cdot {}_{p}\gamma_{xy} \cdot S_p +
$$

$$+ \frac{p\bar{n}_x}{2}\iint_{S_p}\left(\frac{\partial w}{\partial x}\right)^2 dx\,dy + \frac{p\bar{n}_y}{2}\iint_{S_p}\left(\frac{\partial w}{\partial y}\right)^2 dx\,dy + p\bar{n}_{xy}\iint_{S_p}\left(\frac{\partial w}{\partial x}\right)\left(\frac{\partial w}{\partial y}\right) dx\,dy \Bigg\} \qquad 3.7$$

S_p = area of element p

The integral $\iint_{S_p}$ represents the integral of the function over the area S_p of element p.

Equation 3.7 became, when it was re-written using the loading parameter ϕ, and equation 3.1 is substituted for w:-

$$V_1 = \phi^2 K_2 + \phi \sum_{n=1}^{N}\sum_{m=1}^{N} A_n A_m K_{3nm} \qquad 3.8$$

where

$$K_2 = \frac{1}{2}\sum_{p=1}^{N_e}\left\{ p\bar{n}_x \cdot p\bar{\varepsilon}_x + p\bar{n}_y \cdot p\bar{\varepsilon}_y + p\bar{n}_{xy} \cdot p\gamma_{xy} \right\} S_p \qquad 3.9$$

and

$$K_{3nm} = \frac{1}{2}\sum_{p=1}^{N_e}\left\{ \frac{p\bar{n}_x}{2}\iint_{S_p} f'(x)^2 \cdot g_n(y) \cdot g_m(y)\, dx\,dy + \frac{p\bar{n}_y}{2}\iint_{S_p} f(x)^2 \cdot g_n'(y) \cdot g_m'(y)\, dx\,dy \right.$$
$$\left. + p\bar{n}_{xy}\iint_{S_p} f'(x) \cdot f(x)\, g_n(y) \cdot g_m'(y)\, dx\,dy \right\} \qquad 3.10$$

The total strain energy V is

$$V = V_1 + V_2$$

i.e.
$$= \sum_{n=1}^{N}\sum_{m=1}^{N} A_n \cdot A_m K_{1nm} + \phi^2 K_2 + \phi \sum_{n=1}^{N}\sum_{m=1}^{N} A_n \cdot A_m K_{3nm} \qquad 3.11$$

The expression for V can be re-written in matrix form as

$$V = \phi^2 K_2 + \phi [A]^T [K_{3nm}] \{A\} + [A]^T [K_{1nm}] \{A\} \qquad 3.12$$

At the point of buckling, the out-of-plane deflections are infinitesimally small. The effect of a virtual deflection or infinitesimally small variation in the out-of-plane deflections in a plate with its loaded edges assumed to be

fixed at some unspecified displacement will therefore not produce a change in the external potential. This means that only the strain energy requires to be minimised. Minimising the strain energy with respect to the deflection coefficients produces the following set of simultaneous equations

$$\frac{\partial V}{\partial \{A\}} = 2.\left[[K_{1nm}] + \phi[K_{3nm}]\right]\{A\} = 0 \qquad 3.13$$

Equation 3.13 is an eigenvalue problem. The solution is that either the vector $\{A\}$ is zero, and hence ϕ can take any value, or the eigenvector $\{A\}$ has an indeterminate value at certain values of ϕ, the eigenvalue, such that the determinant of the expression in the square brackets in equation 3.13 is zero, i.e.

$$\left|[K_{1nm}] + \phi[K_{3nm}]\right| = 0$$

The second variation of strain energy is

$$\frac{\partial^2 V}{\partial \{A\}\,\partial \{A\}} = [K_{1nm}] + \phi[K_{3nm}] \qquad 3.14$$

A condition of neutral equilibrium exists when the determinant of the second variation is zero (reference 4) i.e.

$$\left|[K_{1nm}] + \phi[K_{3nm}]\right| = 0 \qquad 3.15$$

This has already been satisfied by the non-trivial solution of equation 3.13 and hence the eigenvalues and eigenvectors are points of neutral equilibrium. The points of neutral equilibrium are the transition or bifurcation

points between different deformation modes, and therefore the smallest eigenvalue ϕ corresponds to the point of initial instability.

3.2.2 Application of the Stability Analysis

The function chosen to represent the deflected shape of the simply supported plate shown in Figure 3.1 was

$$w = \sin \frac{k\pi x}{a} \sum_{n=1}^{N} A_n \cos \frac{n\pi y}{2b} \qquad n = 1, 3, 5 \ldots\ldots \qquad 3.16$$

The analysis was carried out for square and rectangular plates of aspect ratio 2:1, with a range of hole sizes from 0.0 to 0.7 times the plate width. It was necessary to examine the buckling loads for various buckle wavelengths in the loaded direction in order to determine the minimum buckling load and its associated buckling mode. It was found that three terms of equation 3.16 were enough to reduce the variation in buckling load to less than 1% in all cases.

The integration of the energy expressions was performed by the numerical integration of the functions over each element area. The solution for the eigenvalue equation 3.13 was performed using the simple iterative method described in Appendix Two, which allowed the minimum eigenvalue to be calculated. The iteration was stopped when subsequent values of the eigenvalue had converged to less than 0.1%. The convergence of the normalised eigenvector was slower, but when the iterations were stopped, the smallest element of the eigenvector had generally converged to three significant figures.

The theoretical variation of buckling load with hole size is presented in Figure 3.9 for simply supported rectangular plates with uniformly displaced loaded edges , and in Figure 3.10 for simply supported square plates for both constant displacement and constant stress loading conditions.

3.3 Post-Buckling Analysis

3.3.1 General Description of the Post-Buckling Analysis

In a plate loaded through uniformly displaced edges, the middle surface stress distribution was regarded as the sum of two stress distributions. The first, represented by the Airey stress function F_1, was the stress distribution in a plate with no out-of-plane deflections produced by the applied displacements. The second, represented by the Airey stress function F_2, was the stress distribution produced by the stretching of the middle surface of the plate into the out-of-plane deflections, with no displacement of the loaded edges. The first stress distribution was dependent only on the magnitude of the applied displacements and the second, F_2, depended on out-of-plane deflection. Because F_2 does not affect the loaded edge displacements, any variation in deflection, while it does affect the external load, does not produce external work. This means that a variation in the total potential energy is a variation in the total strain energy, and that therefore only the strain energy requires to be minimised as a condition for equilibrium.

Marguerre (29), Yamaki (22) and Rhodes and Harvey (30) amongst others, derived stress functions for the post-buckling

behaviour of unperforated rectangular plates, all of which could be separated into an F_1 and F_2 for uniformly displaced loaded edges. In each of these investigations, the deflection function was represented by selected terms of a Fourier series, which were inserted into the compatibility equation 2.8. The resulting equation was then solved for the stress function F. Marguerre (29) only used the particular integral for the solution of stress function F and employed one and three term analyses. Yamaki (22) used both the particular integral and the complementary function, and employed four terms of the deflection function. Rhodes and Harvey (30) assumed the shape fixed in the loaded direction but used several terms to represent the deflections across the plate. The solution for the stress function F, used a particular integral and one term of the complementary function.

In order to relate the out-of-plane deflection coefficients to the applied displacements, Marguerre and Rhodes and Harvey satisfied the condition of external equilibrium by minimising the total potential energy, whereas Yamaki used the Galerkin method. Levy (32) in his post-buckling analysis of square plates with unloaded edges held straight, substituted the equations for F and w back into the equilibrium equation 2.9 in order to relate out-of-plane deflections to applied load.

In a plate containing a hole, the stress distribution representing F_1 can be obtained from plane stress finite element analysis as the stress resultants. The applied displacement can be related to parameter ϕ, as in equations 3.5a to 3.5c used in the stability analysis. The problem of

finding a stress function F_2, which satisfied the boundary conditions along the straight edge of the plate and at the edge of the hole, is very difficult, and to overcome this problem a third stress system, F_3, was used with the stress function F_2, of a plate with no hole. The stress function F_3 was a plane stress function, which when superimposed on stress function F_2, produced zero normal direct and shear stresses at the edge of the hole, and did not disturb the displacements produced by F_2 on the loaded edge. The boundary conditions for F_3 are the same as those for F_2.

The stress function F_3 was obtained by finite element plane stress analysis in terms of the stress resultants ${}_p n_{x3}$, ${}_p n_{y3}$ and ${}_p n_{xy3}$. For the case of a simply supported square or rectangular plate having the overall boundary conditions of uniformly displaced loaded edges and stress free unloaded edges, the boundary conditions for stress functions F_2 and F_3 are that the loaded edges should remain undisplaced and free of shear stresses and that the unloaded edges should remain stress free. The boundary conditions for F_2 and F_3 are stated as follows:-

1) The loaded edges are undisplaced and the shear stresses are zero at this edge, i.e. for the plate shown in Figure 3.1

$$u|_{x=a} = u|_{x=0} = 0$$

$$N_{xy}|_{x=0} = N_{xy}|_{x=a} = 0$$

2) The unloaded edges are stress free, i.e. the normal and shear stress resultants are zero.

$$N_{xy}|_{y=\pm b} = 0$$

$$N_y \Big|_{y=\pm b} = 0$$

The deflected shape of the plate shown in Figure 3.1 was the same as that used in the stability analysis, i.e.

$$w = \sin \frac{k\pi x}{a} \sum_{n=1}^{N} A_n \cos \frac{n\pi y}{2b} \qquad n = 1, 3, 5 \ldots\ldots \qquad 3.16$$

This meant that the buckled shape was fixed in the loaded direction, and was a good approximation for an unperforated plate. The substitution of equation 3.16 into equation 2.8 produced an equation which can be solved to give a function for F_2, which fits the appropriate boundary conditions, and is of the following form

$$F_2 = \sum_{n=1}^{N} \sum_{m=1}^{N} A_n . A_m \; h_{nm}(x,y) \qquad 3.17$$

The derivation of $h_{nm}(x,y)$ is described in the following section.

The nodal loads required to produce static equilibrium at the edge of a hole in a plate containing the stress distribution represented by Airey stress function F_2 were calculated from stress function F_2. A nodal load P_i was calculated from F_2 as being in the form of

$$P_i = \sum_{n=1}^{N} \sum_{m=1}^{N} A_n . A_m \; P_{nmi}(x_i, y_i) \qquad 3.18$$

where P_{nmi} was a function of x and y.

It is obvious that if a multi-term solution was used

for the post-buckling behaviour, then the stress resultants ${}_p n_{x3}$, ${}_p n_{y3}$ and ${}_p n_{xy3}$ would have to be evaluated from the loads described by equation 3.18 for each combination of $A_n . A_m$ at some unit value. In order to reduce the labour involved, the approximation was made that the buckled shape did not change from the initial buckling mode, but that only its magnitude changed. The magnitude of the out-of-plane deflections was represented by a coefficient A_r such that

$$A_n = A_r . \bar{A}_n \qquad n = 1, 3, 5 \ldots . \qquad 3.19$$

A_r was selected as the largest deflection coefficient and therefore the values $\bar{A}_n$ were the values of the critical eigenvector normalised with respect to the largest value of the eigenvector.

The nodal loads P_i can be re-written as

$$P_i = A_r^2 \sum_{n=1}^{N} \sum_{m=1}^{N} \bar{A}_n . \bar{A}_m \; P_{nmi} (x_i , y_i) \qquad 3.20$$

The application of these nodal loads produced a set of stress resultants related to the deflection coefficient A_r, as follows

$$ {}_p n_{x3} = A_r^2 \; {}_p \bar{n}_{x3} $$

$$ {}_p n_{y3} = A_r^2 \; {}_p \bar{n}_{y3} $$

$$ {}_p n_{xy3} = A_r^2 \; {}_p \bar{n}_{xy3} \qquad 3.21a,b,c $$

where ${}_p \bar{n}_{x3}$ is the stress resultant calculated with reference to some unit level of A_r.

This allows the stress resultants to be written as follows:-

$$N_x = \phi_p \bar{n}_{x_1} + A_r^2 t \sum_{n=1}^{N} \sum_{m=1}^{N} \bar{A}_n \bar{A}_m \frac{\partial^2 (h_{nm}(x,y))}{\partial y^2} + A_r^2 p \bar{n}_{x_3}$$

$$N_y = \phi_p \bar{n}_{y_1} + A_r^2 t \sum_{n=1}^{N} \sum_{m=1}^{N} \bar{A}_n . \bar{A}_m \frac{\partial^2 (h_{nm}(x,y))}{\partial x^2} + A_r^2 p \bar{n}_{y_3}$$

$$N_{xy} = \phi_p \bar{n}_{xy_1} + A_r^2 t \sum_{n=1}^{N} \sum_{m=1}^{N} \bar{A}_n . \bar{A}_m \frac{\partial^2 (h_{nm}(x,y))}{\partial x \partial y} + A_r^2 p \bar{n}_{xy_3}$$

3.22a,b,c

The substitution of equation 3.1 into the expression, described by equation 2.14, for bending strain energy gives equation 3.2, i.e.

$$V_2 = \sum\sum A_n . A_m . K_{1nm} \qquad 3.2$$

The strain energy due to in-plane stresses can be calculated by the substitution of equations 3.22 a, b, c into equation 2.11. Collection together of terms of similar order produces an equation for the total strain energy of the form

$$V = A_r^4 \bar{K}_4 + A_r^2 (\bar{K}_1 + \phi \bar{K}_3) + \bar{K}_2 \phi^2 \qquad 3.23$$

In order to satisfy overall equilibrium the strain energy was minimised with respect to the out-of-plane deflection coefficient A_r. This was done by examining the turning points of the equation for the strain energy i.e. when

$$\frac{dV}{dA_r} = 0 \qquad 3.24$$

Substituting equation 3.23 into equation 3.24 produces

$$\frac{dV}{dA_r} = 4A_r^3 \bar{K}_4 + 2A_r(\bar{K}_1 + \phi \bar{K}_3) = 0 \qquad 3.25$$

The solutions for equation 3.25 are

$$A_r = 0$$

or

$$A_r = \pm \sqrt{\frac{\bar{K}_1 + \phi \bar{K}_3}{2\bar{K}_4}}$$

The solution $A_r = 0$ was rejected as being the trivial solution, and the relationship

$$A_r = \sqrt{\frac{\bar{K}_1 + \phi \bar{K}_3}{2\bar{K}_4}} \qquad 3.26$$

was adopted as the solution.

The end load on a plate is made up from three components, P_1, P_2 and P_3. The first, P_1, is the end load required to produce the uniform edge displacement ϕ in a plate with no out-of-plane deflections. The second component P_2, comes from the stretching of a plate without a hole to the assumed deflected shape, with the condition that the loaded edge remains undisplaced. The final component of the total end load, P_3, arises from the loads applied at the edge of the hole in order to produce a free surface.

In calculating ${}_p n_{x1}$, ${}_p n_{y1}$, ${}_p n_{xy1}$ for a plate with uniformly displaced loaded edges, a unit displacement was applied in the finite element analysis, and the end load produced by this was the sum of the nodal reaction loads at that edge of the plate. The end load, $\bar{P}_1$, developed by

the edge displacement ϕ was therefore

$$P_1 = \phi \bar{P}_1 \qquad 3.27$$

The end load P_2 was calculated from the stress resultant in the direction of the applied load at the loaded edge. This stress resultant is calculated from the stress function F_2, i.e.

$$P_2 = \int_{-b}^{b} n_{x2}\Big|_{x=a}\, dy = t\int_{-b}^{b} \frac{\partial^2 F_2}{\partial y^2}\Big|_{x=a}\, dy \qquad 3.28$$

This meant that P_2 could be written in terms of A_r, i.e.

$$P_2 = A_r^2 \bar{P}_2$$

where $\bar{P}_2$ comes from equations 3.28 and 3.17, i.e.

$$\bar{P}_2 = t\sum_{n=1}^{N}\sum_{m=1}^{N} \bar{A}_n.\bar{A}_m \left[\frac{\partial (h_{nm}(a,y))}{\partial y}\Big|_{y=b} - \frac{\partial (h_{nm}(a,y))}{\partial y}\Big|_{y=-b} \right] \qquad 3.29$$

Because the stress function F_2 was expressed in terms of A_r^2, the end load P_3 produced in satisfying equilibrium at the hole edge was also expressed in terms of A_r^2, i.e.

$$P_3 = A_r^2 \bar{P}_3 \qquad 3.30$$

The total end load is the sum of the end loads P_1, P_2 and P_3, described by equations 3.27, 3.29 and 3.30, and can be written as

$$P = \phi \bar{P}_1 + A_r^2 (\bar{P}_2 + \bar{P}_3) \qquad 3.31$$

The substitution of equation 3.26 into equation 3.31 allowed the end load to be related to the applied displacement, i.e.

$$P = \phi\left[\bar{P}_1 + (\bar{P}_2 + \bar{P}_3).\frac{\bar{K}_3}{2\bar{K}_4}\right] + \frac{(\bar{P}_2 + \bar{P}_3)}{2\bar{K}_4}.\bar{K}_1 \qquad 3.32$$

The post-buckling stress distributions were calculated by superimposing all the stress distributions as described by equations 3.22 a, b, c. By writing

$$\bar{n}_{x2} = t\sum_{n=1}^{N}\sum_{m=1}^{N}\bar{A}_n\bar{A}_m\frac{\partial^2(h_{nm}(x,y))}{\partial y^2}$$

etc., the equations 3.22 a, b, c for the post-buckling stress resultants can be written as

$$N_x = \phi_p\bar{n}_{x1} + A_r^2(\bar{n}_{x2} + {}_p\bar{n}_{x3})$$

$$N_y = \phi_p\bar{n}_{y1} + A_r^2(\bar{n}_{y2} + {}_p\bar{n}_{y3})$$

$$N_{xy} = \phi_p\bar{n}_{xy1} + A_r^2(\bar{n}_{xy2} + {}_p\bar{n}_{xy3}) \qquad 3.33a,b,c$$

Substituting equation 3.26 for the deflection coefficient into equations 3.33 a, b, c allows these equations to be rewritten solely in terms of the applied displacement, i.e.

$$N_x = \phi\left[{}_p\bar{n}_{x1} + \frac{\bar{K}_3}{2\bar{K}_4}({}_p\bar{n}_{x3} + \bar{n}_{x2})\right] + \frac{\bar{K}_1}{2\bar{K}_4}({}_p\bar{n}_{x3} + \bar{n}_{x2}) \qquad 3.34a$$

Thus the applied load and the internal stresses can be defined solely in terms of the applied displacement. The derivation of $\bar{F}_2$ for plates with uniformly displaced loaded edges is described in the following section 3.3.2.

However, for plates loaded by uniform stresses some changes have to be made in the analysis. The loaded edge boundary conditions for F_2 and F_3 become

$$N_x|_{x=a} = N|_{x=0} = 0$$

instead of

$$u|_{x=a} = u|_{x=0} = 0$$

In this case the movement of the loaded edge caused by a virtual out-of-plane deflection makes it necessary to minimise the total potential energy instead of only the strain energy for the uniform applied displacement case.

3.3.2 Application of the Post-Buckling Analysis

The application of the theoretical post-buckling analysis to simply supported plates with uniformly displaced loaded edges is described in this section.

The stress function F_2 was evaluated from the compatibility equation 2.8 and the out-of-plane deflection function, w equation 3.16. Substitution of equation 3.16 into equation 2.8 gave the following equation:-

$$\nabla^4 F_2 = E\left[\left(\frac{k\pi}{a}\right)^2 \frac{1}{2} \sum_{n=1}^{N}\sum_{m=1}^{N} A_n A_m \left(nm\left(\frac{\pi}{2b}\right)^2 \sin\frac{n\pi y}{2b}\sin\frac{m\pi y}{2b} - \left(\frac{n\pi}{2b}\right)^2 \cos\frac{n\pi y}{2b}\cos\frac{m\pi y}{2b}\right)\right.$$

$$\left. + \left(\frac{k\pi}{a}\right)^2 \cdot \frac{1}{2}\cos\frac{2k\pi x}{a} \sum_{n=1}^{N}\sum_{m=1}^{N} A_n A_m \left(nm\left(\frac{\pi}{2b}\right)^2 \sin\frac{n\pi y}{2b}\sin\frac{m\pi y}{2b} + \left(\frac{n\pi}{2b}\right)^2 \cos\frac{n\pi y}{2b}\cdot\cos\frac{m\pi y}{2b}\right)\right] \qquad 3.35$$

Equation 3.35 shows that the function F_2 can be separated into a function of y only and into a function of x and y, i.e.

$$F_2 = F_{2A} + F_{2B} \cos \frac{2k\pi x}{a} \qquad 3.36$$

where F_{2A} and F_{2B} are functions of y only. Substituting equation 3.36 into the LHS of equation 3.35 gave

$$\left(\frac{2k\pi}{a}\right)^4 F_{2B} \cos\frac{2k\pi x}{a} - 2F_{2B}^{II}\left(\frac{2k\pi}{a}\right)^2 \cos\frac{2k\pi x}{a} + F_{2B}^{IV} \cos\frac{2k\pi x}{a} + F_{2A}^{II}$$

$$= \text{RHS equation } 3.35 \qquad 3.37$$

Two equations were then separated from equation 3.37 i.e.

$$F_{2A}^{IV} = \frac{E}{2}\left(\frac{k\pi}{a}\right)^2 \sum_{n=1}^{N}\sum_{m=1}^{N} A_n A_m \left(nm\left(\frac{\pi}{2b}\right)^2 \sin\frac{n\pi y}{2b}\cdot\sin\frac{m\pi y}{2b} - \left(\frac{n\pi}{2b}\right)^2 \cos\frac{n\pi y}{2b}\cdot\cos\frac{m\pi y}{2b}\right) \qquad 3.38$$

and $$\left[\left(\frac{2k\pi}{a}\right)^4 \cdot F_{2B} - 2\left(\frac{2k\pi}{a}\right)^2 F_{2B}^{II} + F_{2B}^{IV}\right] \cos\frac{2k\pi x}{a} =$$

$$\frac{E}{2}\left(\frac{k\pi}{a}\right)^2 \cos\frac{2k\pi x}{a}\left[\sum_{n=1}^{N}\sum_{m=1}^{N} A_n A_m \left(nm\left(\frac{\pi}{2b}\right)^2 \sin\frac{n\pi y}{2b}\sin\frac{m\pi y}{2b} + \left(\frac{n\pi}{2b}\right)^2 \cos\frac{m\pi y}{2b}\cdot\cos\frac{n\pi y}{2b}\right)\right] \qquad 3.39$$

Because F_{2A} is a function of y only, any derivatives of F_{2A} with respect to x are zero, hence equation 3.38 was not solved for any derivatives of F_{2A} lower than the second order.

$$F_{2A}^{II} = \frac{E\pi^2 k^2}{4a^2} \sum_{n=1}^{N}\sum_{m=1}^{N} A_n A_m \cos\frac{n\pi y}{2b}\cos\frac{m\pi y}{2b} + B_1 y + B_2 \qquad 3.40$$

A solution to equation 3.39 for F_{2B} was found by combining the symmetrical terms of the particular integral and a single term of the complementary function, i.e.

$$F_{2B} = \frac{E}{2}\left(\frac{k\pi}{a}\right)^2 \sum_{n=1}^{N}\sum_{m=1}^{N} A_n A_m \left(J_{2nm} \cos\frac{(n-m)\pi y}{2b} + J_{3nm} \cos\frac{(n+m)\pi y}{2b} \right.$$

$$\left. + C_{1nm} \cosh\frac{2k\pi y}{a} + C_{4nm} \frac{y}{b} \sinh\frac{2k\pi y}{a} \right)$$

3.41

Coefficients J_{2nm} and J_{3nm} were obtained by substituting equation 3.41 into equation 3.39 and equating similar terms.

$$J_{2nm} = \frac{n^2 + mn}{2\left[\left(\frac{n-m}{2b}\right)^2 + \left(\frac{2k}{a}\right)^2\right]^2 (2\pi b)^2}$$

3.42

$$J_{3nm} = \frac{n^2 - mn}{2\left[\left(\frac{n+m}{2b}\right)^2 + \left(\frac{2k}{a}\right)^2\right]^2 (2\pi b)^2}$$

3.43

The remaining two coefficients in F_{2B}, C_{1nm} and C_{4nm}, were calculated by the application of the boundary conditions on the unloaded edge, which were, zero shearing stress resultant, and zero stress resultant normal to the edge, i.e.

$$N_{xy}\big|_{y=\pm b} = 0 \qquad N_y\big|_{y=\pm b} = 0$$

i.e.

$$\frac{\partial^2 F_2}{\partial x\,\partial y}\bigg|_{y=\pm b} = 0 \qquad \frac{\partial^2 F}{\partial x^2}\bigg|_{y=\pm b} = 0$$

Because F_{2A} is a function of y only, these boundary conditions become

$$F_{2B}^{I} = 0 \qquad \text{and} \qquad F_{2B}^{II} = 0$$

The substitution of equation 3.41 into these boundary conditions gave two simultaneous equations in C_{1nm} and C_{4nm}, which were solved to give

$$C_{1nm} = -\frac{\left(J_{2nm}\cos\frac{(n-m)\pi}{2} + J_{3nm}\cos\frac{(n+m)\pi}{2} + C_{4nm}\sinh\frac{2k\pi b}{a}\right)}{\cosh\frac{2k\pi b}{a}} \qquad 3.44$$

where C_{4nm} is a function of J_{2nm} and J_{3nm} only, i.e.

$$C_{4nm} = \frac{\left[J_{2nm}\left(\left(\frac{n-m}{2b}\right)\pi\sin\frac{(n-m)\pi}{2} + \frac{2k\pi}{a}\tanh\frac{2k\pi b}{a}\cos\frac{(n-m)\pi}{2}\right) + J_{3nm}\left(\left(\frac{n+m}{2b}\right)\pi\sin\frac{(n+m)\pi}{2} + \frac{2k\pi}{a}\tanh\frac{2k\pi b}{a}\cos\frac{(n+m)\pi}{2}\right)\right]}{\left(\frac{1}{b}\sinh\frac{2k\pi b}{a} + \frac{2k\pi}{a}\cosh\frac{2k\pi b}{a} - \frac{2k\pi}{a}\sinh\frac{2k\pi b}{a}\tanh\frac{2k\pi b}{a}\right)} \qquad 3.45$$

The two remaining unknown coefficients B_1 and B_2, in F_{2A}^{II} were determined by applying the boundary conditions at the loaded edge. For the stress function F_2, these were:-

1) zero shear stress, which is satisfied innately by F_{2A} and F_{2B}.

2) undisplaced loaded edges i.e.

$$u|_{x=a} = u|_{x=0} = 0$$

The displacement of the end $x=a$ of the plate can be written as:-

$$u|_{x=a} = \int_0^a \left[\varepsilon_x - \frac{1}{2}\left(\frac{\partial w}{\partial x}\right)^2\right] dx$$

The substitution of equations 3.16, 3.36 and 2.4a into the above equation gave:-

$$u\big|_{x=a} = \int_0^a \left\{ \frac{1}{E}\left[F_{2A}^{II} + F_{2B}^{II}\cos\frac{2k\pi x}{a} + \nu\left(\frac{2k\pi}{a}\right)^2 F_{2B}\cos\frac{2k\pi x}{a}\right] - \left(\frac{k\pi}{2a}\right)^2\left(\cos\frac{2k\pi x}{a} + 1\right)\sum_{n=1}^{N}\sum_{m=1}^{N} A_n A_m \cos\frac{n\pi y}{2b}\cos\frac{m\pi y}{2b}\right\} dx$$

Integration with respect to x led to

$$u\big|_{x=a} = \left[x\left(\frac{F_{2A}^{II}}{E} - \frac{1}{4}\left(\frac{k\pi}{a}\right)^2 \sum_{n=1}^{N}\sum_{m=1}^{N} A_n A_m \cos\frac{n\pi y}{2b}\cdot\cos\frac{m\pi y}{2b}\right)\right]_0^a \qquad 3.46$$

Substitution of equation 3.40 for F_{2A} into equation 3.46 gave

$$u\big|_{x=a} = \frac{a}{E}\left(B_1 y + B_2\right) = 0$$

Since the displacement is zero in the y-direction

$$B_1 = B_2 = 0$$

The stress function cannot be written down directly, as only F_{2A}^{II} was calculated. However, the stress resultants calculated from $F_2 = F_{2A} + F_{2B}\cos\frac{2k\pi x}{a}$ can be written down as follows.

$$n_{x2} = tE\left(\frac{k\pi}{2a}\right)^2 \sum_{n=1}^{N}\sum_{m=1}^{N} A_n \cdot A_m \cos\frac{n\pi y}{2b}\cos\frac{m\pi y}{2b} + \frac{tE}{2}\left(\frac{k\pi}{a}\right)^2 \cos\frac{2k\pi x}{a}\sum_{n=1}^{N}\sum_{m=1}^{N} A_n A_m \left[-J_{2nm}\left(\frac{n-m}{2b}\right)^2\pi^2\cos\frac{(n-m)\pi y}{2b} - J_{3nm}\left(\frac{n+m}{2b}\right)^2\pi^2\cos\frac{(n+m)\pi y}{2b} + C_{1nm}\left(\frac{2k\pi}{a}\right)^2\cosh\frac{2k\pi y}{a} + C_{4nm}\left(\frac{4k\pi}{ab}\cosh\frac{2k\pi y}{a} + \frac{y}{b}\left(\frac{2k\pi}{a}\right)^2\sinh\frac{2k\pi y}{a}\right)\right] \qquad 3.47a$$

$$n_{y2} = -2Et\left(\frac{k\pi}{a}\right)^4 \cos\frac{2k\pi x}{a} \sum_{n=1}^{N}\sum_{m=1}^{N} A_n A_m \left(J_{2nm} \cos\frac{(n-m)\pi y}{2b} + J_{3nm} \cos\frac{(n+m)\pi y}{2b} + C_{1nm} \cosh\frac{2k\pi y}{a} + C_{4nm} \frac{y}{b} \sinh\frac{2k\pi y}{a} \right) \qquad 3.47b$$

$$n_{xy2} = -Et\left(\frac{k\pi}{a}\right)^3 \sin\frac{2k\pi x}{a} \sum_{n=1}^{N}\sum_{m=1}^{N} A_n A_m \left[-J_{2nm}\left(\frac{n-m}{2b}\right)\pi \sin\frac{(n-m)\pi y}{2b} - J_{3nm}\left(\frac{n+m}{2b}\right)\pi \sin\frac{(n+m)\pi y}{2b} + C_{1nm}\left(\frac{2k\pi}{a}\right) \sinh\frac{2k\pi y}{a} + C_{4nm}\left(\frac{1}{b}\sinh\frac{2k\pi y}{a} + \frac{y}{b}\cdot\frac{2k\pi}{a}\cdot\cosh\frac{2k\pi y}{a}\right) \right] \qquad 3.47c$$

The nodal loads, P_i, at the hole edge for the calculation of n_{x3}, n_{y3}, n_{xy3} were calculated from the stress resultants n_{x2}, n_{y2}, n_{xy2} described by equations 3.47a, b, c, using the normalised values of the critical eigenvector. The stress resultants were calculated for a unit value of A_n, so that equations 3.21a, b, c could be written.

The coefficients $\bar{K}_1$, $\bar{K}_3$ and $\bar{K}_4$ in equation 3.23 for the total strain energy were evaluated from the deflection function 3.16 and the equations for the stress resultants 3.33a, b, c. These coefficients can be expressed as:-

$$\bar{K}_1 = \frac{D}{2} \sum_{n=1}^{N}\sum_{m=1}^{N} \bar{A}_n \bar{A}_m \int_A \left\{ \sin^2\frac{k\pi x}{a} \cos\frac{m\pi y}{2b} \cos\frac{n\pi y}{2b} \left(\left(\frac{k\pi}{a}\right)^2 + nm\left(\frac{\pi}{2b}\right)^2 \right)^2 - 2(1-\nu)\left[\left(\frac{k\pi}{a}\right)^2 nm\left(\frac{\pi}{2b}\right)^2 \sin^2\frac{k\pi x}{a} \cos\frac{n\pi y}{2b} \cos\frac{m\pi y}{2b} - nm\left(\frac{\pi}{2b}\right)^2\left(\frac{k\pi}{a}\right)^2 \cos^2\frac{k\pi x}{a} \sin\frac{n\pi y}{2b} \sin\frac{m\pi y}{2b} \right] \right\} dx\,dy \qquad 3.48$$

$$\bar{K}_2 = \frac{1}{2tE} \sum_{p=1}^{Ne} S_p \left({}^p\bar{n}_{x1}^2 + {}^p\bar{n}_{y1}^2 - 2\nu\, {}^p\bar{n}_{x1}\, {}^p\bar{n}_{y1} + 2(1+\nu)\, {}^p\bar{n}_{xy1}^2 \right)$$

3.49

$$\bar{K}_3 = \sum_{p=1}^{Ne} \left\{ \left[{}^p\bar{n}_{x1} \cdot {}^p\bar{n}_{x3} + {}^p\bar{n}_{y1}\, {}^p\bar{n}_{y3} - \nu \left({}^p\bar{n}_{x3}\, {}^p\bar{n}_{y1} + {}^p\bar{n}_{x1} \cdot {}^p\bar{n}_{y3} \right) + 2(1+\nu)\, {}^p\bar{n}_{xy1}\, {}^p\bar{n}_{xy3} \right] \frac{S_p}{tE} \right.$$

$$\left. + \frac{1}{Et} \sum_{n=1}^{N} \sum_{m=1}^{N} \bar{A}_n \bar{A}_m \iint_{S_p} \left[{}^p\bar{n}_{x1} \cdot \bar{n}_{x2} + {}^p\bar{n}_{y1} \cdot \bar{n}_{y2} - \nu \left({}^p\bar{n}_{y1} \cdot \bar{n}_{x2} + {}^p\bar{n}_{x1} \cdot \bar{n}_{y2} \right) + 2(1+\nu)\, {}^p\bar{n}_{xy1} \cdot \bar{n}_{xy2} \right] dx\, dy \right\}$$

3.50

$$\bar{K}_4 = \sum_{p=1}^{Ne} \left\{ \left({}^p\bar{n}_{x3}^2 + {}^p\bar{n}_{y3}^2 - 2\nu\, {}^p\bar{n}_{x3}\, {}^p\bar{n}_{y3} + 2(1+\nu)\, {}^p\bar{n}_{xy3}^2 \right) \frac{S_p}{2tE} \right.$$

$$+ \frac{1}{Et} \sum_{n=1}^{N} \sum_{m=1}^{N} \bar{A}_n \bar{A}_m \iint_{S_p} \left[{}^p\bar{n}_{x1} \cdot \bar{n}_{x2} + {}^p\bar{n}_{y3} \cdot \bar{n}_{y2} - \nu \left({}^p\bar{n}_{x3} \cdot \bar{n}_{y2} + {}^p\bar{n}_{y3} \cdot \bar{n}_{x2} \right) + 2(1+\nu)\, {}^p\bar{n}_{xy3} \cdot \bar{n}_{xy2} \right] dx\, dy$$

$$\left. + \frac{1}{2Et} \sum_{n=1}^{N} \sum_{m=1}^{N} \sum_{p=1}^{N} \sum_{q=1}^{N} \bar{A}_n \bar{A}_m \bar{A}_p \bar{A}_q \iint_{S_p} \left[\bar{n}_{x2}^2 + \bar{n}_{y2}^2 - 2\nu\, \bar{n}_{x2}\, \bar{n}_{y2} + 2(1+\nu)\, \bar{n}_{xy2} \right] dx\, dy \right\}$$

3.51

The integration of these coefficients was carried out in the same way as in the stability analysis, and the coefficients were inserted directly into equations 3.26, 3.32 and 3.34. The end load P_2 developed by F_2 and described by equation 3.29 was obtained by substituting equation 3.47a into equation 3.28 to give

$$P_2 = A_r^2 . \bar{P}_2$$

where

$$\bar{P}_2 = Et\left(\frac{k\pi}{a}\right)^2 \sum_{n=1}^{N} \sum_{m=1}^{N} \bar{A}_n \bar{A}_m \left[C_{1nm} \frac{2k\pi}{a} \sinh \frac{2k\pi b}{a} + C_{4nm} \left(\frac{1}{b} \sinh \frac{2k\pi b}{a} + \frac{2k\pi}{a} \cosh \frac{2k\pi b}{a} \right) \right] \quad 3.52$$

The analysis was carried out for square and rectangular plates with a breadth to thickness ratio of 160. The rectangular plates had sides of ratio of length to breadth of 2 to 1, and the range of hole sizes studied for both square and rectangular plates was from a diameter of 0.0 to 0.6 times the plate width. The post-buckling analysis of rectangular plates was carried out for plates with two or three half-waves in the loaded direction, depending on the buckling mode calculated from the stability analysis.

The variation of the deflection coefficient A_r with applied load is illustrated in Figures 3.11 and 3.12 for square and rectangular plates with various hole diameters.

3.4 A Simplified Failure Analysis

The collapse of a plate with large elastic buckles is a complex phenomenon, involving the growth of plasticity on the surface of the buckles, and the formation of plastic hinges. In both perforated and unperforated plates, the plastic hinges, which produce collapse, grow from the supported edges. It was therefore assumed that collapse was associated with the yield stress being reached at or near the supported edges. Von Karman and Sechler (34) and Winter (33) made the assumption that the ultimate load, P_{ult} was related to the yield stress σ_y and to the effective width for this corresponding maximum stress by the expression

$$P_{ult} = \sigma_y \cdot b_e \qquad 3.53$$

The effective width b_e is the width of the plate over which the maximum stress is considered to act for a given load. This is illustrated in Figure 3.13. If accurate approximations can be made on the redistribution of stresses following the introduction of a hole, the effect of the hole on the effective width of an unperforated plate may be assessed.

If the relationship between applied load and effective width of a plate with no hole is known, and the general pattern of post-buckling stress distribution is also known, then the ultimate loads of centrally perforated plates can be calculated, by making the following assumptions

1) The ultimate load of a plate is reached when the maximum stress in the loaded direction reaches yield stress.

2) The redistribution of stresses in a plate with a

centrally located hole follows the same trends as in a plate with no hole, i.e. the maximum stresses become redistributed towards the edge of the plate.

3) The redistribution of stresses in the plate is such that the tensile and compressive loads due to the tensile and compressive components of the membrane stress distribution are unchanged by the introduction of a hole.

4) The compressive and tensile stresses formerly in a region with a hole can be redistributed over the respective compressive and tensile regions of the stress distribution of a plate with no hole in order to represent the stresses in a plate with a hole.

The first assumption was that made by Von Karman and Sechler (34) and by Winter (33) and is expressed by equation 3.53.

The second assumption was justified by the theoretical and experimental results described in Chapter Five and discussed in Chapter Six.

The post-buckling distribution of stresses in unperforated plates was investigated for square and rectangular plates by Coan (21) and Yamaki (22). The post-buckling stresses in the loaded direction take the form of the distributions illustrated diagrammatically in Figure 13.4.1. for simply supported plates with unloaded edges held straight, and in Figure 13.4.2 for simply supported plates with unloaded edges allowed to warp. These stress distributions

can be represented with sufficient accuracy by functions of the form

$$\sigma_x = A + B \cos\left(\frac{k\pi y}{b}\right) \qquad 3.54$$

where k = 1 for plates with straight unloaded edges

or k = 0.5 for plates with stress free unloaded edges.

The constants A and B were evaluated from data on effective widths of plates with the appropriate boundary conditions. The effective width of a plate was defined by:-

$$b_e = \frac{2}{\sigma_{x\,max}} \int_0^b \sigma_x \, dy \qquad 3.55$$

Substitution of equation 3.54 into equation 3.55 allowed the effective width, b_e, to be expressed in terms of constants A and B, i.e.

$$b_e = \frac{2}{\sigma_{x\,max}} \left[A.b + B.\frac{b}{k\pi} \sin k\pi \right] \qquad 3.56$$

In the cases where the maximum stress occurred at the edge of the plate, $\sigma_{x\,max}$ was written in terms of A and B :-

$$\sigma_{x\,max} = A + B \cos k\pi \qquad 3.57$$

At a given constant load P, the value of effective width corresponding to maximum stress $\sigma_{x\,max}$ can be found if the relationship between load P and effective width b_e is known.

The coefficients A and B were found in terms of b_e and $\sigma_{x\,max}$ from equations 3.56 and 3.57, i.e.

$$A = \frac{\left(\frac{b_e}{2b}\cos k\pi - \frac{1}{k\pi}\sin k\pi\right)}{\left(\cos k\pi - \frac{1}{k\pi}\sin k\pi\right)}\,\sigma_{x_{max}} \qquad 3.58$$

$$B = \frac{\left(1 - \frac{b_e}{2b}\right)\sigma_{x_{max}}}{\left(\cos k\pi - \frac{1}{k\pi}\sin k\pi\right)} \qquad 3.59$$

The third and fourth assumptions implied that when a hole was introduced into a plate, the compressive stresses formerly carried by the area removed from the cross-section by the hole can be redistributed over the compressive region of the stress distribution in a plate with no hole between the hole edge and supported edge in order to represent the post-buckling stress distribution of a plate with a hole. This redistribution was assumed to occur uniformly. This also implied that in plates where the area removed by the hole was completely under tension, the introduction of the hole caused no change in the maximum compressive stresses, and therefore did not affect the ultimate load.

The compressive stresses in a plate, where the post-buckling stress distribution is represented by Figure 3.15, start at a distance C_r from the centre line, where

$$C_r = 0 \qquad A > -B$$

or $$C_r = \frac{1}{k\pi}\cos^{-1}\left(-\frac{A}{B}\right) \qquad A < -B$$

The compressive load formerly carried by the cross-sectional area removed by a hole of radius C was therefore

$$P_H = 2t \int_{c_r}^{c} \sigma_x \, dy \qquad 3.60$$

if $C > c_r$

or $P_H = 0$ if $c_r > C$ 3.61

The constant average compressive stress to be added to the compressive stress region was written as

$$\Delta\sigma = \frac{1}{(b-c)} \int_{c_r}^{c} \sigma_x \, dy \qquad 3.62$$

i.e. by substitution of equation 3.54, equation 3.60 became

$$\Delta\sigma = \frac{1}{(b-c)} \left[A(c-c_r) + B.\frac{b}{k\pi} \left(\sin\frac{k\pi c}{b} - \sin\frac{k\pi c_r}{b} \right) \right] \qquad 3.63$$

where A and B were defined by equations 3.58 and 3.59. Equation 3.63 is valid for $c > c_r$, otherwise $\Delta\sigma = 0$.

The maximum stress then became, after the addition of the constant stress $\Delta\sigma$:-

$$\bar{\sigma}_{x_{max}} = \sigma_{x_{max}} + \Delta\sigma \qquad 3.64$$

The applied load P was assumed to remain constant and was defined in terms of maximum stress $\sigma_{x_{max}}$ and effective width b_e of a plate with no hole, and could therefore be defined in terms of the new maximum stress $\bar{\sigma}_{x_{max}}$ and a 'corrected' effective width b_{ec} : i.e.

$$P = b_e \sigma_{x_{max}} = b_{ec} \bar{\sigma}_{x_{max}}$$

Thus the corrected effective width b_{ec} could be written as:-

$$b_{ec} = \frac{b_e \sigma_{x_{max}}}{\bar{\sigma}_{x_{max}}}$$

By substitution of equations 3.58, 3.59 and 3.63

$$b_{ec} = \frac{b_e}{\left[1 + \frac{(c - c_r)}{(b - c)} \cdot \frac{\left(\frac{b_e}{2b} \cos k\pi - \frac{1}{k\pi} \sin k\pi\right)}{\left(\cos k\pi - \frac{1}{k\pi} \sin k\pi\right)} + \frac{\left(1 - \frac{b_e}{2b}\right) \frac{b}{k\pi} \left(\sin \frac{k\pi c}{b} - \sin \frac{k\pi c_r}{b}\right)}{(b - c)\left(\cos k\pi - \frac{1}{k\pi} \sin k\pi\right)}\right]}$$

3.65

This corrected effective width b_{ec} was the effective width for a plate with a hole, for a given load P. Therefore, where the relationship for end load P and the effective width is known, and the stress distribution can be written as a simple expression, as in equation 3.54, then the relationship between applied load P and 'corrected' effective width can be established as the approximate relationship between applied load and the effective width of a plate with a hole.

The relationship between applied load and effective width was derived by Rhodes and Harvey (30) for plates with

simply-supported stress free edges and loaded by constant edge displacements. This relationship between applied load and effective width can be converted into a graph of maximum stress in the loaded direction against effective width, and this is illustrated in Figure 3.16. Equation 3.65 allows a family of curves to be derived for a range of hole sizes, relating maximum stress to 'corrected' effective width b_{ec}. These are illustrated in Figure 3.16.

The first assumption enabled the collapse of a plate with a hole to be calculated using Figure 3.16. From equation 3.53, the ultimate load became:-

$$P_{ult} = \sigma_Y \, b_{ec} \qquad 3.66$$

where b_{ec} was the corrected effective width for the given hole size at σ_Y; and was obtained from Figure 3.16.

A curve showing the variation in ultimate load with hole size was constructed for plates with the nominal dimensions of those plates under test, and was presented in Figure 3.17. This figure illustrates a reduction in ultimate load caused by the introduction of a hole. Comparison with observed results was made in Chapter Five and was discussed in Chapter Six.

Tables of corrected effective width are presented for the range of effective widths $\frac{b_e}{b} = 1.0 - 0.3$ and hole diameters 0.0 to 0.7 times the plate width. Table 3.1 presents corrected effective widths for simply supported plates with uniformly compressed loaded edges, and stress free unloaded edges i.e. $k = 0.5$, and Table 3.2 presents corrected effective

widths for simply supported plates with uniformly compressed edges and straight unloaded edges.

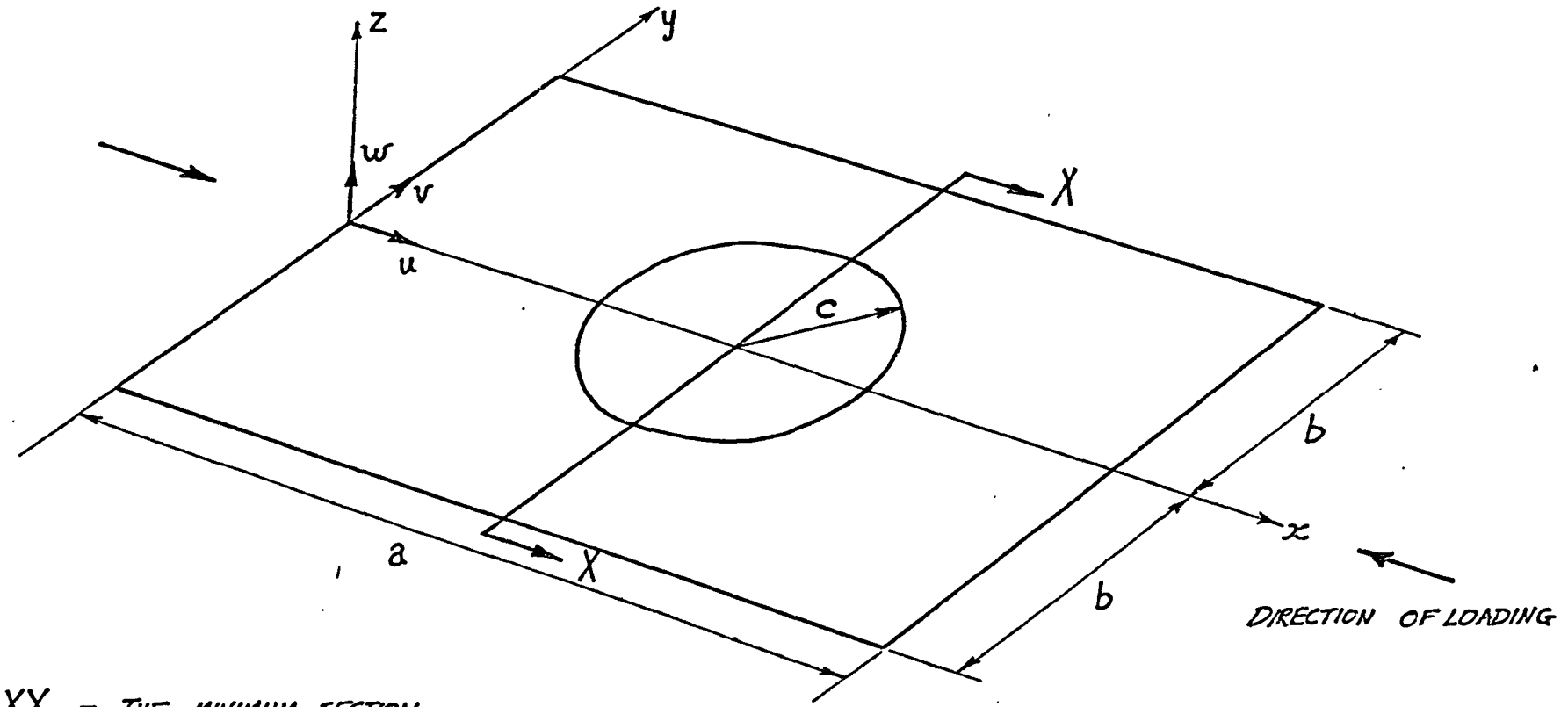

XX - THE MINIMUM SECTION

FIGURE 3.1 THE PLATE CO-ORDINATES AND DIMENSIONS

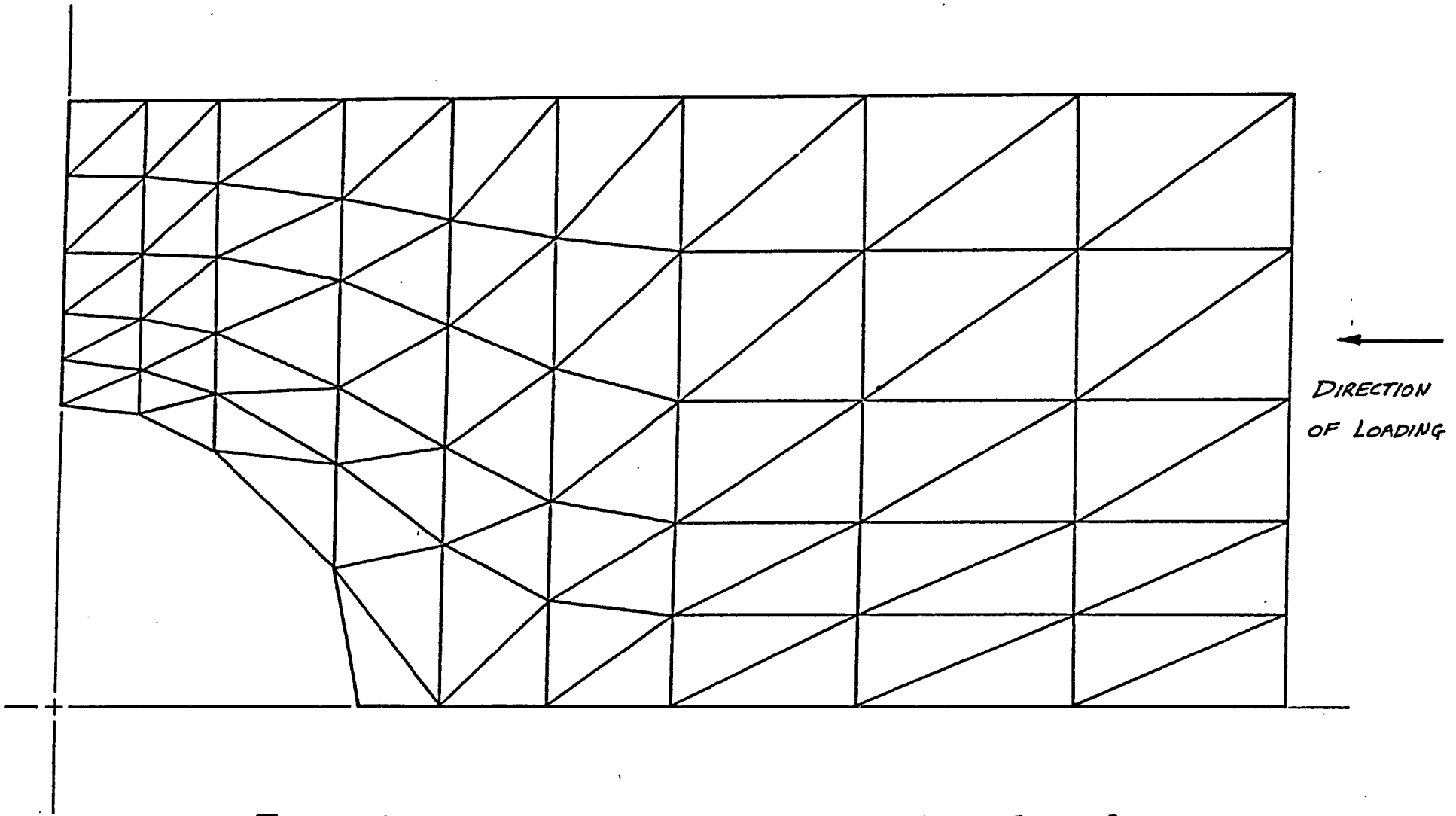

FIGURE 3.2 A TYPICAL FINITE ELEMENT MESH FOR A RECTANGULAR PLATE

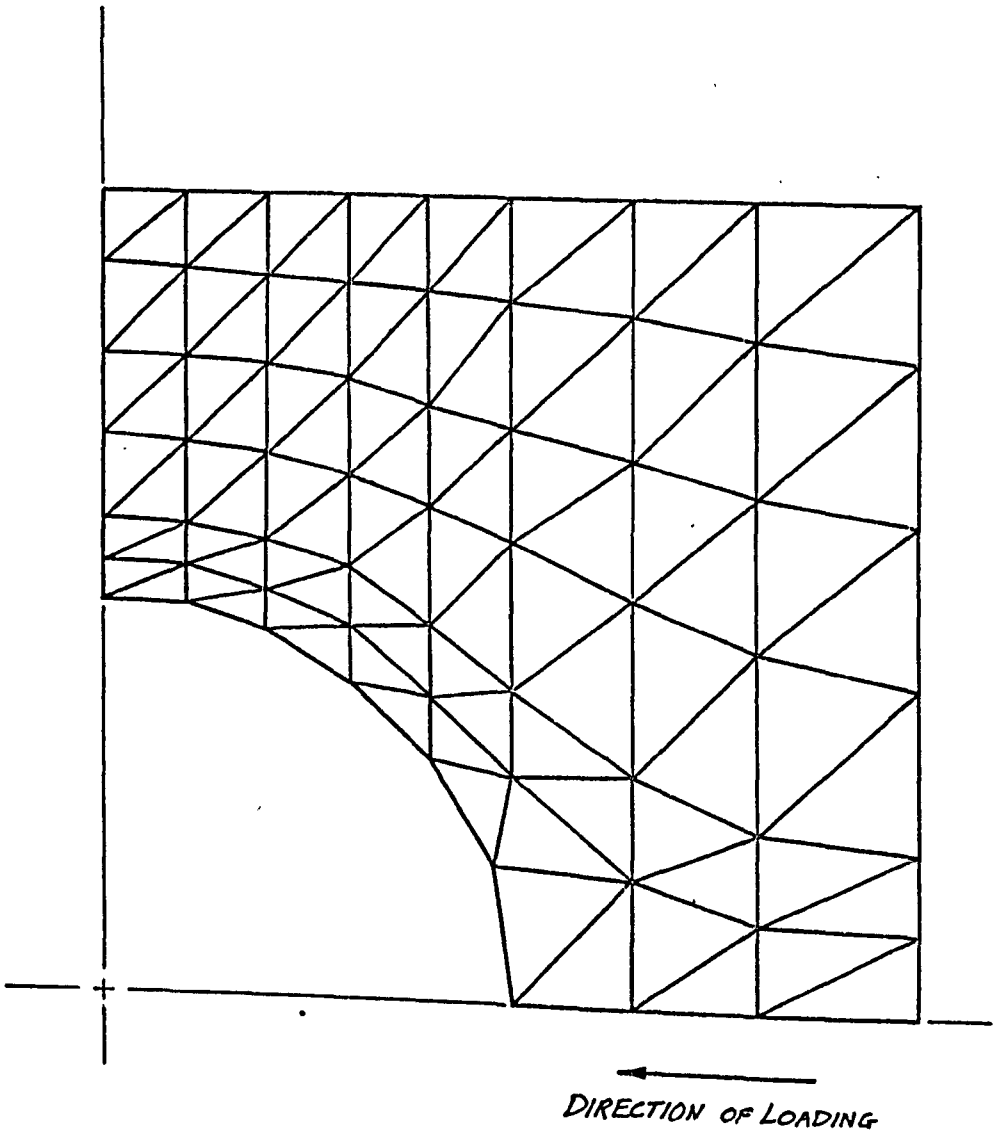

FIGURE 3.3 A TYPICAL FINITE ELEMENT MESH FOR A SQUARE PLATE

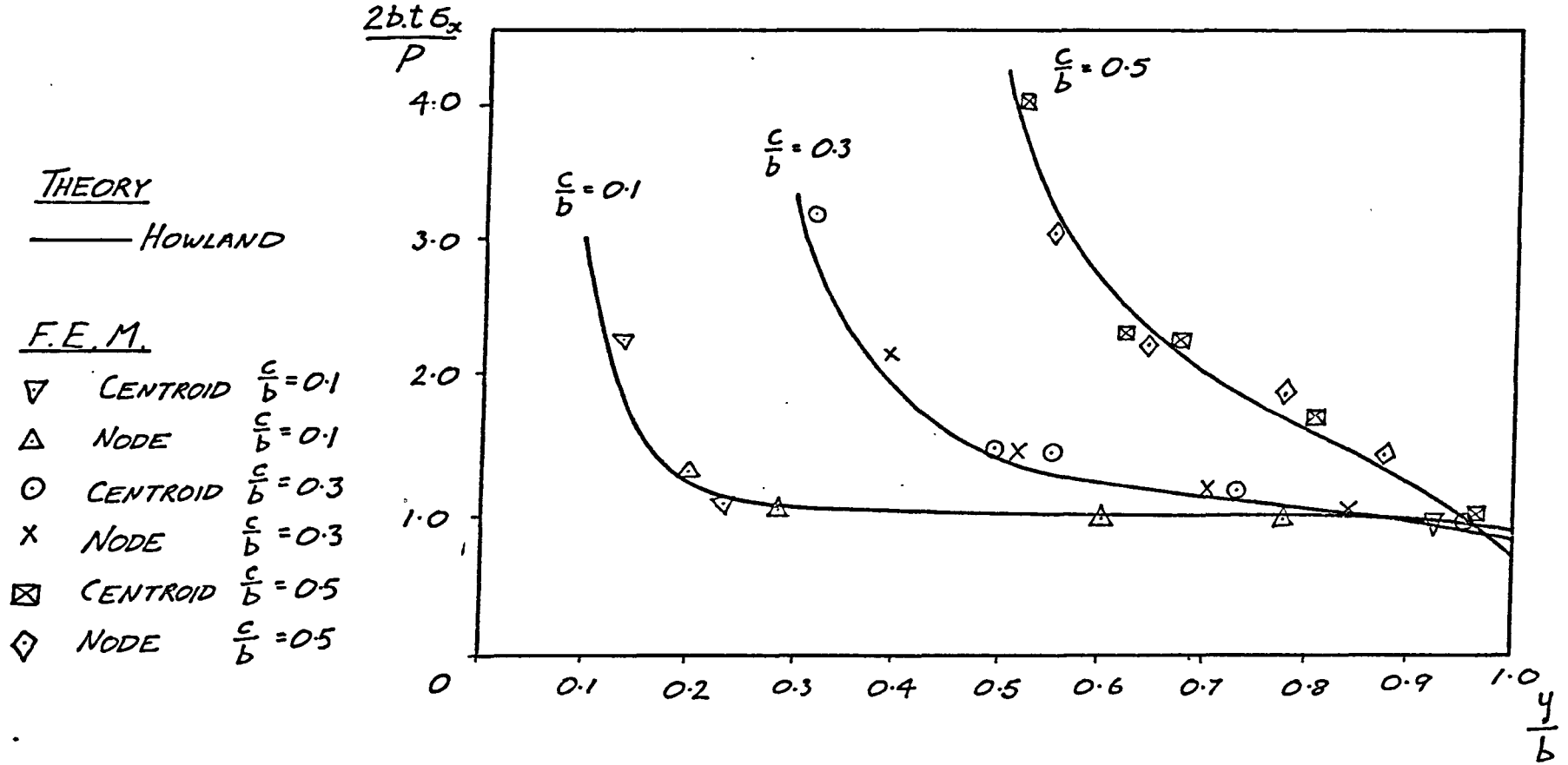

FIGURE 3·4 DISTRIBUTION OF σ_x STRESSES ACROSS THE MINIMUM SECTION OF A RECTANGULAR PLATE. COMPARISON BETWEEN FEM RESULTS AND THEORETICAL RESULTS

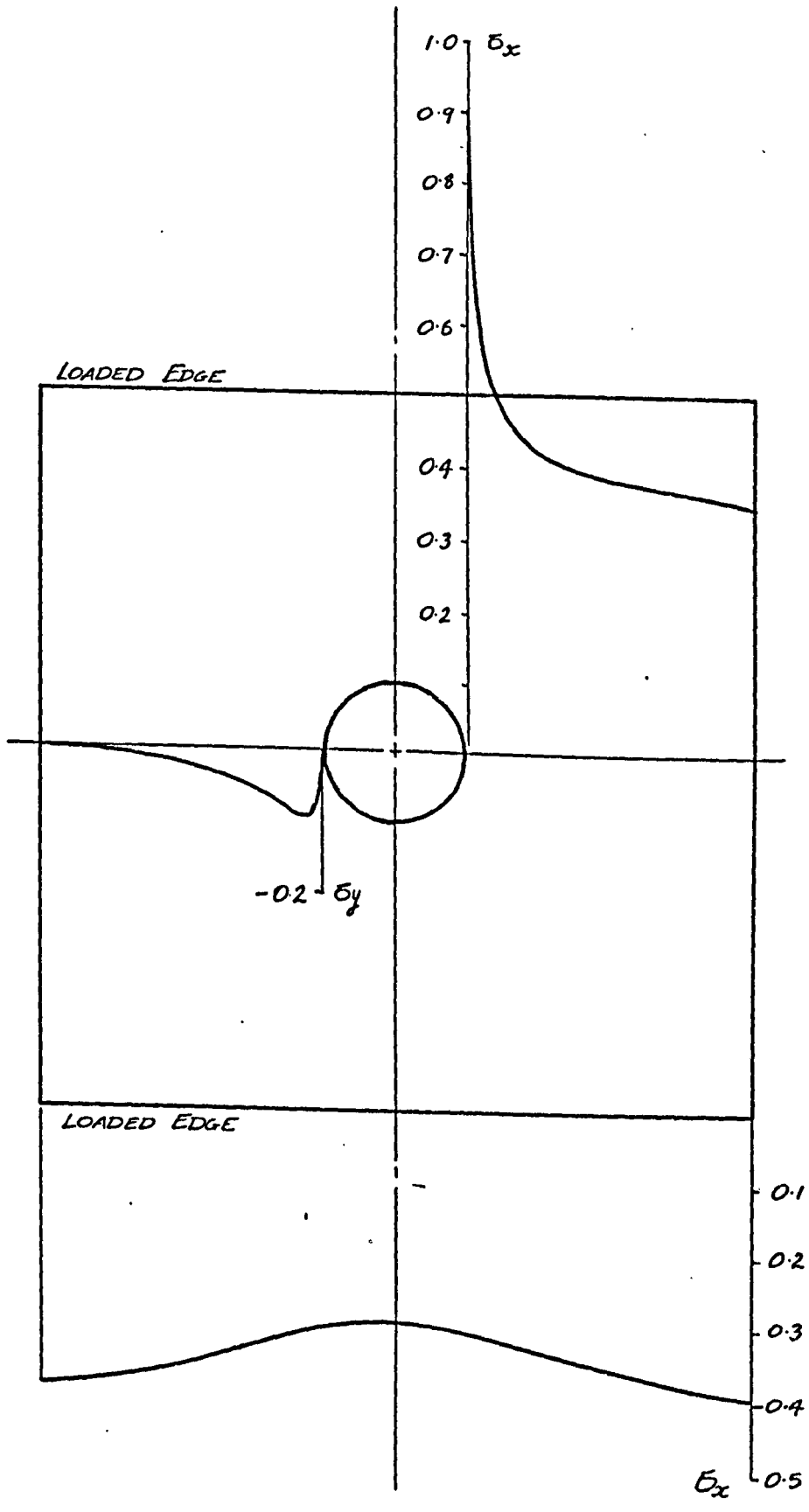

FIGURE 3·5 THE PREBUCKLING DISTRIBUTION OF STRESSES IN A SQUARE PLATE LOADED BY UNIFORM DISPLACEMENTS

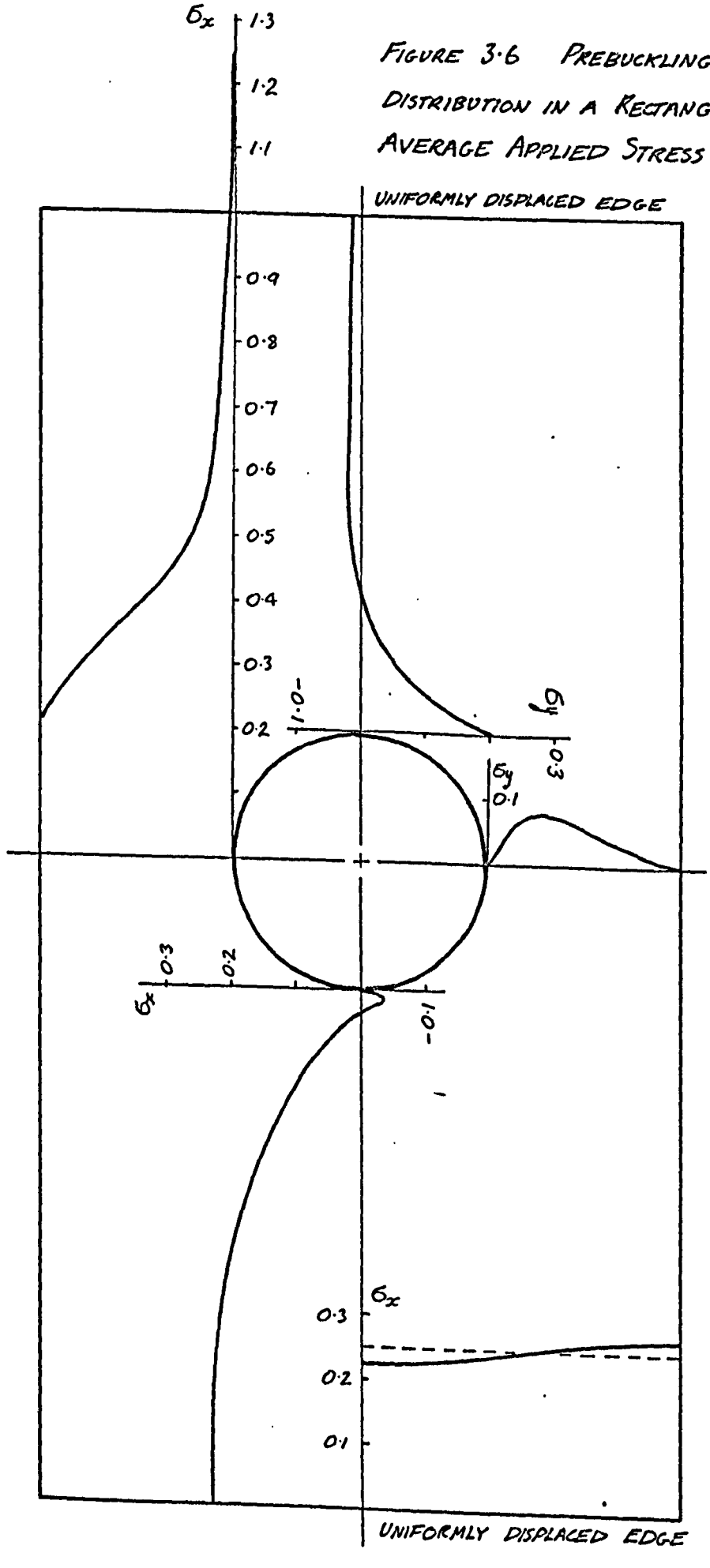

FIGURE 3·6 PREBUCKLING STRESS DISTRIBUTION IN A RECTANGULAR PLATE AVERAGE APPLIED STRESS = 0·25

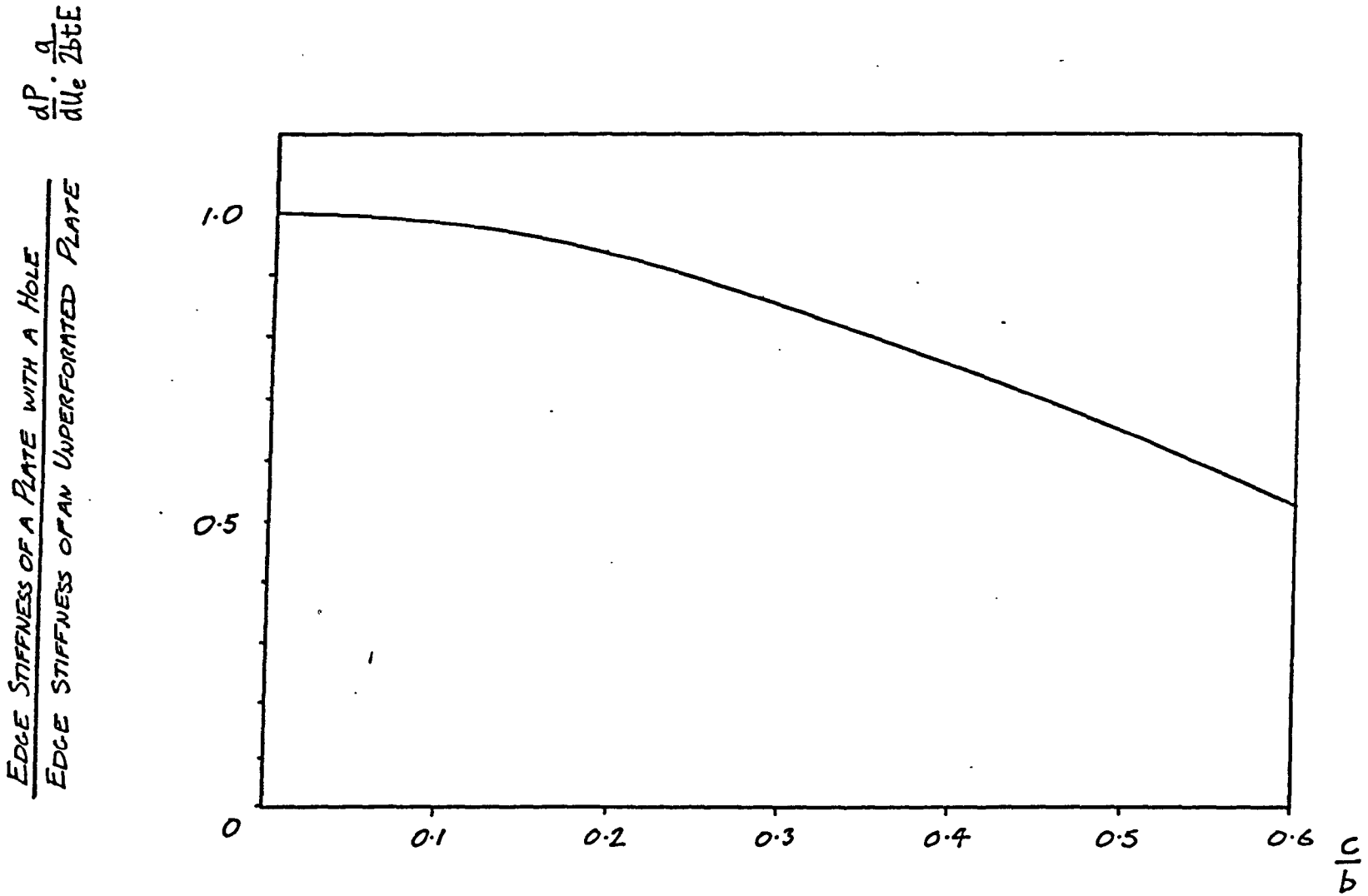

FIGURE 3·7 VARIATION OF THE PRE-BUCKLING EDGE STIFFNESS OF A SQUARE PLATE WITH THE HOLE DIAMETER

FIGURE 3·8 VARIATION OF THE PRE-BUCKLING EDGE STIFFNESS OF A RECTANGULAR PLATE WITH THE HOLE DIAMETER

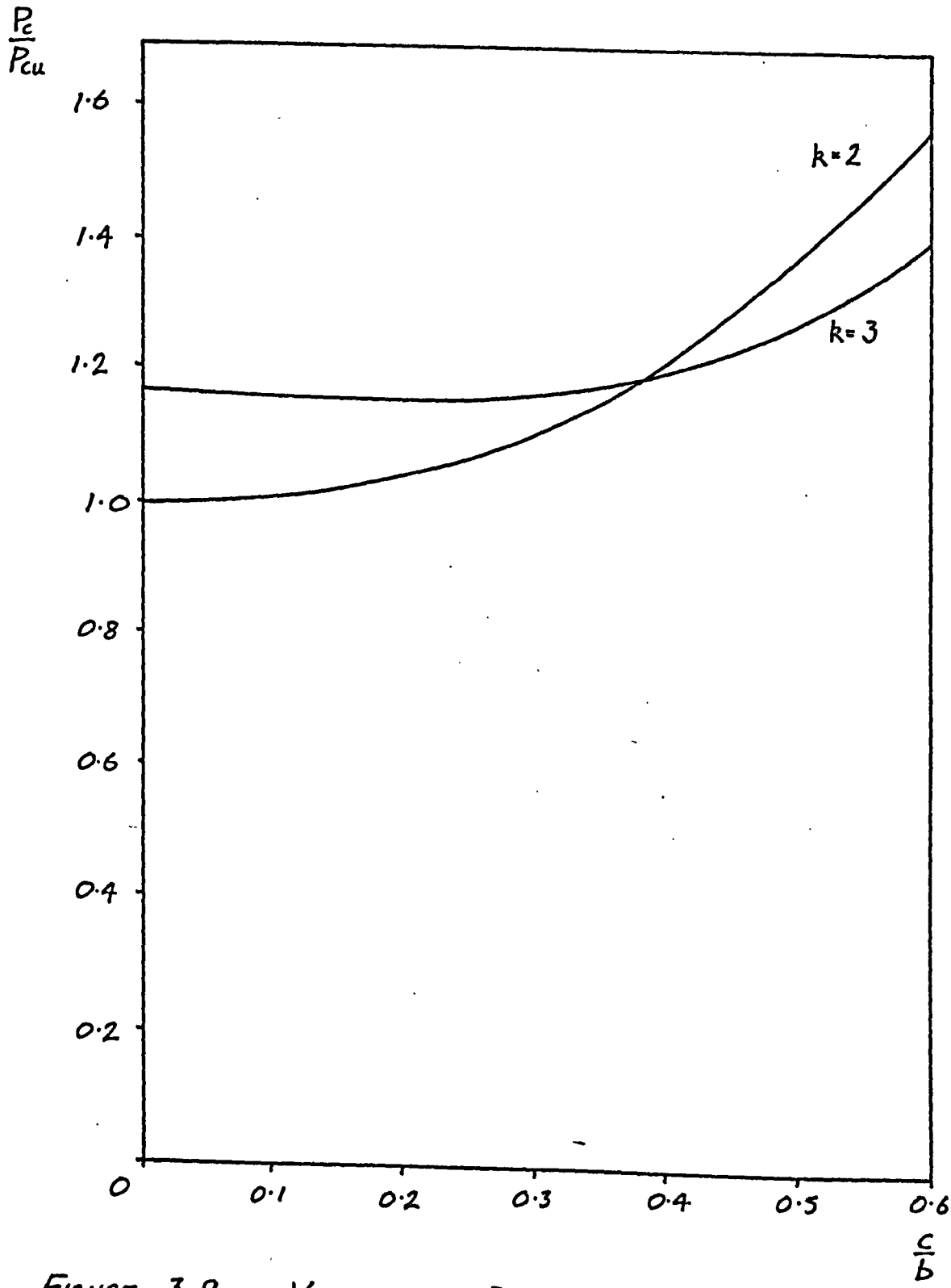

FIGURE 3.9 VARIATION OF BUCKLING LOAD WITH HOLE RADIUS FOR SIMPLY SUPPORTED RECTANGULAR PLATES WITH UNIFORMLY DISPLACED EDGES
k = NUMBER OF BUCKLES IN THE DIRECTION OF LOADING

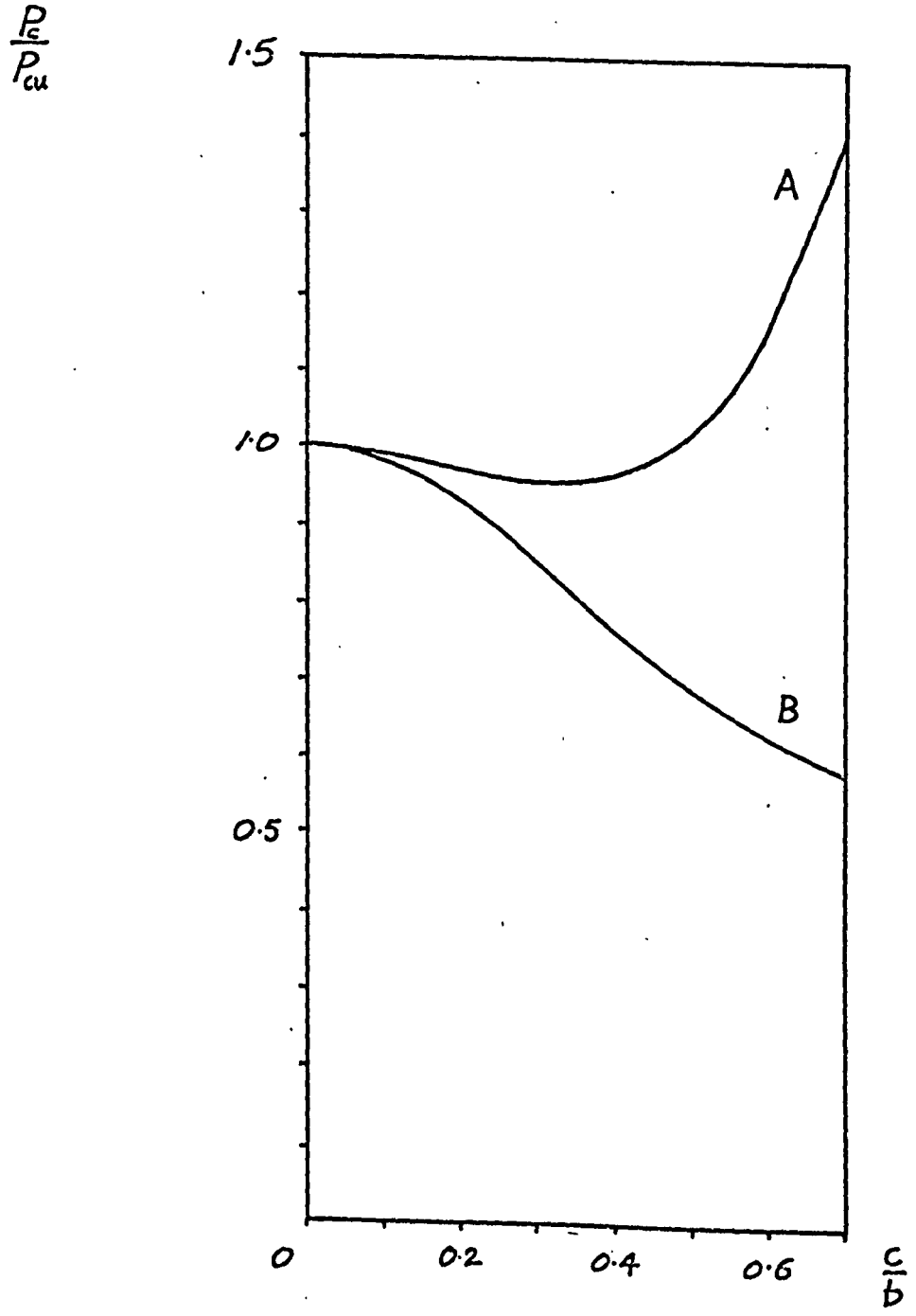

FIGURE 3.10 VARIATION OF BUCKLING LOAD WITH HOLE RADIUS FOR SIMPLY SUPPORTED SQUARE PLATES

CURVE A UNIFORM DISPLACEMENT LOADING

CURVE B " STRESS "

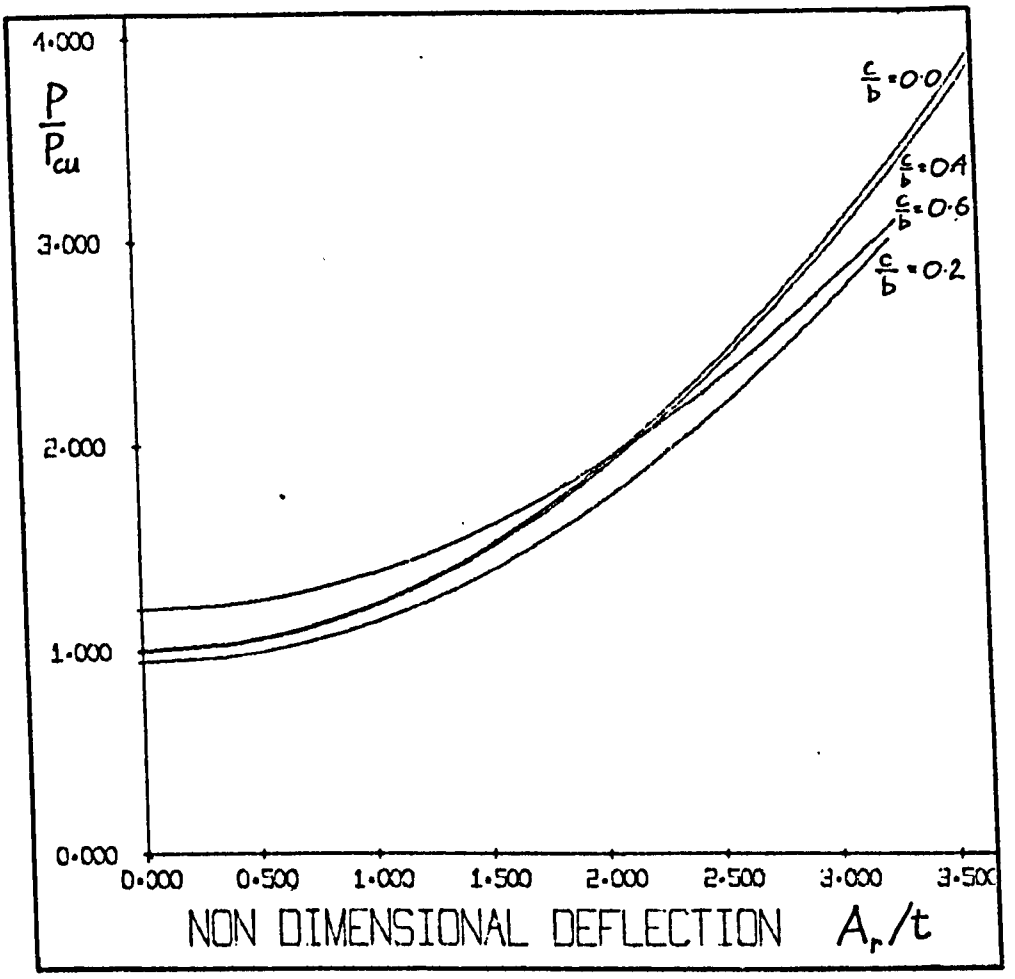

FIGURE 3.11 THE THEORETICAL LOAD – OUT OF PLANE DEFLECTION BEHAVIOUR OF A SQUARE PLATE

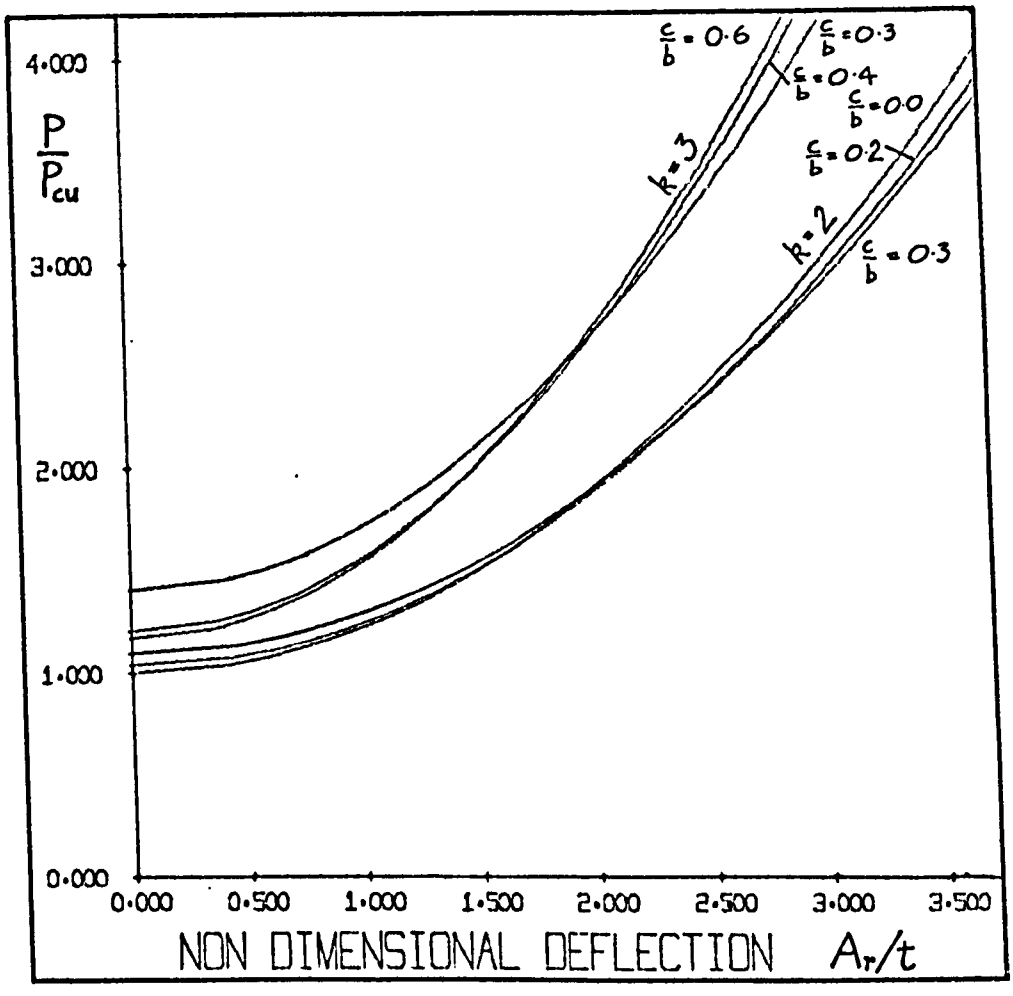

FIGURE 3.12 THE THEORETICAL LOAD – OUT OF PLANE DEFLECTION BEHAVIOUR OF A RECTANGULAR PLATE

k = NUMBER OF BUCKLES IN THE DIRECTION OF LOADING

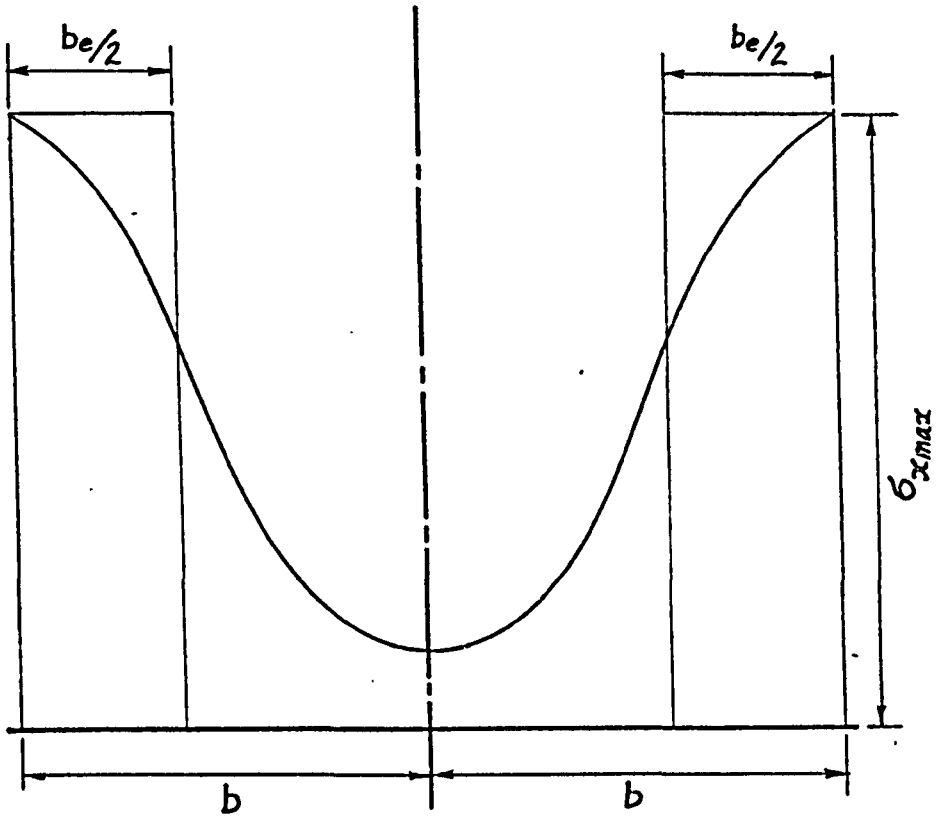

FIGURE 3.13 THE EFFECTIVE WIDTH OF A PLATE

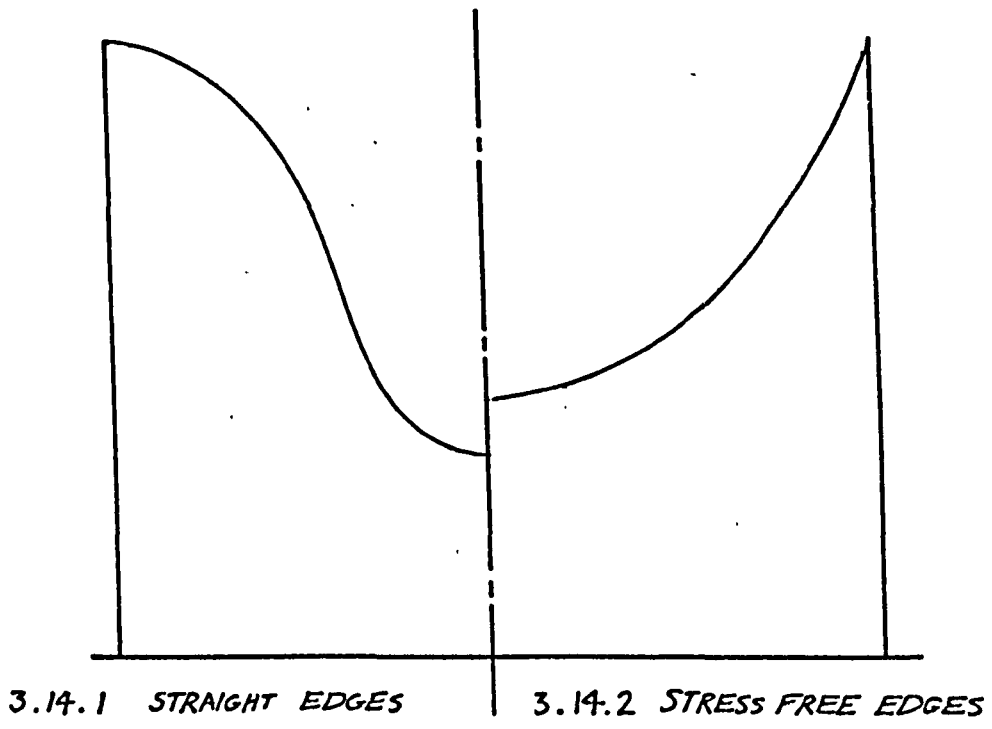

FIGURE 3.14 σ_x STRESS DISTRIBUTION AT MID LENGTH

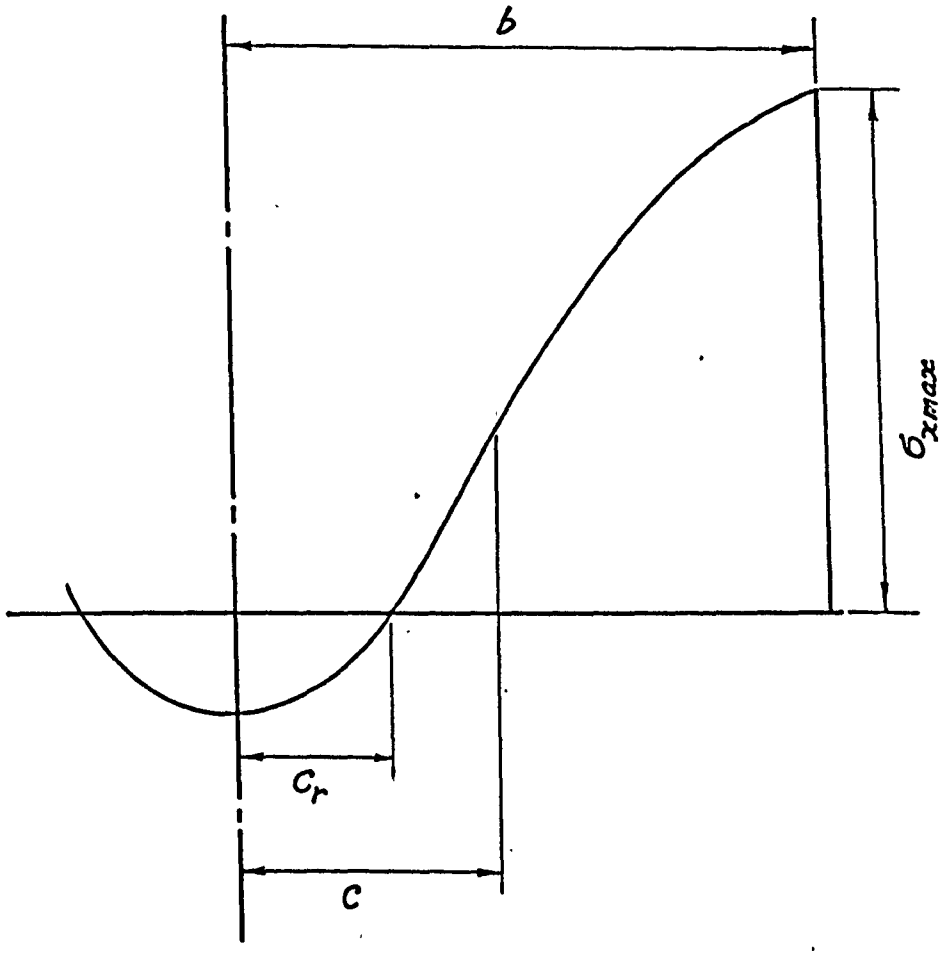

FIGURE 3.15 POST - BUCKLING DISTRIBUTION OF STRESS

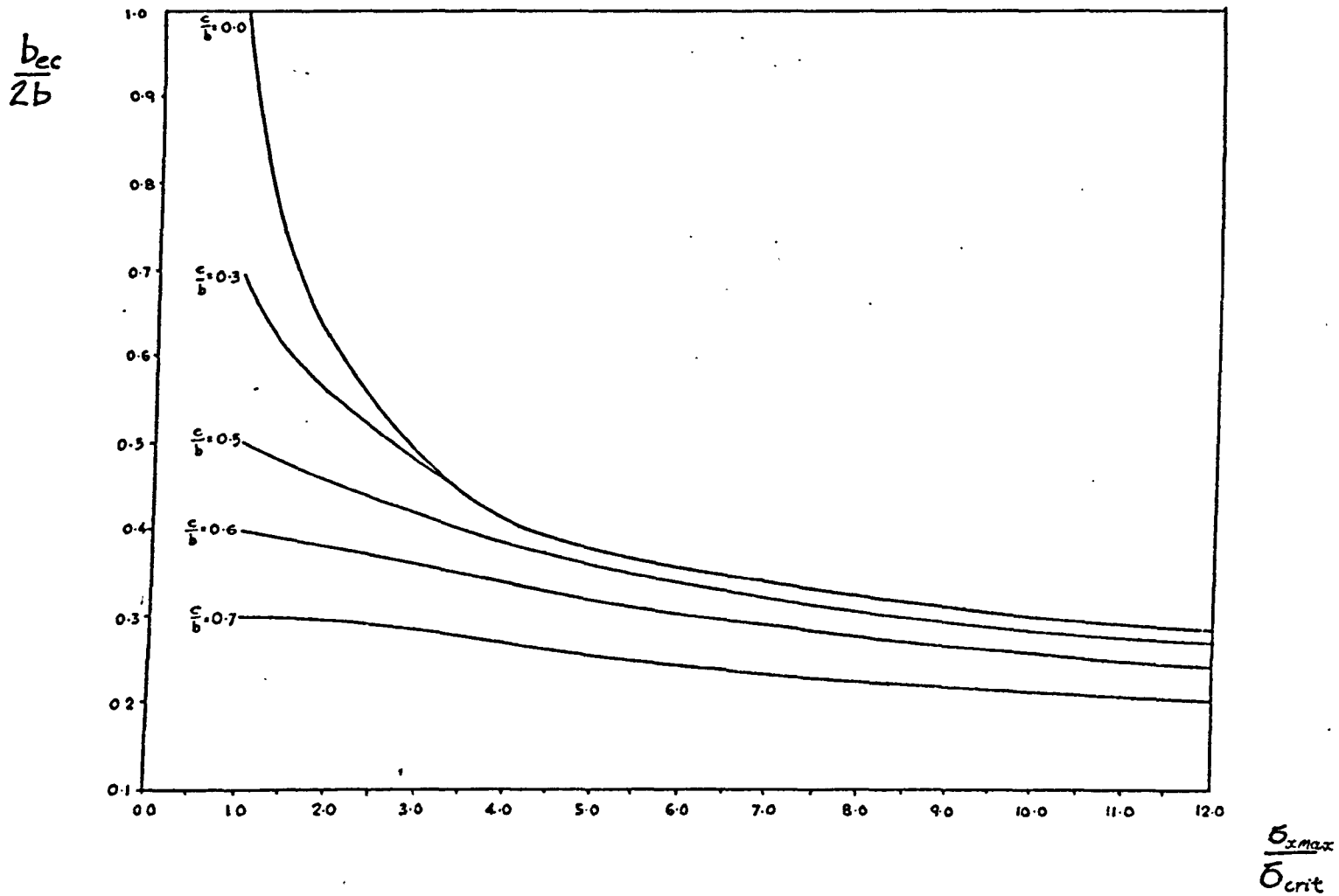

FIGURE 3.16 APPROXIMATE EFFECTIVE WIDTHS FOR SIMPLY SUPPORTED PLATES WITH STRESS FREE UNLOADED EDGES

σ_{CRIT} AVERAGE APPLIED CRITICAL STRESS

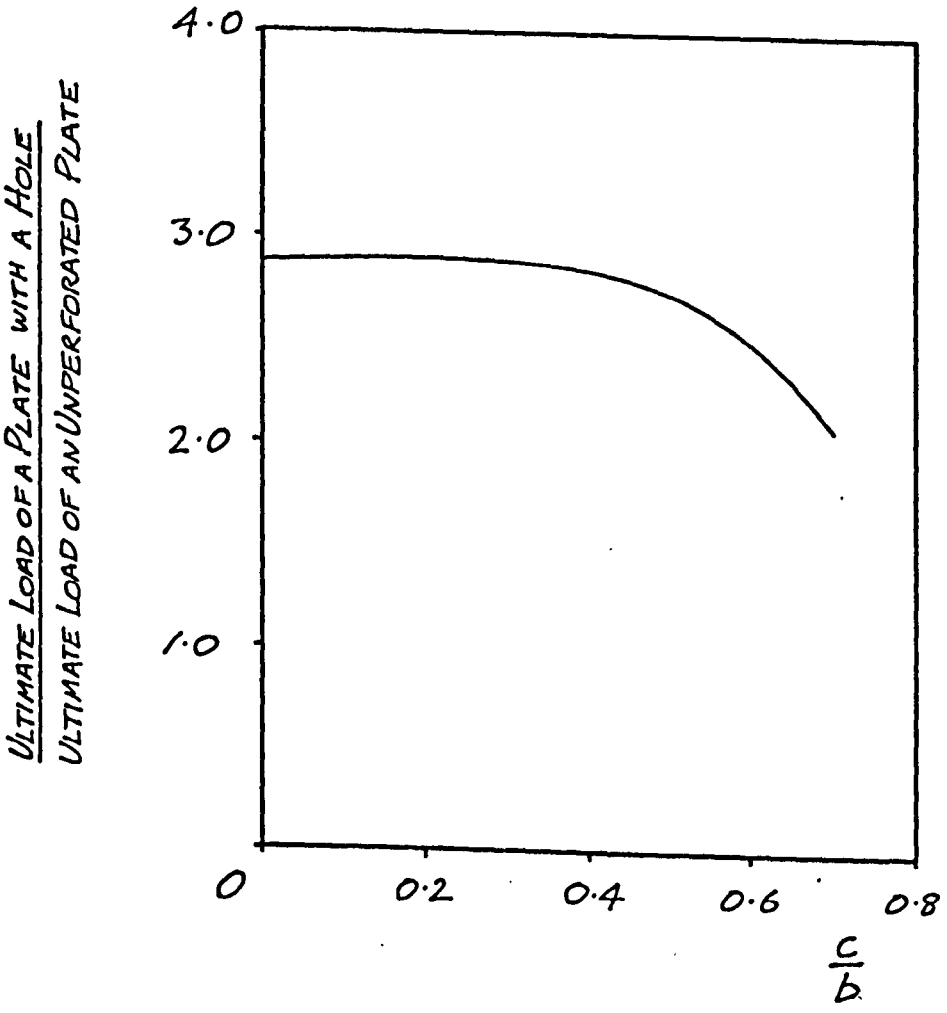

FIGURE 3.17 THE VARIATION OF ULTIMATE LOAD WITH HOLE RADIUS FOR PLATES WITH $\frac{2b}{t} = 160$

b_e	HOLE DIAMETER/ PLATE WIDTH c/b						
	0.1	0.2	0.3	0.4	0.5	0.6	0.7
0.9	0.8229	0.7430	0.6600	0.5737	0.4842	0.3917	0.2964
0.8	0.7433	0.6822	0.6159	0.5439	0.4659	0.3818	0.2920
0.7	0.6610	0.6172	0.5673	0.5099	0.4442	0.3697	0.2866
0.6	0.5760	0.5477	0.5132	0.4707	0.4183	0.3548	0.2797
0.5	0.4882	0.4731	0.4528	0.4249	0.3867	0.3359	0.2705
0.4	0.3973	0.3929	0.3848	0.3707	0.3474	0.3109	0.2578
0.3	0.3000	0.3000	0.3000	0.2967	0.2868	0.2656	0.2282
0.2	0.2000	0.2000	0.2000	0.2000	0.1981	0.1891	0.1678
0.1	0.1000	0.1000	0.1000	0.1000	0.1000	0.0979	0.0897

TABLE 3.1 EFFECTIVE WIDTHS OF SIMPLY SUPPORTED PLATES WITH STRESS FREE UNLOADED EDGES

b_e	HOLE DIAMETER/ PLATE WIDTH c/b						
	0.1	0.2	0.3	0.4	0.5	0.6	0.7
0.9	0.8264	0.7490	0.6672	0.5808	0.4901	0.3957	0.2985
0.8	0.7497	0.6937	0.6303	0.5585	0.4783	0.3905	0.2968
0.7	0.6699	0.6336	0.5884	0.5322	0.4639	0.3840	0.2946
0.6	0.5865	0.5679	0.5405	0.5008	0.4460	0.3756	0.2917
0.5	0.5000	0.4960	0.4853	0.4625	0.4231	0.3645	0.2878
0.4	0.4000	0.4000	0.4000	0.3911	0.3675	0.3241	0.2604
0.3	0.3000	0.3000	0.3000	0.3000	0.2880	0.2599	0.2126
0.2	0.2000	0.2000	0.2000	0.2000	0.1968	0.1816	0.1513
0.1	0.1000	0.1000	0.1000	0.1000	0.1000	0.0939	0.0797

TABLE 3.2 EFFECTIVE WIDTHS OF SIMPLY SUPPORTED PLATES WITH STRAIGHT UNLOADED EDGES

CHAPTER FOUR

The Experimental Investigation

The general object of the investigation was to observe the behaviour of plates with centrally located circular holes under edge compression and to produce data for comparison with theoretical results. Square plates and rectangular plates with aspect ratio 2:1 were tested. The boundary and loading conditions applied to the plates by the test equipment were those which approximated the boundary conditions chosen for study in Chapter One, i.e.

1) Uniformly displaced loaded edges
2) Simply supported edges
3) No restraint in the plane of the plate on the unloaded edges
4) All edges free of shear stress.

The experimental investigation is described under the four main headings, i.e.

4.1 The Test Programme.
4.2 Test Equipment.
4.3 The Specimens.
4.4 Test Procedure.

The experimental results and their comparison with the theoretical analysis are presented and discussed in the following chapters.

4.1 The Test Programme

The test programme was divided into two parts.

Part A — A series of tests designed to produce data on buckling loads, collapse loads, and the out-of-plane deflection behaviour of the plates for comparison with theoretical predictions.

Part B — Four strain investigations to measure the stress distribution in each of four plates for comparison with the theoretically predicted distributions.

Part A of the test programme was intended to produce information on the overall behaviour of the square and rectangular plates under edge compression, with the previously stated loading and boundary conditions.

Part B of the experimental programme was to measure the strains along the axes of the plates at various points, for comparison with the theoretically derived values. This comparison was intended to show to what extent the assumptions made in deriving the stress functions were valid, and to find what limits could be set to the accuracy of the theory in providing information on the stress distribution in post-buckled plates.

The imperfections in the plates allowed the theory to be compared with the behaviour of plates of commercial quality, and thus provided estimates of the extent of application of the theoretical results in practice. The disadvantage of the imperfections was that they made any

detailed examination of the buckled shape of limited value for comparison with the calculated shape.

4.2 Test Equipment

The principal items of equipment used in the tests were as follows:-

4.2.1 The plate test rig

4.2.2 The loading machine

4.2.3 The strain recording apparatus

4.2.1 The Plate Test Rig

The apparatus for supporting the edges of the plates and transmitting applied loading from the loading machine to the edges of the plate is shown in Figures 4.1 and 4.2. The test rig was originally designed and built by W.C. Fok (39) for rectangular plates of length to breadth ratio 2:1, and modifications were made by the author to allow square plates to be tested. Figure 4.1 shows the test rig in its configuration for testing rectangular plates and Figure 4.2 shows the test rig in its configuration for testing square plates.

The main components of the test rig were:-

4.2.1.1 Fixed base

4.2.1.2 Vertical upright supports

4.2.1.3 Vertical knife edges

4.2.1.4 Loading head

4.2.1.5 Roller bearing assembly

These components are described more fully as follows:-

4.2.1.1 The Base

The base consisted of a mild steel plate

machined to 16" x 5" x 1⅜" (406 mm x 127 mm x 34.5 mm) with four ½ inch (12.7 mm) BSW holes tapped to receive the uprights. A 1½" x ⅜" (39 mm x 9.5 mm) locating recess was machined in the upper surface of the base.

4.2.1.2 Vertical Uprights

The uprights were two sections of 5" x 2½" (127 mm x 63.5 mm) plain channel each with a ½" (12.7 mm) thick plate welded to the lower end. Two 9/16" (14.3 mm) holes were drilled through the plate to allow the uprights to be bolted to the base (part 4.2.1.1) A locating key was machined on the plates of both uprights in order to accurately position the uprights on the base. The webs of the plain channel were machined flat and parallel to each other, and then the flange and plate of each upright was machined flat and perpendicular to each other and to the flanges. Holes were drilled in the uprights in order to allow the knife edges to be attached.

4.2.1.3 The Vertical Knife Edges

The knife edges were made of mild steel of 21" x 1½" x ⅜" (534 mm x 38 mm x 9.5 mm) overall size and were attached to the uprights by ⅜" (9.5 mm) cap screws. One knife edge was located on each upright by ⅜" (9.5 mm) dia dowel pins, while the other was allowed to move so that the gap could be adjusted for different plates. The knife edges were machined to a small radius.

4.2.1.4 The Loading Head

The loading head was similar in size and shape to the fixed base, but had four guides attached which ran against the sides of the uprights. A triangular section

block was held on top of the loading head by four 5/16th" (8 mm) capscrews. This triangular block located into a V-shaped slot in the loading head of the loading machine, so that the load was known to be located centrally on the edge of the plate.

4.2.1.5 Roller bearing assembly

The load was applied to the edges of the plate through two cylindrical rollers. These rollers were held, supported by needle bearings, in blocks. One roller was used at each end of the plate. The components of this assembly are illustrated in Figure 4.3 and are as follows:-

(i) The cylindrical roller. The roller was 2" (51 mm) diameter. A flat surface was machined on to the roller and a groove 1.5" (38 mm) wide was machined into the flat along the whole length of the roller.

(ii) Locating strips. These strips fitted into the groove on the rollers, as shown in Figure 4.3, and were machined to allow the plates to be located in the centre of the roller. The strips were made from mild steel of cross section 11/16" x 3/16" (17.5 mm x 4.8 mm)

(iii) Needle bearings. The needle bearings were made up from standard commercial full race bearings. The needles were ½" (12.7 mm) long and ten sets of bearings were used to support each roller.

(iv) The bearing blocks. These blocks were made up from 2.5" x 2.5" x 5" (63.5 mm x 63.5 mm x 127 mm) mild steel in order to contain the needle bearings and the roller. Aluminium strips were bolted over the

edges of the hole in order to contain the needle bearings.

4.2.2 The Loading Machine

The load was applied by a Tinius Olsen Universal testing machine of a maximum 200,000 lbf (889.6 KN) capacity. The loading was of the applied displacement type applied through the loading head, and was measured through the base of the machine by load transducers. The test rig is shown under the loading head of the machine in Figure 4.4. The load was applied through a V-groove, in a block of metal attached to the machine head, to the triangular section block on the loading head of the test rig.

4.2.3 Strain Measuring Equipment

The buckling loads were estimated from the measured strain at various points on each plate. The strains were measured from foil type strain gauges applied to the plate, and connected, using the 'three wire' technique, to the resistance bridge circuit of a MODULOG data logger. Output from the data logger was printed on to a paper roll. For the strain investigations, two gauge rosettes were applied along the axes of the plates, and using the same 'three wire' technique as before, were connected to an ELCOMATIC data logger. Output from this data logger went to a paper printer and to a tape punch. The paper tape produced was used as data for a computer program written by the author in order to produce tables of strain and stress.

The 'three wire' technique is a standard method of connecting strain gauges into a Wheatstone bridge circuit,

which compensates for changes in resistance in the leads from the bridge circuit to the gauges. The wiring diagram is shown in Figure 4.5. The common lead (A) shown in Figure 4.5 between the temperature compensating dummy gauge and the active gauge is in the opposite arm of the bridge from lead (B) and being in close proximity to each other experience almost identical temperature fluctuations. The third lead (C) has no effect, as no current passes through it when the bridge is balanced.

4.3 The Specimen Plates

The plate specimens were cut from hot-dip galvanised mild steel sheeting of nominal thickness 0.063" (1.62 mm). The plates were cut to the overall dimensions 10.125 ins x 10.125 ins (257 mm x 257 mm) and 10.125 ins x 20.125 ins (257 mm x 511 mm), which included a slight margin to allow the knife edges and rollers to hold the edges of the plates. The dimensions of the plate between supports were 10 ins x 10 ins (254 mm x 254 mm) and 10 ins x 20 ins (254 mm x 508 mm) for square and rectangular plates. The loaded edges were filed straight after the holes were cut in the plate in order to remove any distortion of these edges caused by the hole cutting process. Only a small amount of filing was required in order to remove the irregularities on the edges, and a small rat-tail file was used. The loaded edges, although straightened, were not parallel to each other by a very small amount. This slight skewness of the edges was not of importance as the load was applied to the head of the rig by a centrally located pivot.

The smaller holes 1" (25.4 mm) dia. and 2" (50.8 mm) diameter were drilled out, and the larger holes were trepanned. In order to minimise the effect of the trepan causing a bulge in the plate, the holes were cut halfway through the plate from one side and then completed from the other.

The plates all had out-of-plane imperfections. In order to gain an estimate of the magnitude of these imperfections, some of the plates were laid on a surface table, and a dial gauge which had been zeroed to the surface was passed over it. Bulges were found in the plates of an order of 0.006" (0.015 mm) to 0.016" (0.41 mm) peak height in exceptional cases. The out-of-plane deflections were reduced when the plates were held between the knife edges, but this test indicated that initial imperfections in the order of 0.1 - 0.25 times the plate thickness existed. It was felt that an investigation using these plates would be of value, as the results would show the behaviour of plates of commercial standard, and therefore would allow an estimation of the limitations of the theory for practical applications.

4.4 Test Procedure

4.4.1 Test Series A

The plates were prepared with holes in the following ranges of sizes.

Length	Breadth	Range of hole diameters
20" (508 mm)	10" (254 mm)	0"-6" (152 mm) in 1" (25.4 mm) step
10" (254 mm)	10" (254 mm)	0"-6" (152 mm) in 1" (25.4 mm) step

Each plate was numbered before testing and the thickness measured at various points with a micrometer in order to determine an accurate average value. The variation in thicknesses over individual plates was slight. The plates were each loaded into the test rig and tested as follows.

The cap screws fastening the movable knife edges to the vertical uprights were loosened and the plate inserted between the knife edges. The movable knife edges were then tightened against the plate until the plate could just be slipped up and down without any free lateral movement of the plate between the knife edges. G-clamps were used to hold the knife edges in place while the cap screws were tightened.

The dial gauges used to measure the out-of-plane deflections were attached to the uprights by means of their magnetic bases. For rectangular plates, the gauges were generally positioned at the ½ and 1/3 plate length distances from the loaded edge on the 'long' axis of the plate, and at the hole edge. However, the positions varied for different plates and were recorded with the results of each test. For square plates the gauges were placed on a diagonal, halfway between the centre of the plate and the corner, and at the hole edge.

The rig was positioned under the loading head of the Tinius Olsen machine and the loading head was carefully lowered until a small load (approx. 0.1 x buckling load) registered on the machine. This load was intended to settle the plate into its supports and take up any movement between the components of the rig. The load was then

released until the load measured by the machine just registered zero. All the dial gauges on the plate were set to zero and the channels of the MODULOG data logger were zeroed before initial readings of strain and deflection were made. The load was increased from zero and held steady at regular intervals, while readings of strain and deflection were made, until the collapse load of the plate was reached. Collapse was shown on the loading gauge of the Tinius Olsen machine as a sudden reduction in load.

The buckling loads were estimated from the variation of the membrane strain with load at some particular point on each plate. The membrane strains at that point were estimated from surface strain measurements obtained from strain gauges attached to both surfaces of the plate at that point. The strain gauges were connected to the Wheatstone bridge circuit of the MODULOG data logger by the 'three wire' technique, as previously described. Several strain gauge locations and strain directions were tried on an early test, but as there was negligible difference in the buckling load calculated from each, only one position was considered on each plate in subsequent tests.

The estimation of the buckling load from the strain measurements was made by comparing pre- and post-buckling curves of load against membrane strain. The intersection of these two curves was taken as the point of buckling. This method and the various other methods of estimating buckling loads are discussed with the presentation of the experimental results in Chapter Five.

4.4.2 Test Series B. The Strain Investigations

The test procedure for both square and rectangular plates was the same as that used in test series A, with the exception that the ELCOMATIC data logger was used instead of the MODULOG machine. The ELCOMATIC data logger was connected to the strain gauge rosettes on the plates by the 'three wire' technique. The loading was initiated and incremented in the same manner as before. The deflection gauges were used in similar positions to those on plates without strain gauge rosettes.

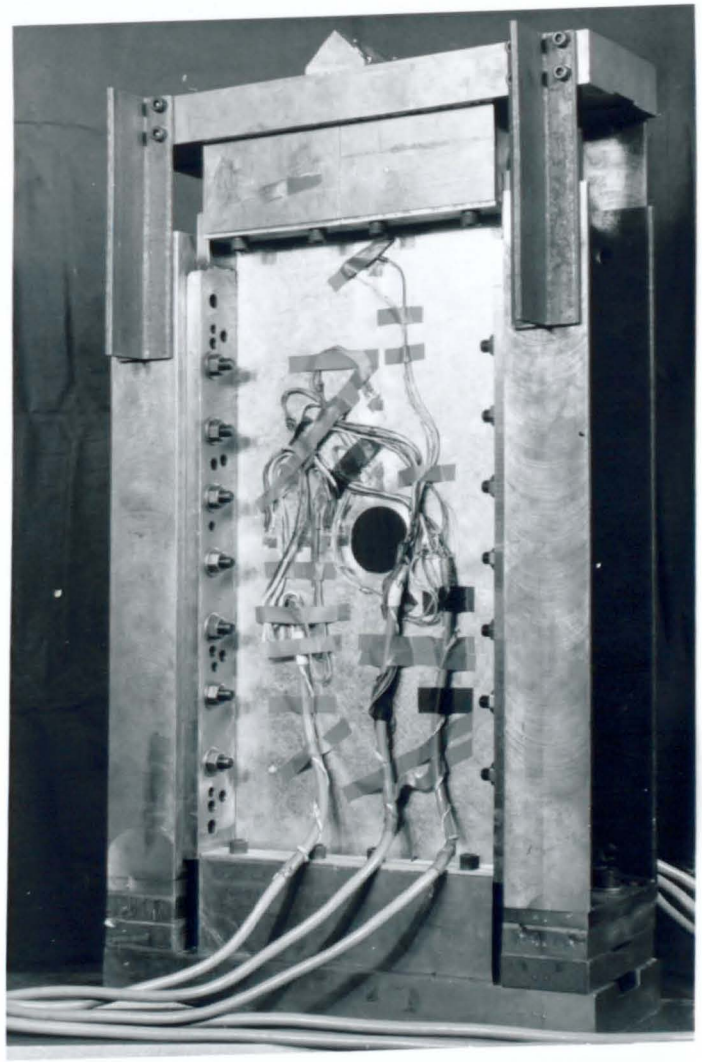

FIGURE 4.1

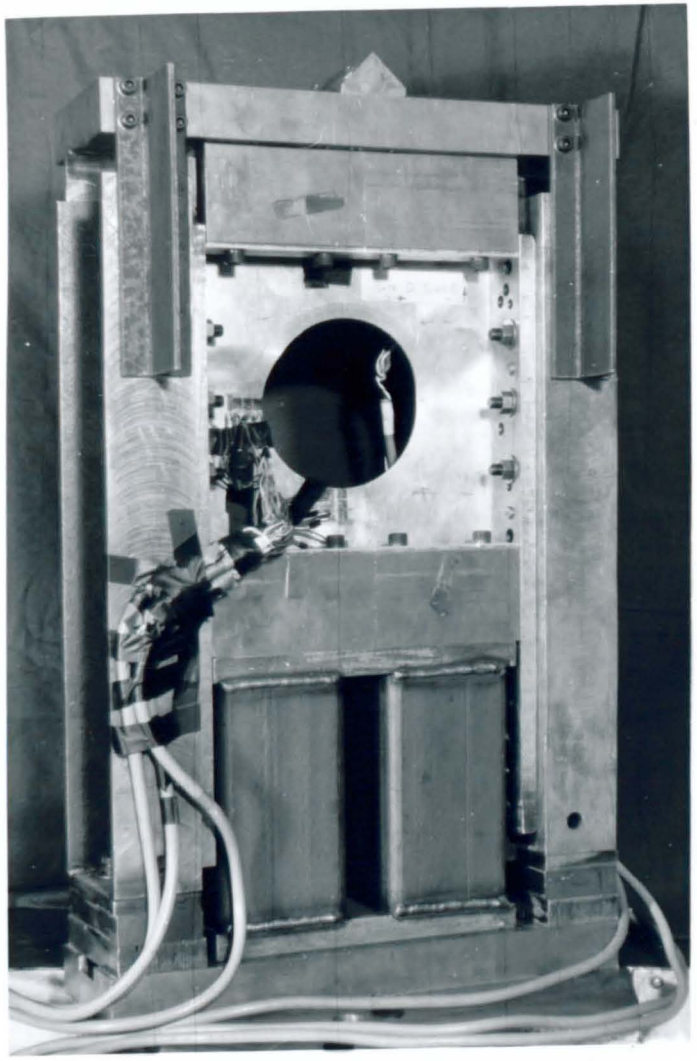

FIGURE 4.2

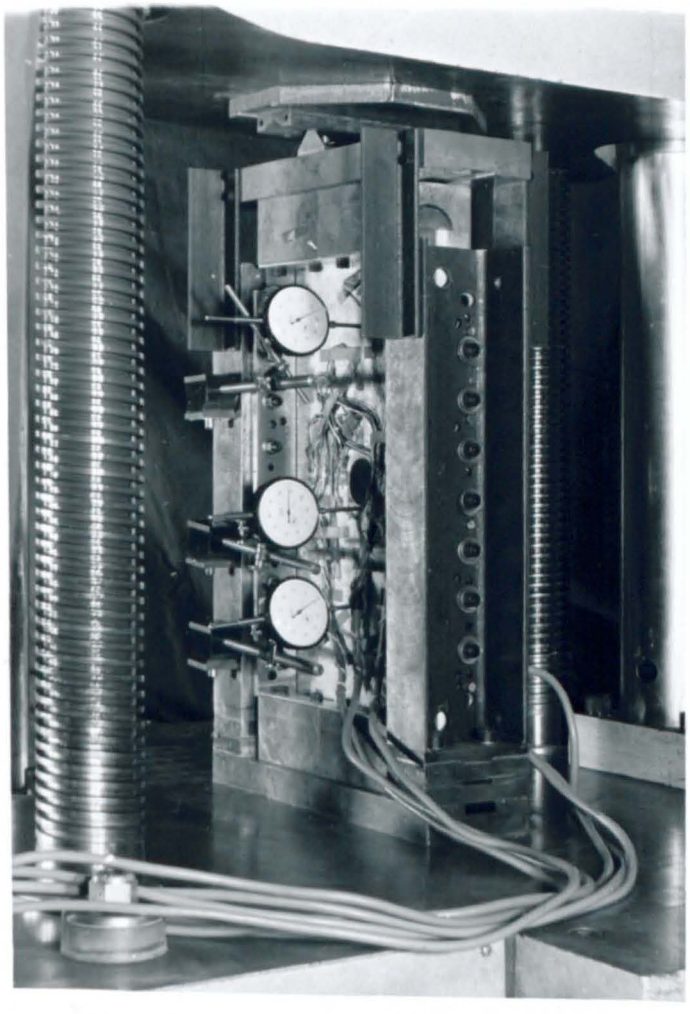

FIGURE 4.4

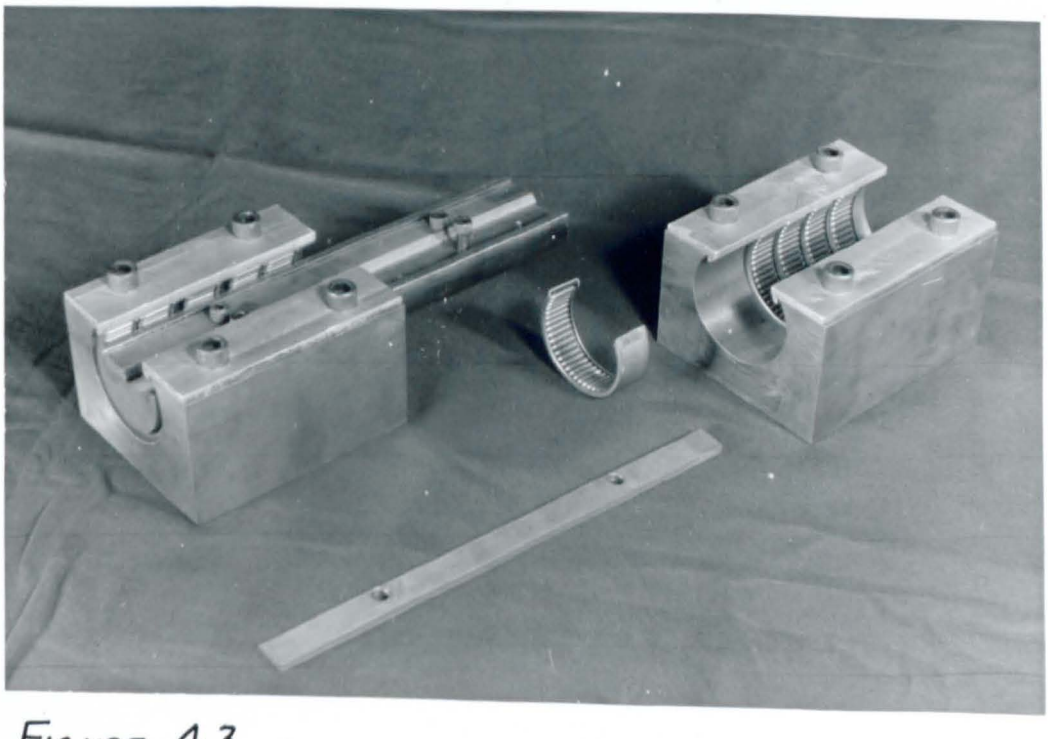

FIGURE 4.3

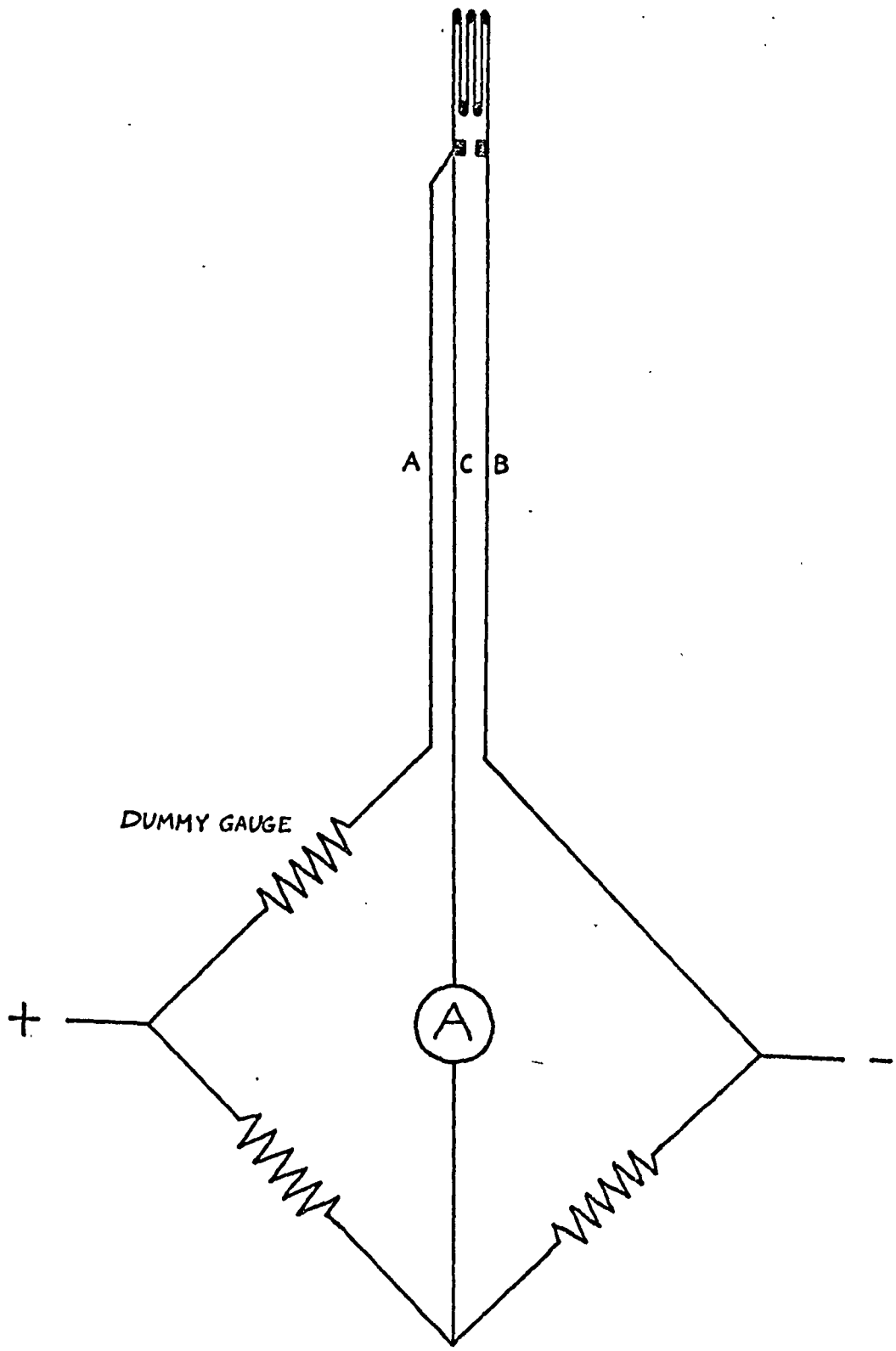

FIGURE 4.5 THE THREE WIRE TECHNIQUE

CHAPTER FIVE

Theoretical and Experimental Results

The theoretical and experimental results and the comparison between them are described under four headings. These headings are as follows:-

5.1 Initial Instability

5.2 Load Deflection Behaviour

5.2.1 Load - out-of-plane deflections

5.2.2 Load - edge displacements

5.3 Ultimate Loads

5.4 Internal Stress Distributions

Typical examples of the plates tested have been selected for comparison with theoretical behaviour. In this chapter, comments are only made on the general patterns of behaviour, whilst detailed discussion of the theoretical analysis and its comparison with experimental results is made in the next chapter.

5.1 Initial Instability

The buckling loads were estimated from the experimental results for the variation of mid surface strain with applied load. The choice of the method was made on the basis of work reported by Coan (21) and Yamaki (22) on plates with initial out-of-plane imperfections. Coan found, from analytical and experimental investigations, that the inflection point of the load-deflection curve corresponded most closely to the buckling load of a flat plate. However, this point cannot readily be identified when out-of-plane imperfections are large. Schlack (19) used numerical analysis

of the load-deflection experimental data to identify this inflection point, but obtained considerable scatter in his results.

Coan studied several methods of estimating the critical load of a flat plate and recommended two methods, using load-strain curves. The first, and more accurate, was to consider that buckling occurred when the tangent to the curve of mid surface strain in the loaded direction became parallel to the deflection axis. The application of this method was considered unreliable, as the scatter of experimental results did not allow a smooth curve to be drawn through them.

The second method described by Coan was to consider that the buckling occurred at the load at the intersection of the tangents to the pre- and post-buckling load - mid surface strain curves. In this method, only straight lines of best fit are required to be drawn through the pre- and post-buckling experimental plots, as illustrated in Figure 5.1. This method was described as being less accurate than the previous two but consistent in underestimating the buckling loads.

It was decided to adopt the second load - mid surface strain method as the potentiality for error was considered to be less than that of the other methods described. In addition, Rhodes (35) found this method to give reliable and consistent results when applied to the local buckling of wide flange beams.

5.1.1 Comparison of Experimental and Theoretical Results

5.1.1.1 Square Plates

The theoretical relationships between buckling load and the hole diameter for simply supported square plates under constant stress and uniform displacement edge loading are presented in Figure 5.2. The theoretical curves show the differences in behaviour between the two types of loading. The experimentally derived results for constant edge displacement are also plotted on Figure 5.2, and the observed mode of buckling was a single half-wave, which was the same as the predicted mode.

5.1.1.2 Rectangular Plates (length/breadth = 2:1)

The theoretical relationships between buckling load and hole size for simply supported rectangular plates, of the overall dimensions and geometry tested, are illustrated in Figure 5.4 for constant stress loading, and in Figure 5.3 for constant edge displacement loading.

The variation in buckling load for constant displacement loading is presented in Figure 5.3 for buckling modes of two and three half-waves. The change in buckling mode at a hole diameter of approximately 0.35 times the plate width, indicated by these results, was observed in the tests, where the majority of plates tested took up the theoretical buckling mode.

5.1.2

5.1.2 Comparison of the theoretical results with the results of other investigators

5.1.2.1 Simply Supported Square Plates with Constant Stress Loaded Edges

The theoretical relationship between buckling load and hole size established by Levy (16), Kumai (18) and Kawai and Ohtsubo (24) are presented with the author's theoretical relationship in Figure 5.5. The experimental results of Kumai (18) and Yoshiki et al. (23) are also plotted in Figure 5.5.

The derivation of these authors' results has already been described in Chapter One.

5.1.2.2 Simply Supported Plates with Uniformly Displaced Loaded Edges

The theoretical relationship between buckling load and hole size, derived by Kawai and Ohtsubo, is illustrated in Figure 5.6 in comparison with the author's theoretical relationship.

5.2 Theoretical and Experimental Load-Deflection Behaviour

The two types of deformations of thin plating under compressive loading which are of greatest interest are:-

5.2.1 Out-of-plane deflections

5.2.2 In-plane displacements of the loaded edges.

The ability to predict these out-of-plane deflections is important, as the redistribution of post-buckling stress and change in axial stiffness are dependent on the derivatives of these deflections. Out-of-plane deflections are easily measurable by the methods described in Chapter Four.

Measurement of the end compression was not attempted, due to lack of suitable reference points on the plates or test rig, which were not affected by the motions of the plate and the flexibility of the test rig. However, the theoretical results are presented.

5.2.1 Out-of-plane Deflections

Comparison was made between the theoretical load - out-of-plane deflection curve derived by Yamaki (22) for simply supported plates, and that derived by the author, as a check on the performance of the author's theory for the limiting case of a plate with no hole. The comparison is illustrated in Figure 5.7.

This also allows the performance of the test rig with plates having no holes to be checked against an established mathematical theory, by reference to the comparison between the author's theoretical and experimental results for these plates.

5.2.1.1 Square Plates

Figure 5.8 illustrates the theoretical variation in load deflection behaviour of plates with various hole sizes. The deflections in Figure 5.8 are fictitious as they represent the hypothetical deflection at the centre of the plates. However, they provide a comparison of the relative magnitudes of the deflections of the plate.

Comparisons were made between the theoretical and experimentally measured load-deflection behaviour, and typical comparisons throughout the range of hole sizes are presented in Figures 5.9 - 5.15.

Figures 5.13 and 5.15 are of interest in that the deflections remote from the hole suggest that a change in waveform took place prior to collapse. This is discussed in Chapter Six.

5.2.1.2 Rectangular Plates

The theoretical load-maximum deflection curves for various hole sizes are compared for two and three half-wave buckling modes in Figures 5.16 and 5.17 respectively. Comparison between the two and three half-wave buckled shapes for a plate with a hole diameter of 0.3 times the plate width was made in Figure 5.18.

Comparisons between experimental load-deflection behaviour and theoretical behaviour are presented for typical plates in Figures 5.19 to 5.27. Figures 5.19 to 5.22 show results for plates with the range of hole sizes 0.0 to 0.2 times the plate width, which buckled into two half-waves, and Figures 5.24 - 5.27 show the results for the range of plates, having hole diameters of 0.4 - 0.6 times the plate width, which buckled into three half-waves. Figure 5.23 shows the comparison of theoretical and experimental results for a plate with a hole diameter of 0.3 times the plate width, which buckled into three half-waves.

5.2.2 Load-Edge Displacement Behaviour

Theoretical curves derived by Yamaki (22) representing the uniform loaded edge displacements with applied load are compared in Figure 5.28 with the theoretical curves derived by the author for the limiting case of a plate with no hole, which has square buckles.

The graph of the theoretical variation of uniform edge displacement with applied load for square plates with a centrally located circular hole and the experimental boundary conditions are shown in Figure 5.29. The post-buckling slopes are all similar to those of a plate with no hole, and the variation of pre- and post-buckling axial stiffness with hole size is shown in Figure 5.30.

The theoretical loaded edge displacement variation with applied load for the rectangular plates under test is illustrated for the two and three half-wave buckled shapes in Figures 5.31 and 5.32. The variation of the post-buckling stiffnesses with hole size is presented in Figure 5.33 for both buckled shapes. This shows the variation of the two and three half-wave post-buckling stiffnesses in comparison to the variation of pre-buckling stiffness with hole size.

The load-edge displacement curve in Figure 5.34 represents a rectangular plate with hole diameter to plate width ratio equal to 0.3, and shows the intersection of the curves arising from the two and three half-wave buckling modes, which suggests that coupled modes of buckling are possible under certain conditions.

5.3 Ultimate Loads

Two types of failure were observed in the plates. The first type occurred in plates with relatively small holes of diameter less than 0.3 times the plate width and is illustrated in Figure 5.35. This mode of failure was the type observed in unperforated plates.

The second type of failure is illustrated in Figures

5.36 and 5.37, and occurred mainly in plates with holes of diameter greater than 0.3 - 0.4 times the plate width. Plastic hinges or folds grew across the narrowest section of the plate between the hole edge and the supported edge. This either took the form of a kink, or two half-waves developed, as shown diagrammatically in Figure 5.38. The development of these two half-waves can be seen in the load-deflection curves presented in Figures 5.13 and 5.15.

Experimentally measured collapse loads were plotted against hole size in Figure 5.39. This showed that the collapse loads tended to decrease appreciably with increase in hole diameters greater than 0.3 to 0.4 times the plate width.

5.4 The Internal Stress Distributions

The general objects of the experimental strain investigation are explained in Chapter Four.

The four plates tested in this investigation were selected from the stock of plates prepared for the general series of tests, and no special preparations were made, other than those necessary to make the surface suitable for the application of strain gauges. The nominal dimensions of each of the four plates tested are set down in Table 5.1.

Plate	Length ins(mm)	Breadth ins(mm)	Thickness ins(mm)	Hole dia. ins (mm)
A	20 (508)	10 (254)	0.0622 (1.6)	2 (50.8)
B	20 (508)	10 (254)	0.0622 (1.6)	6 (152.4)
C	10 (254)	10 (254)	0.0622 (1.6)	5 (127.0)
D	10 (254)	10 (254)	0.0622 (1.6)	3 (76.2)

Table 5.1

Each plate was strain gauged along both centre lines with two-gauge 90° rosettes. The strain measurements were used to calculate stresses from the following relationships between stress and strain.

$$\sigma_x = \frac{E}{(1-\nu^2)} (\varepsilon_x + \nu \varepsilon_y)$$

$$\sigma_y = \frac{E}{(1-\nu^2)} (\varepsilon_y + \nu \varepsilon_x)$$

The stresses calculated from the strain measurements are presented in comparison to theoretical stresses derived in the manner described in Chapter Three.

5.4.1 Rectangular Plates

5.4.1.1 Plate A

Plate A was a rectangular plate with a hole of diameter 0.2 times the plate width, having the dimensions described in Table 5.1. The layout of the strain gauges along each axis is shown in Figure 5.40.

The plate buckled into a two half-wave shape as predicted by the theoretical analysis and collapsed prematurely at an applied load of 5930 lbf (27.2 KN) when one of the plate edges slipped from between the knife edge supports.

The theoretical stresses in each direction along both of the principal axes were drawn to the same scale and set out on the same diagram in Figure 5.41 for an applied load of approximately twice the buckling load, in order to demonstrate the relative magnitudes of these stresses. Figure 5.41 shows clearly that the dominant stresses are

the σ_x stresses along the y-axis.*

The σ_x stress distribution along the y-axis is presented in Figures 5.42 and 5.48 for both the experimentally and theoretically derived results. In the post-buckling range the redistribution of stresses is clearly shown in Figures 5.44 - 5.48. The σ_y stresses along the y-axis are also presented in Figures 5.42 - 5.48 in order to show the relative magnitudes of stresses in both x and y directions.

Figures 5.49 - 5.53 show the theoretical and experimental σ_x stress distributions on the x-axis and the corresponding σ_y stresses are shown in Figures 5.54 - 5.56. These figures have been portrayed with relatively larger scales than the σ_x stress distributions on the y-axis.

5.4.1.2 Plate B

Plate B was a rectangular plate with a hole of diameter 0.6 times the plate width, having the dimensions stated in Table 5.1. The plate buckled into three half-waves as predicted by the buckling analysis and reached an ultimate load of 7780 lbf (34.6 KN).

The layout of strain gauges is shown in Figure 5.57.

The theoretical and experimental σ_x stress distributions on the y-axis are illustrated in Figures 5.58 - 5.62. The corresponding σ_y stress distributions are also plotted in these figures in order to illustrate the relative orders of magnitude of the stresses in each direction.

On the x-axis the theoretical and experimental σ_x stress distributions are shown in Figures 5.63 to 5.68 and

* For the purpose of comparison of theoretical and experimental results the x and y axes of the plate are taken to pass through the centre of the plate.

the σ_y stress distributions are illustrated in Figures 5.69 - 5.73.

5.4.2 Square Plates

5.4.2.1 Plate C

Plate C was a square plate with a hole of diameter 0.5 times the plate width. The plate buckled into a single half-wave and collapsed at a load of 9000 lbf (40.1 KN). The layout of the strain gauges is shown in Figure 5.74.

Comparison between theoretical and experimental σ_x stresses on the y-axis is made in Figures 5.75 - 5.78. The stress distributions on the x-axis were not presented. The high stress gradients on the x-axis cause relatively large experimental error and it was felt the finite element analysis had too few elements in this region to represent the stresses accurately. Therefore it was felt that valid comparison between theory and experiment was not possible.

5.4.2.2 Plate D

Plate D was a square plate with a hole of diameter 0.3 times the plate width, and nominal dimensions described in Table 5.1. The plate buckled into a single half-wave and collapsed at a load of 8400 lbf (37.4 KN). The layout of gauges on the plate centre lines is shown in Figure 5.79.

Graphs of theoretical and experimentally derived σ_x stress distributions on the y-axis are shown in Figures 5.80 - 5.84. The distribution of the experimental points was unexpected and indicates some experimental error, which makes the rest of these results invalid for comparison with the theoretical analysis.

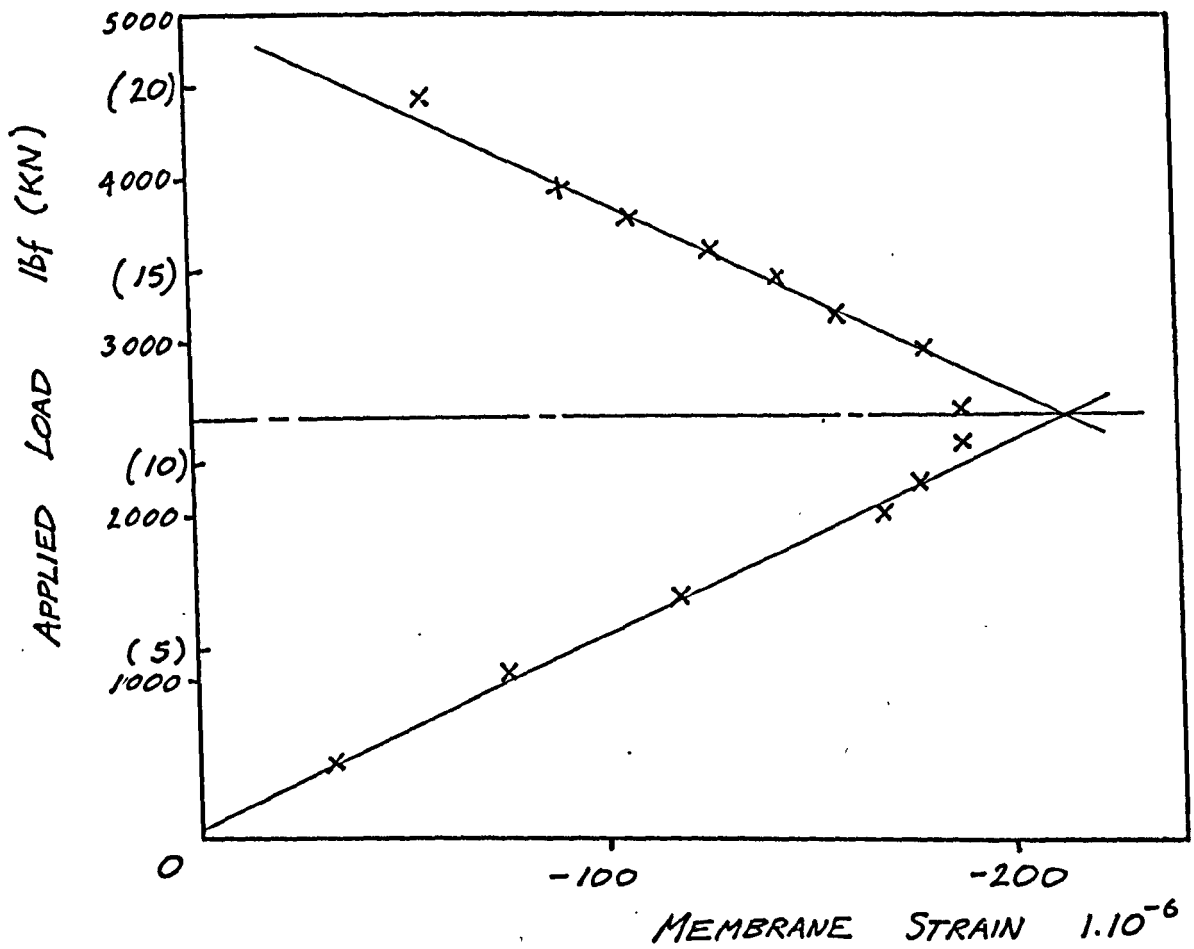

FIGURE 5.1 ESTIMATION OF BUCKLING LOAD FROM MEASURED VALUES OF MEMBRANE STRAIN

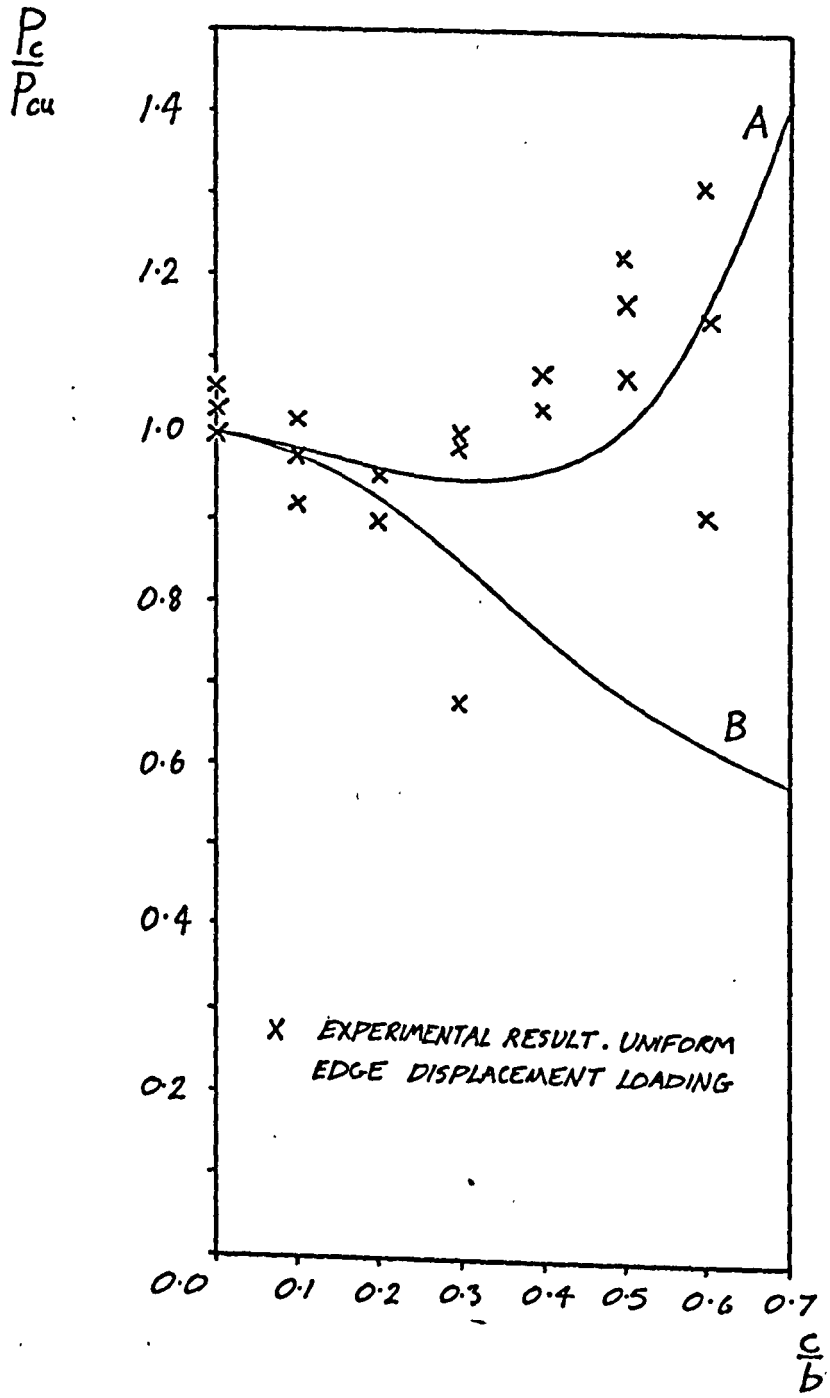

FIGURE 5.2 THEORETICAL AND EXPERIMENTAL VARIATION OF BUCKLING LOAD WITH HOLE RADIUS FOR SIMPLY SUPPORTED SQUARE PLATES

A - UNIFORM EDGE DISPLACEMENT LOADING

B - " " STRESS "

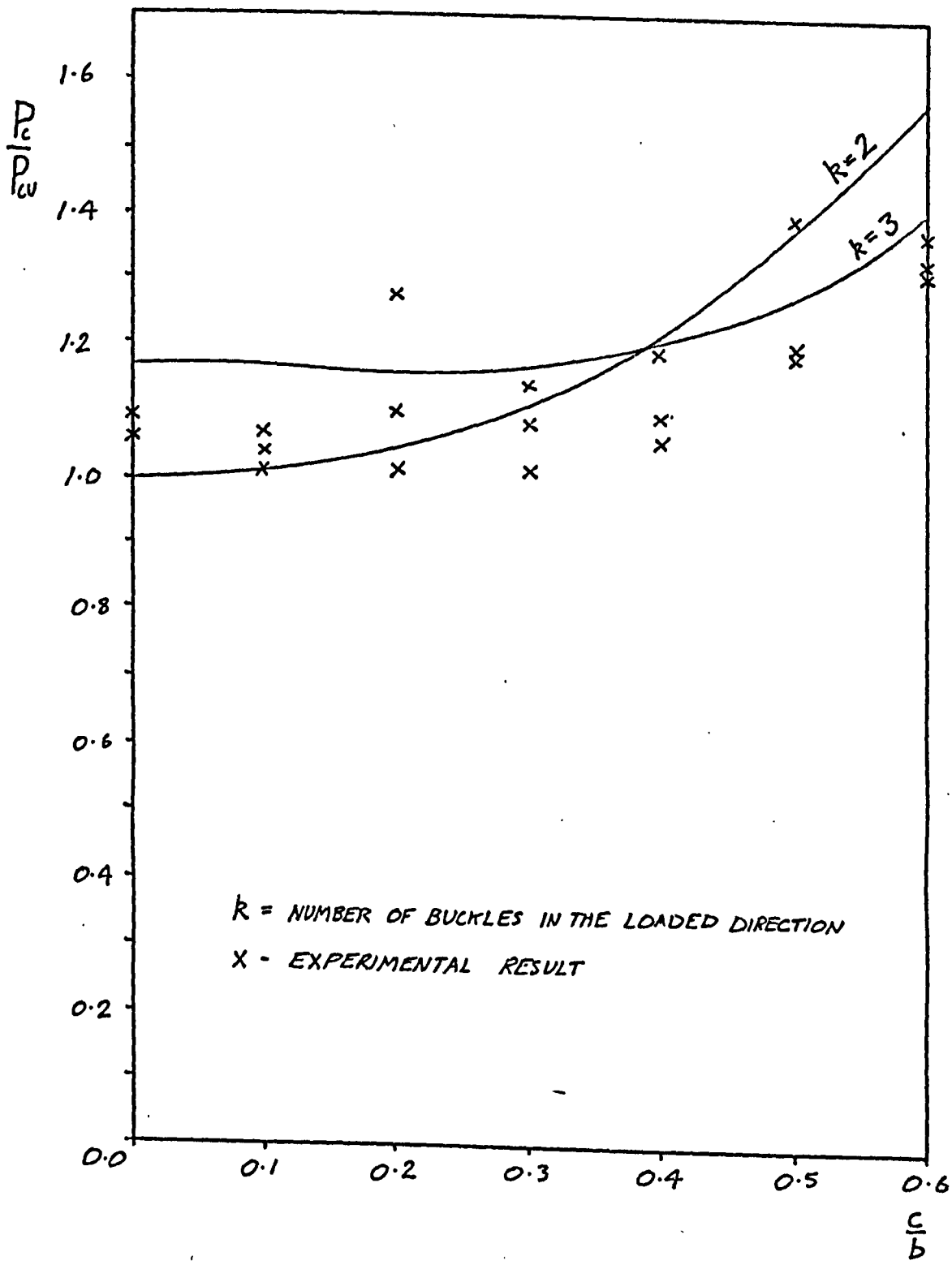

FIGURE 5.3 THEORETICAL AND EXPERIMENTAL VARIATION OF BUCKLING LOAD WITH HOLE RADIUS FOR RECTANGULAR PLATES WITH UNIFORMLY DISPLACED LOADED EDGES AND SIMPLE SUPPORTS.

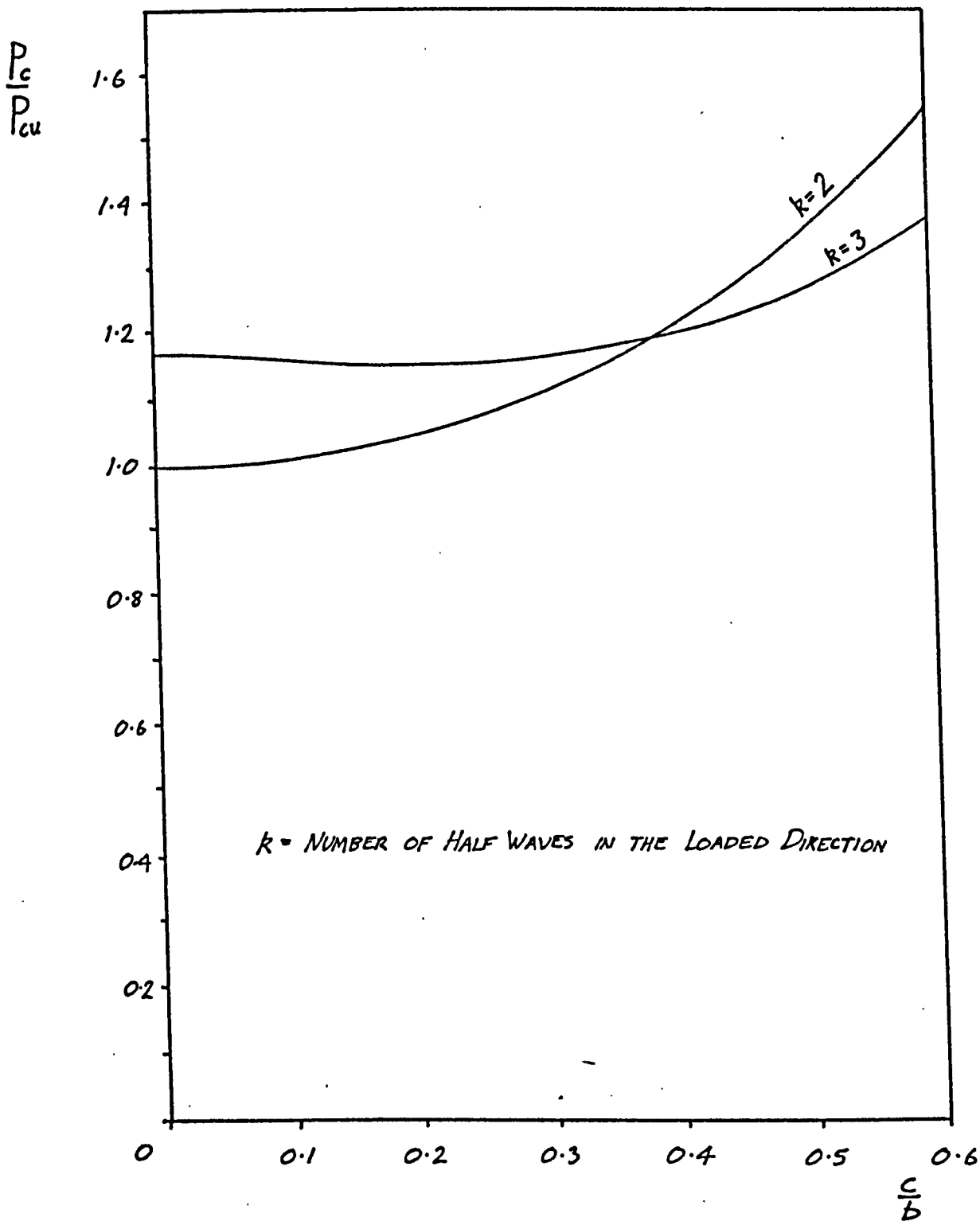

FIGURE 5.4 THEORETICAL VARIATION OF BUCKLING LOAD WITH HOLE RADIUS FOR SIMPLY SUPPORTED RECTANGULAR PLATES WITH UNIFORM STRESS LOADING.

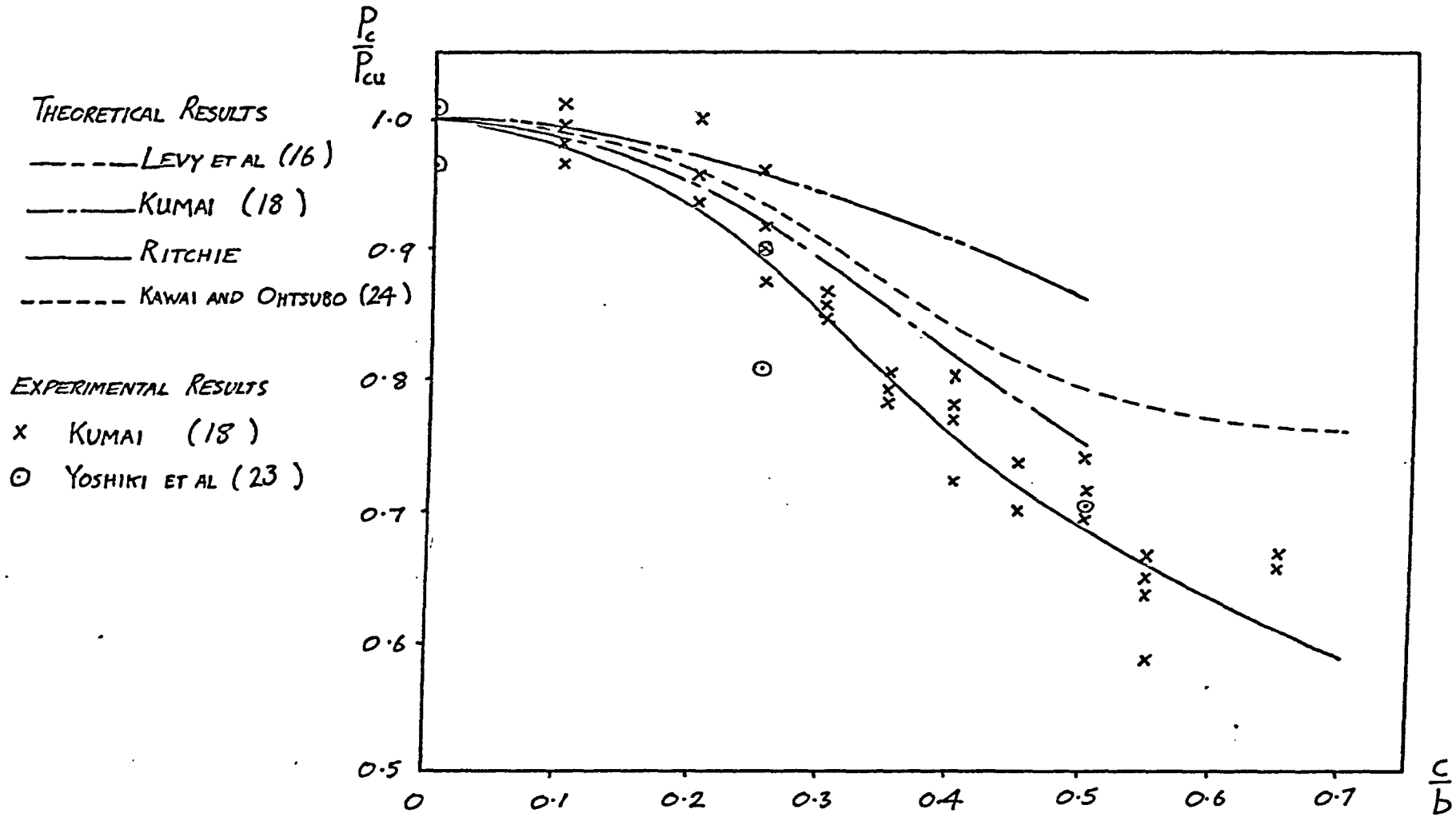

FIGURE 5.5 COMPARISON OF VARIOUS THEORETICAL AND EXPERIMENTAL RESULTS FOR SIMPLY SUPPORTED SQUARE PLATES UNDER UNIFORM STRESS LOADING.

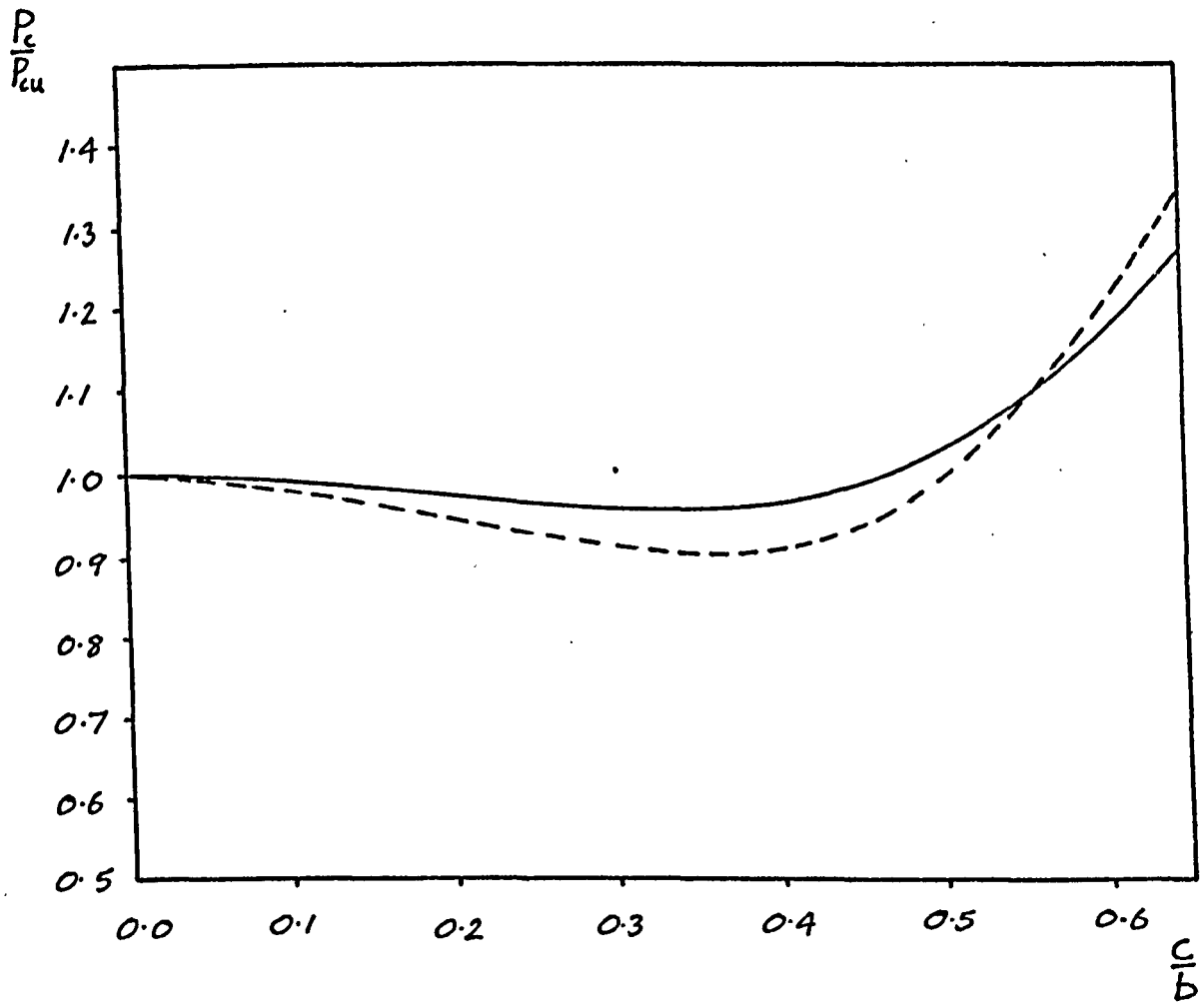

FIGURE 5.6 THEORETICAL VARIATION OF BUCKLING LOAD WITH HOLE RADIUS FOR SIMPLY SUPPORTED SQUARE PLATES WITH UNIFORM EDGE DISPLACEMENT LOADING

——— RITCHIE

- - - - - - KAWAI AND OHTSUBO (24)

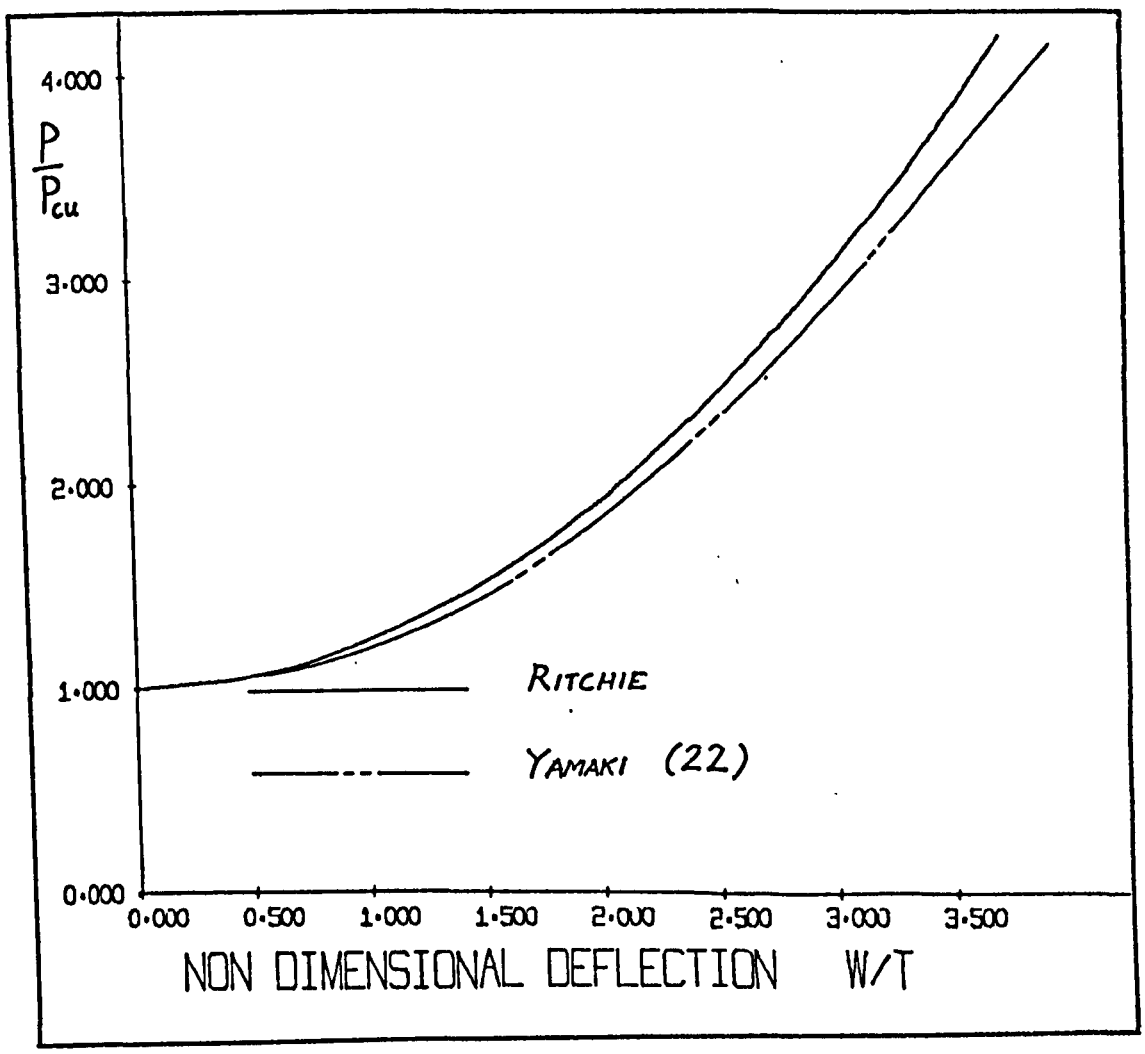

FIGURE 5.7 LOAD – OUT OF PLANE DEFLECTION BEHAVIOUR OF A SIMPLY SUPPORTED UNPERFORATED SQUARE PLATE.

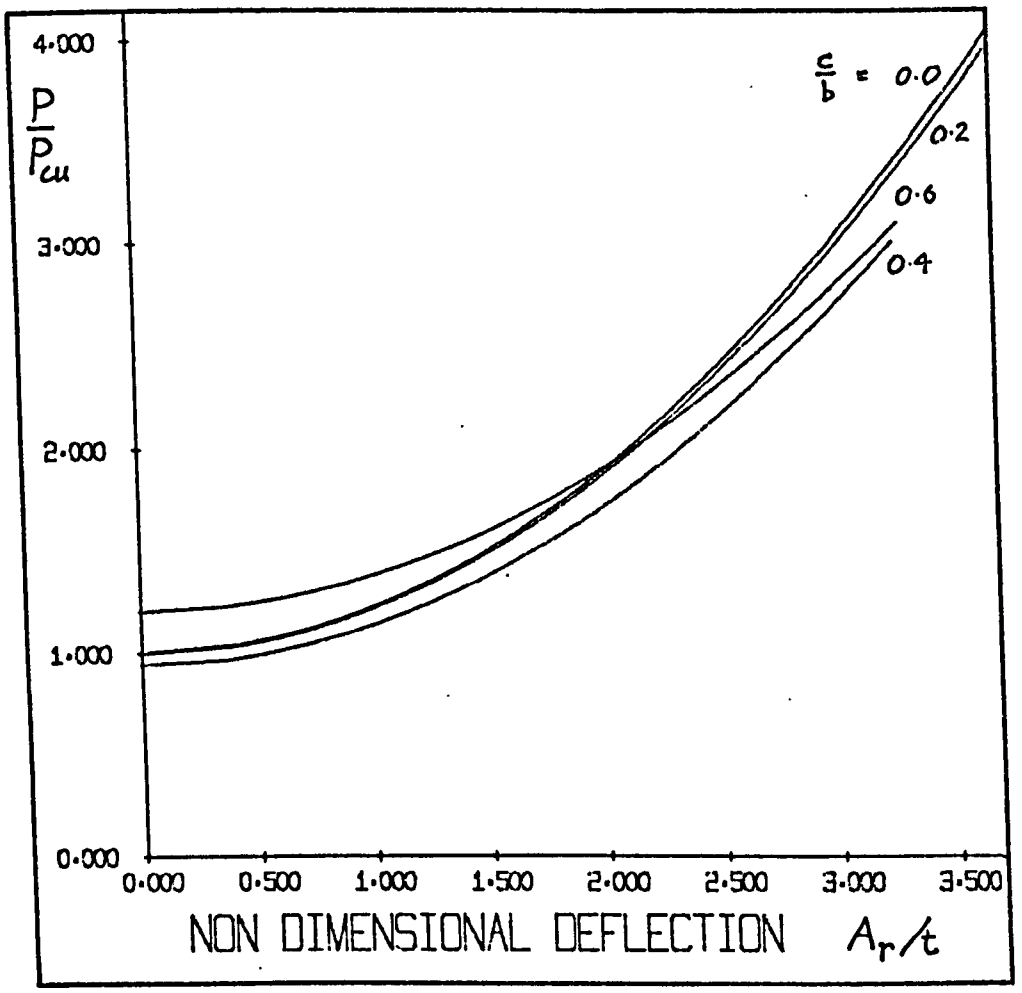

FIGURE 5.8 LOAD - OUT OF PLANE DEFLECTION BEHAVIOUR OF SIMPLY SUPPORTED SQUARE PLATES

Figure 5.9 Out-of-plane deflections of a square plate $\frac{c}{b} = 0.0$

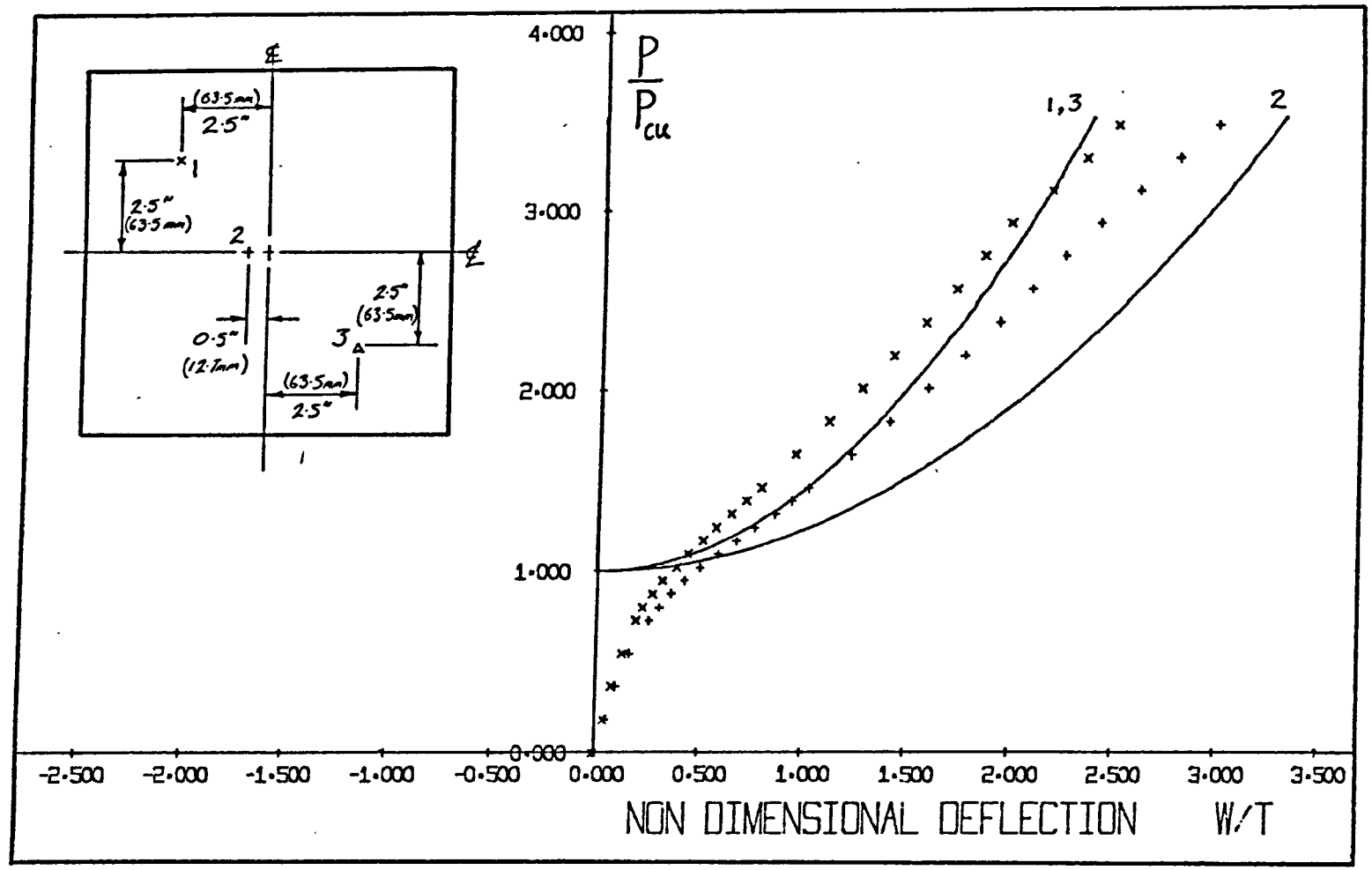

Figure 5.10 Out-of-plane deflections of a square plate $\frac{c}{b} = 0.0$

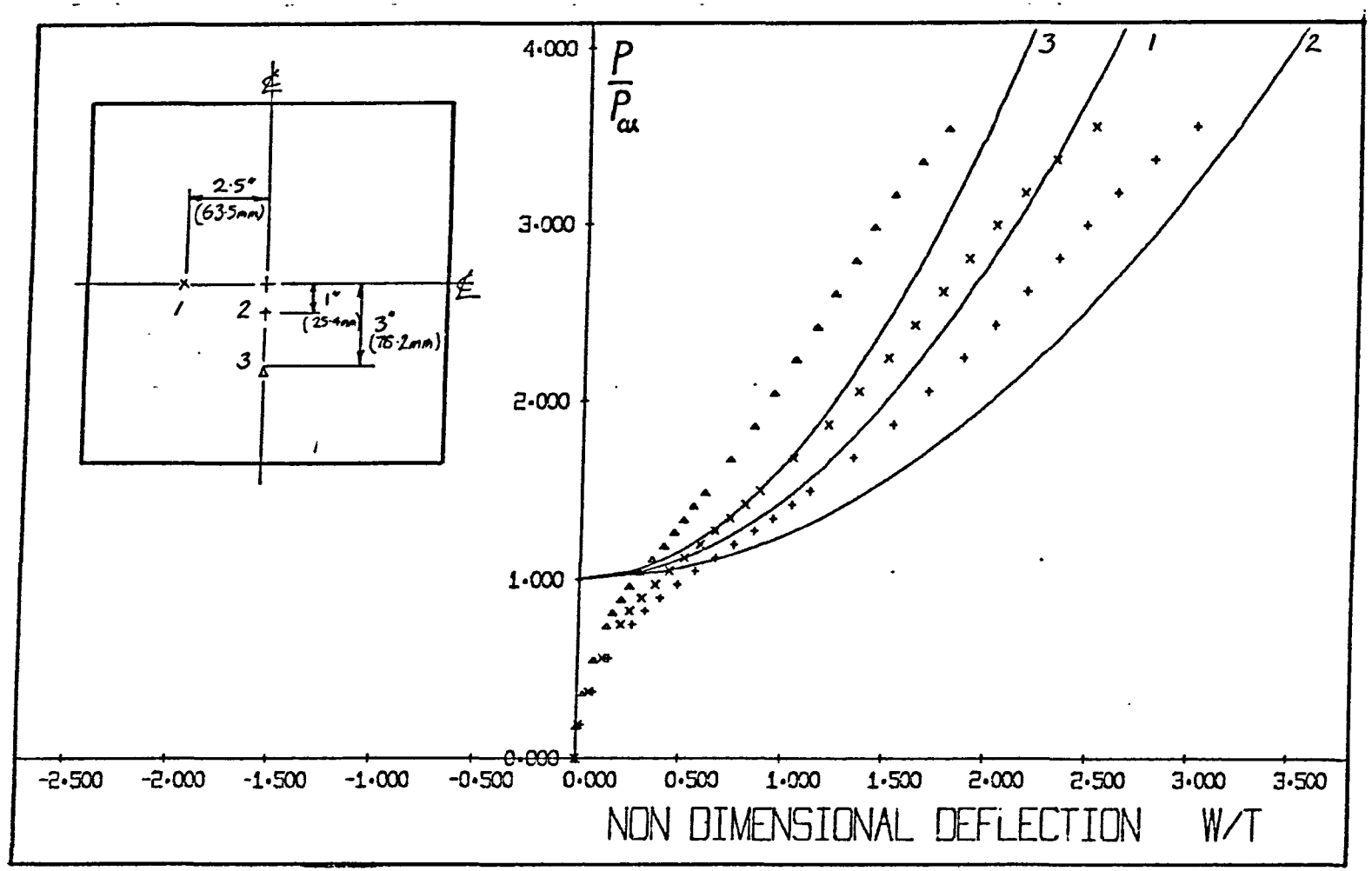

Figure 5.11 Out-of-plane deflections of a square plate $\frac{c}{b} = 0.1$

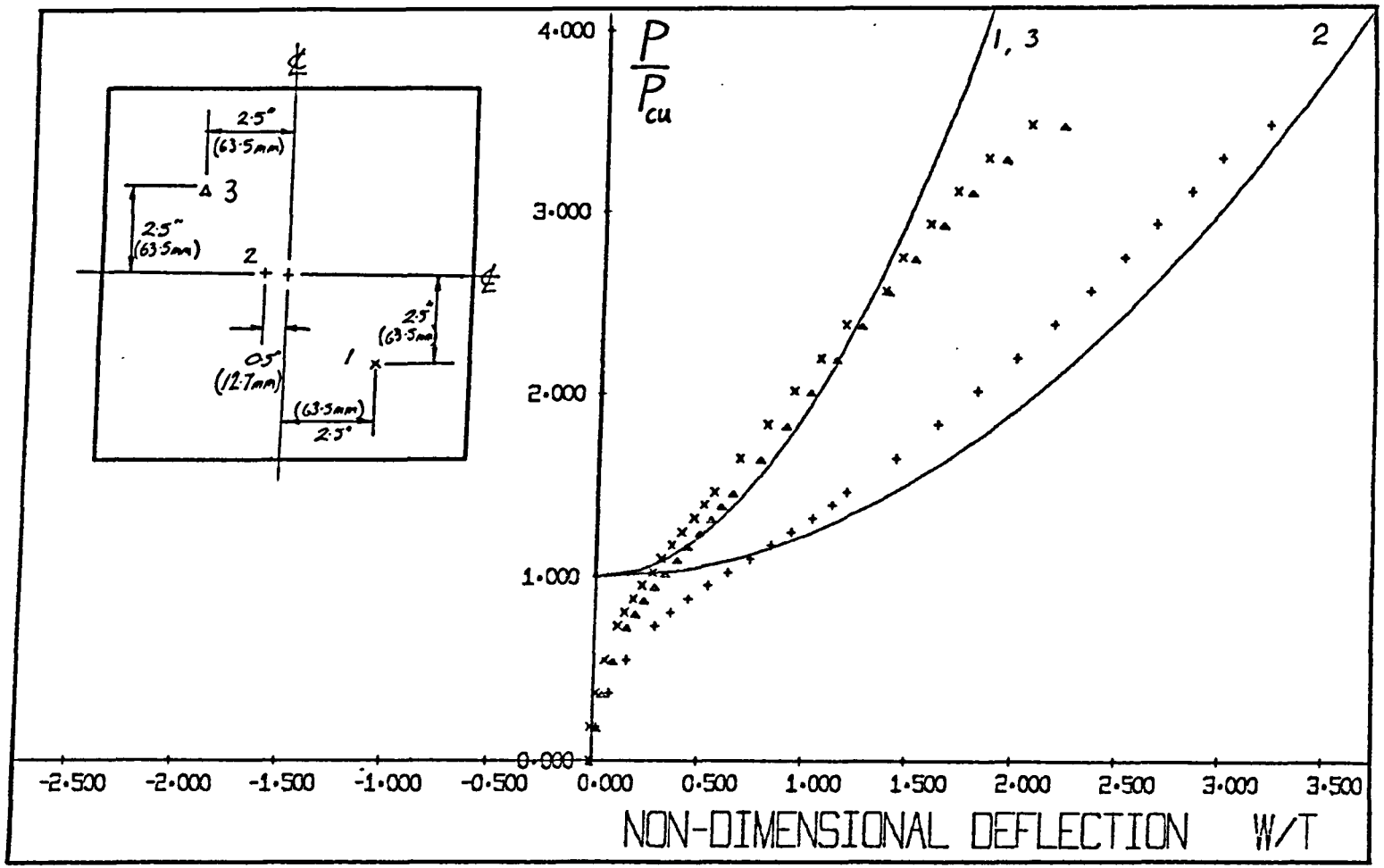

Figure 5.12 Out-of-plane deflections of a square plate $\frac{c}{b} = 0.2$

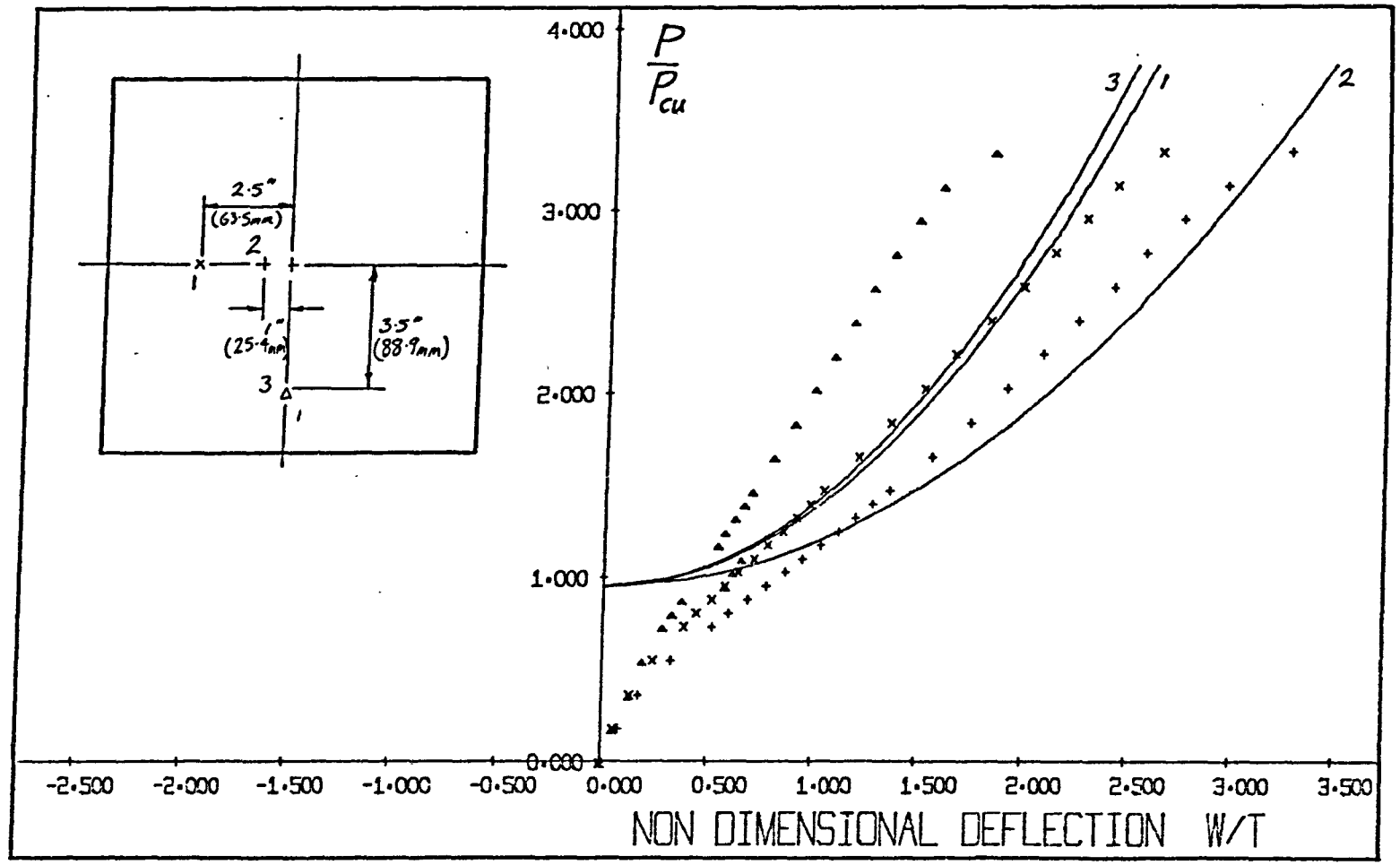

Figure 5.13 Out-of-plane deflections of a square plate $\frac{c}{b} = 0.4$

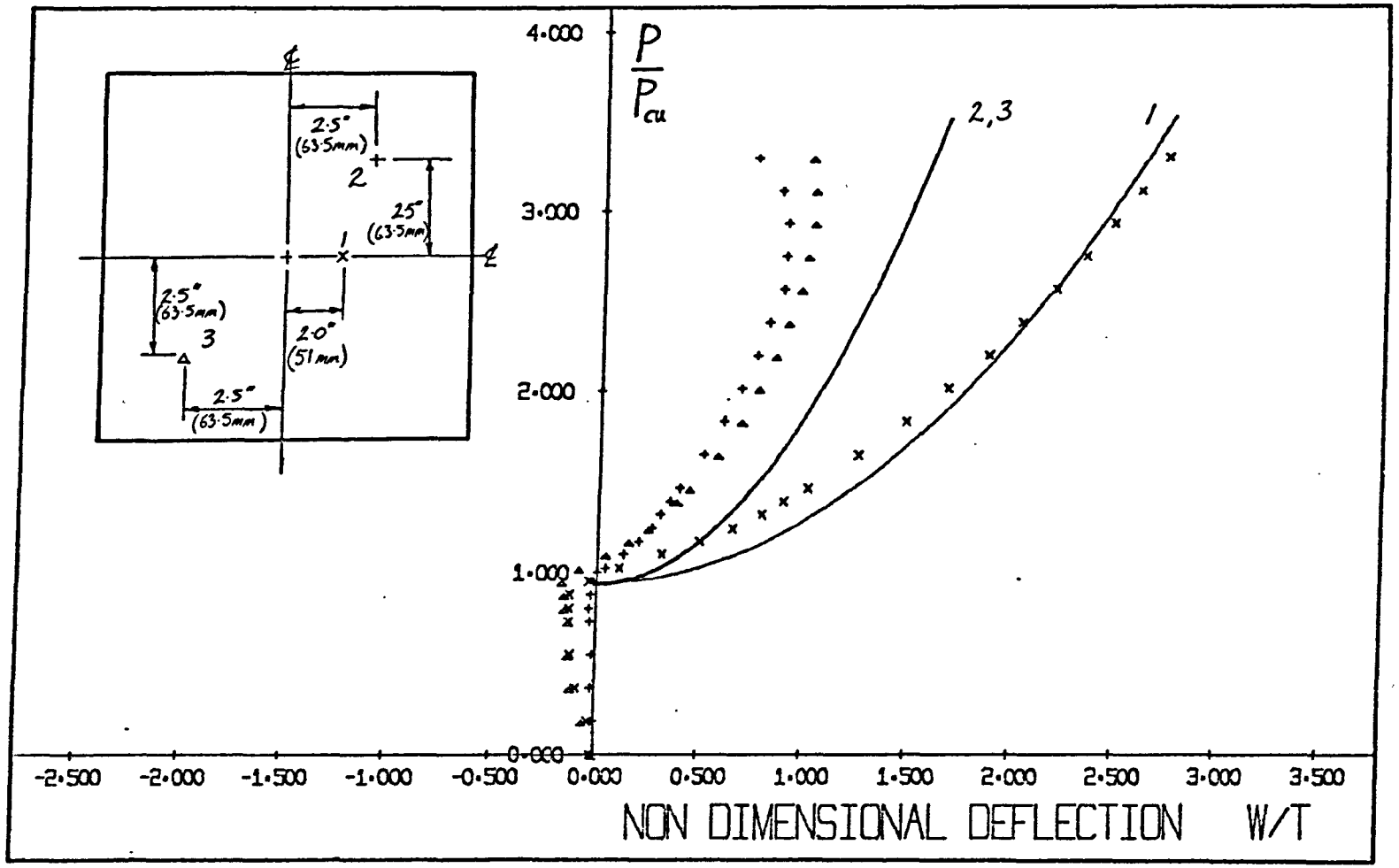

Figure 5.14 Out-of-plane deflections of a square plate $\frac{c}{b} = 0.5$

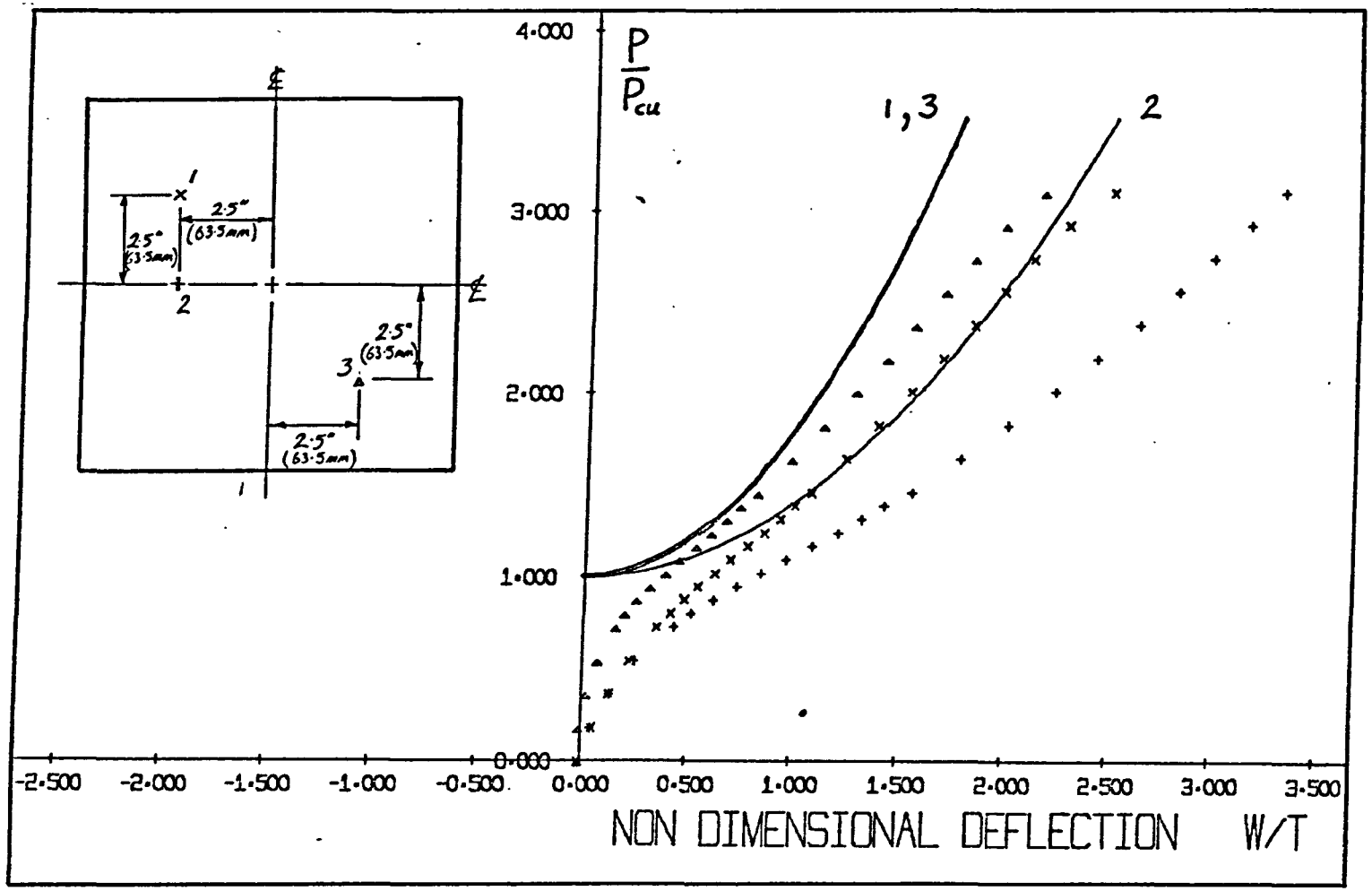

Figure 5.15 Out-of-plane deflections of a square plate $\frac{c}{b} = 0.6$

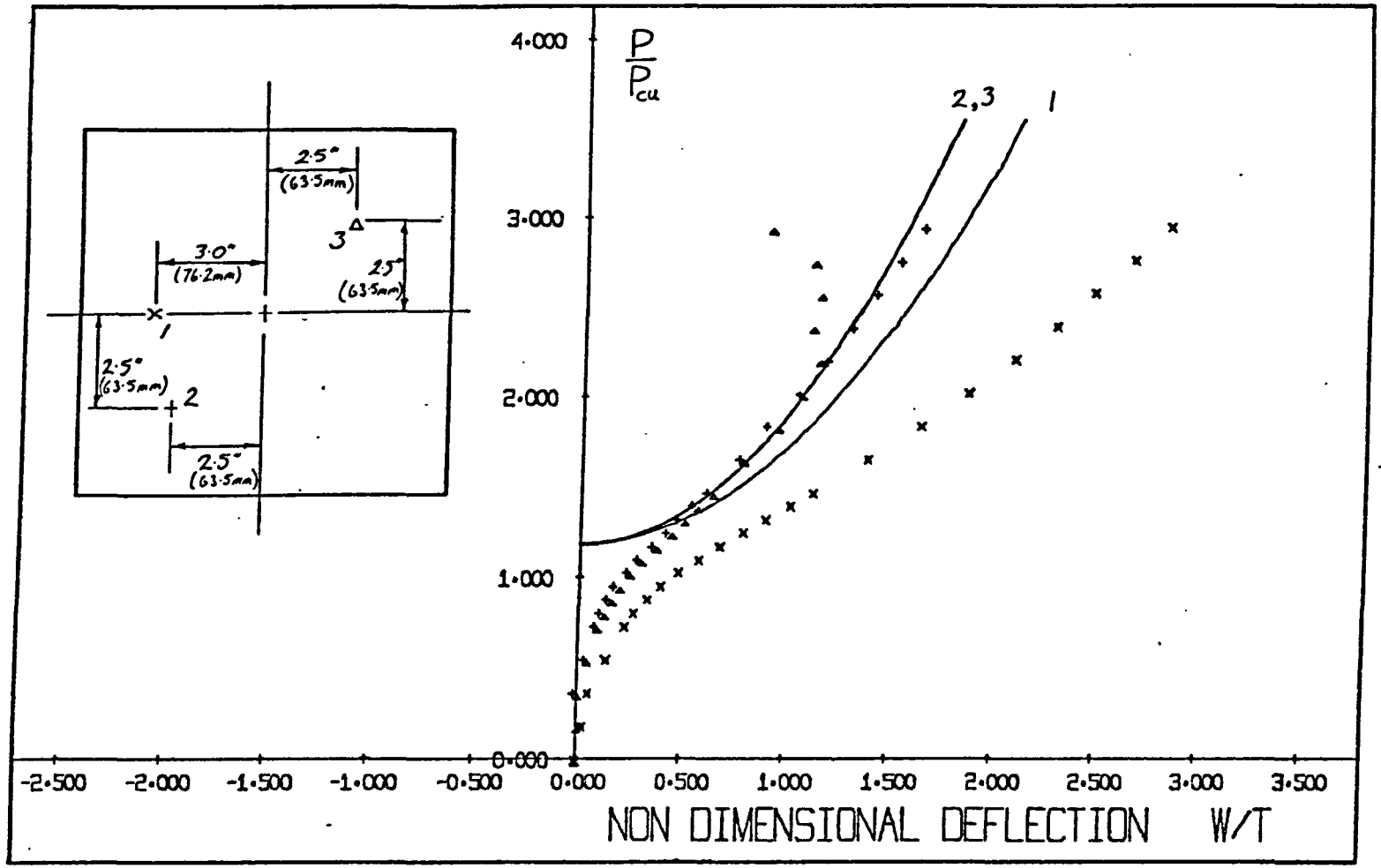

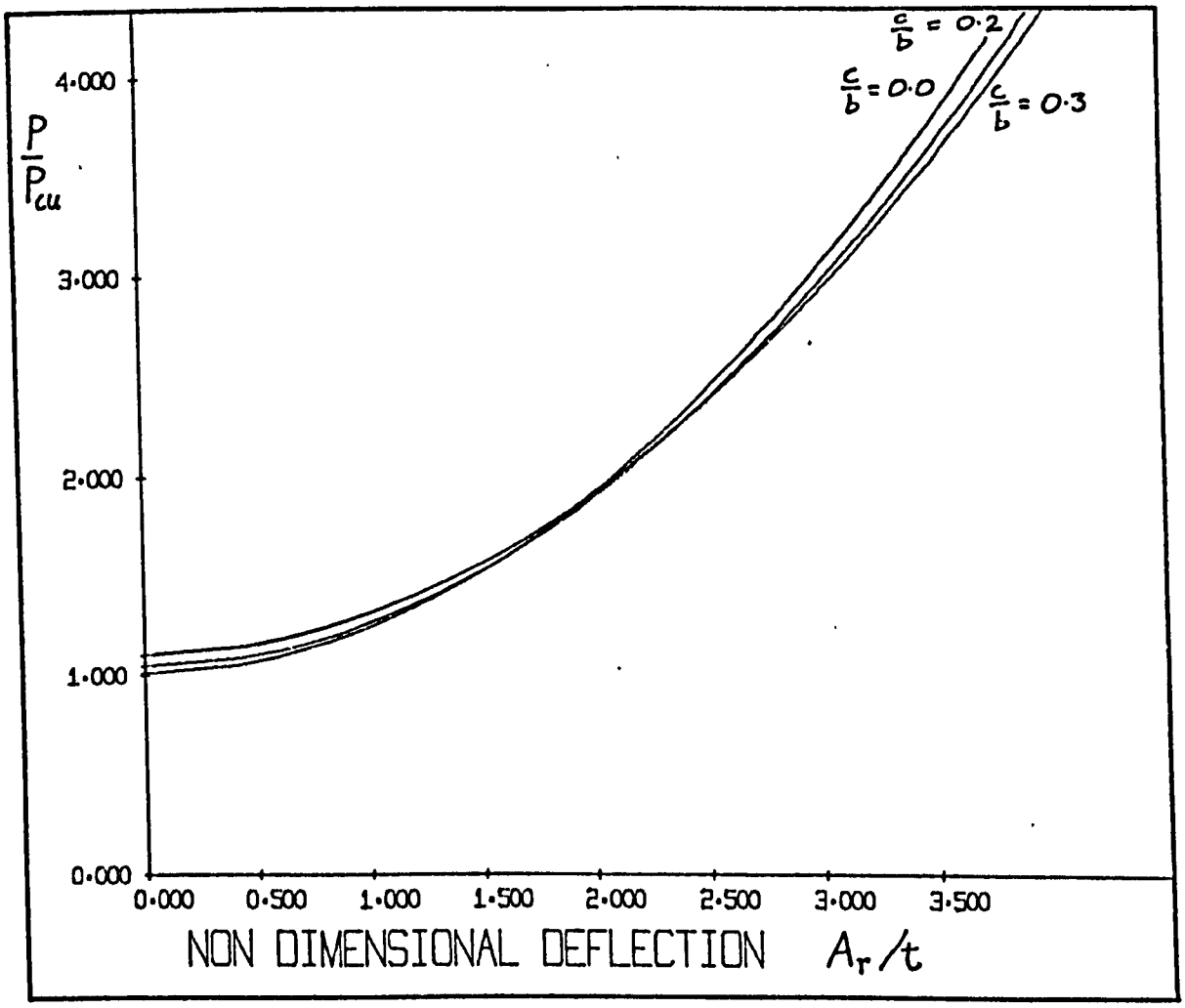

FIGURE 5.16 THEORETICAL LOAD - OUT OF PLANE DEFLECTION BEHAVIOUR OF SIMPLY SUPPORTED RECTANGULAR PLATES BUCKLED WITH TWO HALF WAVES

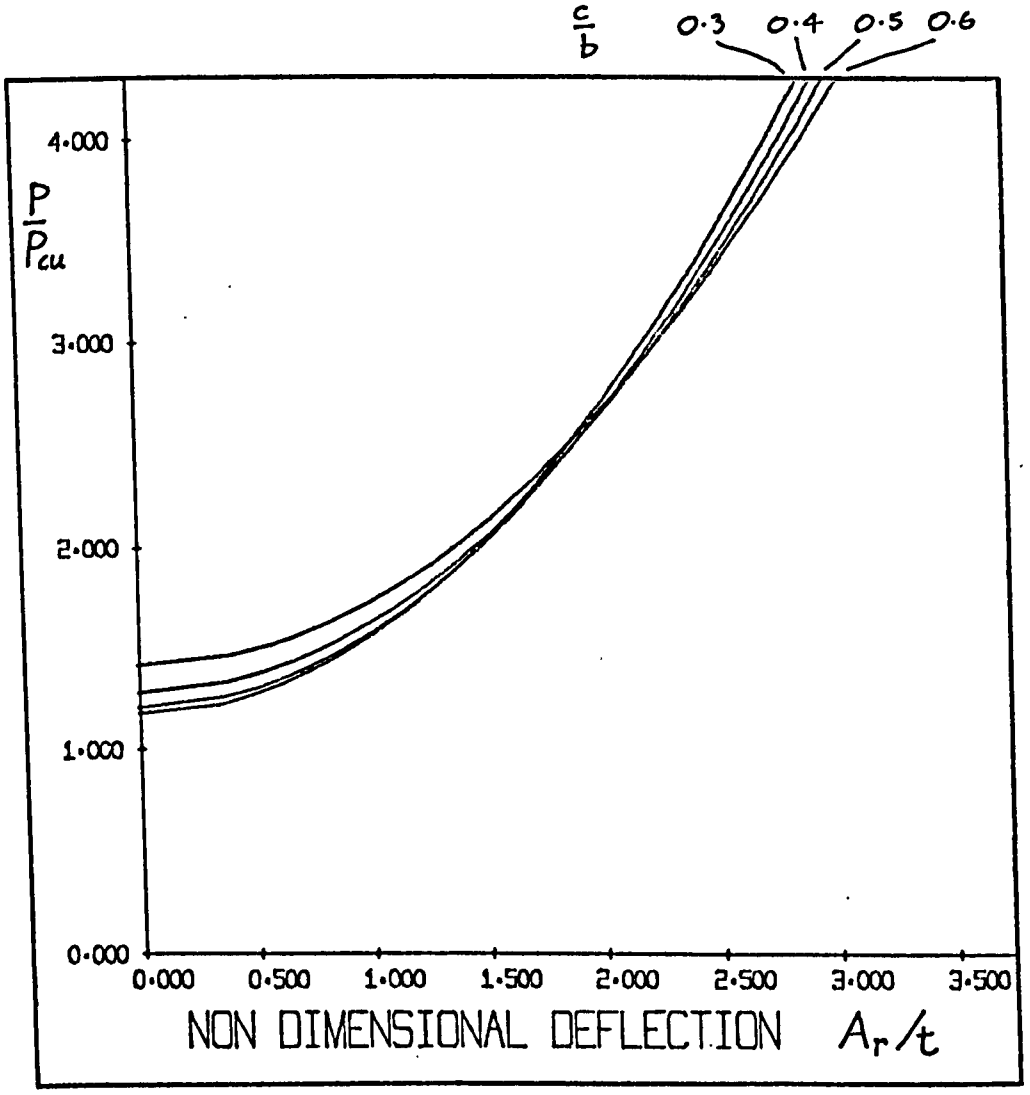

FIGURE 5.17 THEORETICAL LOAD - OUT OF PLANE DEFLECTION BEHAVIOUR OF SIMPLY SUPPORTED RECTANGULAR PLATES BUCKLED WITH THREE HALF WAVES

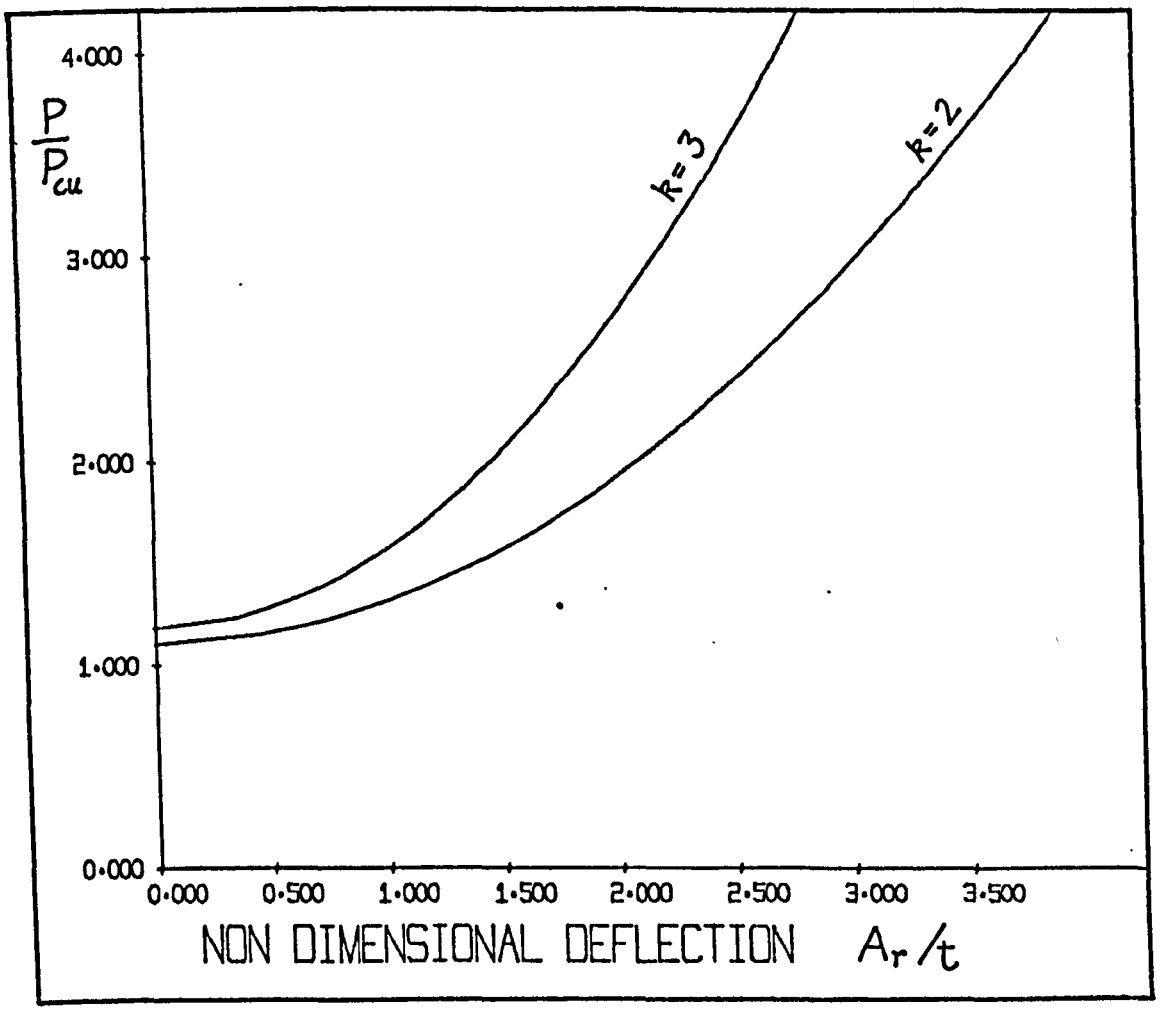

FIGURE 5.18 LOAD - OUT OF PLANE DEFLECTION BEHAVIOUR OF A SIMPLY SUPPORTED RECTANGULAR PLATE WITH A HOLE OF DIAMETER 0·3 x PLATE WIDTH

k = NUMBER OF HALFWAVES IN THE DIRECTION OF LOADING

Figure 5.19 Out-of-plane deflections of a rectangular plate $\frac{c}{b} = 0.0$

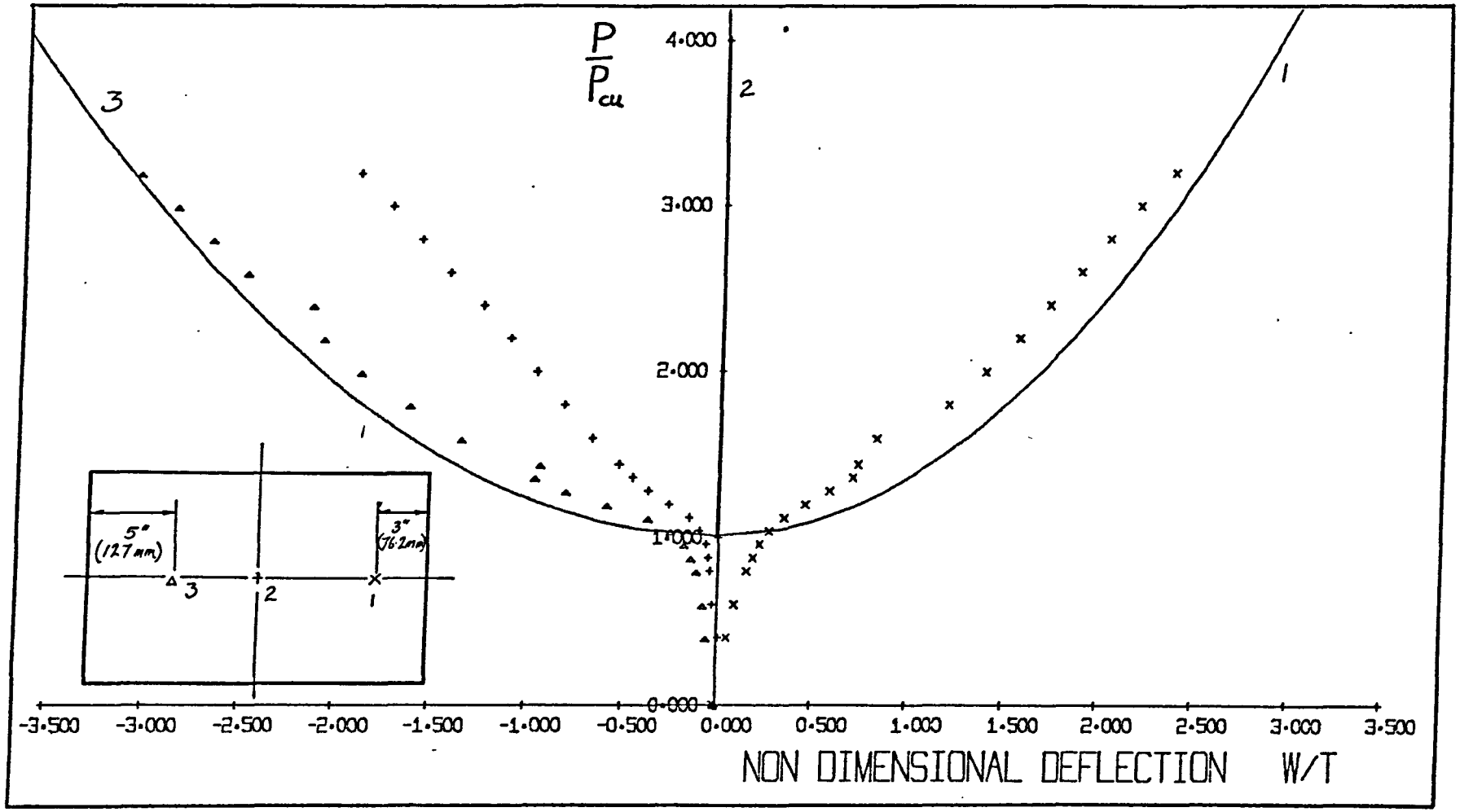

Figure 5.20 Out-of-plane deflections of a rectangular plate $\frac{c}{b} = 0.1$

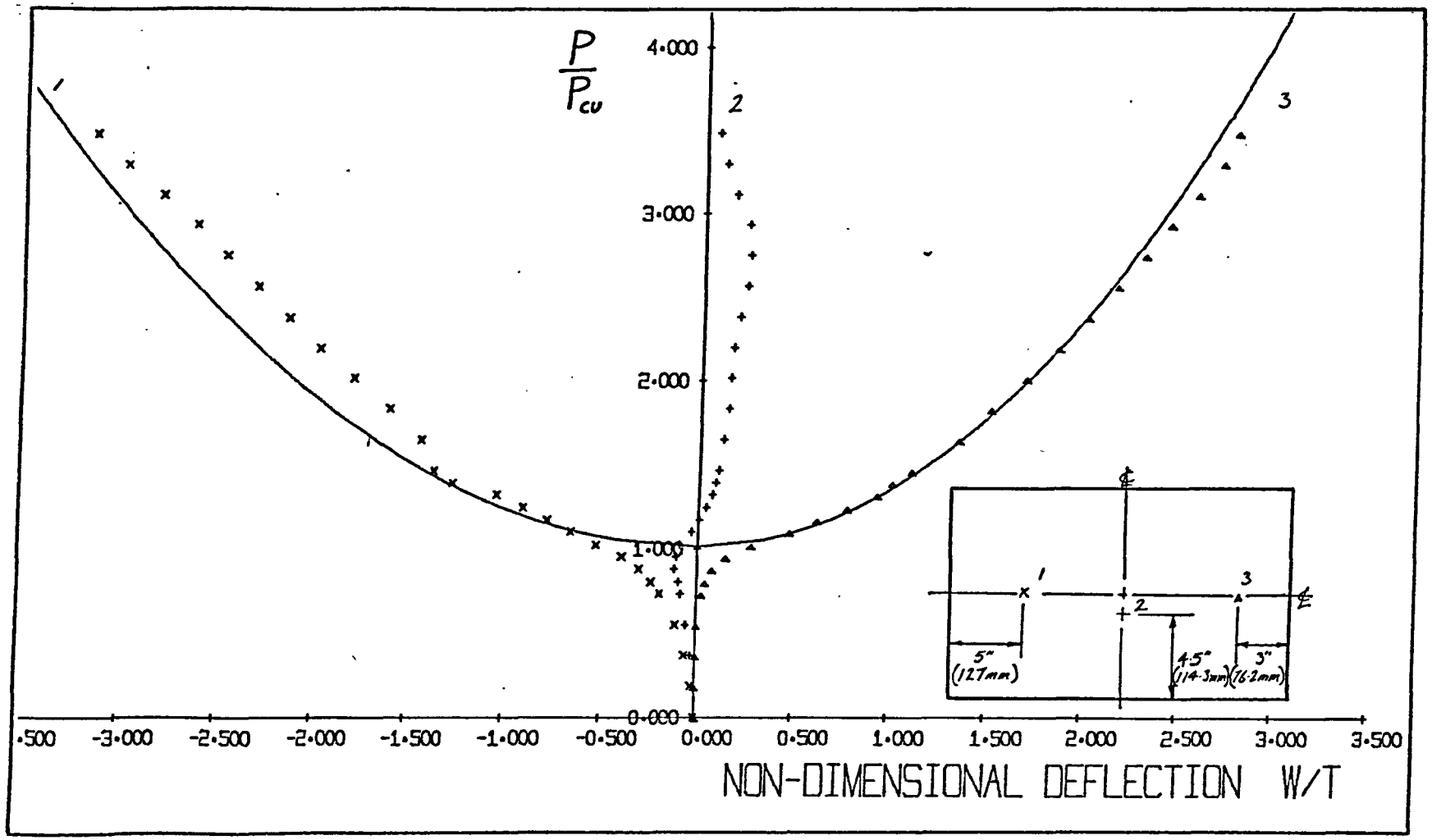

Figure 5.21 Out-of-plane deflections of a rectangular plate $\frac{c}{b} = 0.1$

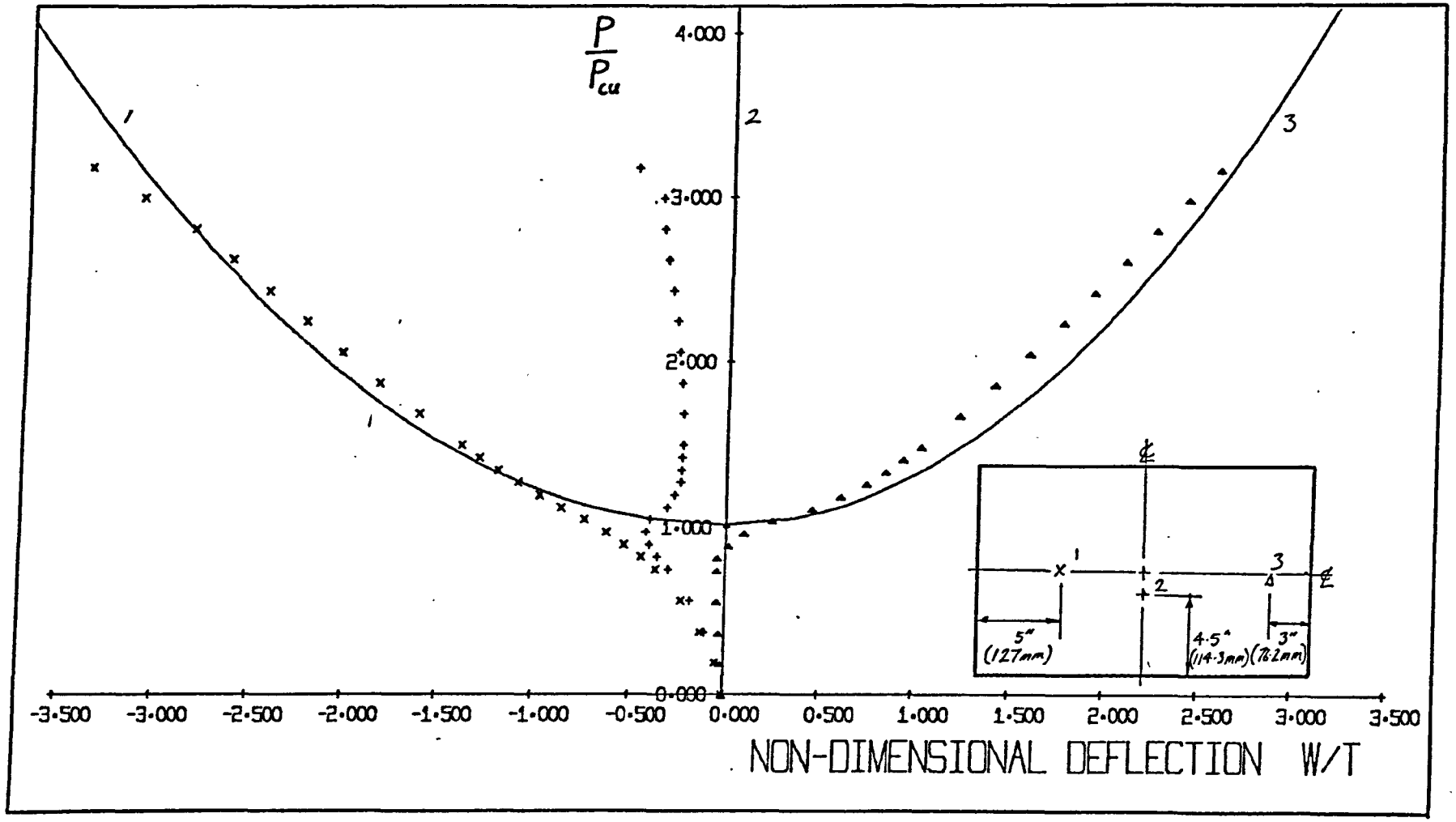

Figure 5.22 Out-of-plane deflections of a rectangular plate $\frac{c}{b} = 0.2$

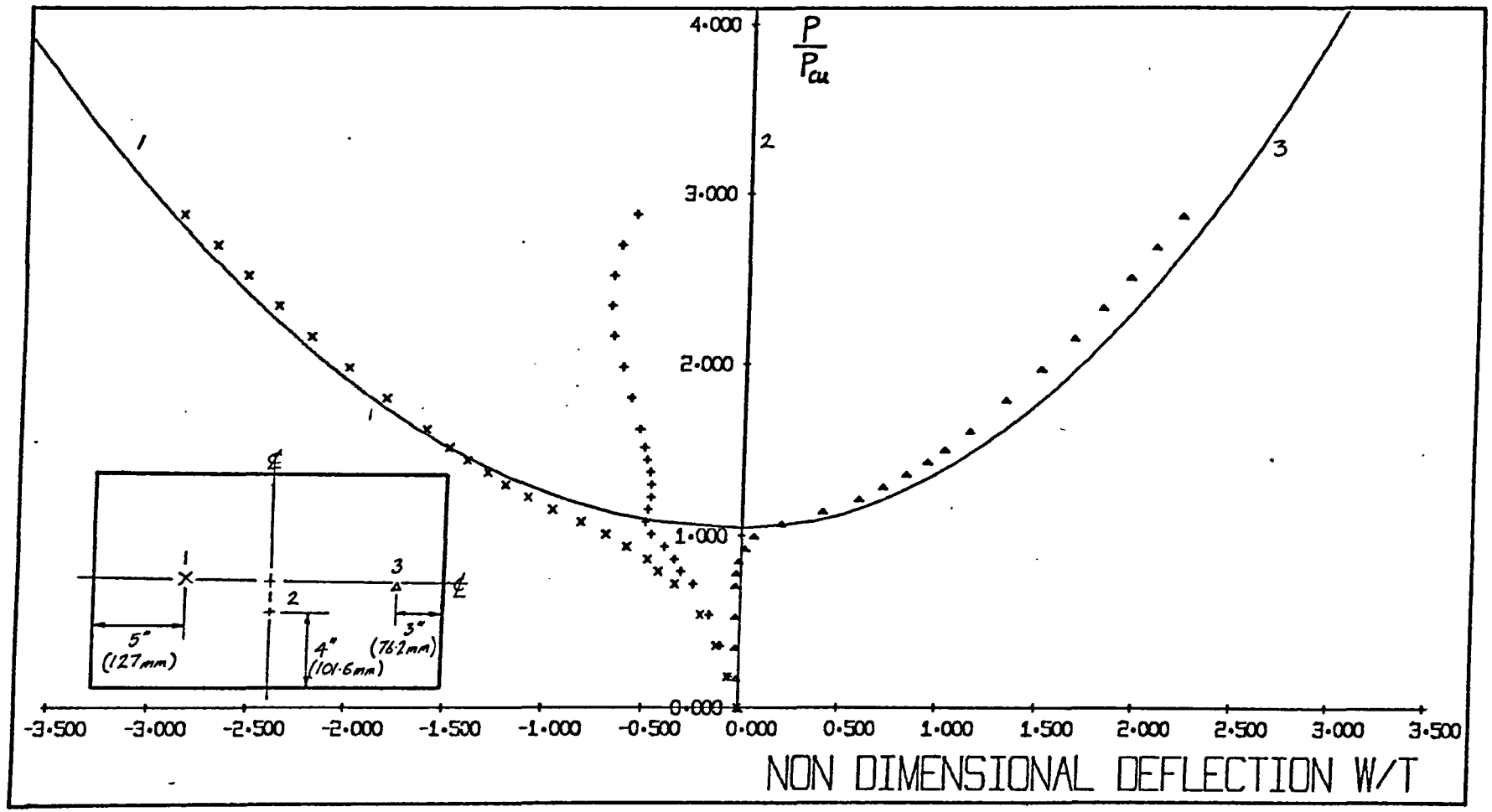

Figure 5.23 Out-of-plane deflections of a rectangular plate $\frac{c}{b} = 0.3$

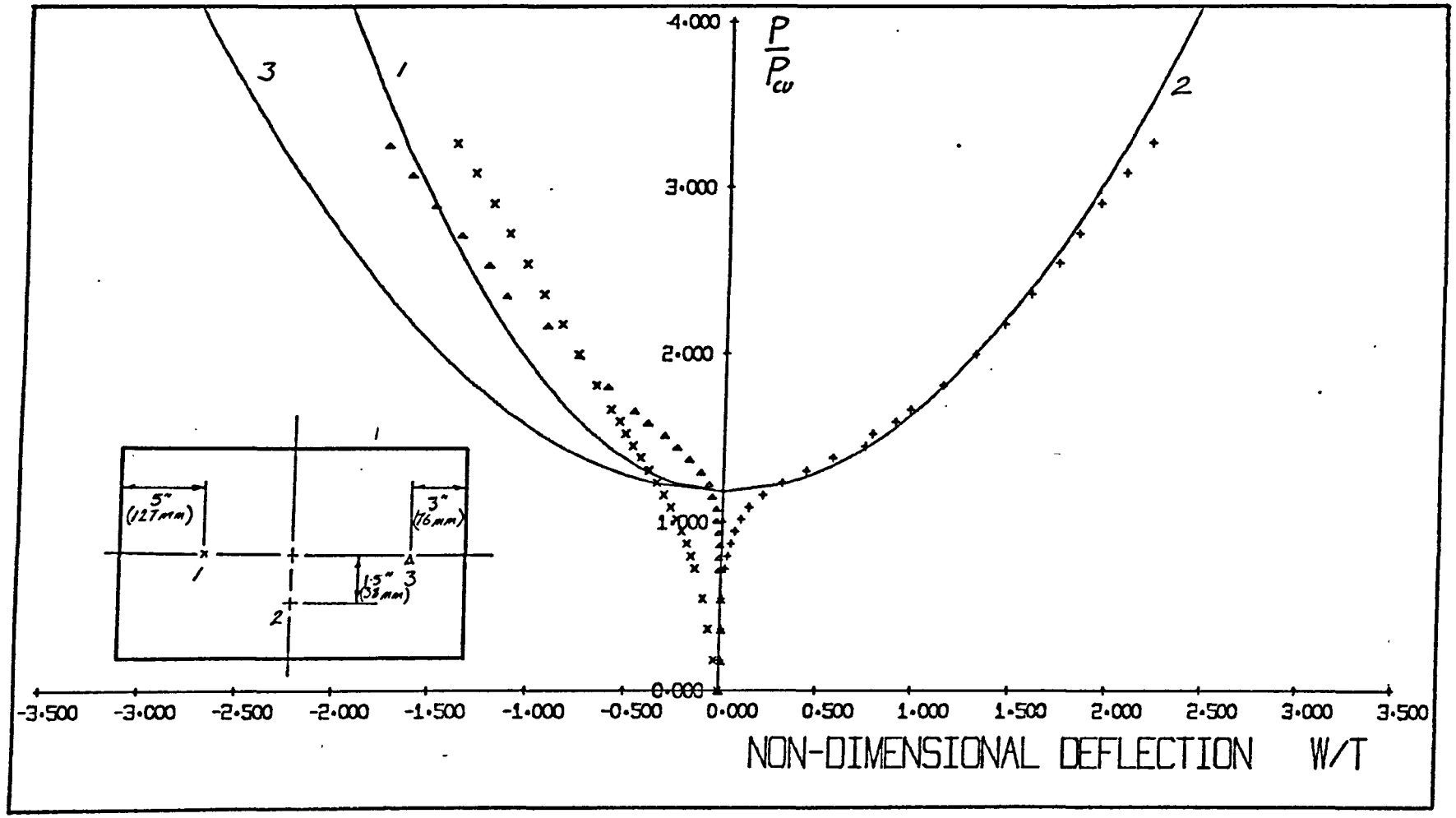

Figure 5.24 Out-of-plane deflections of a rectangular plate $\frac{c}{b} = 0.4$

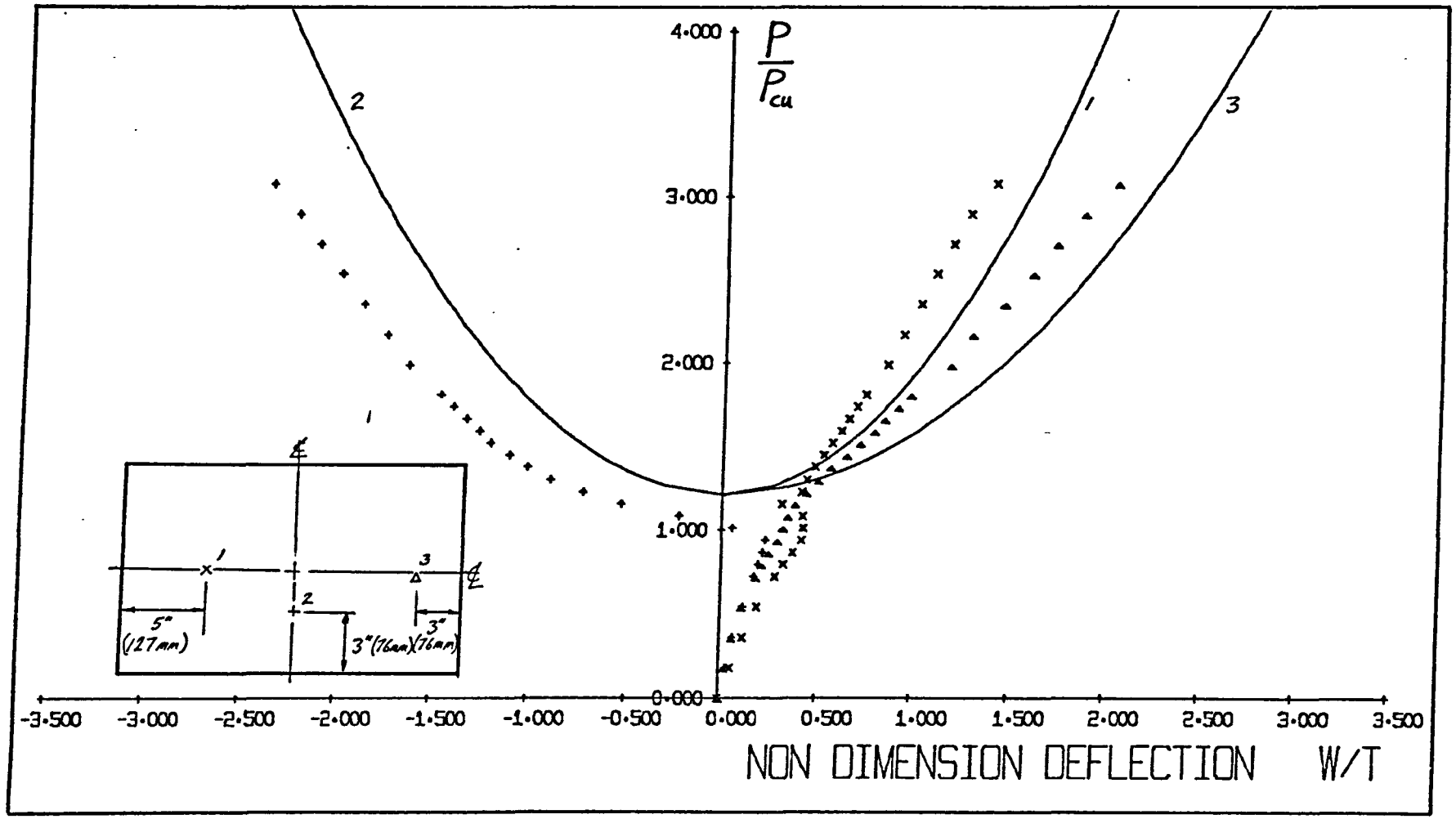

Figure 5.25 Out-of-plane deflections of a rectangular plate $\frac{c}{b} = 0.5$

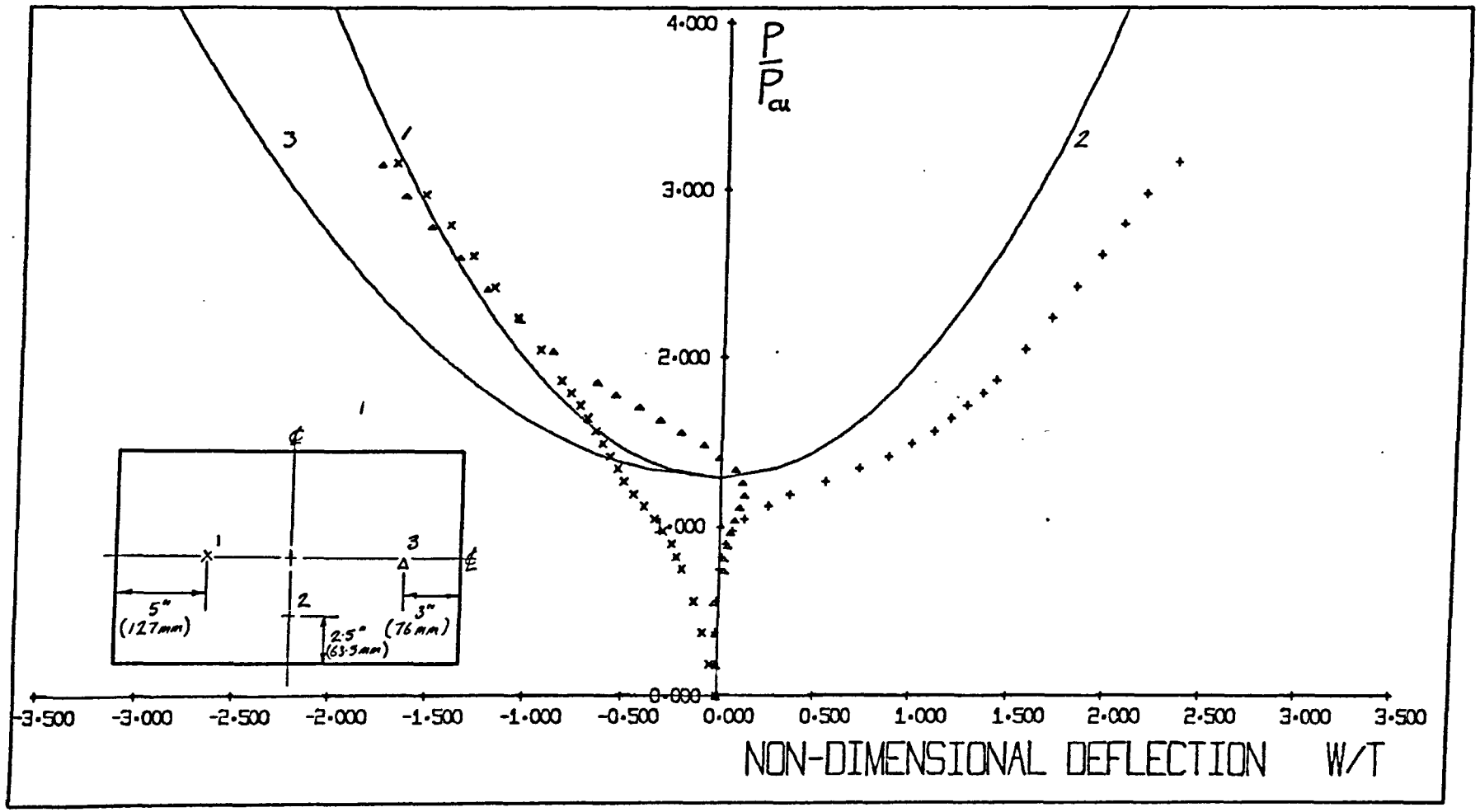

Figure 5.26 Out-of-plane deflections of a rectangular plate $\frac{c}{b} = 0.5$

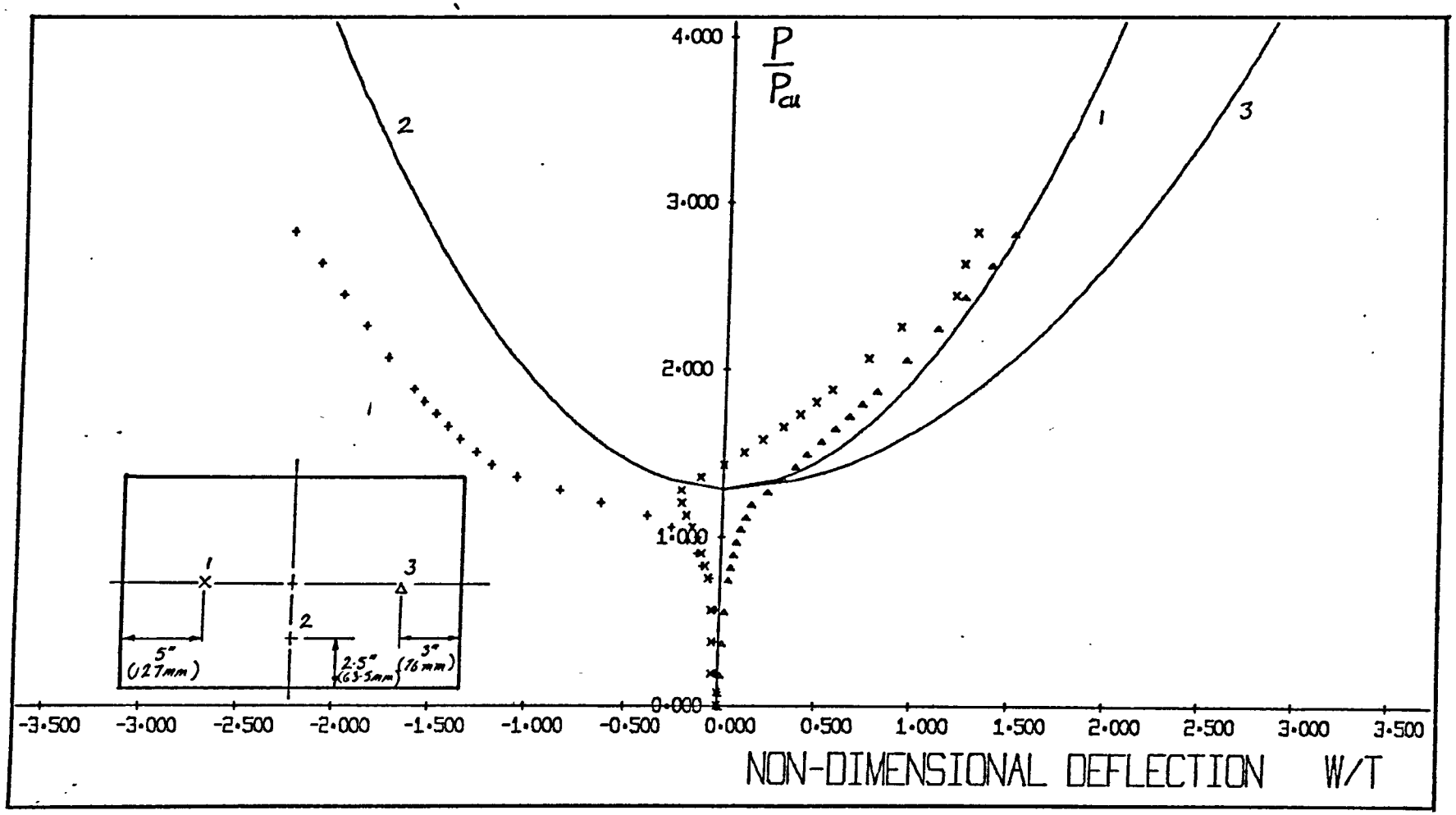

Figure 5.27 Out-of-plane deflections of a rectangular plate $\frac{c}{b} = 0.6$

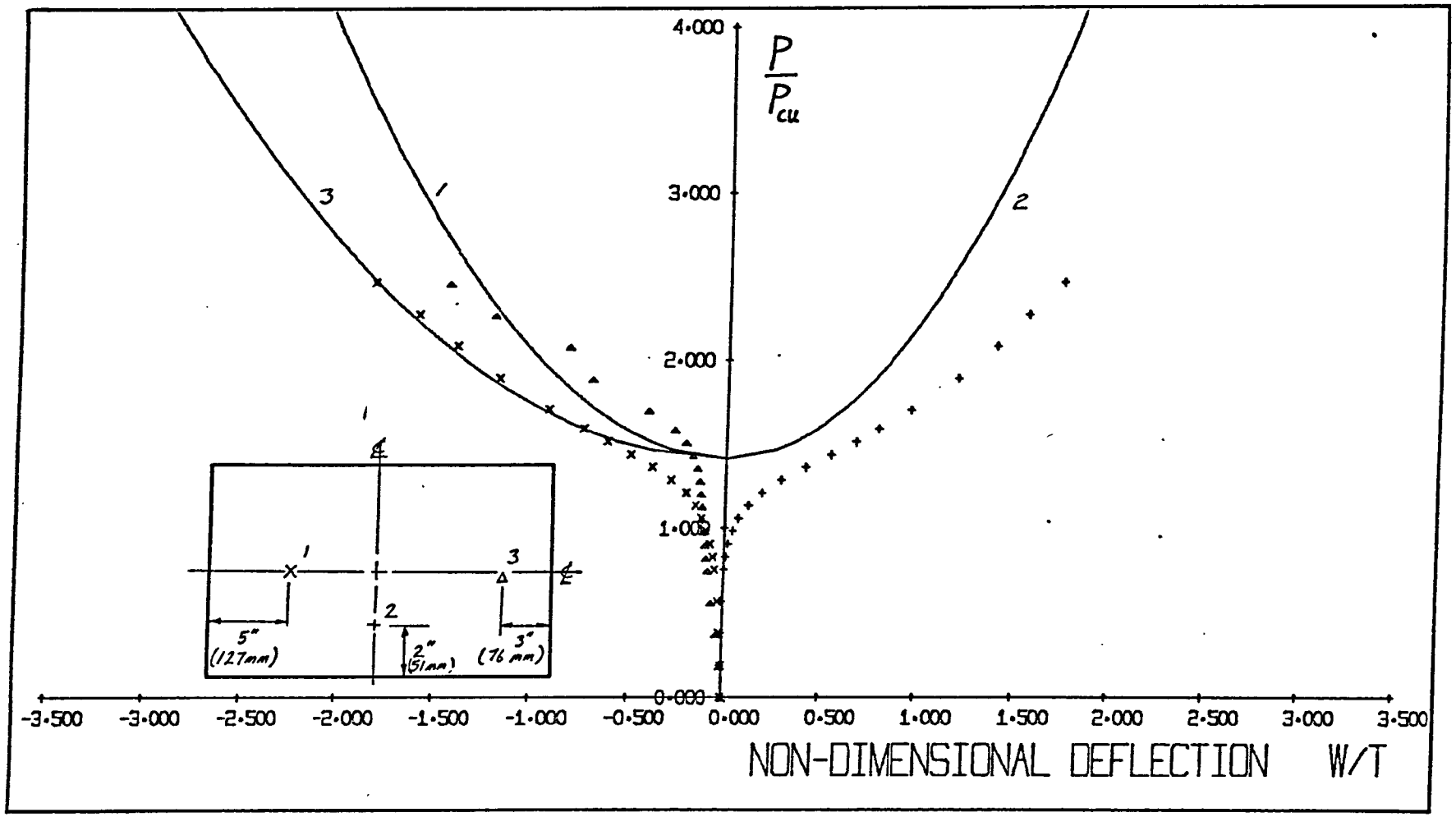

FIGURE 5.28 LOAD - EDGE COMPRESSION BEHAVIOUR OF AN UNPERFORATED PLATE

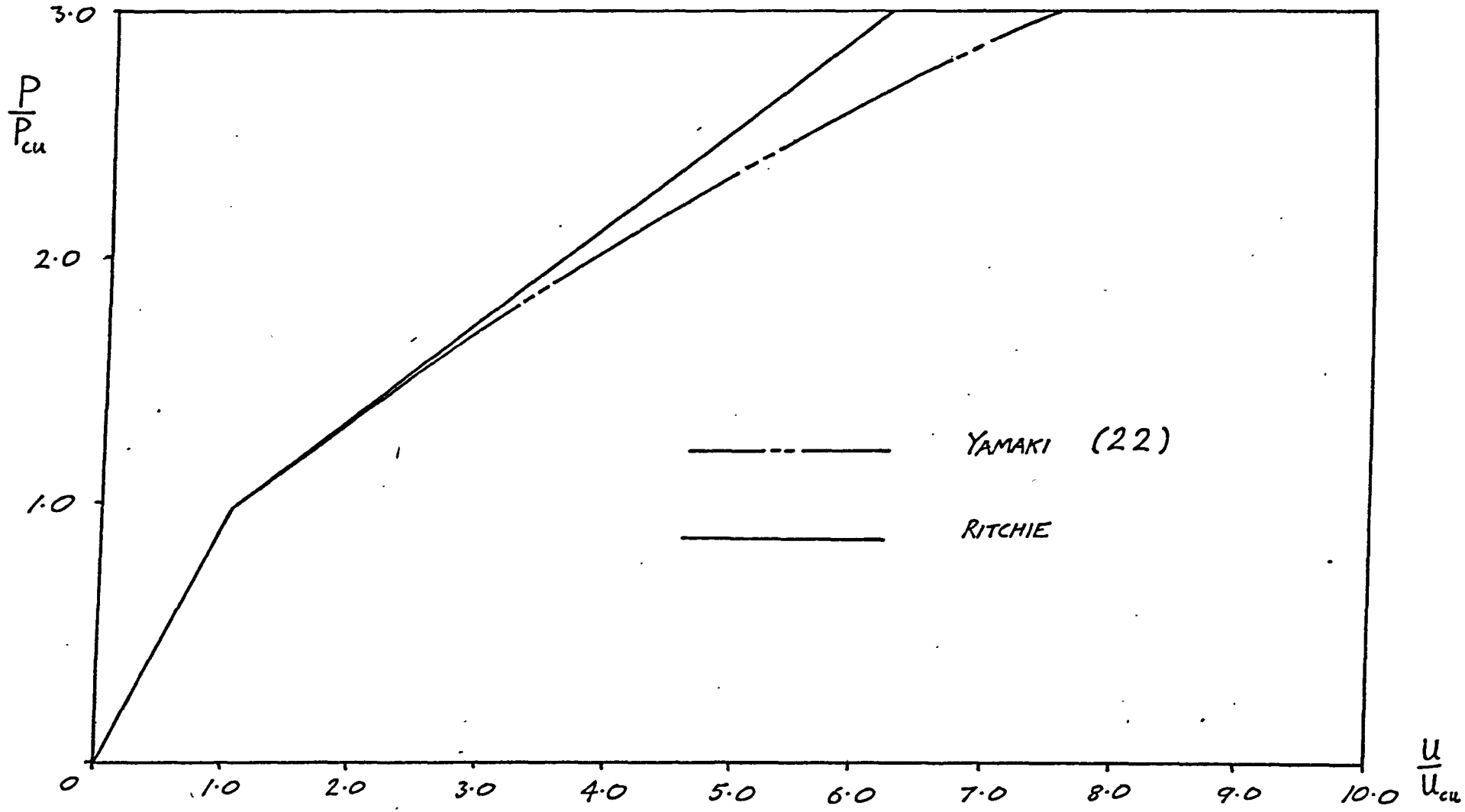

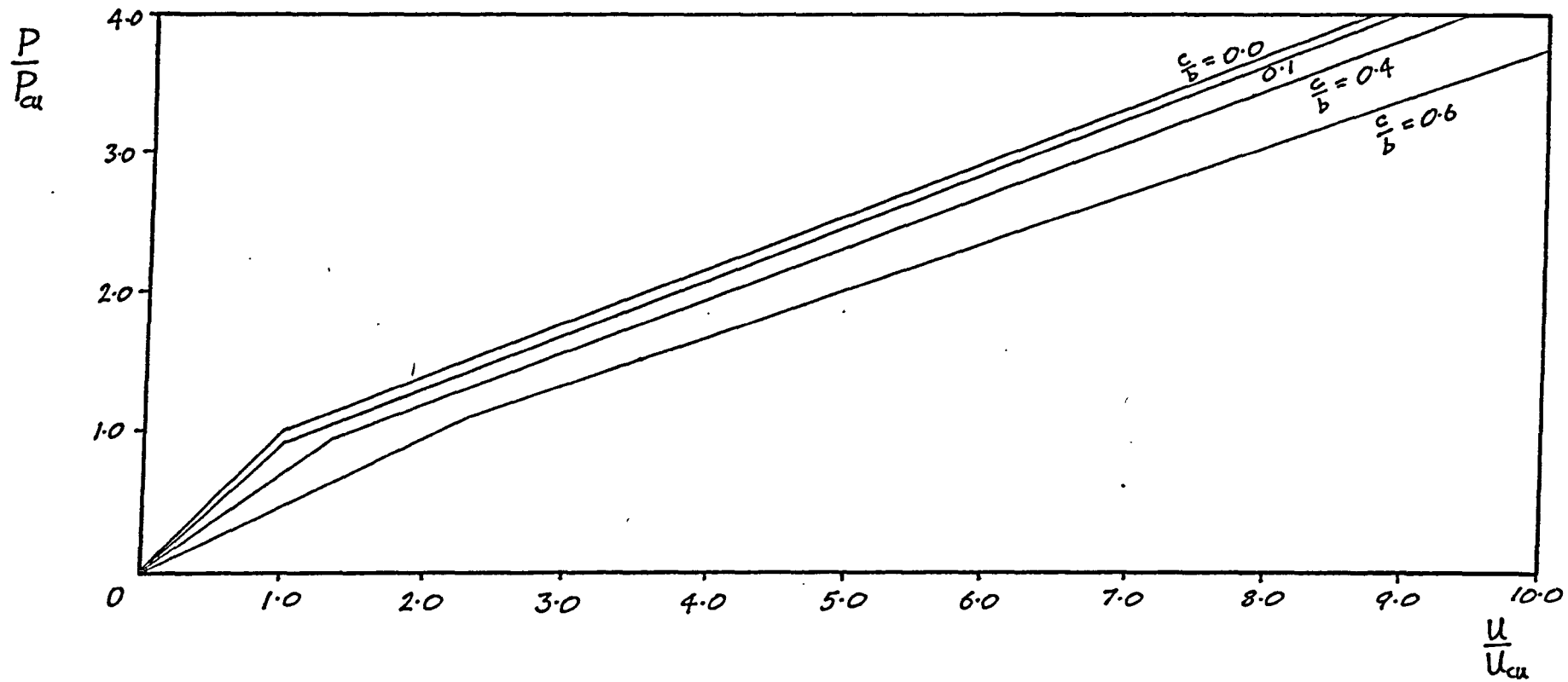

FIGURE 5.29 LOAD - EDGE COMPRESSION BEHAVIOUR OF SQUARE PLATES

FIGURE 5.30 THEORETICAL VARIATION OF THE AXIAL STIFFNESS OF SQUARE PLATES WITH HOLE RADIUS

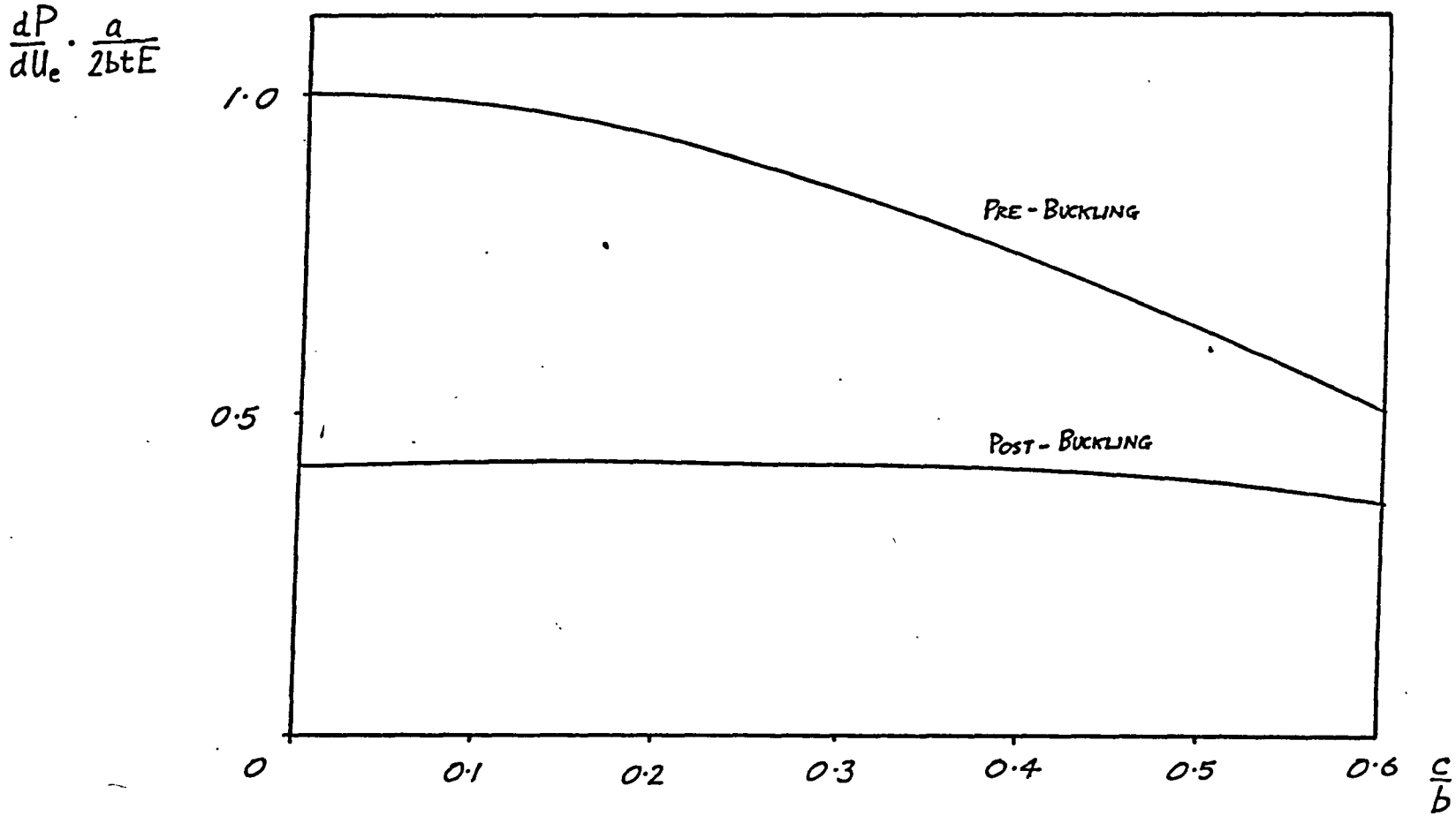

FIGURE 5.31 LOAD EDGE COMPRESSION BEHAVIOUR OF RECTANGULAR PLATES BUCKLED INTO TWO HALF WAVES ie k = 2

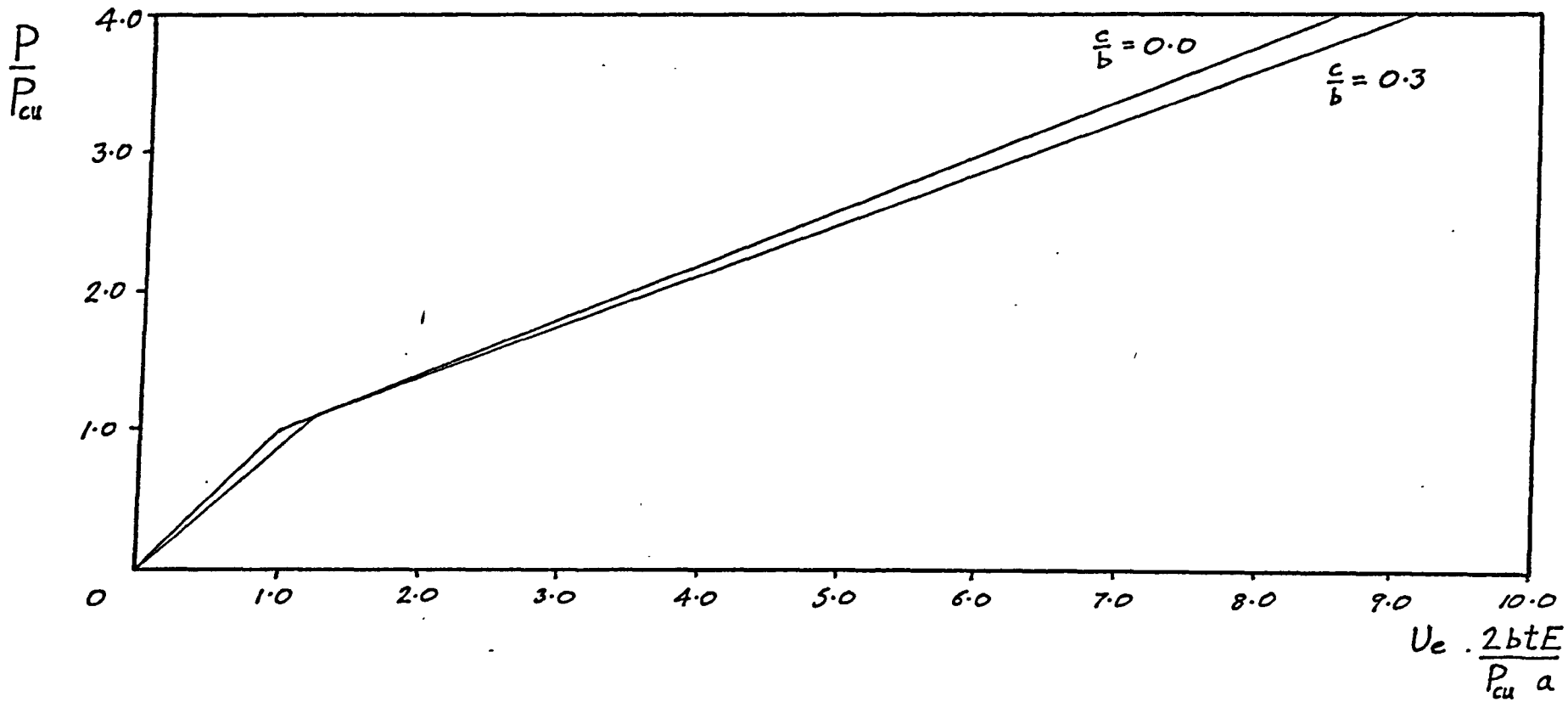

FIGURE 5.32 LOAD - EDGE COMPRESSION BEHAVIOUR OF RECTANGULAR PLATES BUCKLED INTO THREE HALF WAVES ie $k = 3$

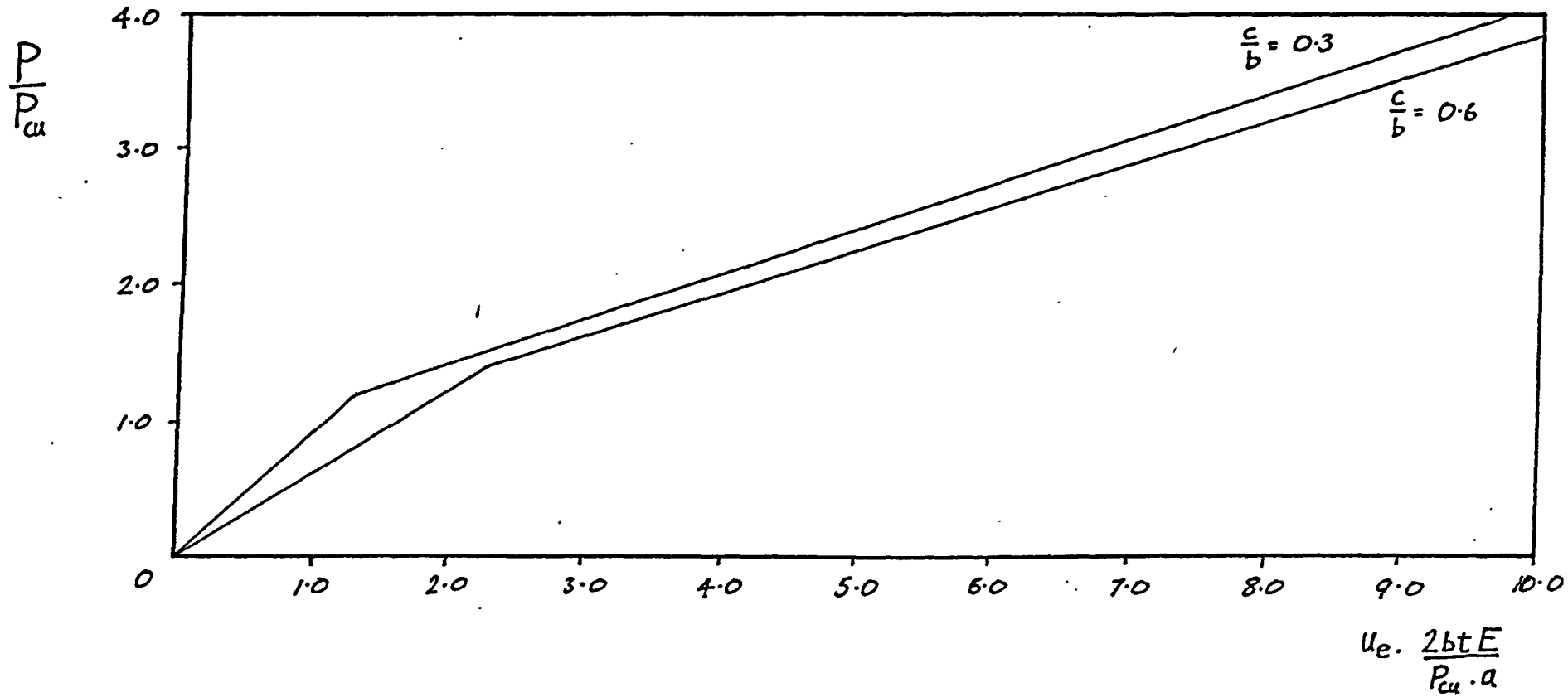

FIGURE 5.33 THEORETICAL VARIATION OF THE AXIAL STIFFNESS OF RECTANGULAR PLATES WITH HOLE RADIUS

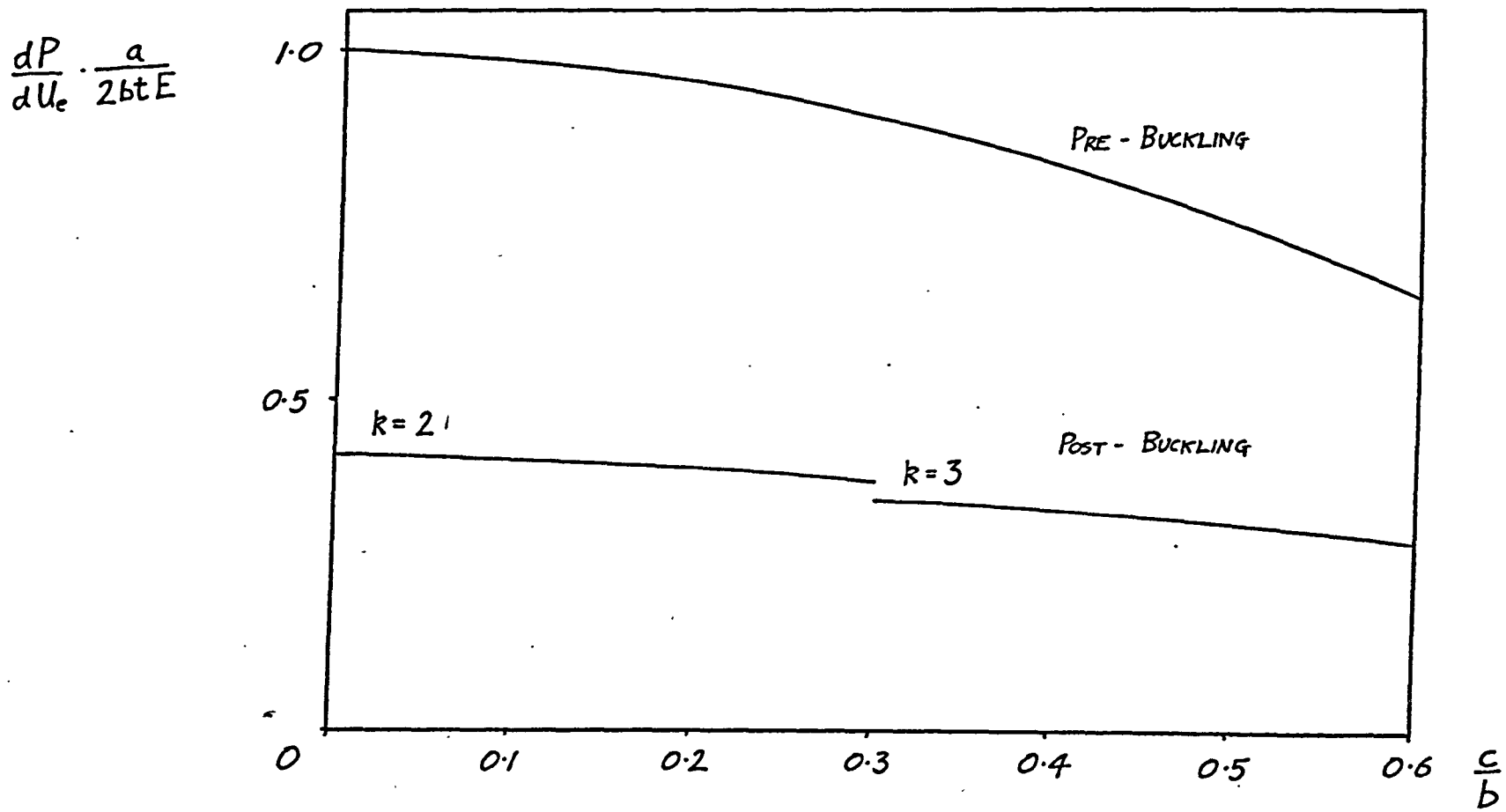

FIGURE 5.34 LOAD - EDGE COMPRESSION BEHAVIOUR OF A RECTANGULAR PLATE WITH A HOLE OF RADIUS $0.3 \times b$

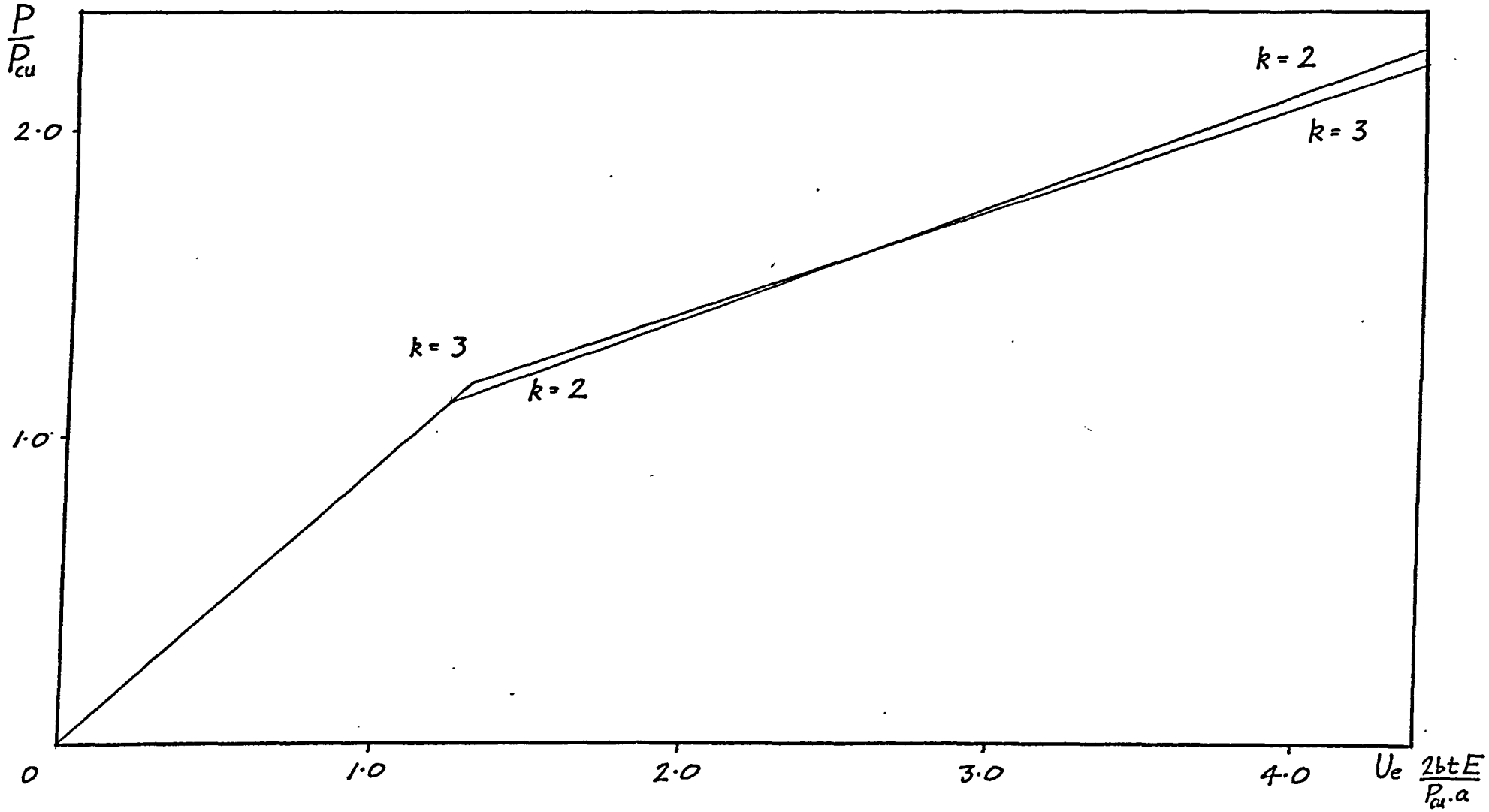

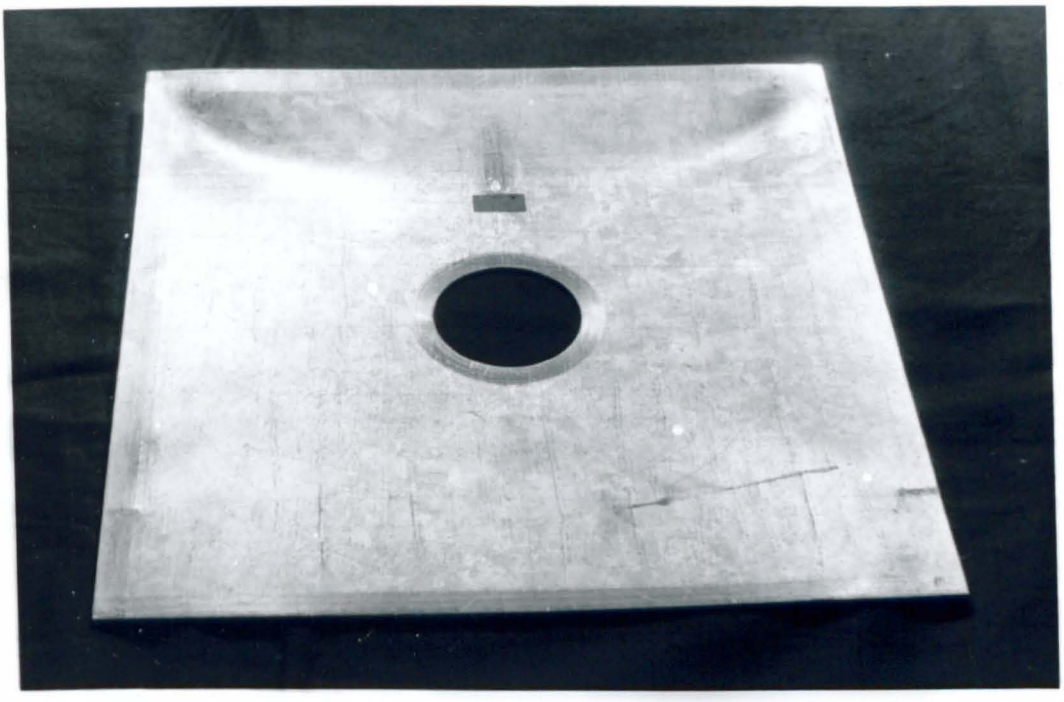

FIGURE 5.35

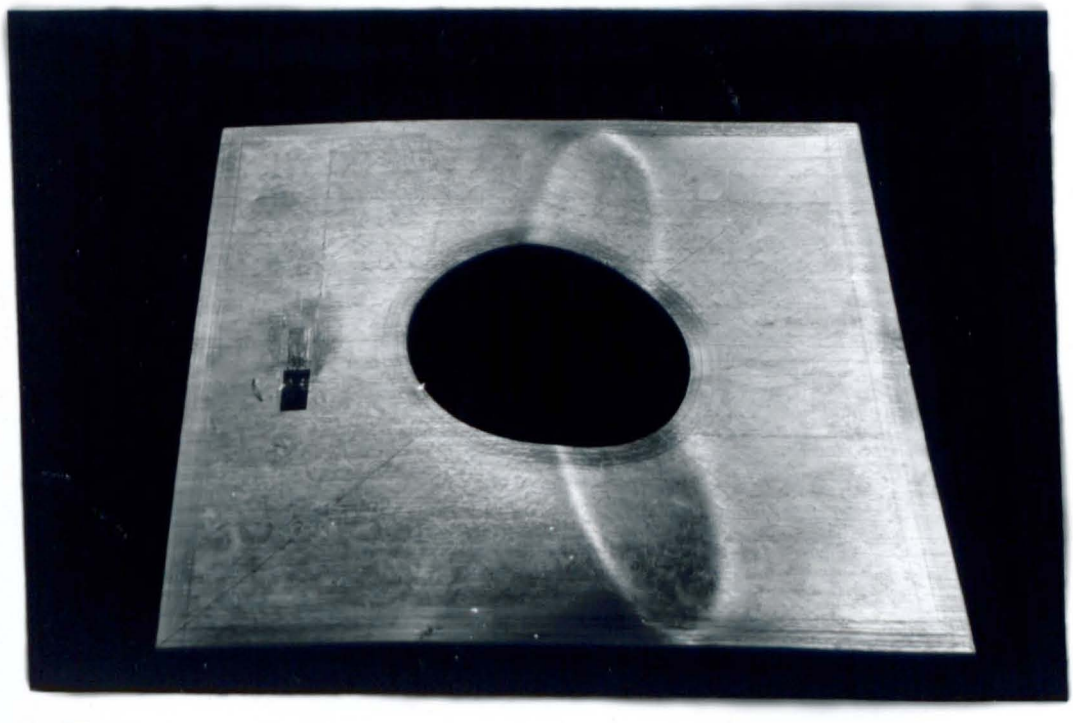

FIGURE 5.36

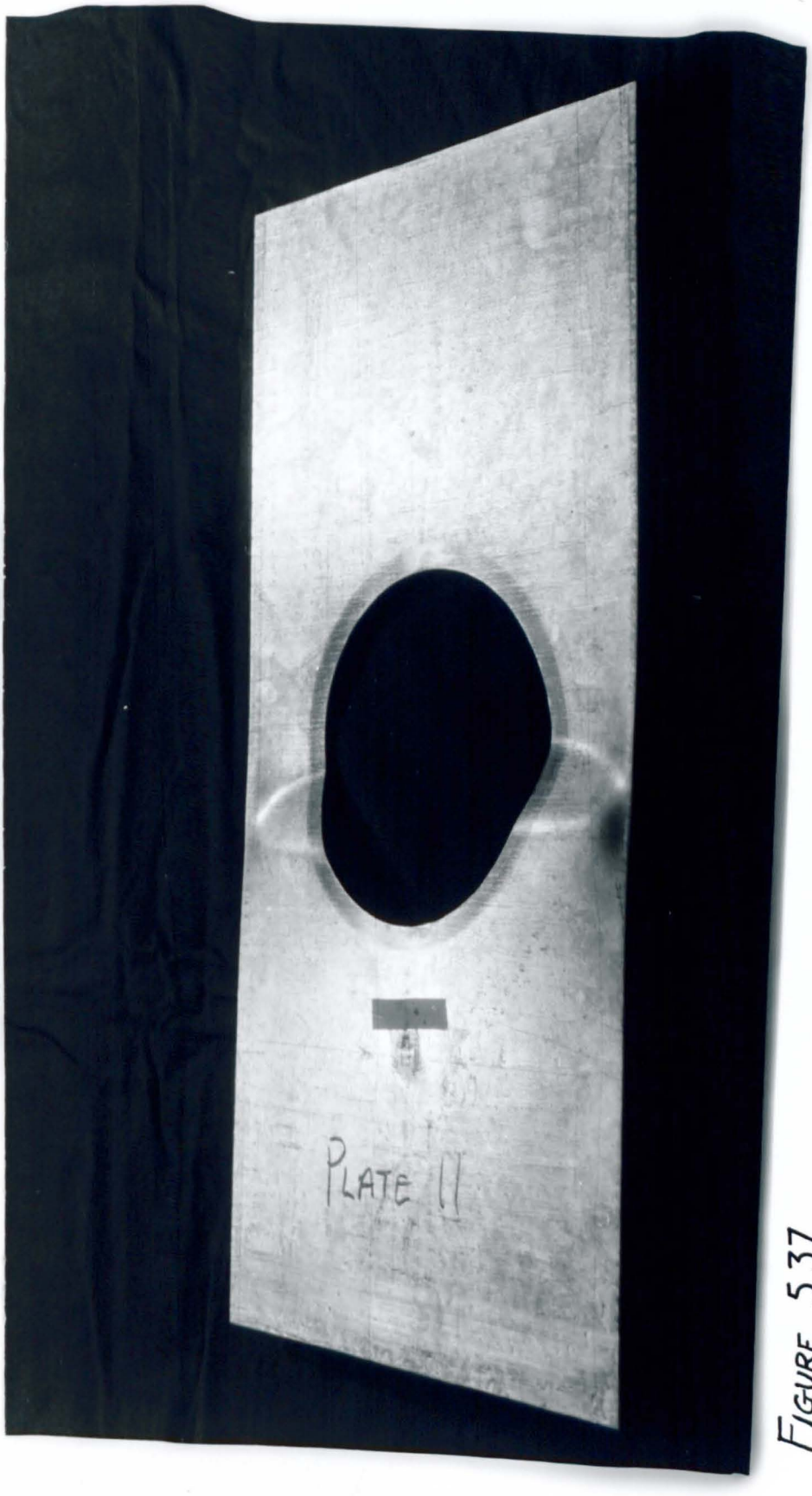

FIGURE 5.37

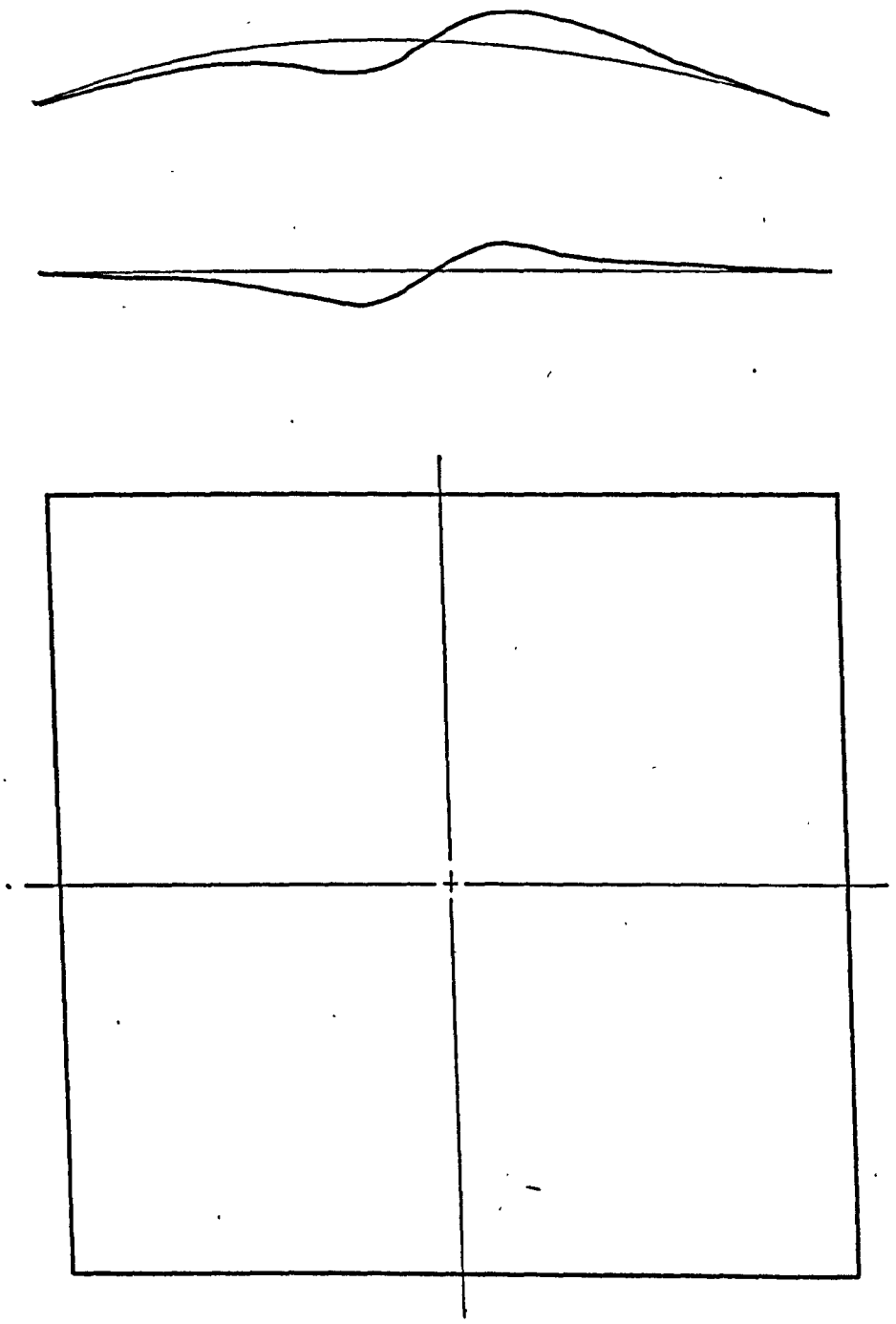

FIGURE 5.38 FAILURE MODES OF A SQUARE PLATE

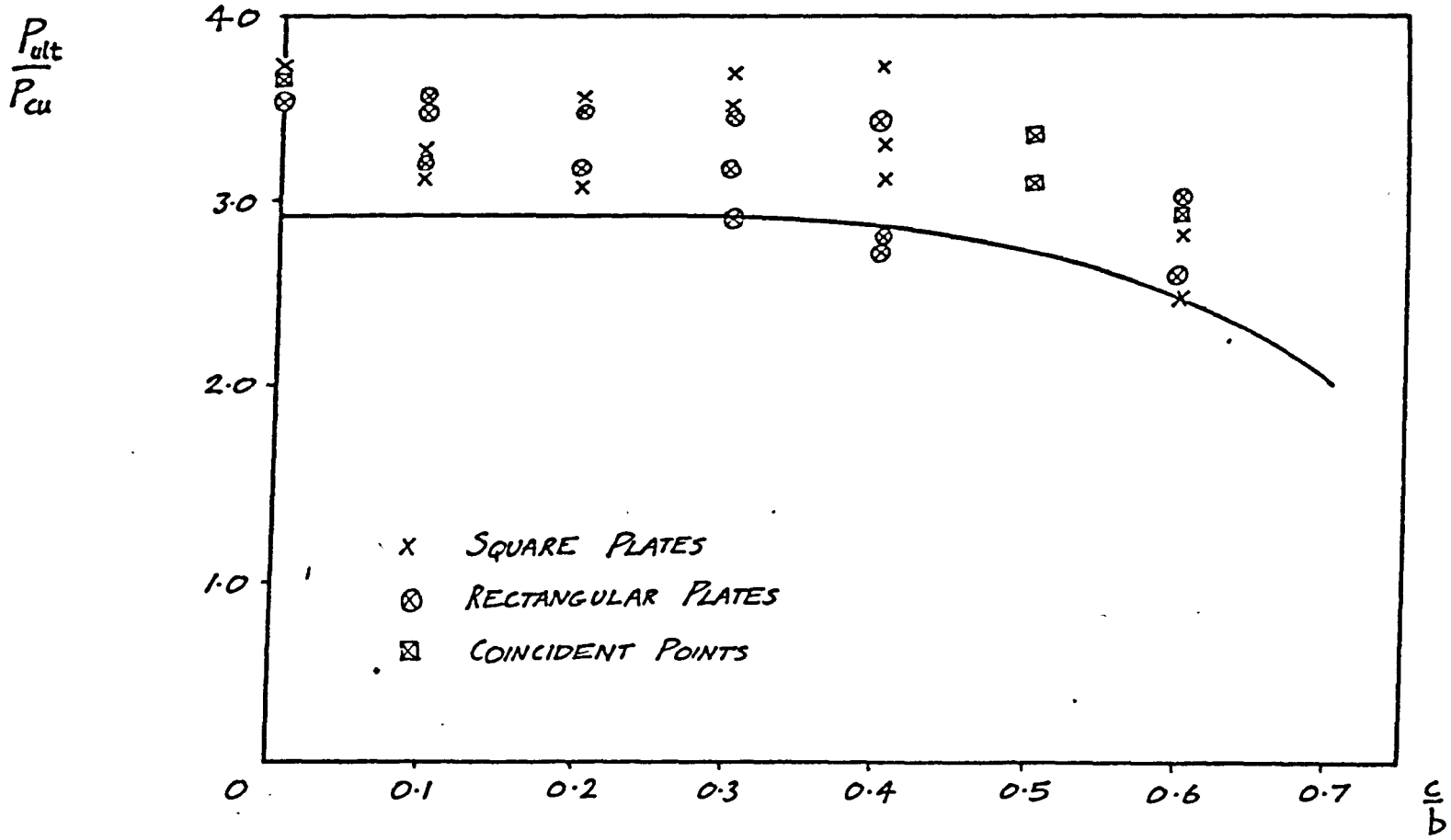

FIGURE 5.39 COMPARISON BETWEEN THEORETICAL AND EXPERIMENTAL ULTIMATE LOADS

For the purpose of comparison of theoretical and experimental results the x and y axes of the plate are taken to pass through the centre of the plate.

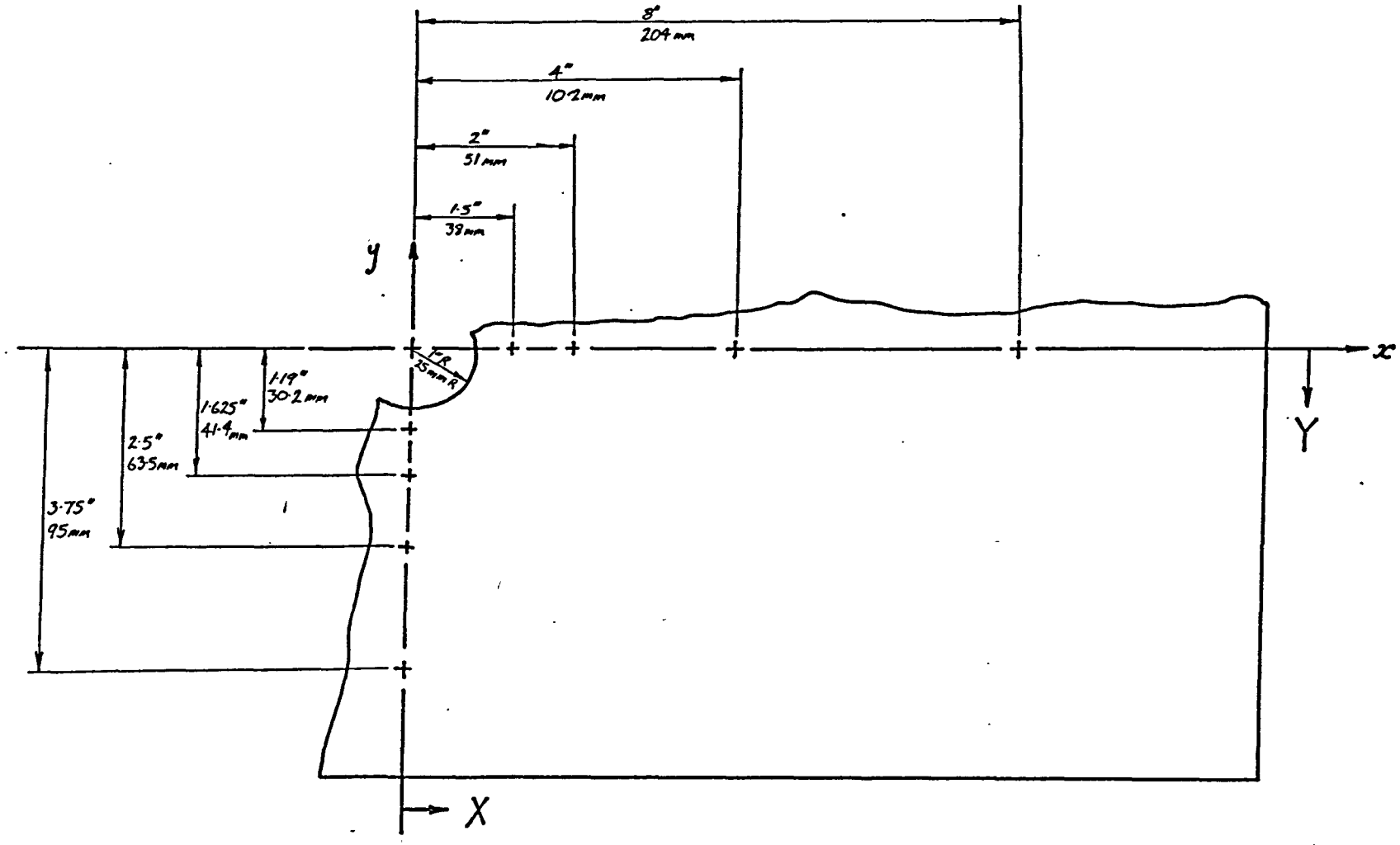

FIGURE 5.40 ARRANGEMENT OF STRAIN GAUGE ROSETTES ON PLATE A

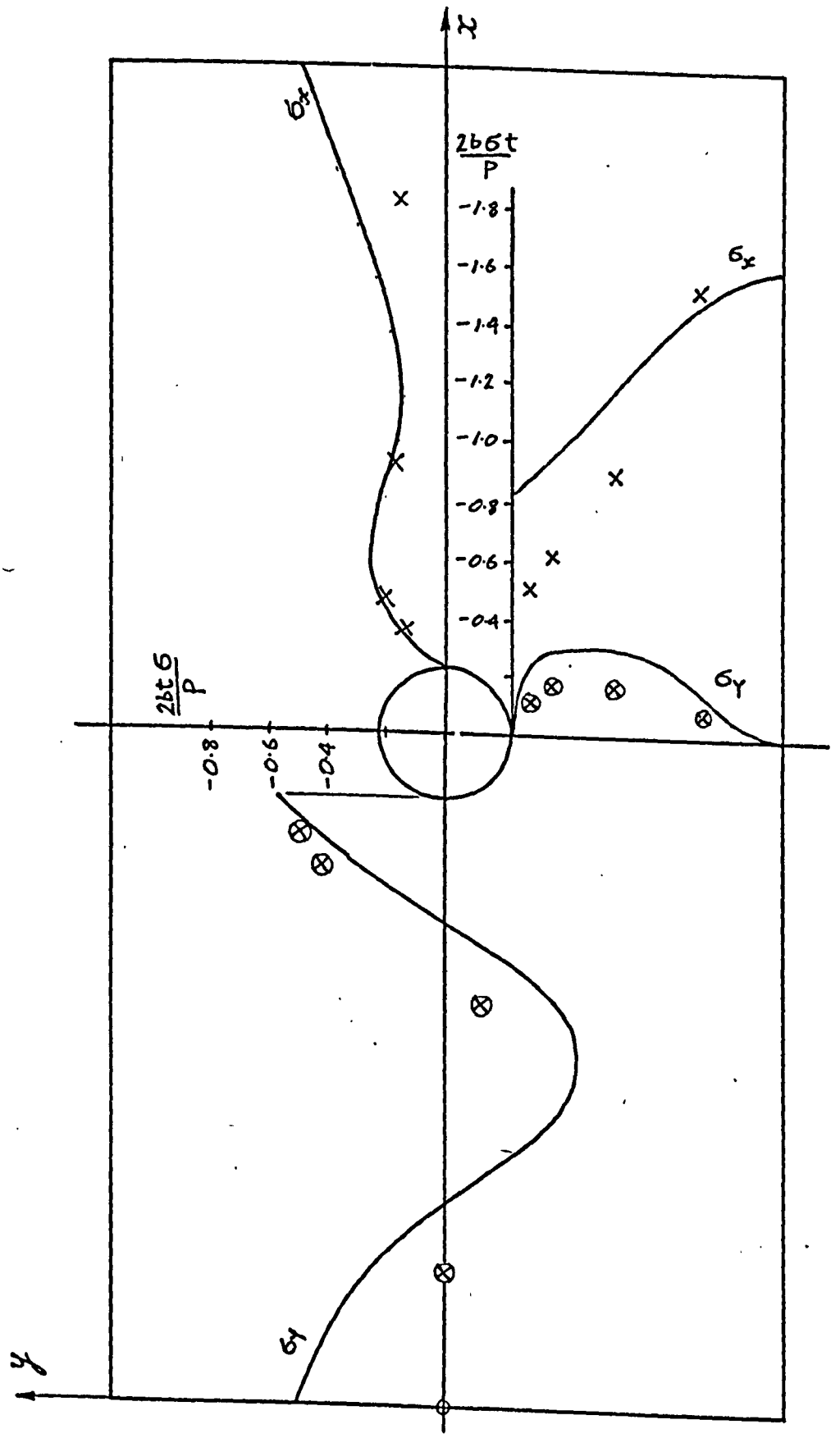

FIGURE 5.41 POST-BUCKLING STRESS DISTRIBUTION IN PLATE A WHEN $P = 2.P_{cu}$

EXPERIMENTAL RESULTS: X - σ_x , ⊗ - σ_y

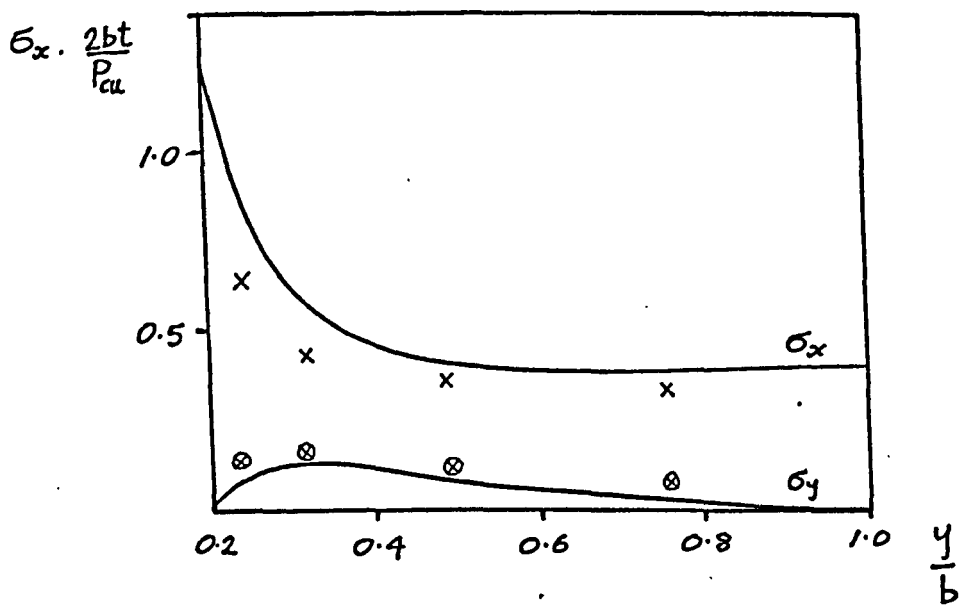

FIGURE 5.42 STRESSES AT THE MINIMUM SECTION. $P = 0.37.\ P_{cu}$

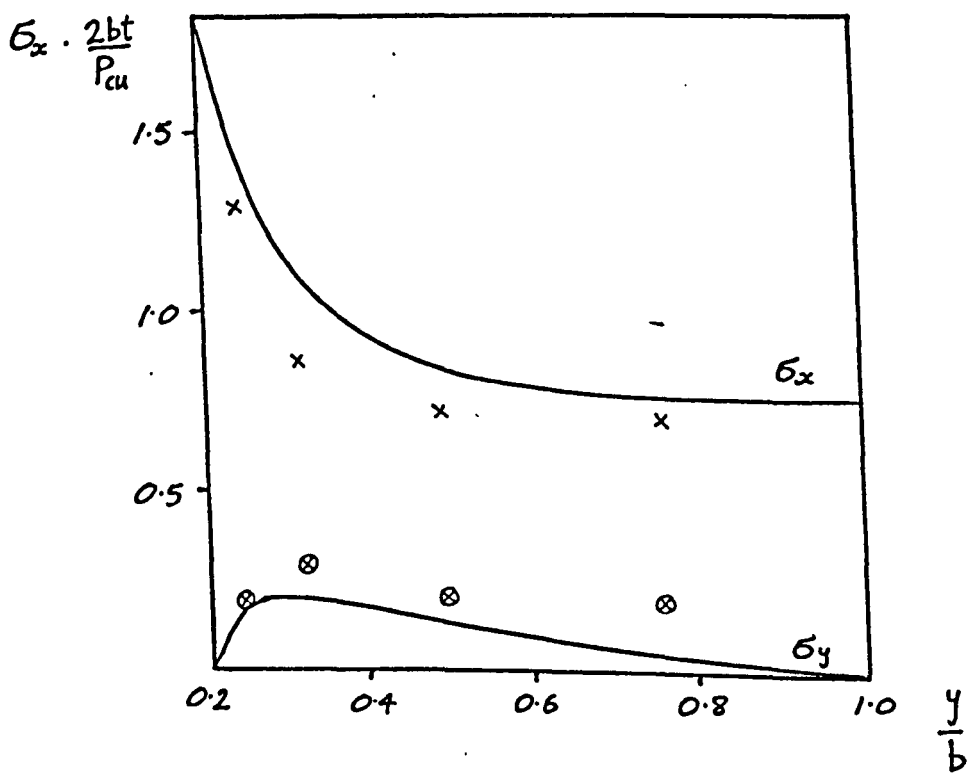

FIGURE 5.43 STRESSES AT THE MINIMUM SECTION. $P = 0.74.\ P_{cu}$

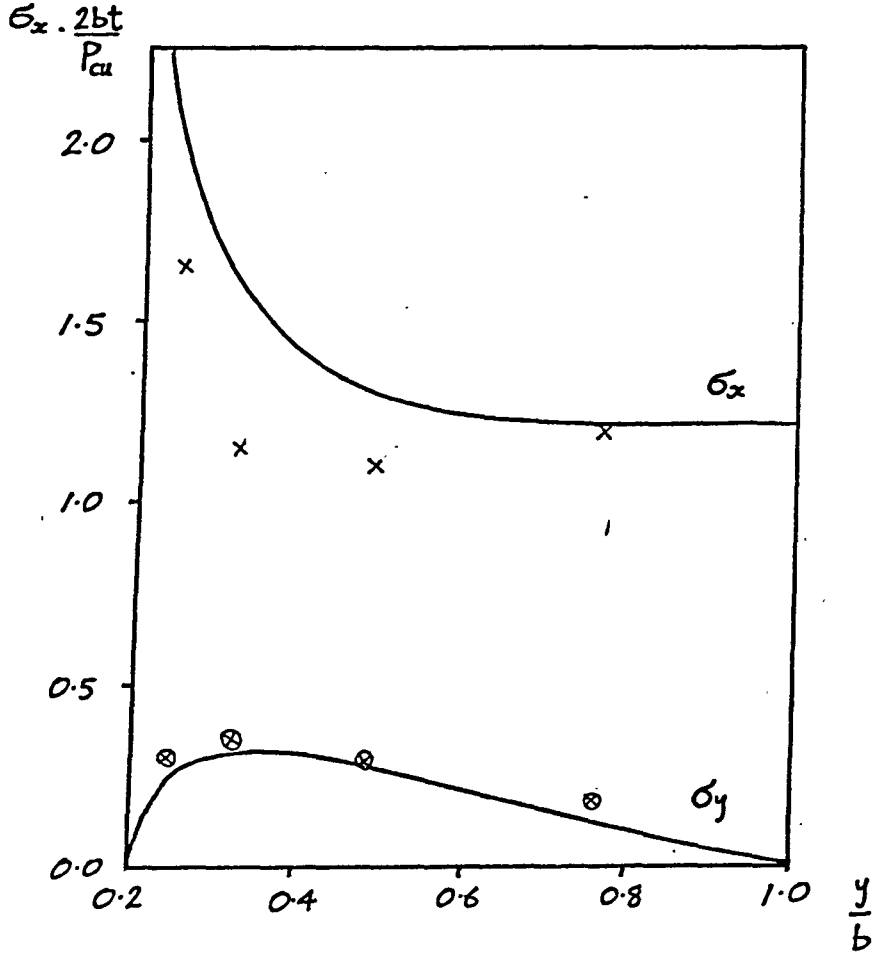

FIGURE 5.44 STRESSES AT THE MINIMUM SECTION. $P = 1{\cdot}11 P_{cu}$

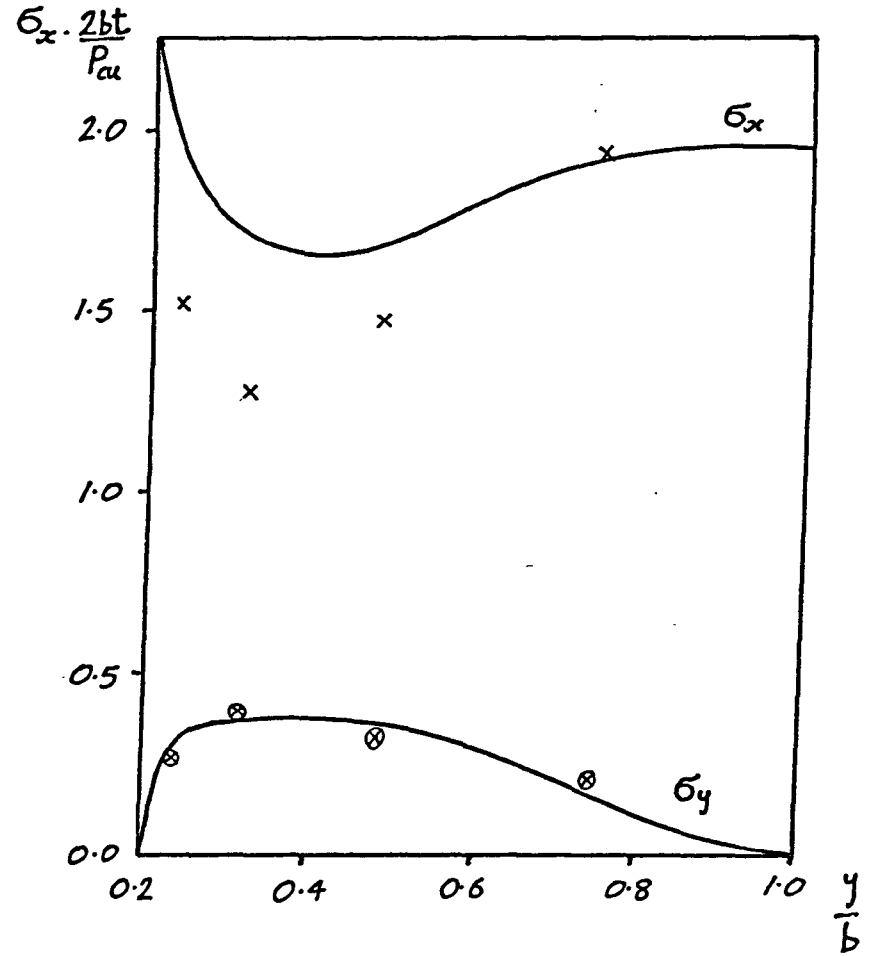

FIGURE 5.45 STRESSES AT THE MINIMUM SECTION $P = 1{\cdot}47 P_{cu}$

FIGURE 5.46 STRESSES AT THE MINIMUM SECTION $P = 1{\cdot}66\, P_{cu}$

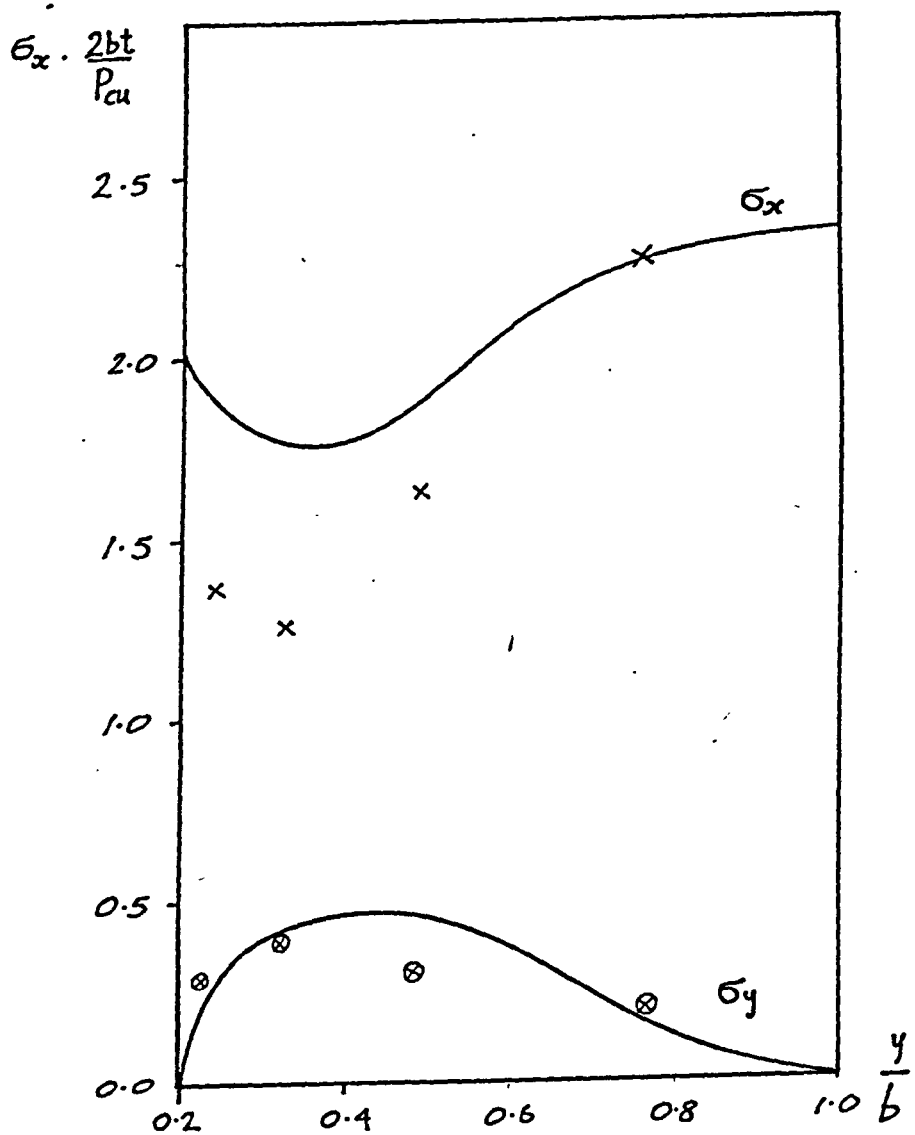

FIGURE 5.47 STRESSES AT THE MINIMUM SECTION $P = 1{\cdot}84\, P_{cu}$

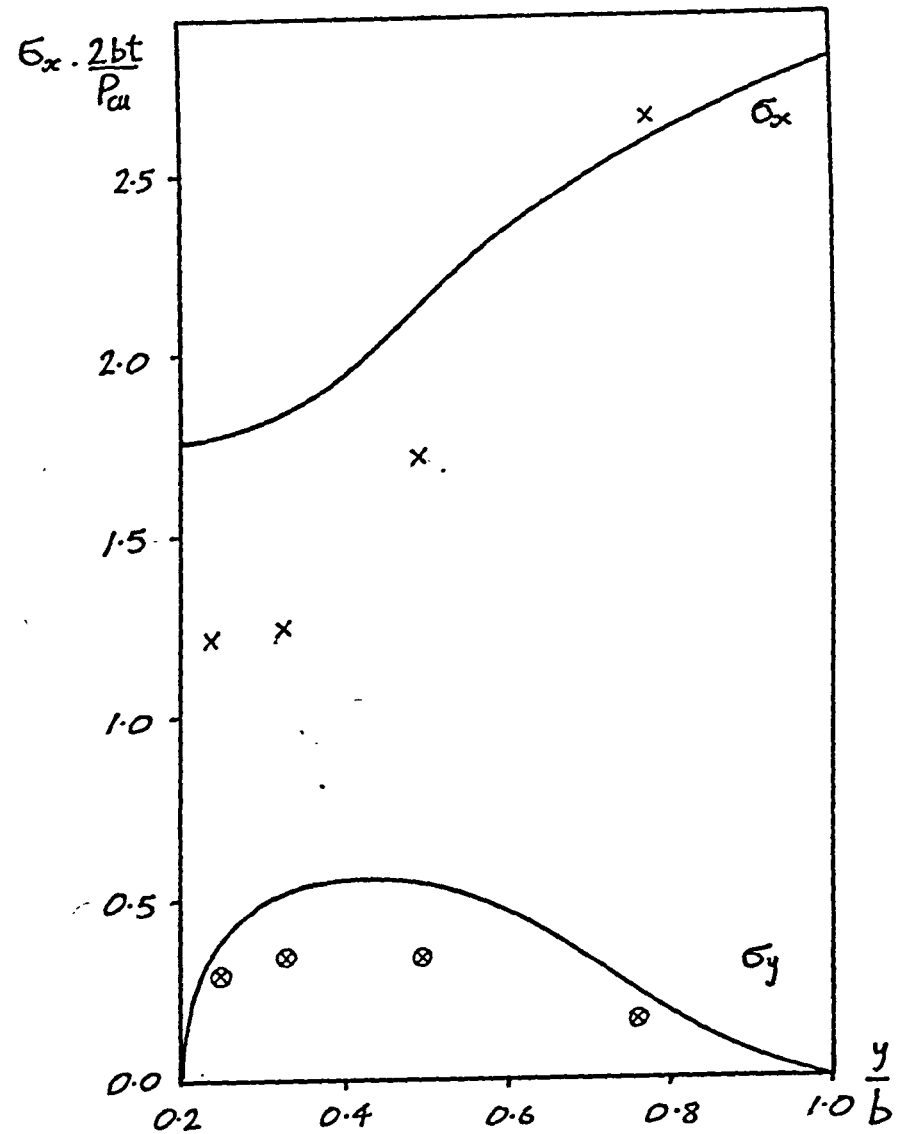

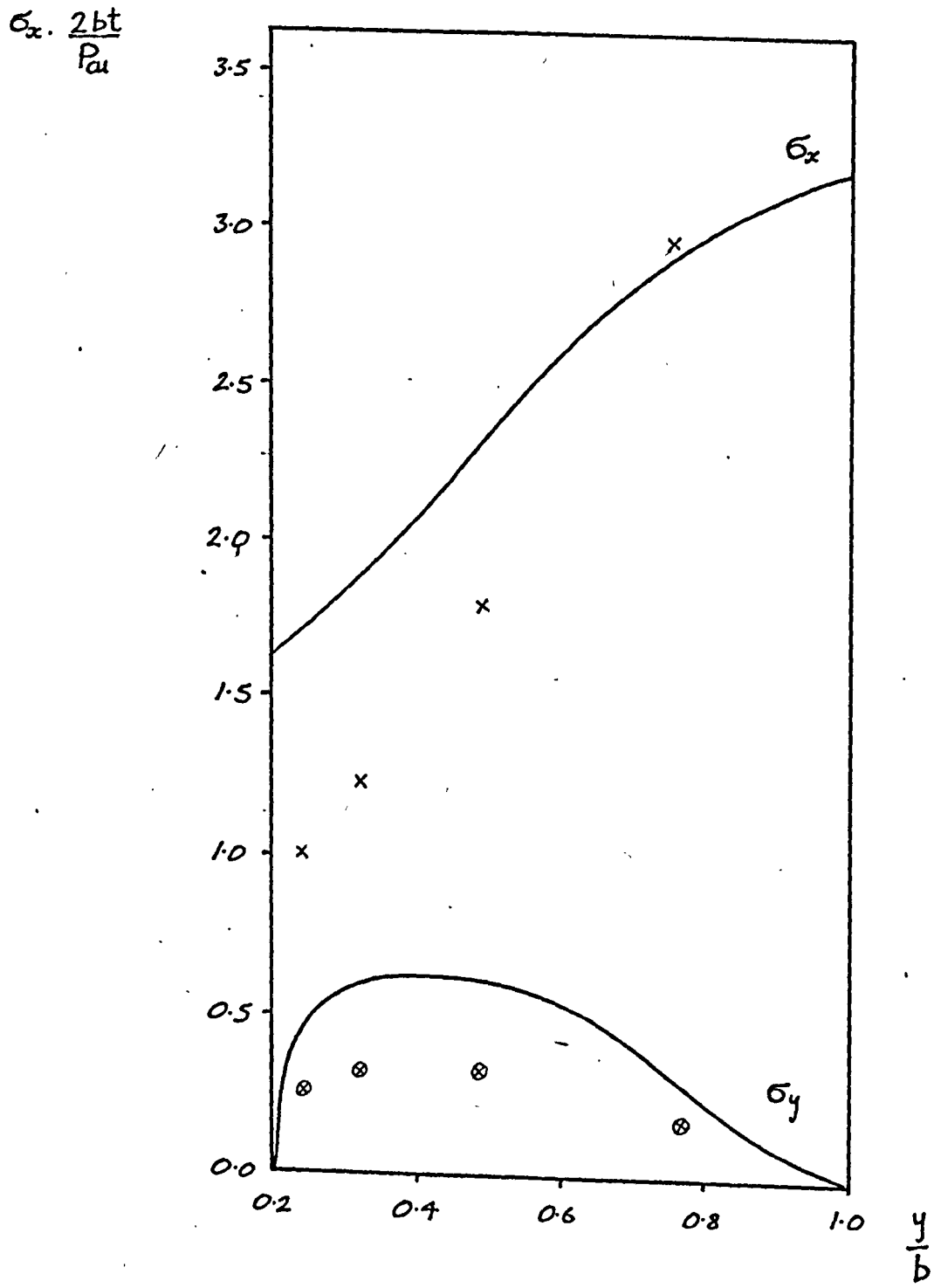

FIGURE 5.48 STRESSES AT THE MINIMUM SECTION $P = 2.03\, P_{cu}$

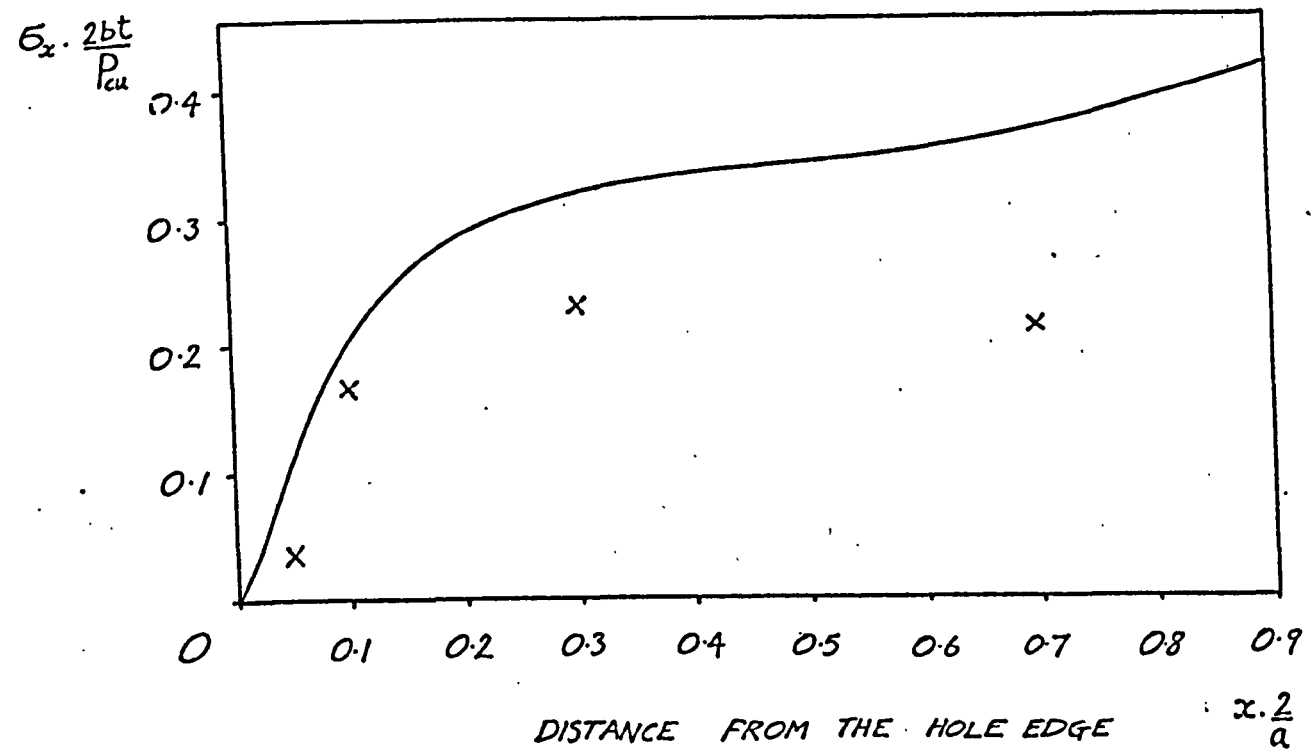

FIGURE 5.49 STRESSES ON THE X-AXIS $P = 0{\cdot}37 \cdot P_{cu}$

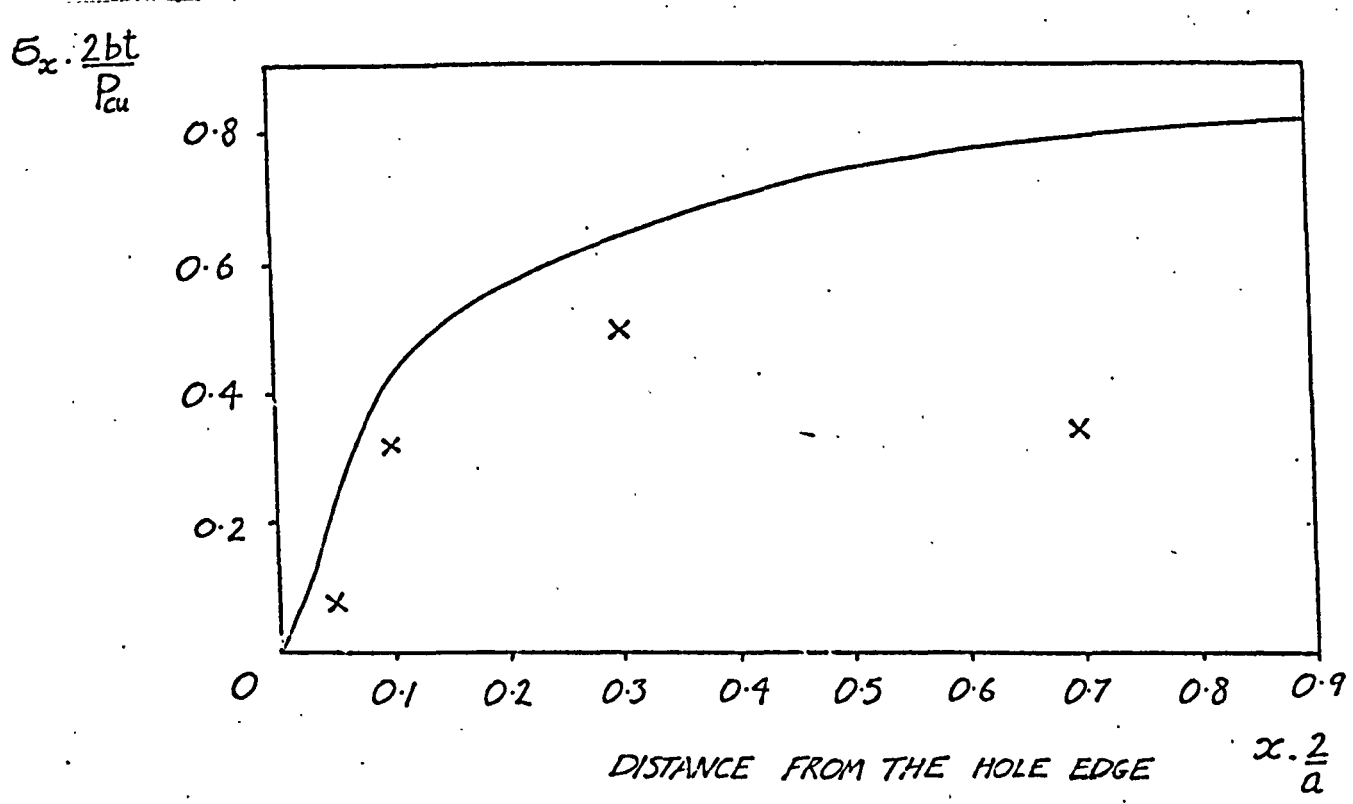

FIGURE 5.50 STRESSES ON THE X-AXIS $P = 0{\cdot}74 P_{cu}$

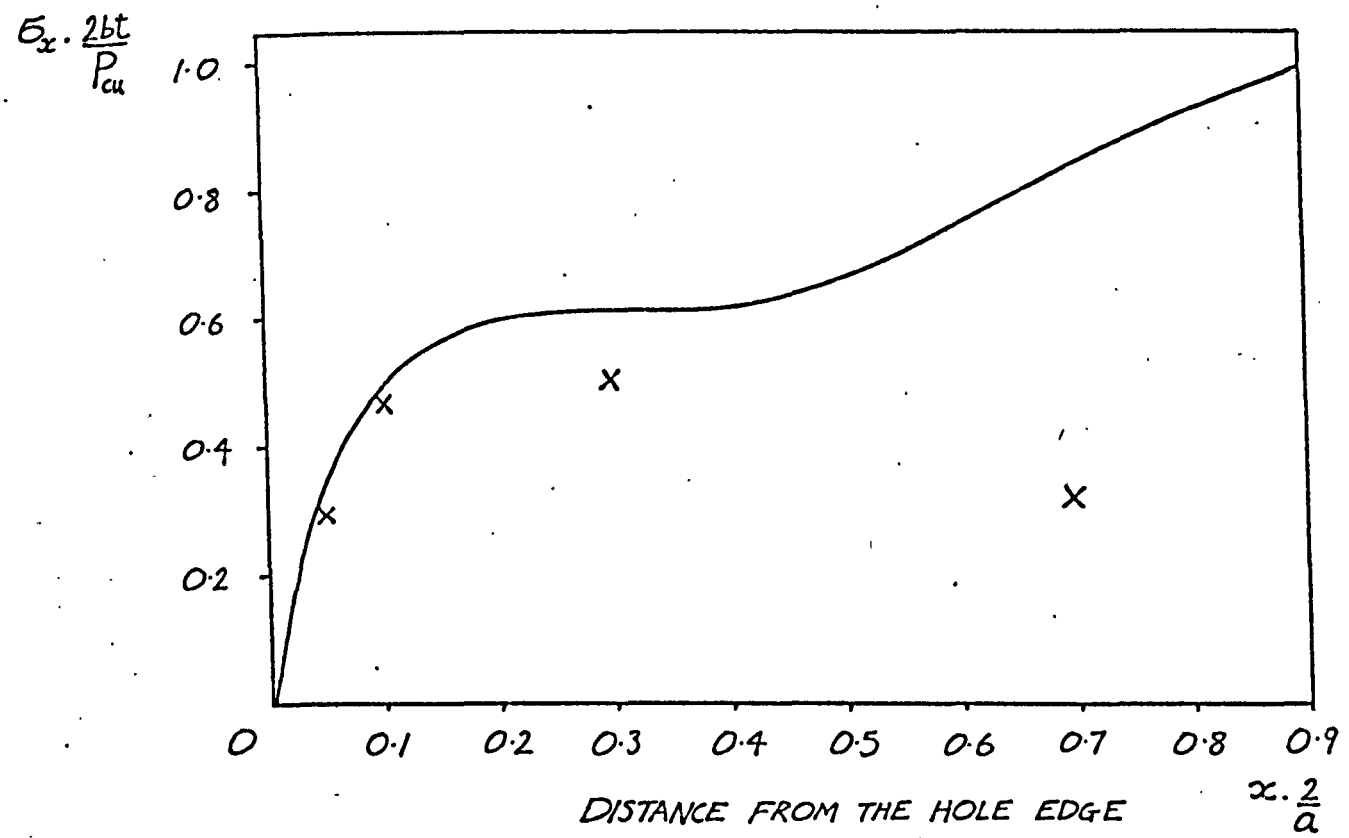

FIGURE 5.51 STRESSES ON THE X-AXIS $P = 1{\cdot}47 . P_{cu}$

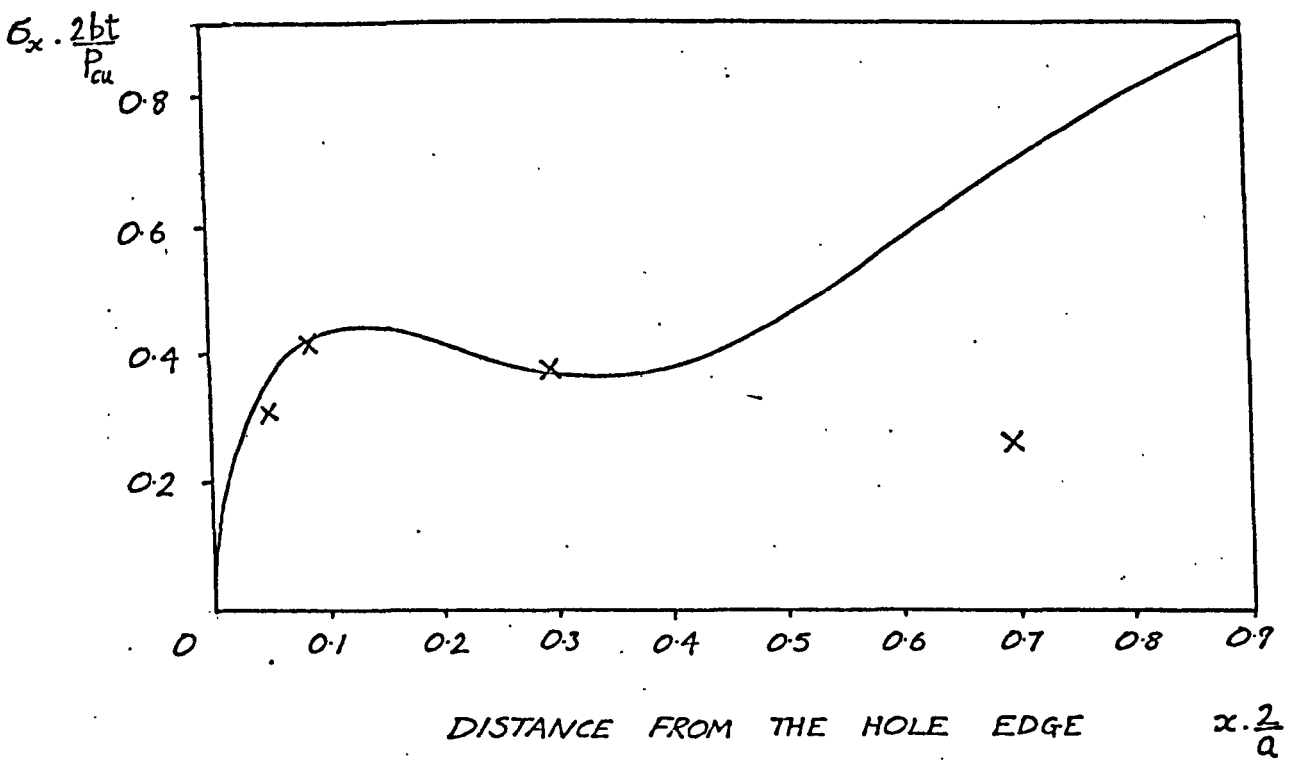

FIGURE 5.52 STRESSES ON THE X-AXIS $P = 1{\cdot}84 . P_{cu}$

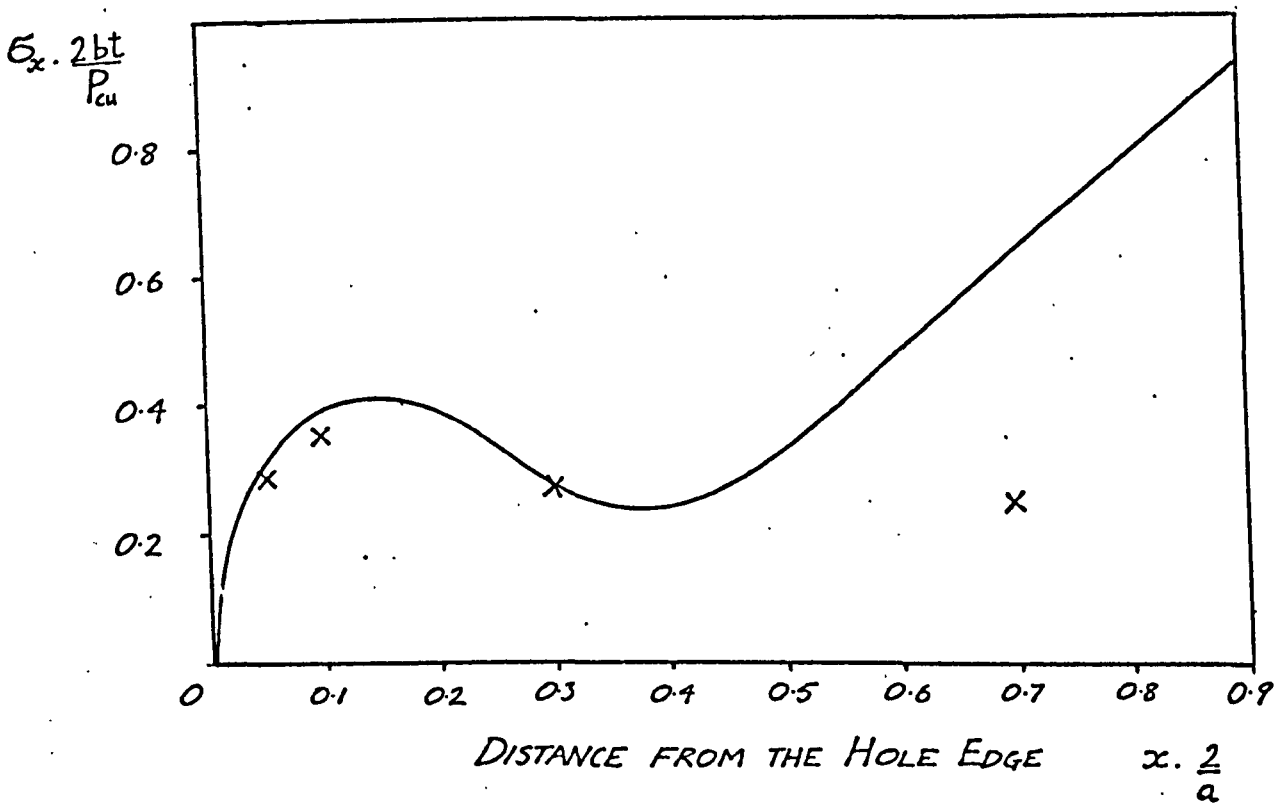

FIGURE 5.53 STRESSES ON THE X-AXIS $P = 2.03\ P_{cu}$

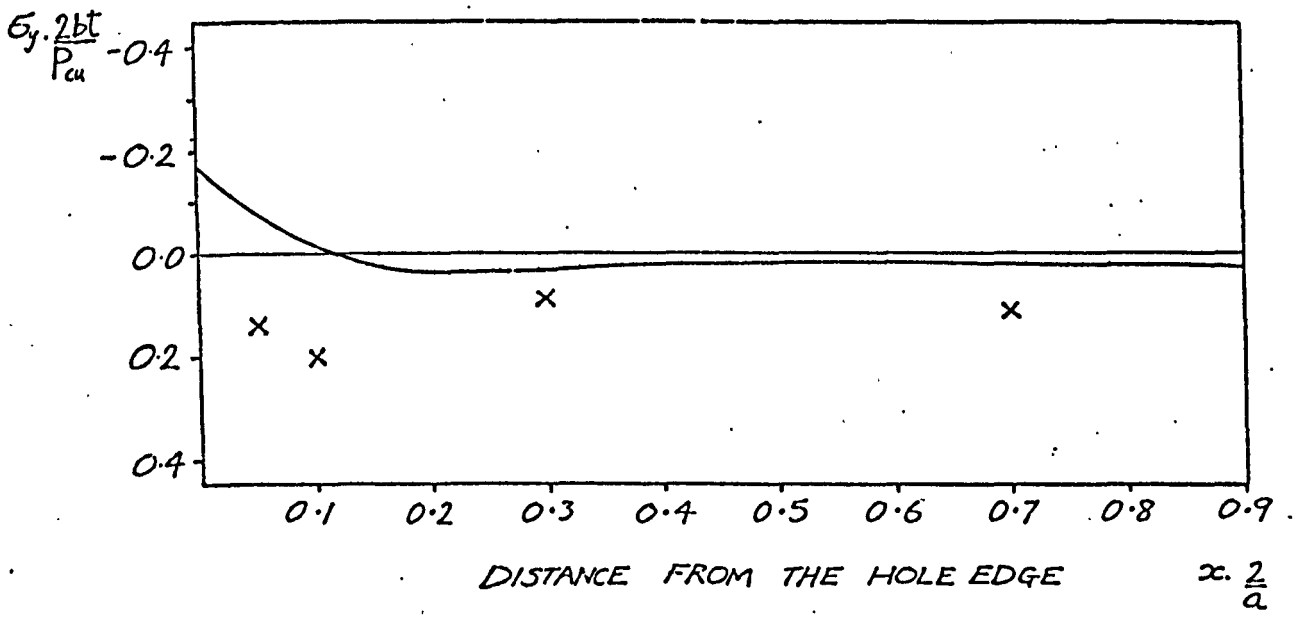

FIGURE 5.54 STRESSES ON THE X-AXIS $P = 1{\cdot}03 . P_{cu}$

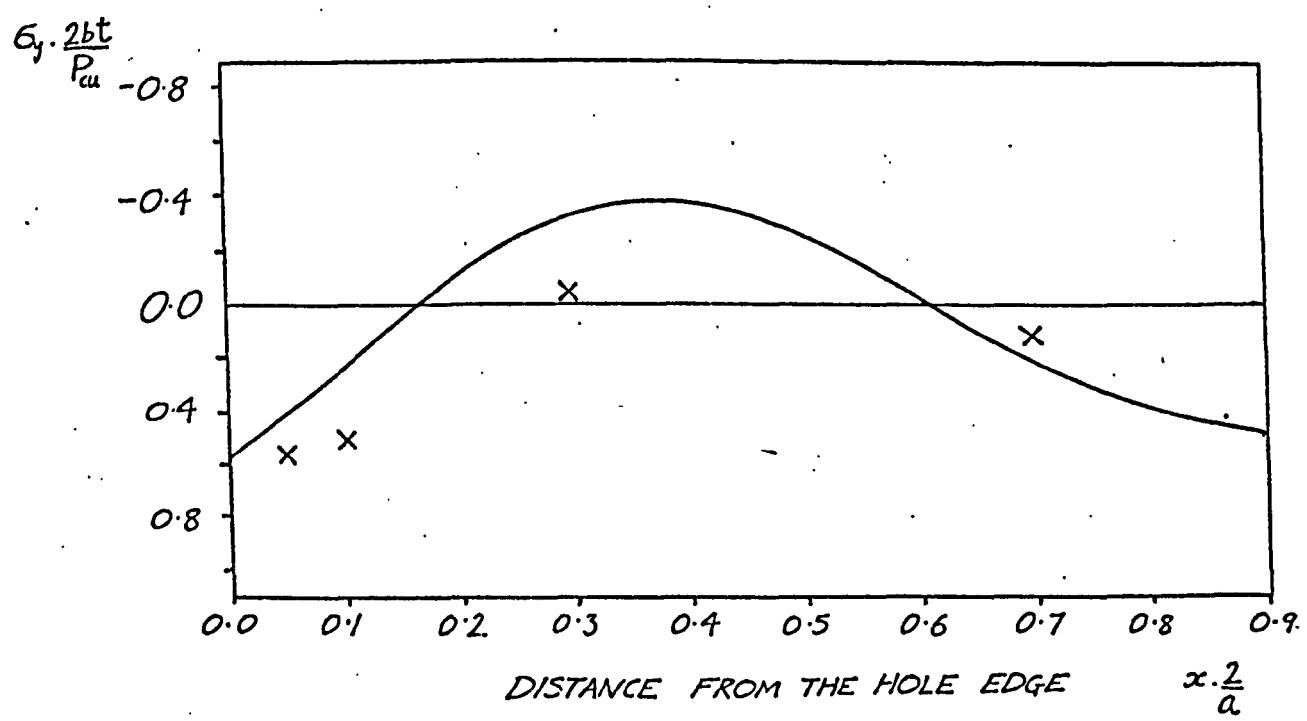

FIGURE 5.55 STRESSES ON THE X-AXIS $P = 1{\cdot}47\, P_{cu}$

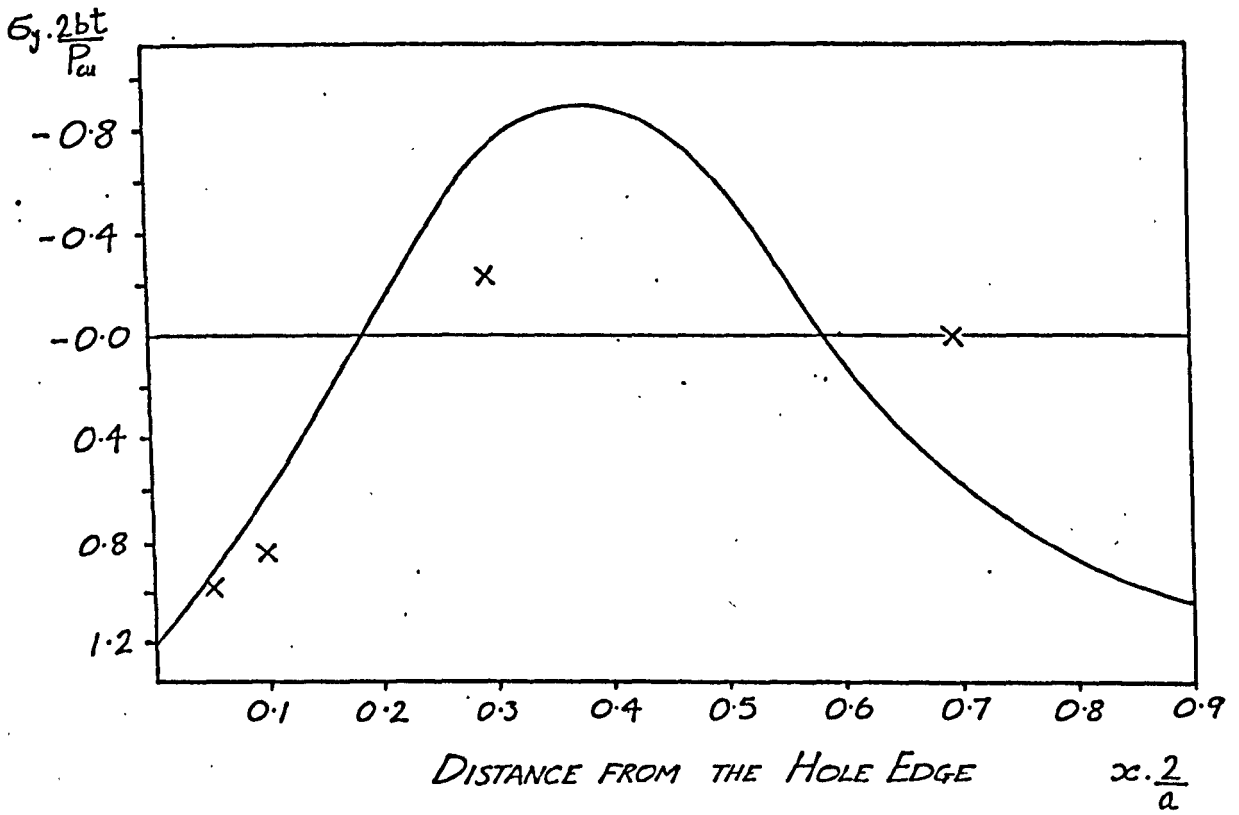

FIGURE 5.56 STRESSES ON THE X-AXIS $P = 2{\cdot}03 . P_{cu}$

For the purpose of comparison of theoretical and experimental results the x and y axes of the plate are taken to pass through the centre of the plate.

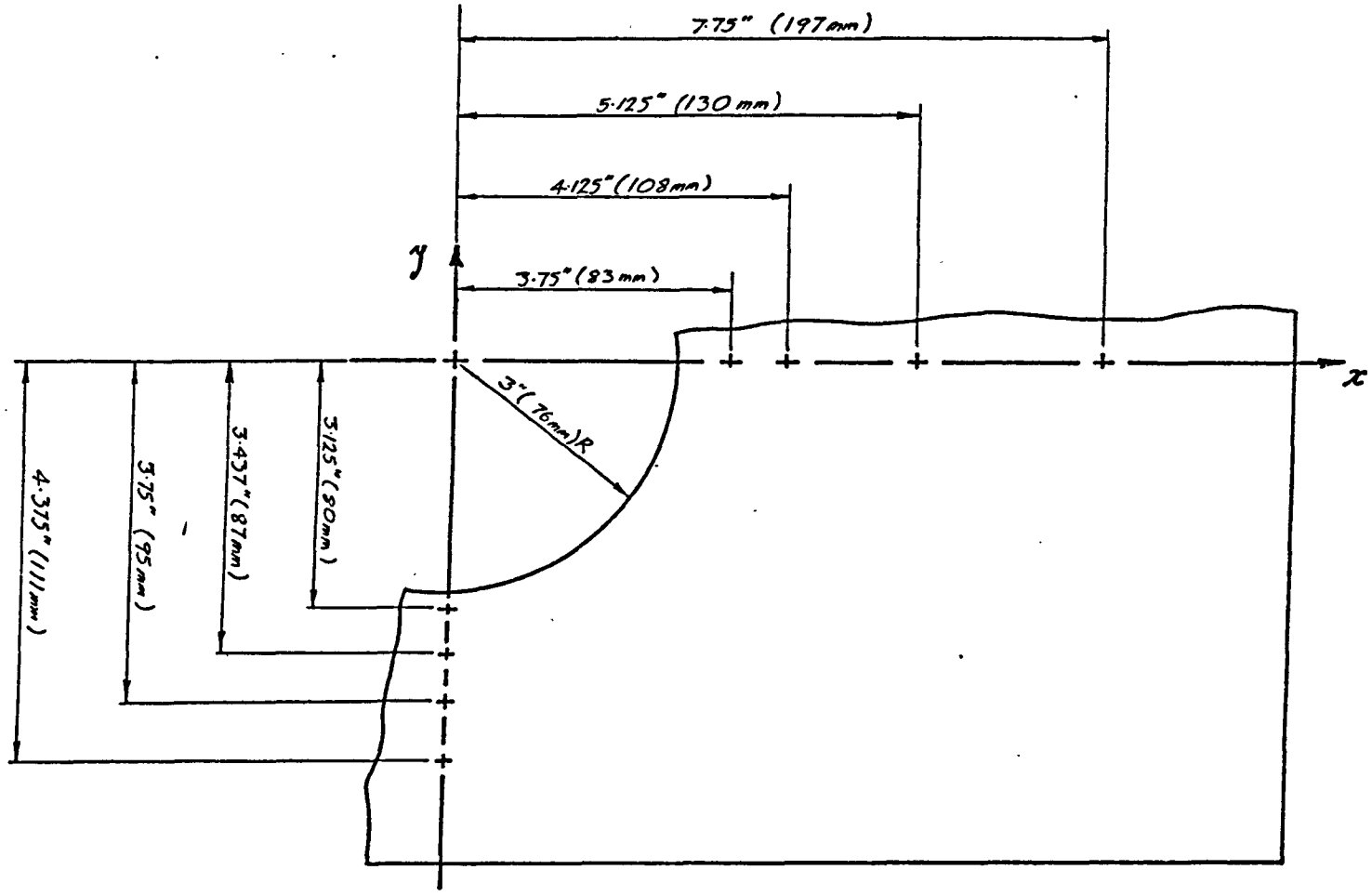

FIGURE 5.57 ARRANGEMENT OF STRAIN GAUGE ROSETTES ON PLATE B

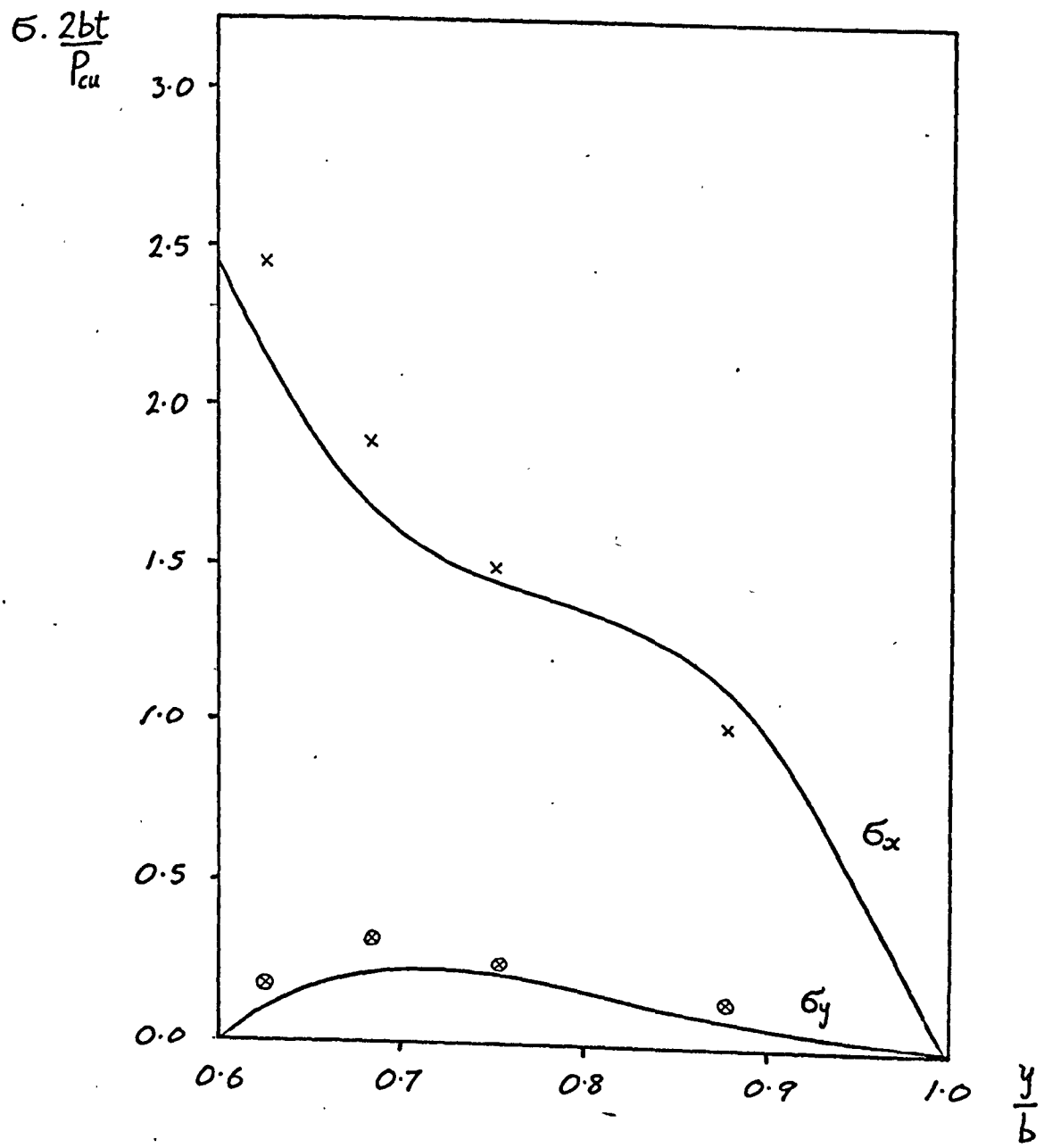

FIGURE 5.58 STRESSES AT THE MINIMUM SECTION. $P = 0.55 P_{cu}$

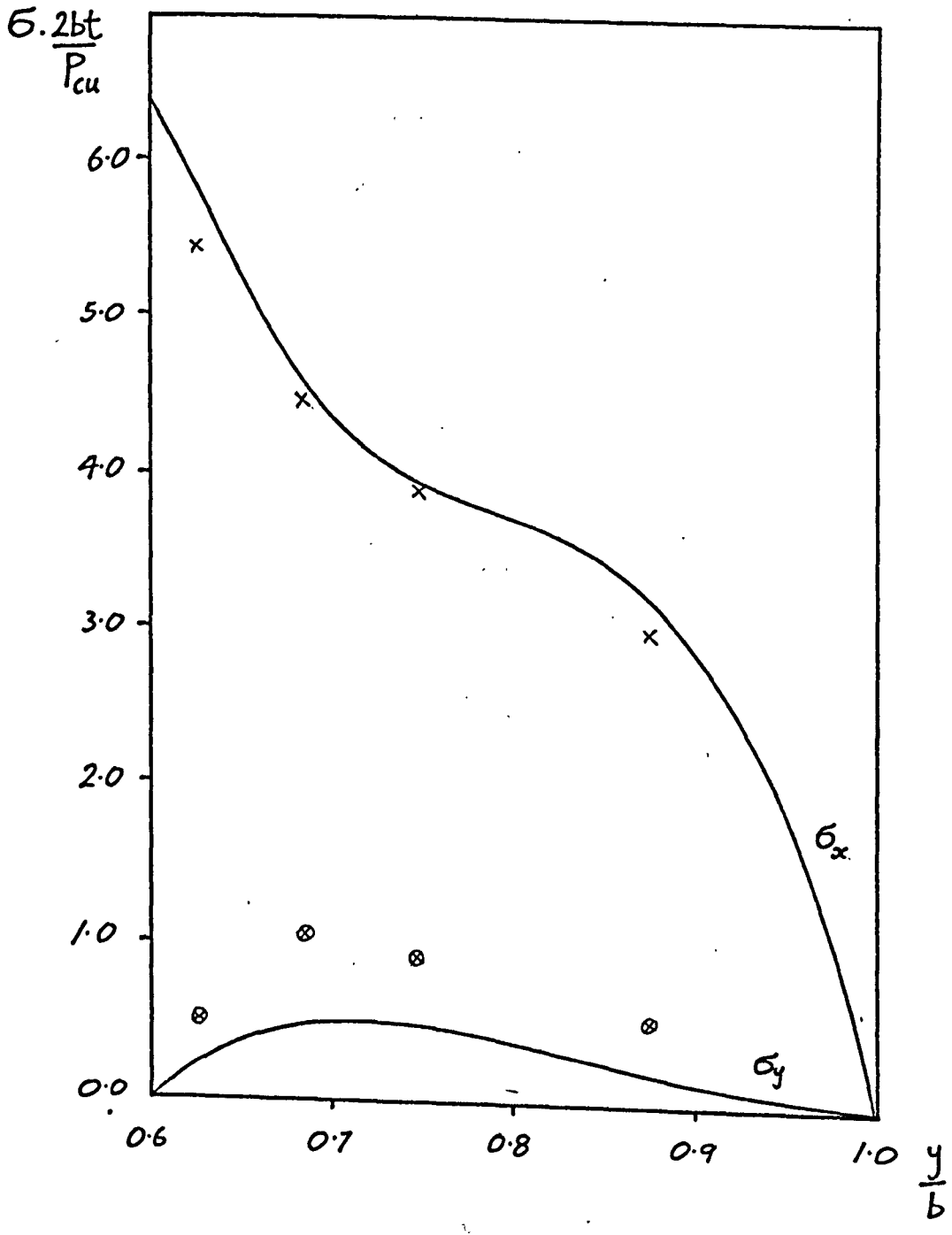

FIGURE 5.59 STRESSES AT THE MINIMUM SECTION. $P = 1.47 P_{cu}$

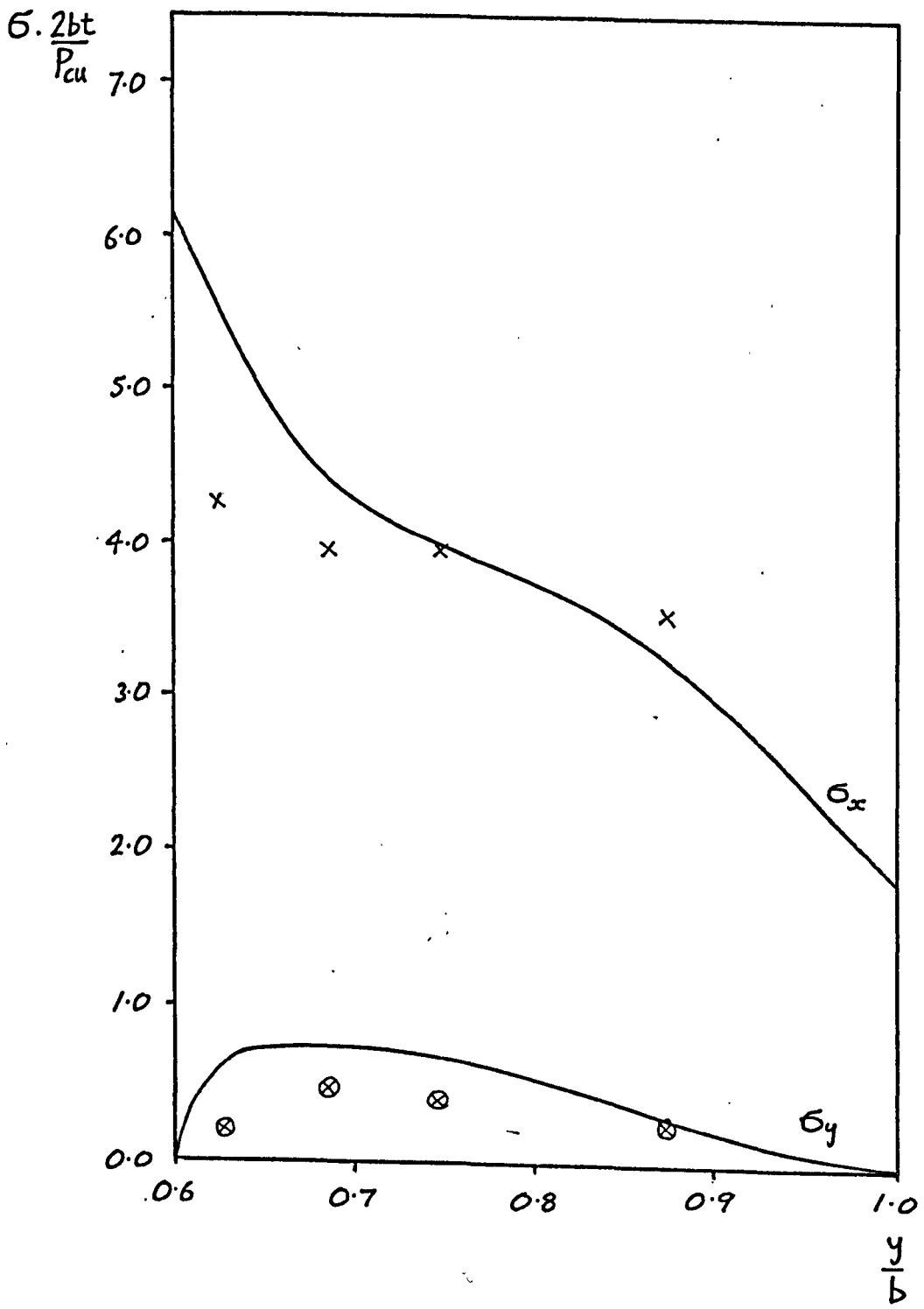

FIGURE 5.60 STRESSES AT THE MINIMUM SECTION. $P = 1{\cdot}84\ P_{cu}$

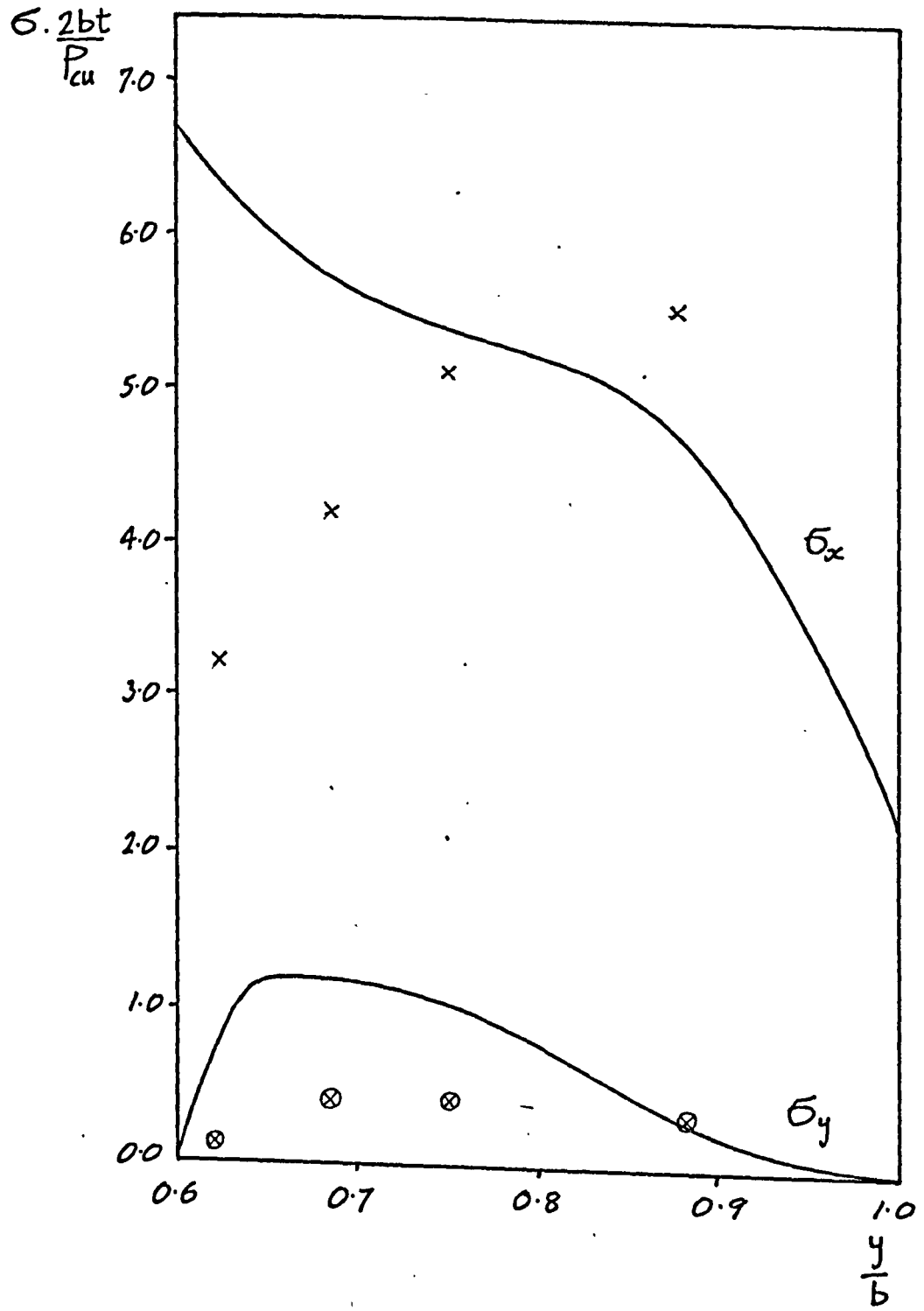

FIGURE 5.61 STRESSES AT THE MINIMUM SECTION. $P = 2.39\, P_{cu}$

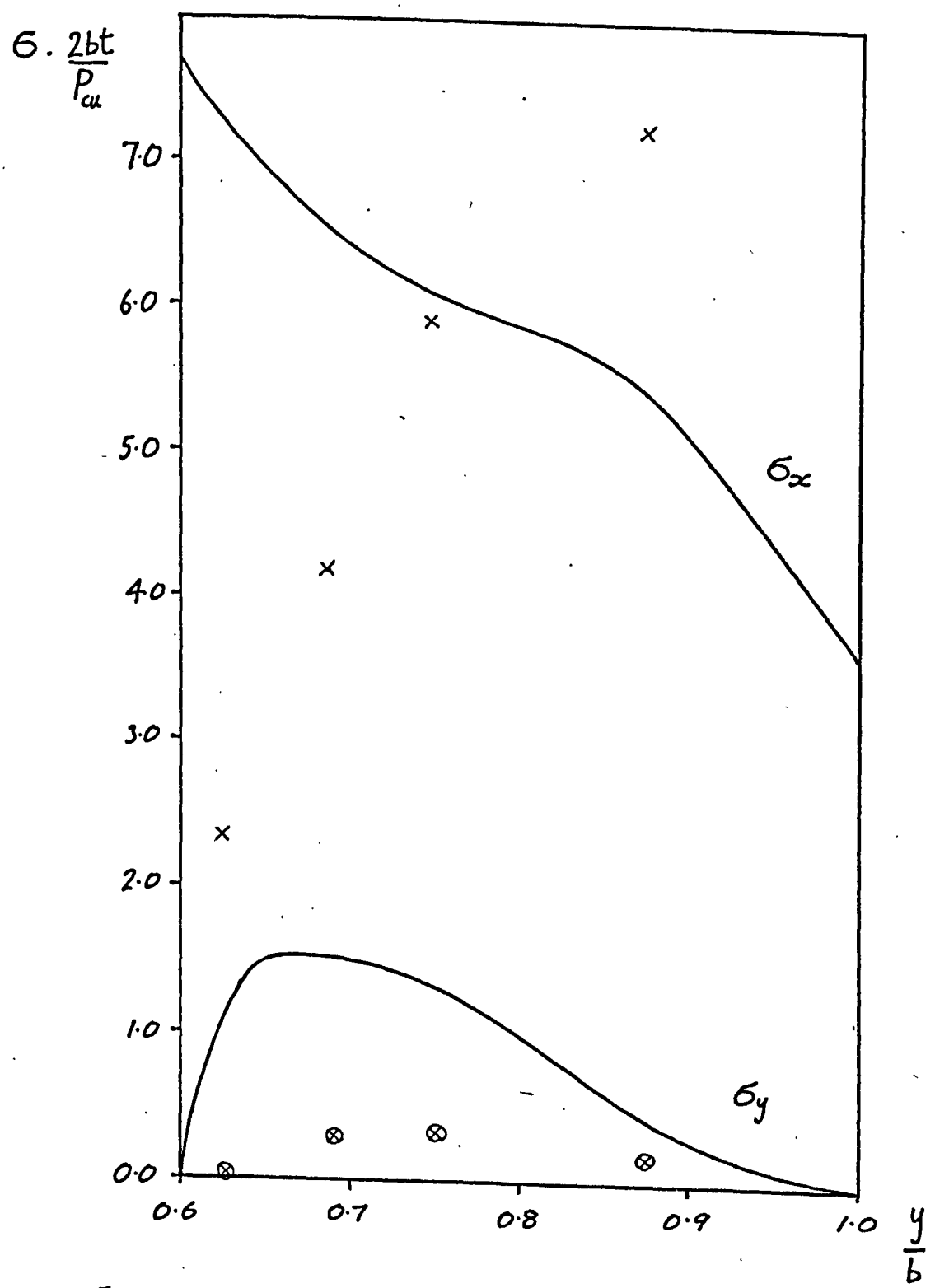

FIGURE 5.62 STRESSES AT THE MINIMUM SECTION. $P = 2{\cdot}76\, P_{cu}$

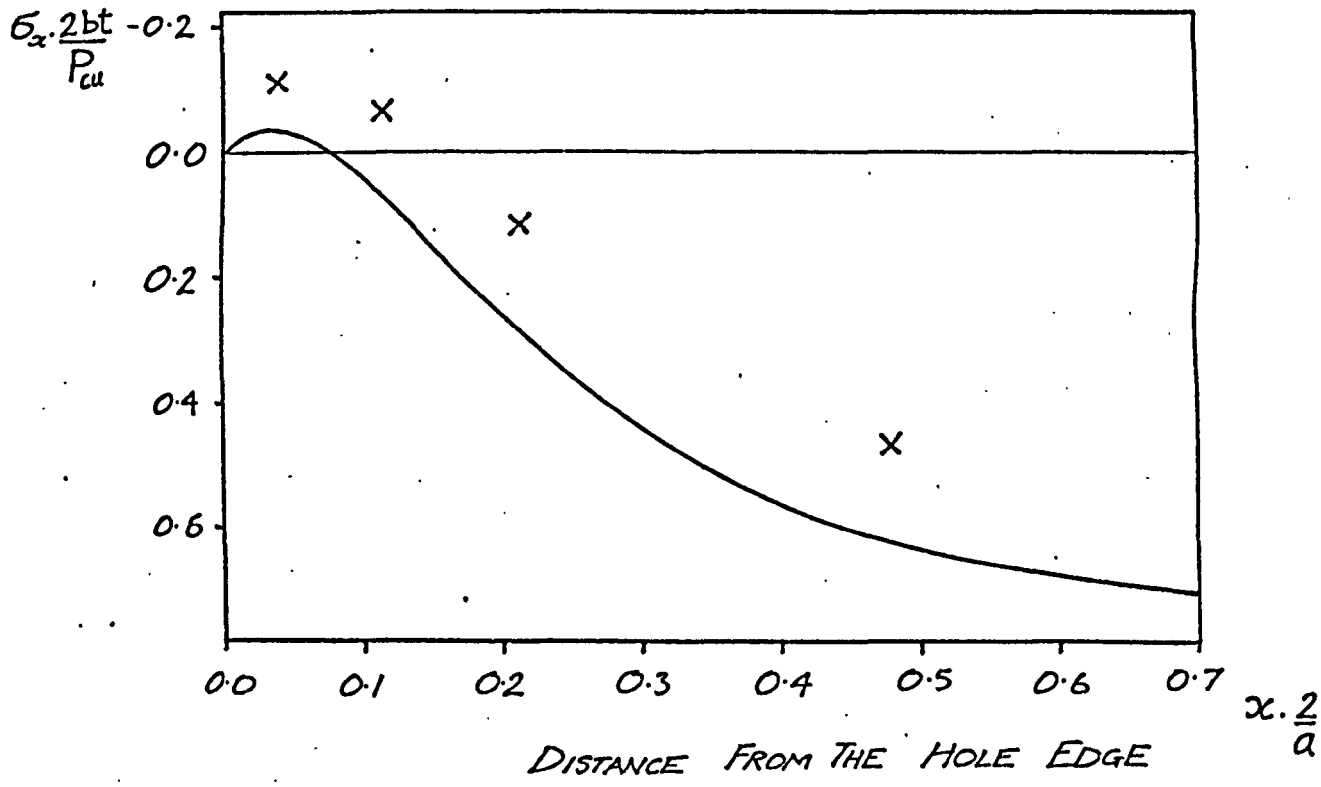

FIGURE 5.63 STRESSES ON THE X-AXIS $P = 0.92\, P_{cu}$

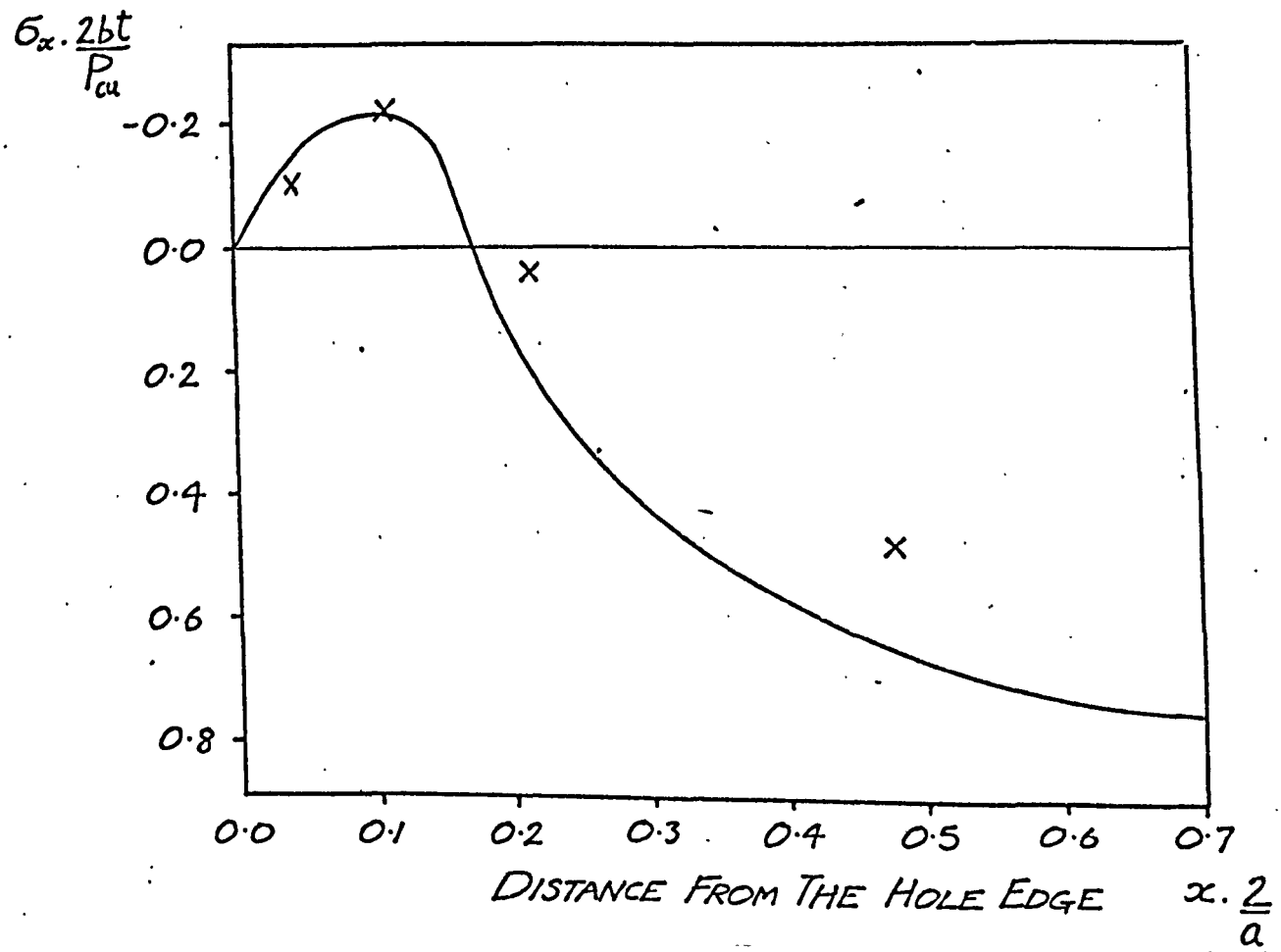

FIGURE 5.64 STRESSES ON THE X-AXIS $P = 1.66\, P_{cu}$

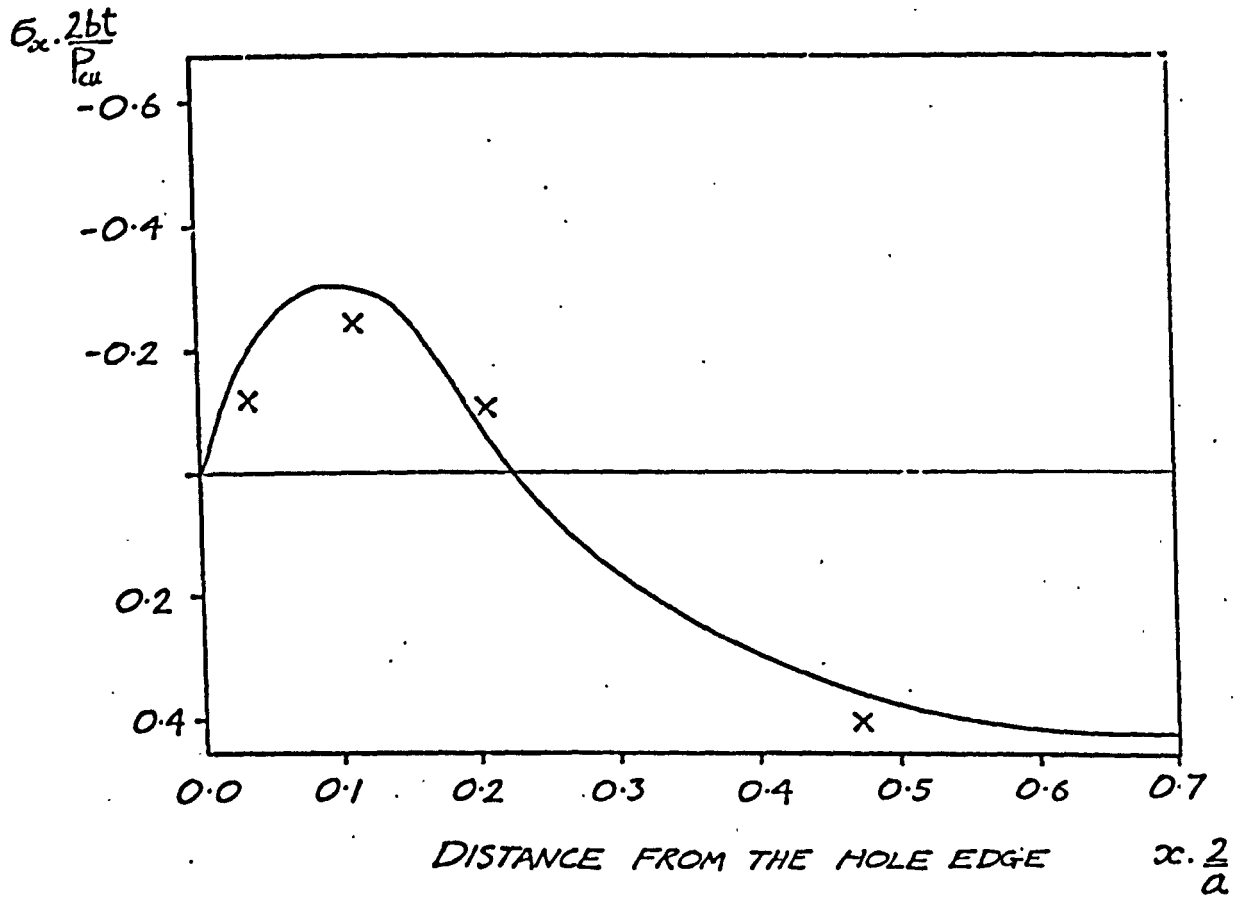

FIGURE 5.65 STRESSES ON THE X-AXIS $P = 2.03 P_{cu}$

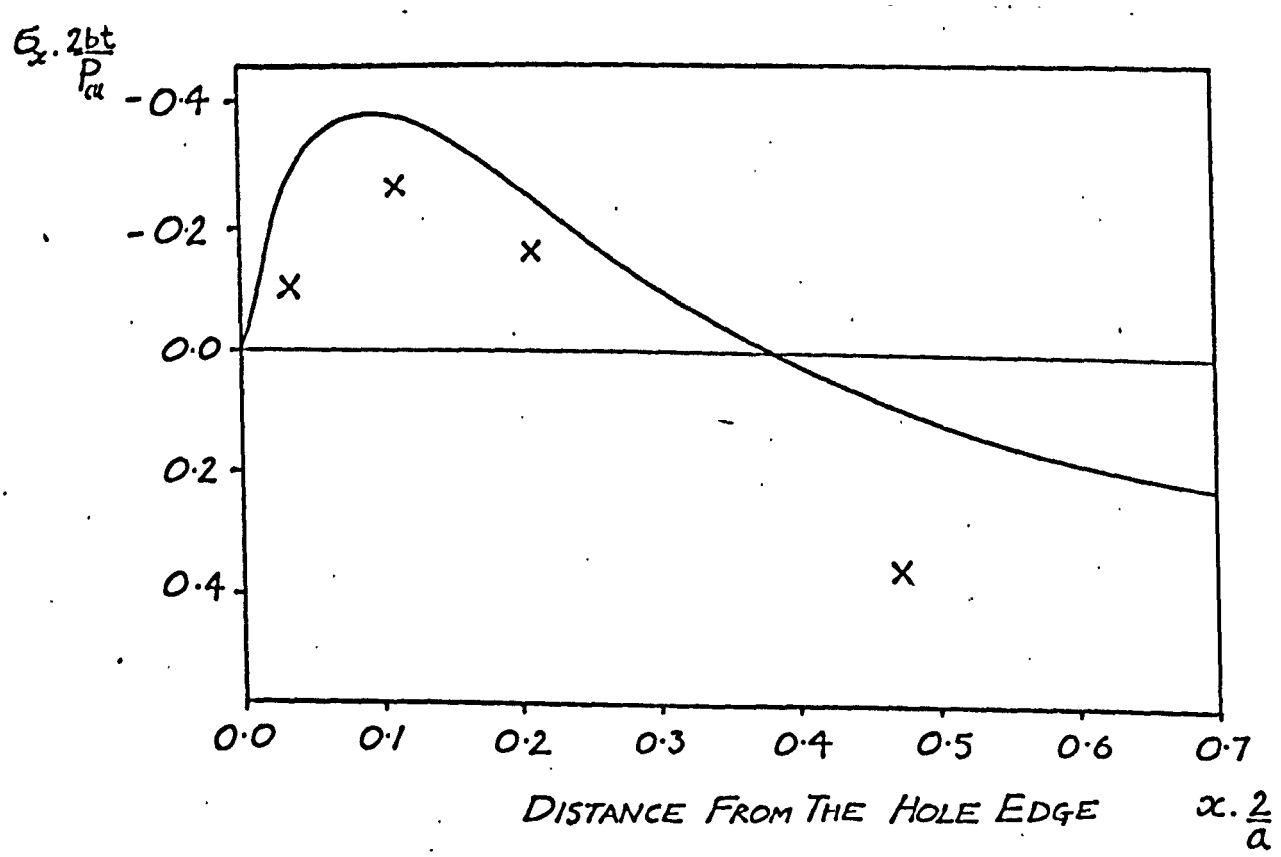

FIGURE 5.66 STRESSES ON THE X-AXIS $P = 2.21 P_{cu}$

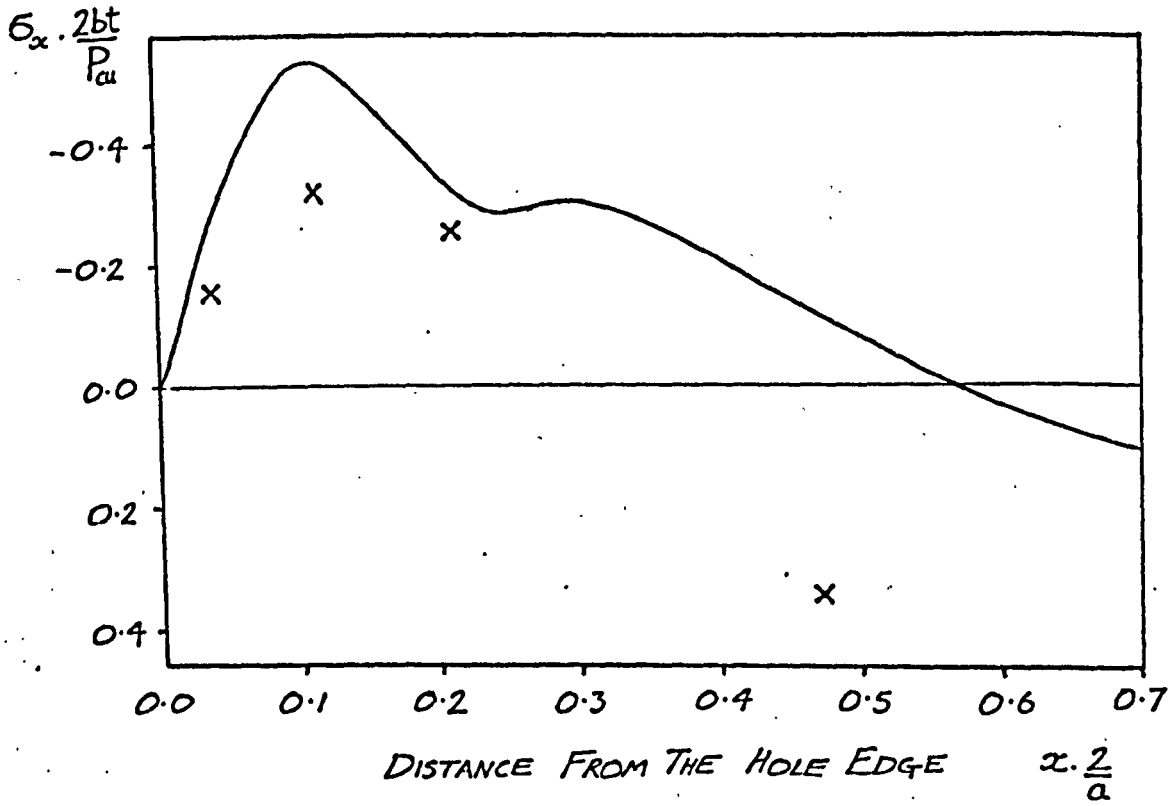

FIGURE 5.67 STRESSES ON THE X-AXIS $P = 2.39 P_{cu}$

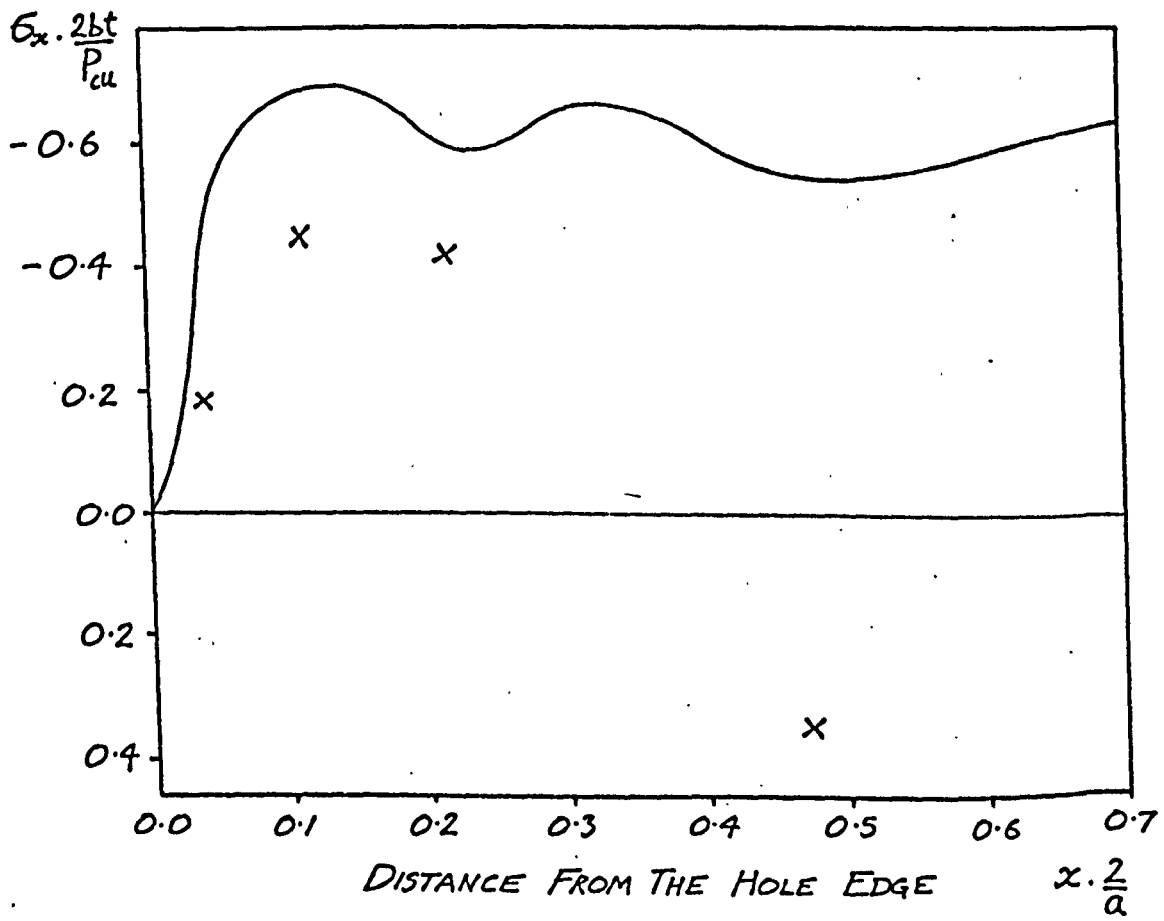

FIGURE 5.68 STRESSES ON THE X-AXIS $P = 2.76 P_{cu}$

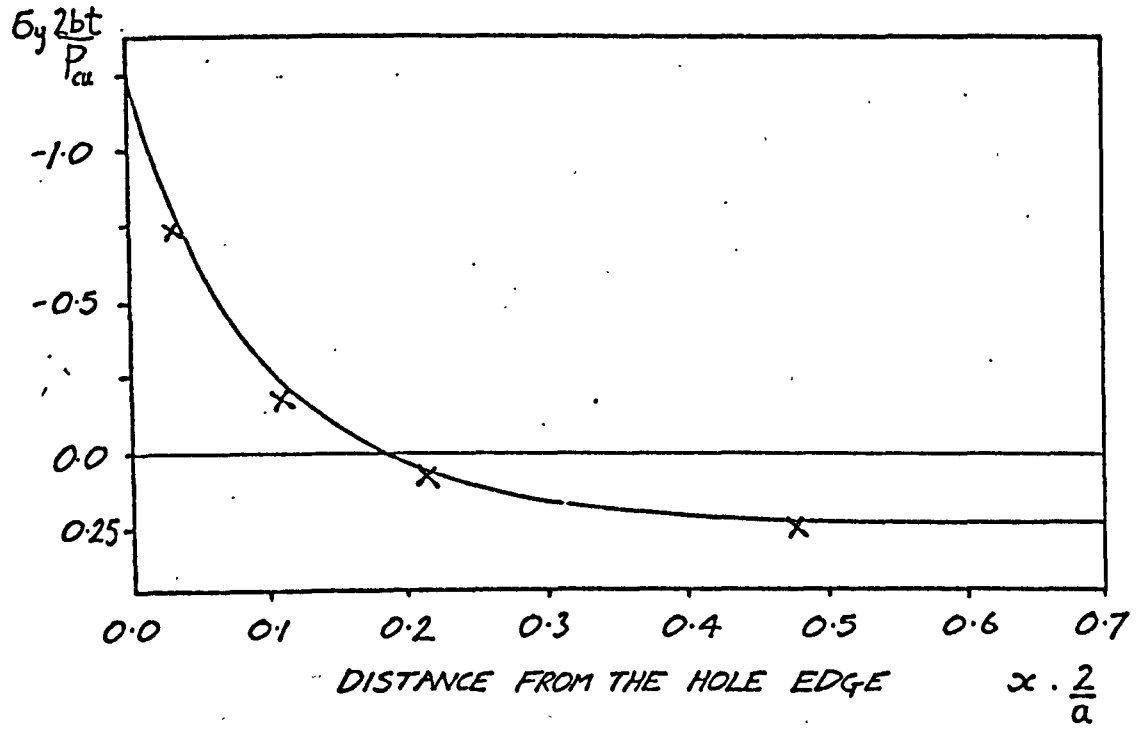

FIGURE 5.69 STRESSES ON THE X-AXIS $P = 0.92\, P_{cu}$

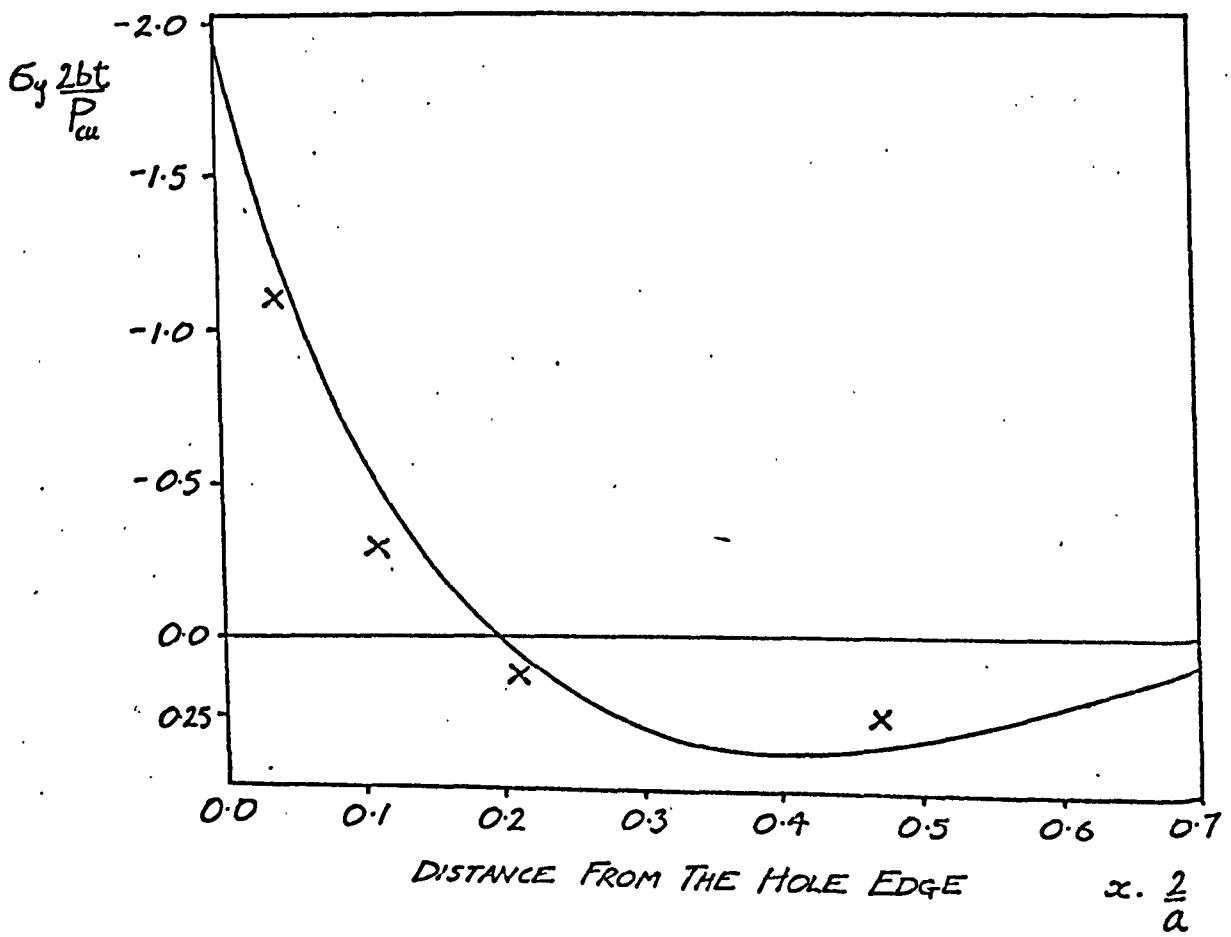

FIGURE 5.70 STRESSES ON THE X-AXIS $P = 1.47\, P_{cu}$

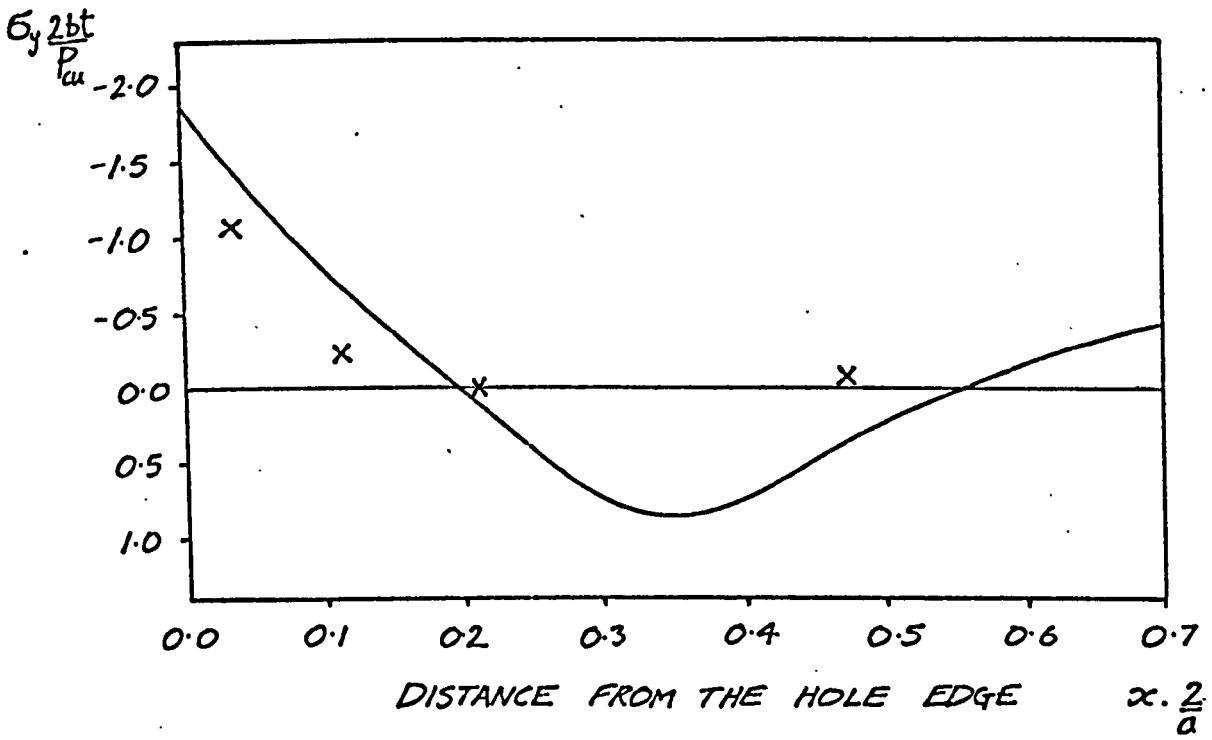

FIGURE 5.71 STRESSES ON THE X-AXIS $P = 2{\cdot}03\ P_{cu}$

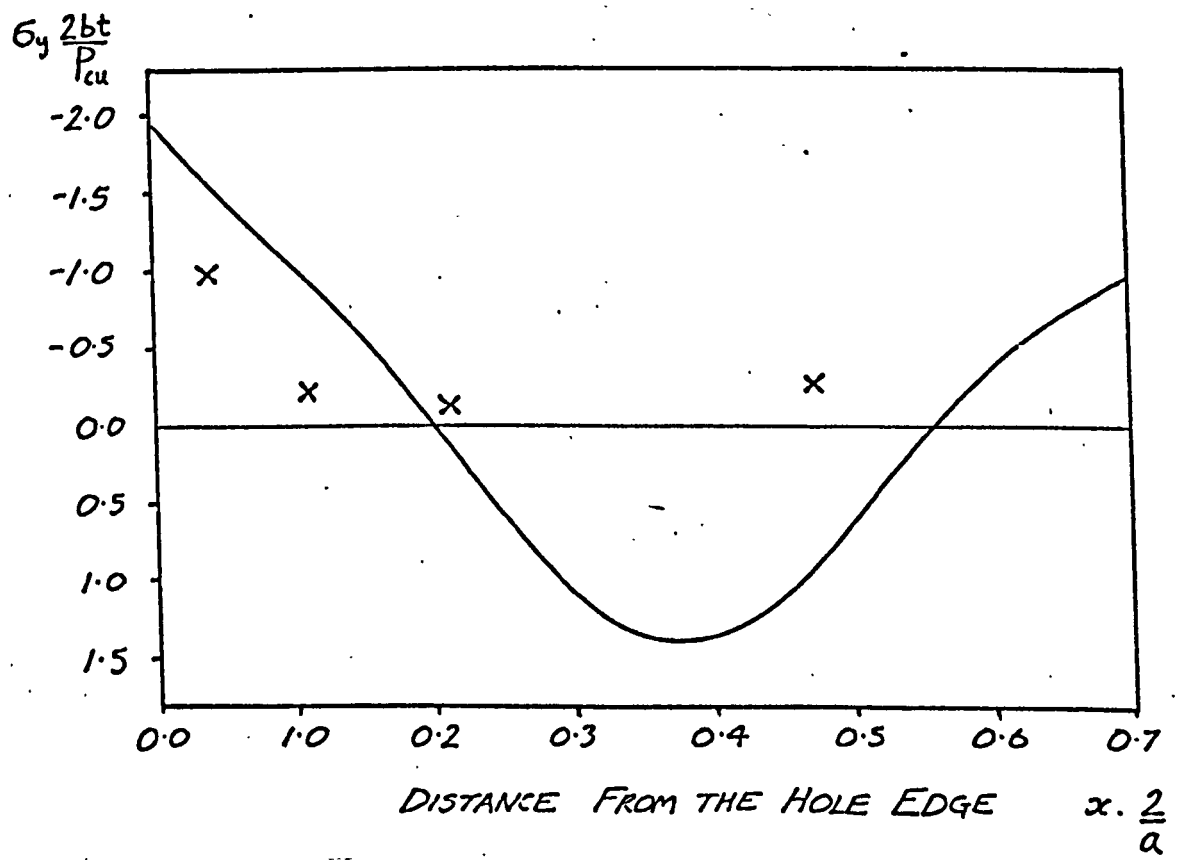

FIGURE 5.72 STRESSES ON THE X-AXIS $P = 2{\cdot}39\ P_{cu}$

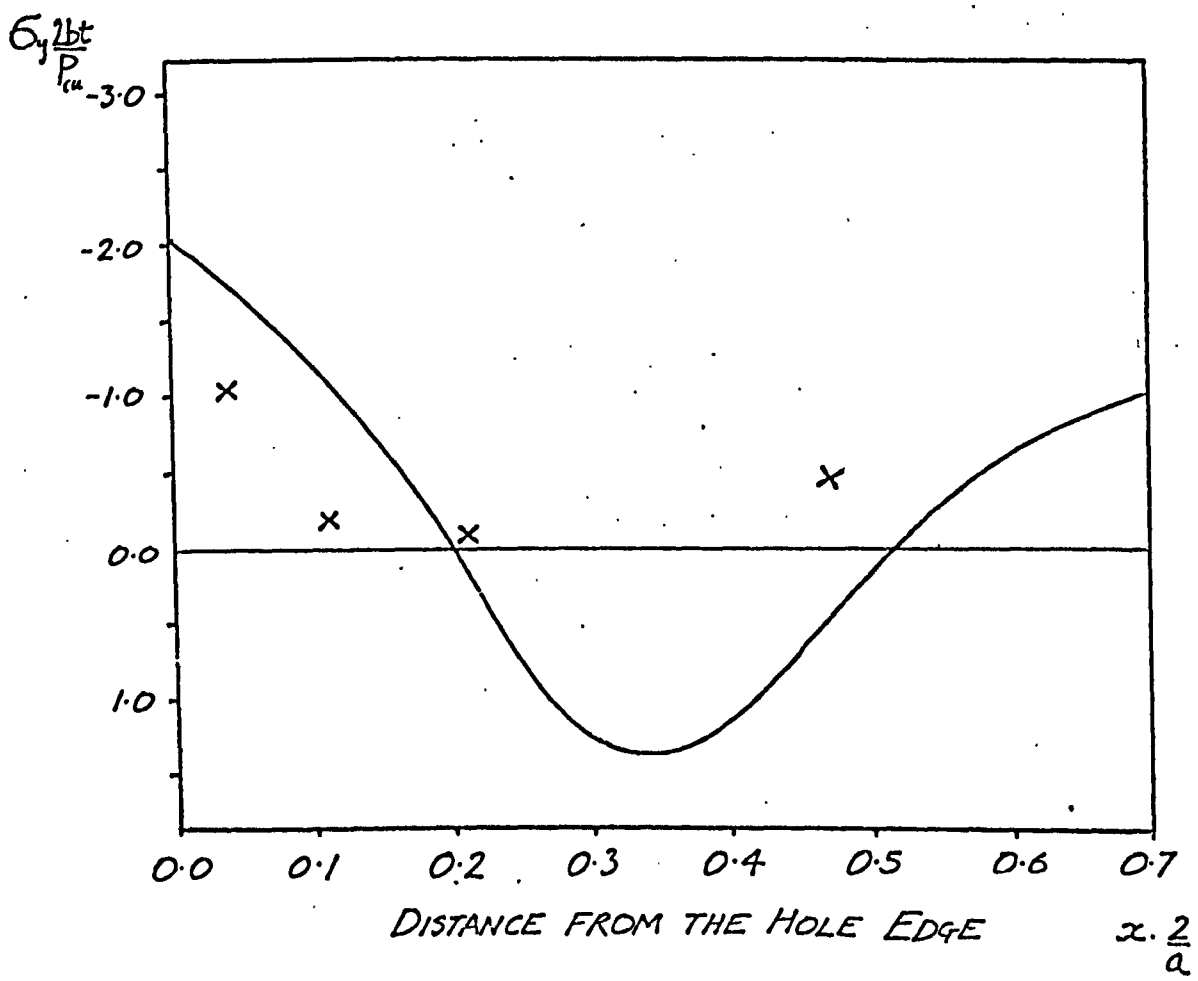

FIGURE 5.73 STRESSES ON THE X-AXIS $P = 2{\cdot}76\ P_{cu}$

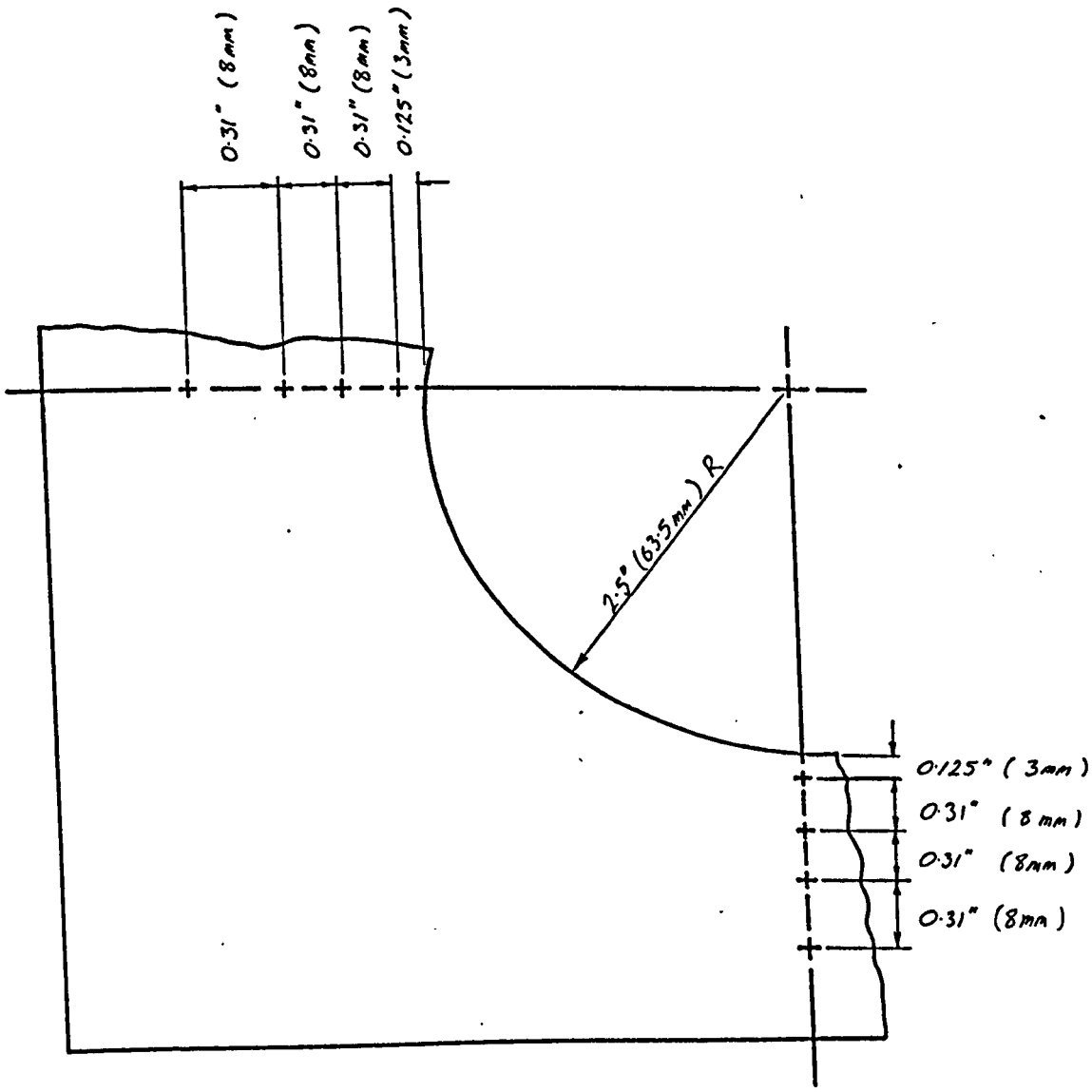

FIGURE 5.74 ARRANGEMENT OF STRAIN GAUGE ROSETTES ON PLATE C

For the purpose of comparison of theoretical and experimental results the x and y axes of the plate are taken to pass through the centre of the plate.

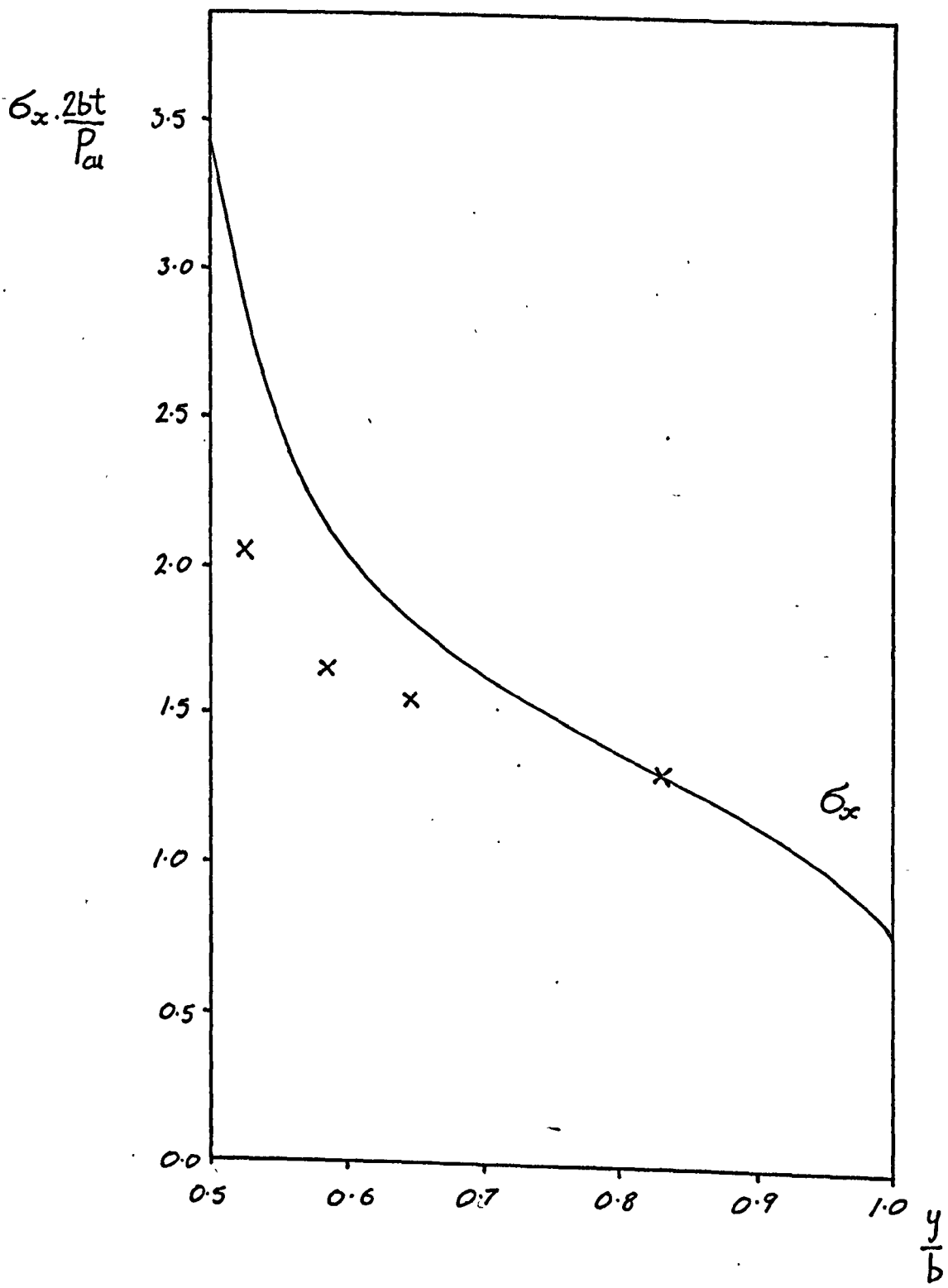

FIGURE 5.75 STRESSES AT THE MINIMUM SECTION $P = 0{\cdot}88 P_{cu}$

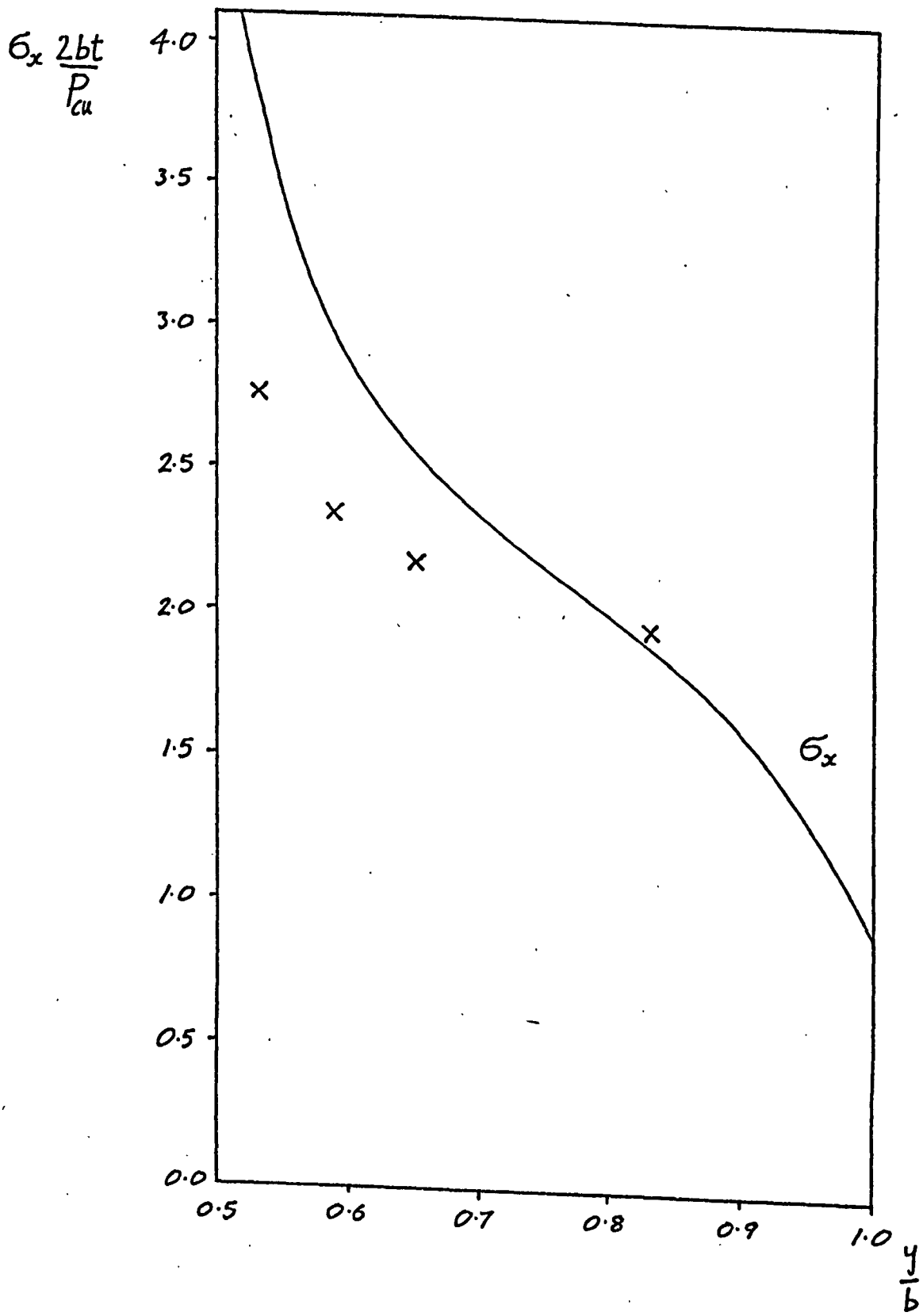

FIGURE 5.76 STRESSES AT THE MINIMUM SECTION $P = 1{\cdot}25\, P_{cu}$

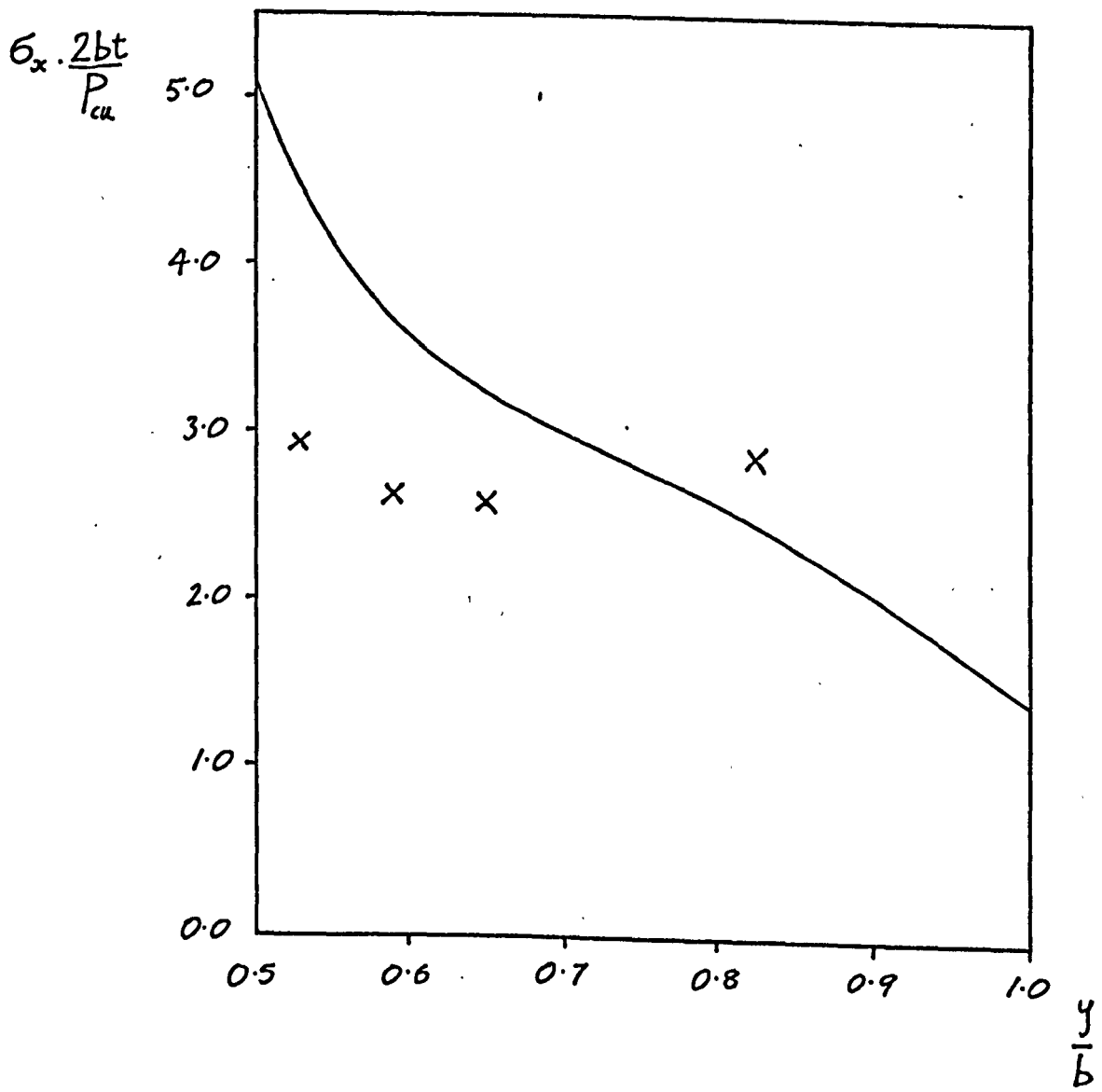

FIGURE 5.77 STRESSES AT THE MINIMUM SECTION $P = 1.66\, P_{cu}$

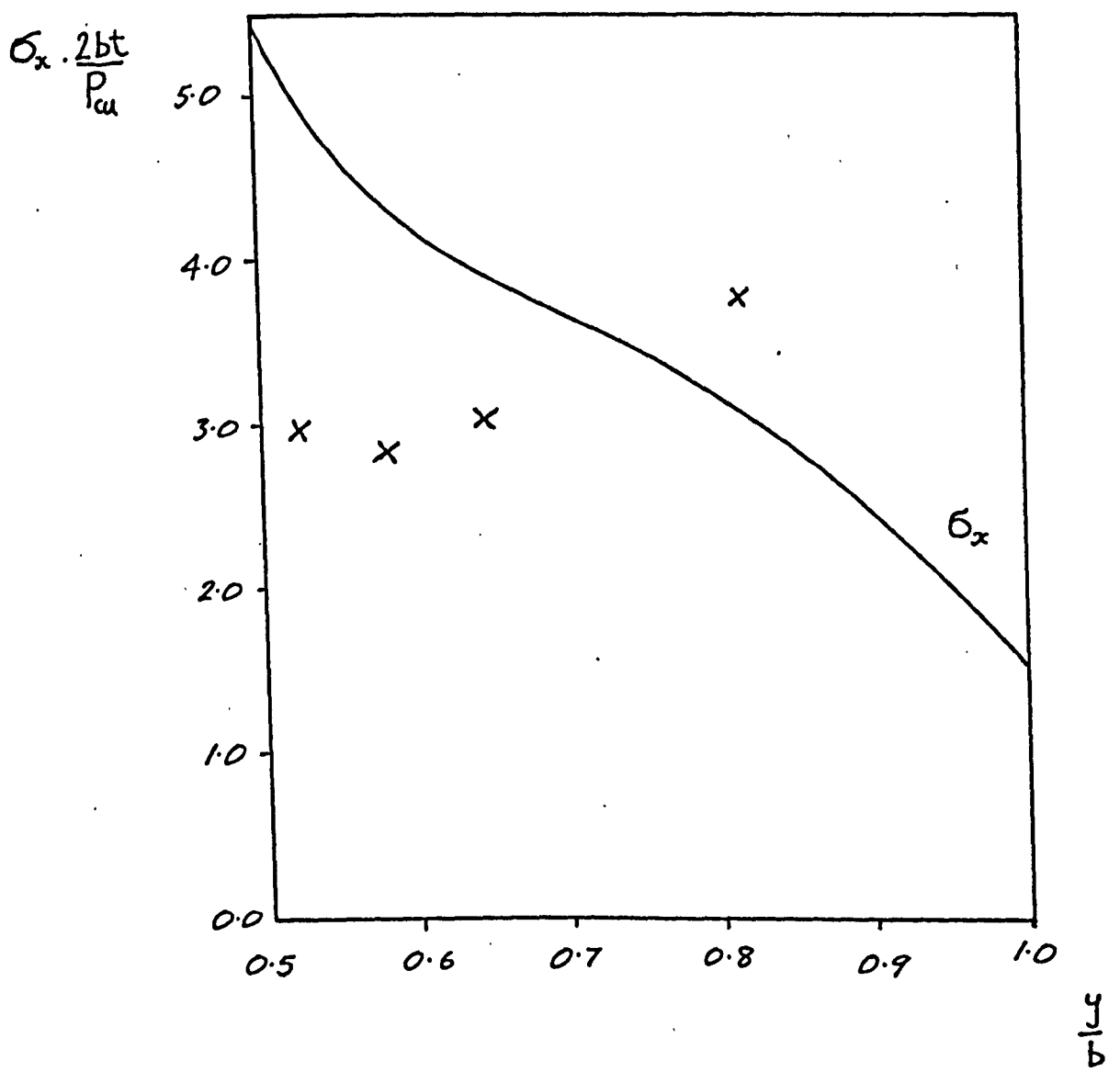

FIGURE 5.78 STRESSES AT THE MINIMUM SECTION $P = 2{\cdot}03\, P_u$

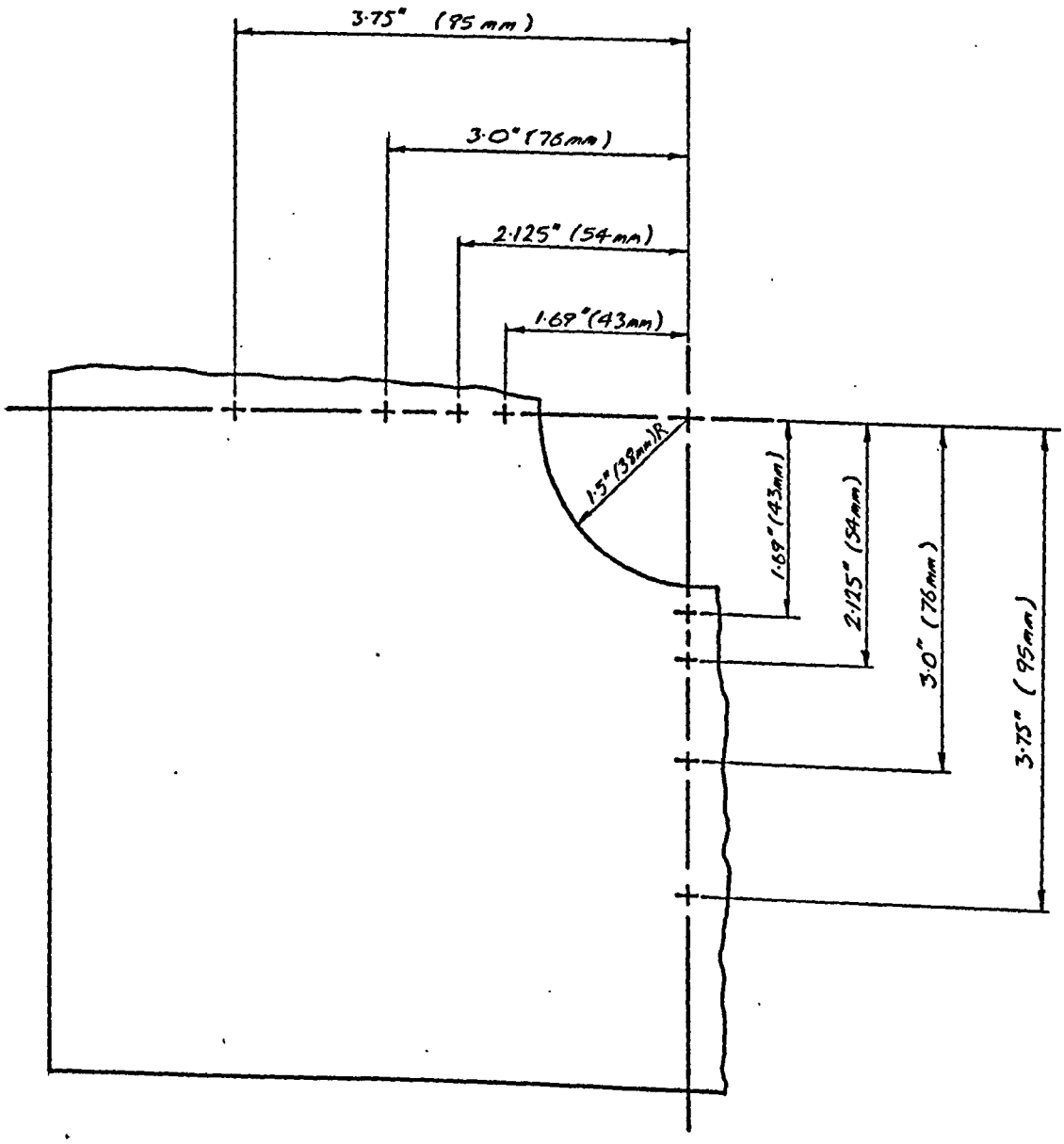

FIGURE 5.79 ARRANGEMENT OF STRAIN GAUGE ROSETTES ON PLATE D

For the purpose of comparison of theoretical and experimental results the x and y axes of the plate are taken to pass through the centre of the plate.

FIGURE 5.80 STRESSES AT THE MINIMUM SECTION. $P=0.96P_{cu}$

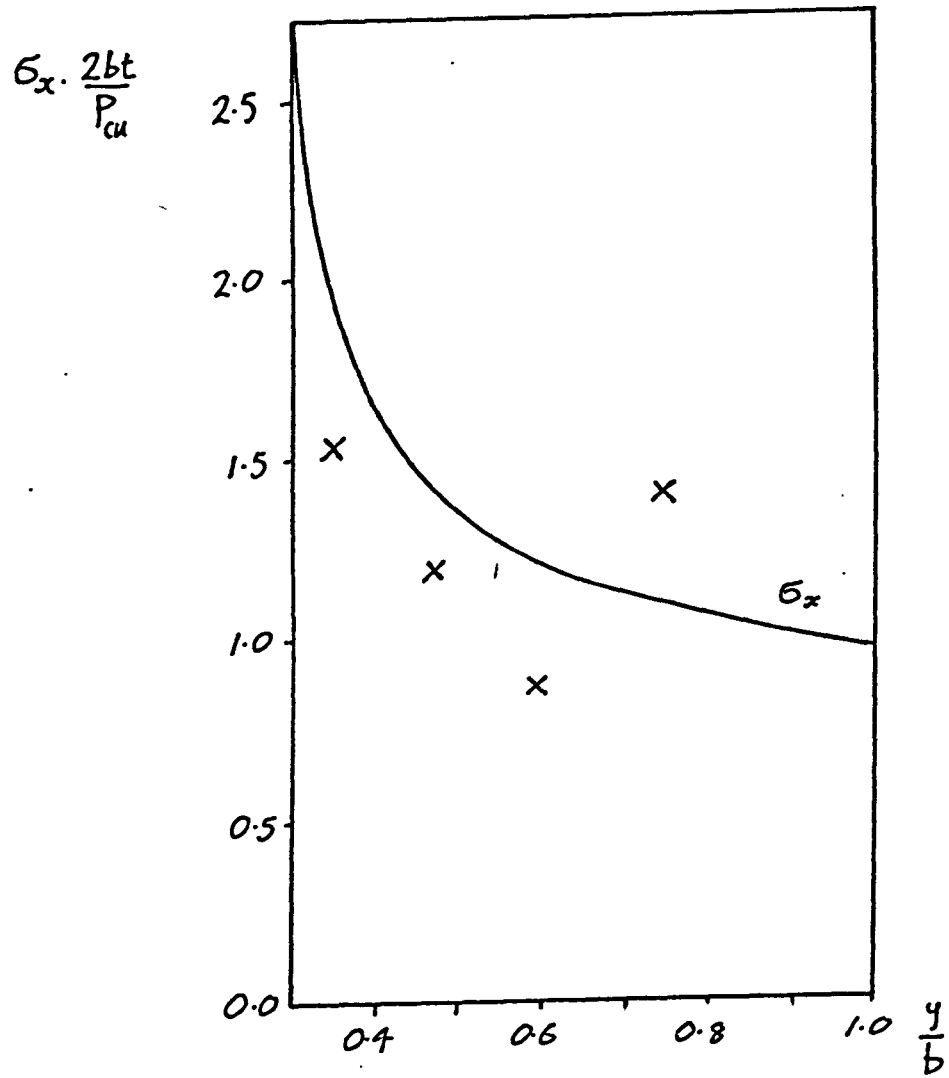

FIGURE 5.81 STRESSES AT THE MINIMUM SECTION $P=1.11P_{cu}$

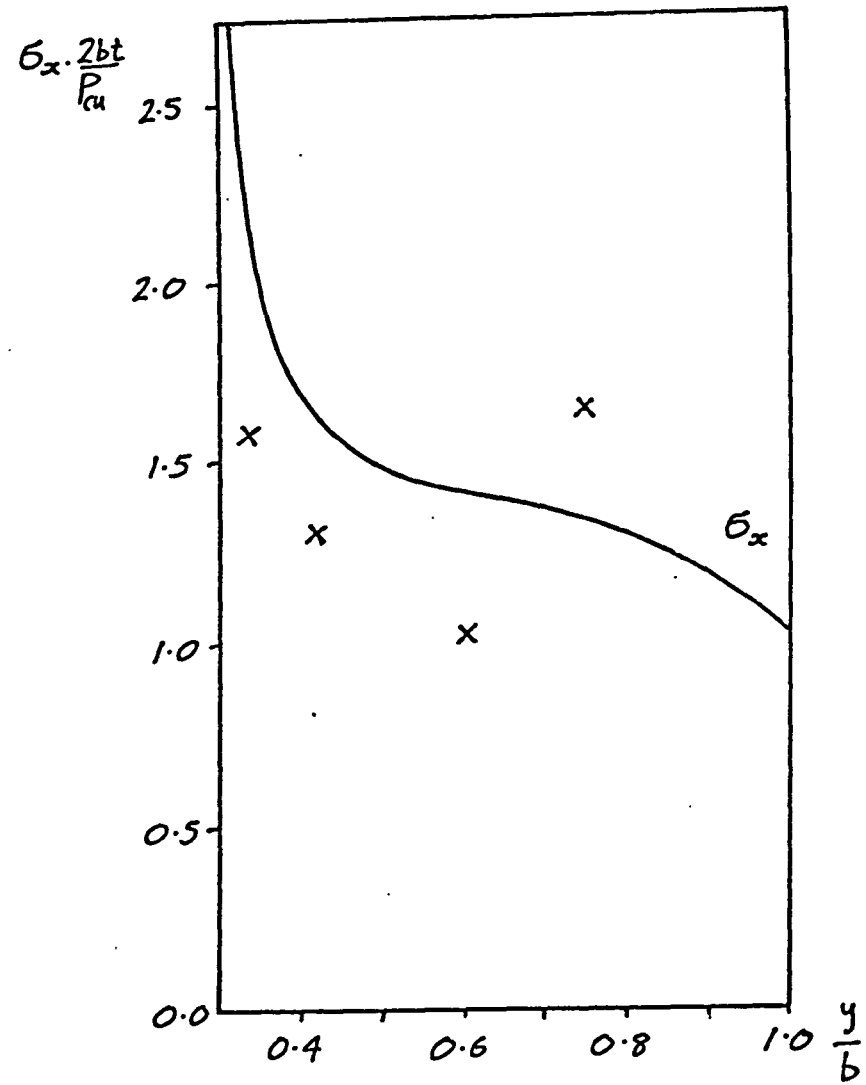

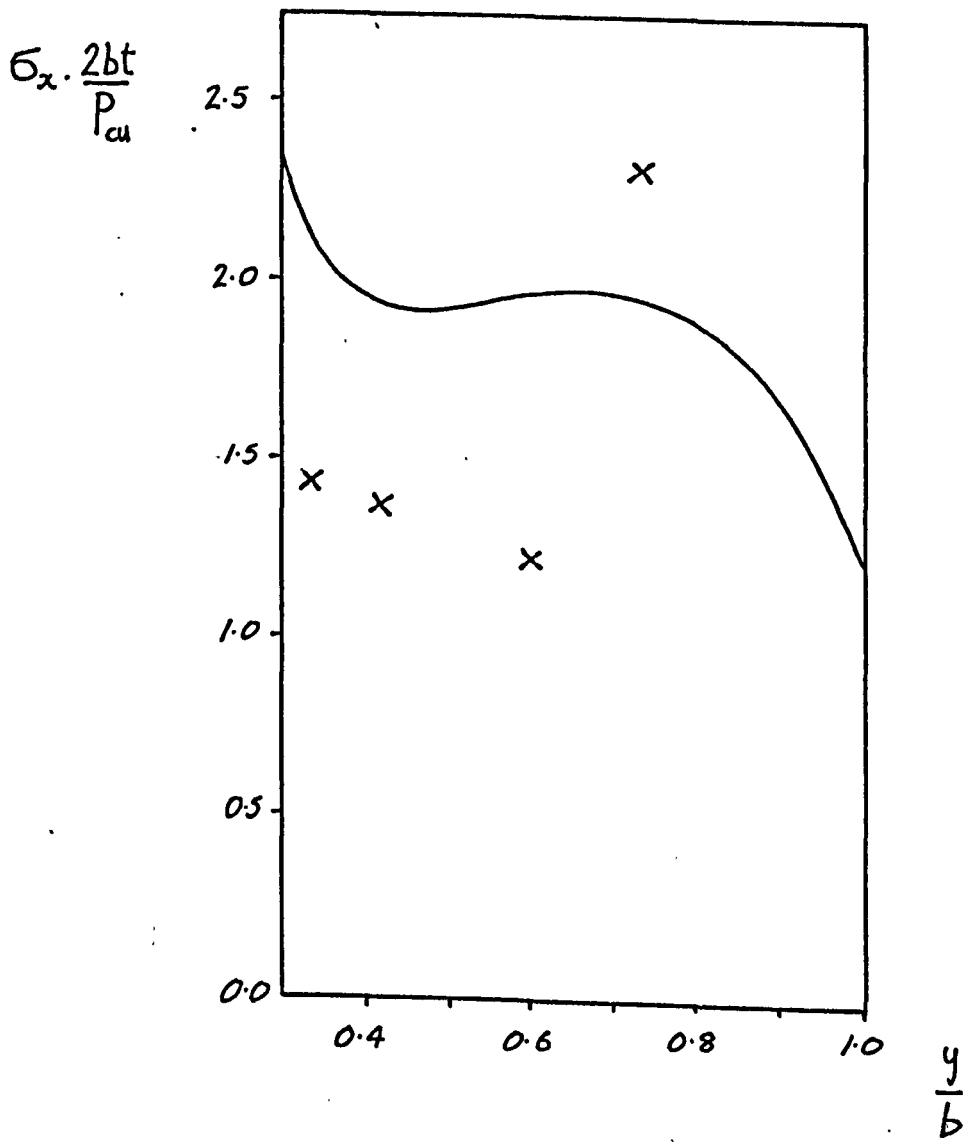

FIGURE 5.82 STRESSES AT THE MINIMUM SECTION $P = 1{\cdot}47 P_{cu}$

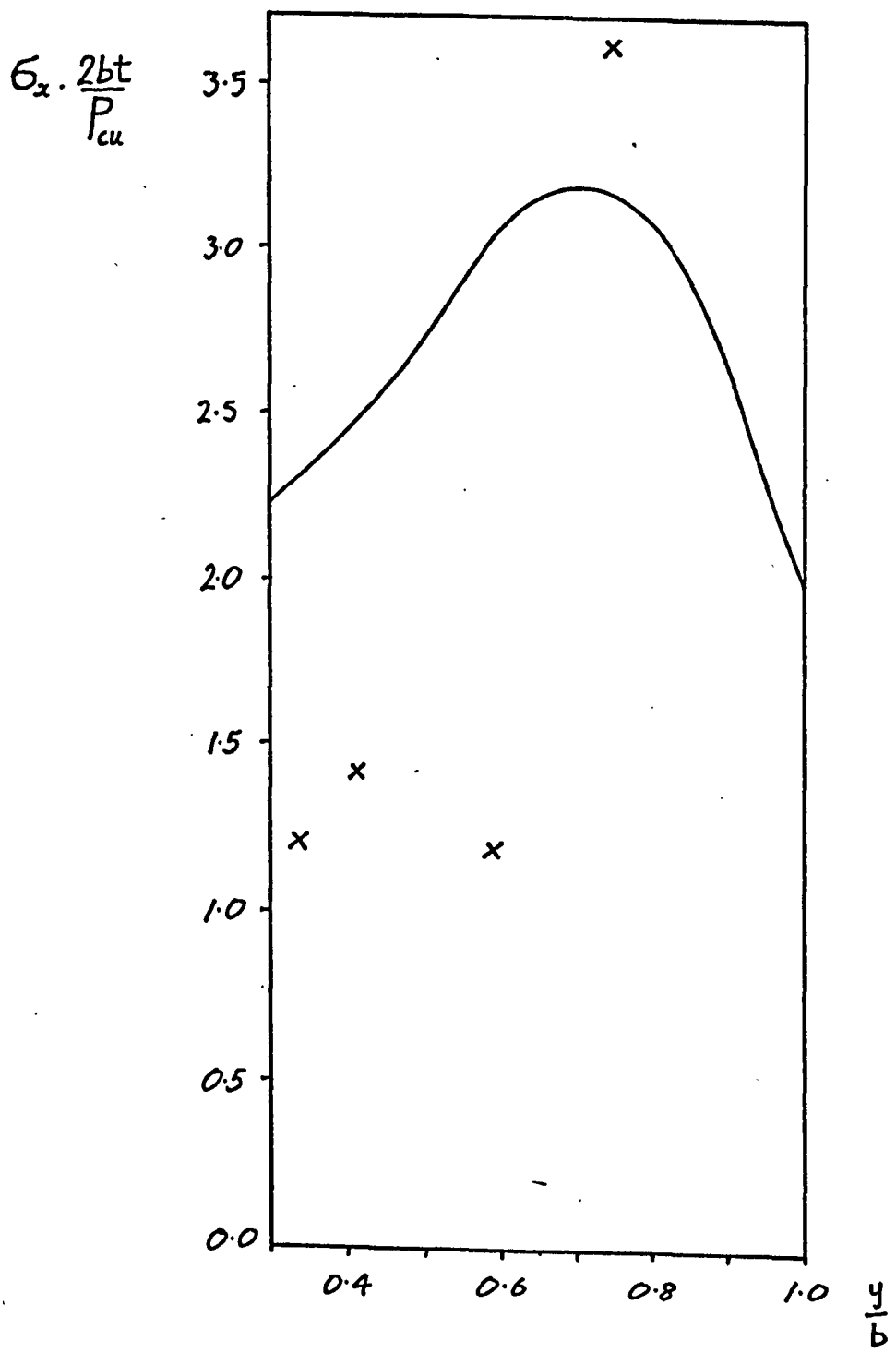

FIGURE 5.83 STRESSES AT THE MINIMUM SECTION $P = 2.21\, P_{cu}$

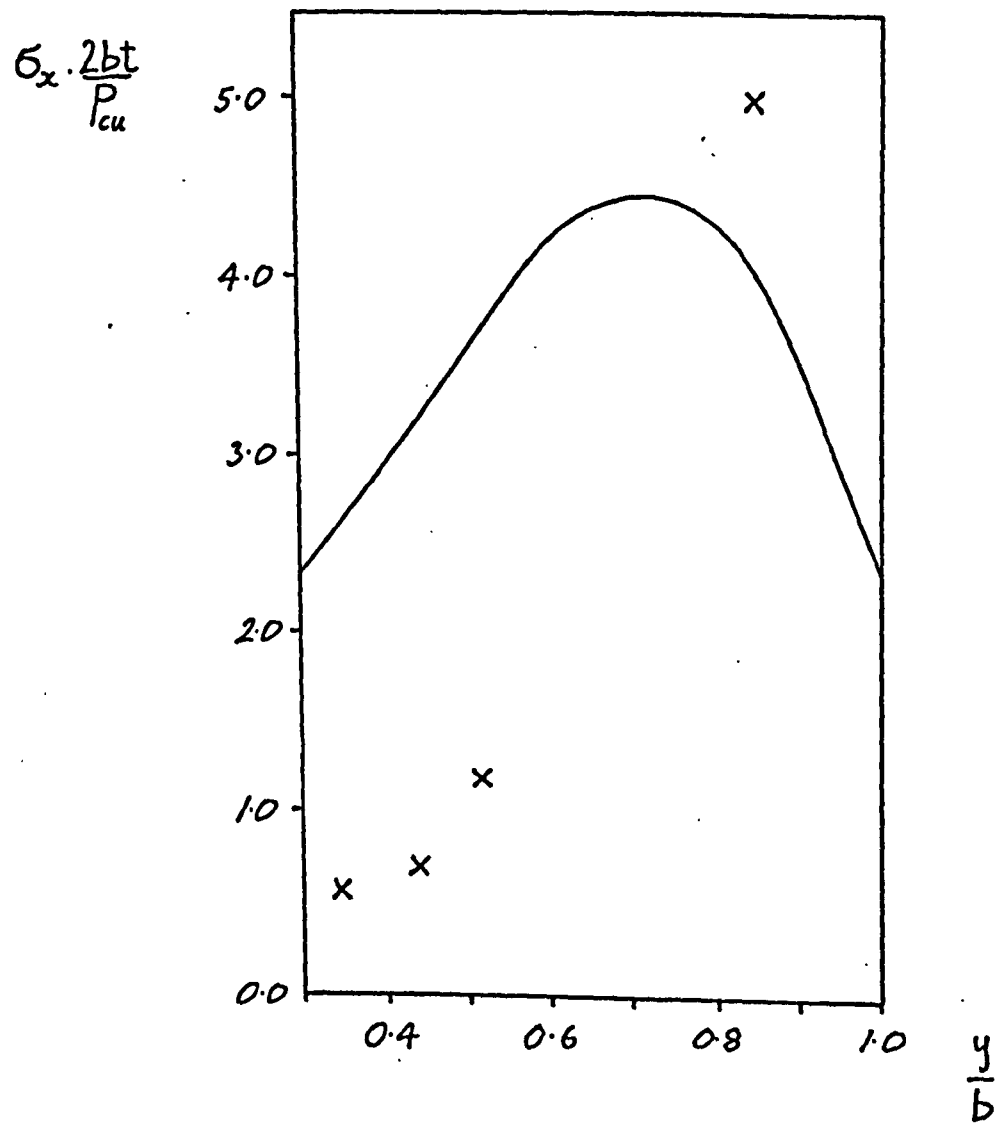

FIGURE 5.84 STRESSES AT THE MINIMUM SECTION $P = 2{\cdot}95\, P_{cu}$

CHAPTER SIX

Discussion of the Theoretical and Experimental Results

6.1 Buckling

Comparison between theoretical and experimental results for the buckling loads of the square plates under test is illustrated in Figure 5.2. There is scatter in the experimental results. However, the trend of increasing buckling load with hole size is clearly seen, and agreement between the theoretical and experimental values is good. Comparison between the author's theoretical results for constant edge displacement loaded square plates and the theoretical results derived by Kawai and Ohtsubo illustrated in Figure 5.6 show some slight differences. However, this can be attributed to the differing deflection functions used, i.e. Kawai and Ohtsubo used a truncated polynomial series of the following type:-

$$w = \sum_{r=1}^{R} \sum_{p=1}^{P} x^p y^r$$

Favourable comparisons can be seen in Figure 5.5 between the author's theoretical results for constant stress loaded square plates and the theoretical results derived by Kumai (18) and Levy (16), and also between the experimental results of Kumai and Yoshiki et al. (23). The author's theoretical results agree more closely with the experimental results of Yoshiki and Kumai than the other theoretical results. Kumai and Levy's theoretical analyses both used infinite plate stress distributions, which limited rigorous

application of their results to plates with hole diameters less than 0.3 times the plate width. In addition, Kumai's out-of-plane deflection equation was invalid for plates with large hole sizes, for the reasons outlined in Chapter One.

Comparison between the theoretical and experimental buckling loads of the rectangular plates tested is shown to be good in Figure 5.3, and the trend of increasing buckling load with increase in hole size is clearly shown. The theoretical analysis generally predicted the buckling mode of the rectangular plates. The few exceptions were plates with hole sizes in the region of the critical hole diameter at which the change in buckling mode occurs. The possible sources of uncertainty over the mode of buckling in this region are, very large initial imperfections interfering with the buckling mode; coupled modes of buckling arising in the immediate post-buckled region; or interaction between the previous two causes.

The presence of large initial imperfections are seen in the experimental load - out-of-plane deflection curves for most of the plates tested. The possibility of coupled modes of buckling is indicated by the load - end displacement graph shown in Figure 5.34 for a plate with a hole diameter of 0.3 times the plate width, in which the curves for the two and three half-wave modes intersect. However, this uncertainty only occurred in a few of the plates with hole diameter near that of the critical size.

6.2 Post-Buckling Behaviour

6.2.1 Out-of-plane Deflections

The author's theoretical results agree well with the results derived by Yamaki for out-of-plane deflections of a plate with a square buckle, and the comparison is illustrated in Figure 5.7. The agreement is particularly close in the immediate post-buckling range, but deteriorates due to the author's theory having a fixed deflected shape corresponding to the buckling mode, and Yamaki's solution having four variable terms. The effectiveness of the test rig in reproducing the plate behaviour under the required boundary conditions can therefore be estimated from the close agreement of the author's theoretical results with the experimental results for plates with no holes, illustrated in Figures 5.9, 5.10 and 5.19.

Comparison of the theoretical and experimental results for out-of-plane deflections of plates with small hole sizes (diameters less than 0.3 times the plate width) is good for both square and rectangular plates, and is illustrated in Figures 5.11, 5.12 and 5.20 to 5.23 for both square and rectangular plates respectively.

The accuracy of agreement between theory and experiment deteriorates with increasing hole size for diameters greater than 0.4 times the plate width, and is illustrated in Figures 5.13 to 5.15 and 5.24 to 5.27 for square and rectangular plates respectively. This deterioration in accuracy arises from the author's theory using a fixed deflected shape, which is unable to reproduce a free edge

boundary condition at the hole edge. This is due to the inaccuracy of the energy expressions increasing with increase in hole diameter because of the discrepancy between the approximate and actual boundary conditions.

In general, the reduction in accuracy of theoretical results with increasing load arises from the theoretical post-buckling deflection being fixed in shape. However, agreement between theory and experimental results is good at low levels of loading.

6.2.2 End Compression

The load - end compression relationships shown in Figures 5.29, 5.31 and 5.32 show an almost constant post-buckling stiffness for each buckled mode for any hole size. This is further illustrated in Figures 5.30 and 5.33, which show the relationship between hole size and pre- and post-buckling stiffnesses for square plates and rectangular plates with various buckling modes.

The post-buckling load - end compression curve for a plate with no hole was tangential to the curve calculated by Yamaki at the point of buckling. The deviation between the two curves was due to Yamaki's solution having four terms of variable magnitude in the post-buckling region. The single degree of freedom allowed by the author's theory overestimated the strain energy of the plate, which caused the stiffness of the plate to be overestimated when the total potential energy was minimised. In this case, this meant that the end displacements were underestimated for any given load, and this was observed in comparison with

Yamaki's solution.

6.2.3 Post-Buckling Stresses

The accuracy of the experimental stresses was dependent upon the accuracy of measurement of the strains, which, in turn, was highly dependent on the gradient of the strain field over the gauge area, and on the magnitude of the strain, as the constant measurement errors obviously became a smaller proprtion as the magnitude of the strain measurement increased. As an example, this reasoning infers that the ε_y strains along the y-axis are relatively less accurate than the ε_x strain along the same axis, the ε_x strains being higher in magnitude, and having less steeply sloping gradients. The corresponding σ_x stresses calculated on the y-axis from the strain measurements will therefore be more accurate than the σ_y stresses.

Figure 5.41 illustrates the relative magnitudes of the theoretical and experimental stresses at approximately twice the buckling load in Plate A. This figure shows that the σ_x stresses across the minimum section are the greatest stresses in the direction of loading. Therefore the effectiveness of the theoretical analysis was assessed by its ability to predict these stresses.

Comparison between theoretical and experimental stresses for Plate A is good until approximately twice the buckling load. Similar trends of redistribution of theoretically and experimentally derived stresses occur for the σ_x stress distribution on the y-axis in Figures 5.42 to 5.48 and for the σ_x and σ_y stress distributions on the x-axis in Figures 5.49 to 5.53 and 5.54 to 5.56. The

theoretical redistribution of σ_x stresses across the minimum section is illustrated for Plate A in Figure 6.1. The theoretical analyses of Plates B and C (hole diameters of 0.6 and 0.5 times the plate width respectively) did not reproduce the observed redistribution of stresses. In plate D (hole diameter 0.3 times the plate width) the theoretical analysis showed the same type of experimentally observed redistribution found in Plates A, B and C. Unfortunately the experimental results for this case were so unrealistic that they were not considered to be valid.

The accuracy of the theoretical deflections strongly affects the accuracy of the calculated post-buckling stresses. The stresses were calculated by the method described in Chapter Three from equations 3.33a - c which are based on squares of the derivatives of the deflection function. Differentiation of the deflection function induces a greater error in the derivatives than in the function. The relatively lower accuracy of the theoretical out-of-plane deflections for large holes (diameters greater than 0.3 times the plate width) than for small holes (diameters less than 0.3 times the plate width) therefore explains the inability of the theory to predict the post-buckling redistribution of stresses in plates with large holes. The reduction in accuracy of the theoretical deflections with increasing load, shown in all the plates tested, also explains the loss in accuracy of the theoretical stress distributions in Plate A beyond approximately twice the buckling load.

6.2.4 Summary of the Discussion on the Post-Buckling Behaviour

The comparison between theoretical and experimental results infers that the application of the results from the theoretical analysis should be confined to within twice the buckling load and to plates with hole diameters less than 0.3 times the plate width for good accuracy of out-of-plane deflections and post-buckling membrane stress. This infers that the theoretical analysis would be useful for studying relatively thick plates where collapse occurred around twice the buckling load, and the membrane stresses produced by out-of-plane deflections were a relatively small proportion of the total stress distribution.

6.3 Collapse

The experimental results presented in Figure 5.39 show that the collapse load only decreased slightly with increase in hole size, and that there are still relatively large reserves of strength left in a plate even with a large hole. A change of collapse mode was observed to occur in both the square and rectangular plates, and this is described in the previous chapter as a change from a mode I to a mode II type failure.

The experimental collapse loads and the results of the failure analysis are compared in Figure 5.39. The failure analysis produced results which followed the trends of reduction in ultimate load observed in the tests. The analysis is described in Chapter Three and the four assumptions made in formulating the analysis were explained in

detail. The first assumption was that collapse occurred when the maximum stress in the loaded direction reached yield, and this allows the ultimate load to be related to the effective width and yield stress. This assumption is accurate if applied to effective widths calculated from collapse loads, as in references 33 and 34, or from elastic stress distributions, as opposed to effective widths calculated from end shortening as in reference 22.

The second assumption on the redistribution of stresses in the post-buckling region was justified by the results of the experimental strain analysis of Plates A, B and C in which the peak stresses occurred at the supported edge of the plate after buckling. This redistribution was accurately predicted in plates with small holes up to approximately twice the buckling load, which made it necessary to resort to an approximate method in order to calculate the effective widths. Because the theoretical analysis was inaccurate over approximately twice the buckling load, it was necessary to base an approximate analysis on a more accurate post-buckling analysis of the load - effective width relationship for a plate with no hole. The analysis chosen for the basis of the collapse analysis was Rhodes and Harveys' (30).

The third and fourth assumptions were on the differences between the post-buckling stress distributions of plates with holes and unperforated plates. The low accuracy of the theoretical stress distributions near collapse load levels did not allow the mode of redistribution to be examined and hence these assumptions could not be improved upon. However,

the theoretical results for the collapse loads are in good agreement with the experimental results.

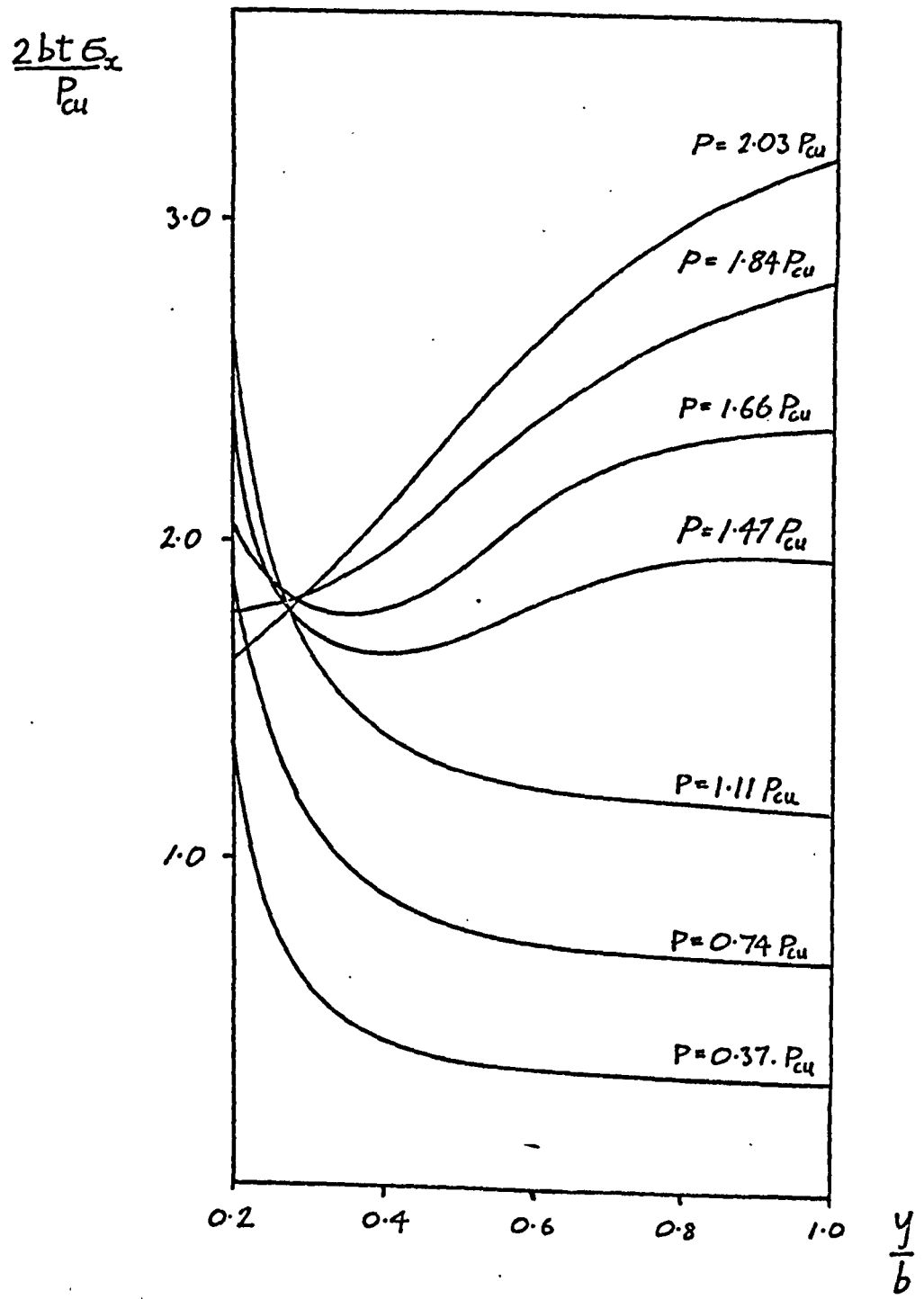

FIGURE 6.1 THE REDISTRIBUTION OF POST-BUCKLING STRESSES IN PLATE A ACROSS THE MINIMUM SECTION

CHAPTER SEVEN

General Discussion on the Buckling and Post-Buckling Behaviour of Plates with Holes

7.1 Buckling

The load at which buckling occurs in a plate is related to the pre-buckling distribution of membrane stress and the amount of rotational or translational restraint on out-of-plane deflections. Buckling more readily occurs when the maximum stresses occur where the out-of-plane restraint is low.

By this reasoning, the introduction of a small hole into a plate causes a decrease in the resistance to buckling, due to the introduction of a free edge with an associated stress concentration, and can be seen in Figures 5.2 and 5.5 for square simply supported plates with no in-plane edge restraint. For relatively large hole sizes the stresses diffuse towards the supported edge in rectangular plates and also in square constant edge displacement loaded plates, due to the relatively low stiffness of the loaded edge opposite the hole. This causes an increase in the buckling load shown in Figures 5.2 and 5.3. This diffusion of stress towards the edges does not happen in constant stress loaded square plates, as illustrated in Figure 7.1, and this produces the decrease in buckling load illustrated in Figure 5.5.

The effect of rotational edge restraint can be seen from a comparison of the results for simply supported square plates with constant stress loaded edges shown in Figure 5.5, with the results obtained by Kumai for clamped plates, shown

in Figure 7.2. The constant stress load produces a decrease in buckling load with increase in hole size in comparison with the increase in buckling load shown by clamped plates for relatively large holes. This increase is due to stresses around the hole being distributed towards a region highly restrained against out-of-plane rotation as well as translation.

The results shown in Figure 1.3 for simply supported square plates tested by Schlack under uniform edge compression showed a decrease in buckling load in comparison with the results obtained by the author. This was due to the additional restraint of holding the unloaded edges straight, which raised the general level of stresses in the plate.

The author's theoretical and experimental work, and the work of other investigators, has allowed the effects of various types of boundary and loading conditions to be qualitatively identified. This allows some speculation, based on fact, to be made about the local buckling behaviour of various plate components to be discussed. Compression flanges and webs of thin walled beams and columns are of interest. Compression flanges have a degree of rotational edge restraint from the neighbouring elements which also impose some constraint on the in-plane edge displacements of the flange. However, this latter restraint is considered to be slight, as it does not prevent the edges of unperforated flanges moving in the post-buckling range. In long rectangular flanges, the differences in stress distribution produced

by different types of loading diffuse in accordance with St. Venants principle. This would tend to cause a slight reduction in buckling load for plates with small holes and an increase for plates with large holes, as previously described. Thus the general trend in behaviour would be expected to be an increasing buckling load with increasing hole size.

The results of local buckling tests performed by Yu and Davis (31) on uniform thickness cold rolled beams and columns, with a centrally located circular hole in the compression flange, are illustrated in Figure 1.6. These results showed a slight reduction in buckling load with increasing hole size, and the theoretical relationship derived by Kawai and Ohtsubo (24) for simply supported square plates under constant stress loading was selected by Yu and Davis as a suitable conservative design curve. However, there is the possibility that in estimating the proportion of the load carried by the flange, the stiffness of the neighbouring flanges was overestimated due to the presence of initial imperfections, which would have introduced errors into the estimation of the buckling loads.

The theoretical buckling analysis described in Chapter Three can be readily applied to thin-walled sections composed of an assembly of thin plates. The out-of-plane deflections can be represented by the deflection functions used in the analysis of thin-walled beams by Rhodes (35) and the pre-buckling membrane stress distributions can be readily obtained from a plate bending and membrane stress finite element analysis.

7.2 Post-Buckling Behaviour and Collapse

The experimental and theoretical investigations of the post-buckling stresses in square and rectangular plates with simply supported edges and uniformly compressed loaded edges, has shown that the mode of redistribution of stresses in plates with holes is similar to that in a plate with no hole. This similarity is in the way that the stresses tend to diffuse towards the supported edges away from the peak of a buckle, so that the maximum stresses occur along the supported edges of a plate. It is therefore a reasonable assumption to consider that the post-buckling distribution of stresses in plates with holes under different boundary conditions and loading conditions follows the same trends as similarly loaded and restrained plates with no holes. By making this assumption, the method of analysis described in Chapter Three can be applied to plates with holes, if an analytical solution exists for the post-buckling behaviour of a similarly loaded and restrained plate with no hole. The limitations on the application of the results of such theoretical analyses cannot be readily assessed. However, the factors affecting the accuracy of the theoretical analysis have been discussed, and the results of these discussions can be used as a basis for planning tests to determine the limits of accuracy for other cases.

The collapse analysis can also be applied to plates with other boundary conditions if there has been a relationship established between applied load and effective width for plates with no holes. This is because the collapse analysis is based on the correction of the post-buckling

stress distribution in a plate with no hole, in order to allow for the redistribution of stresses caused by the introduction of a hole. Only a mathematical approximation to the shape of the post-buckling stress distribution is required.

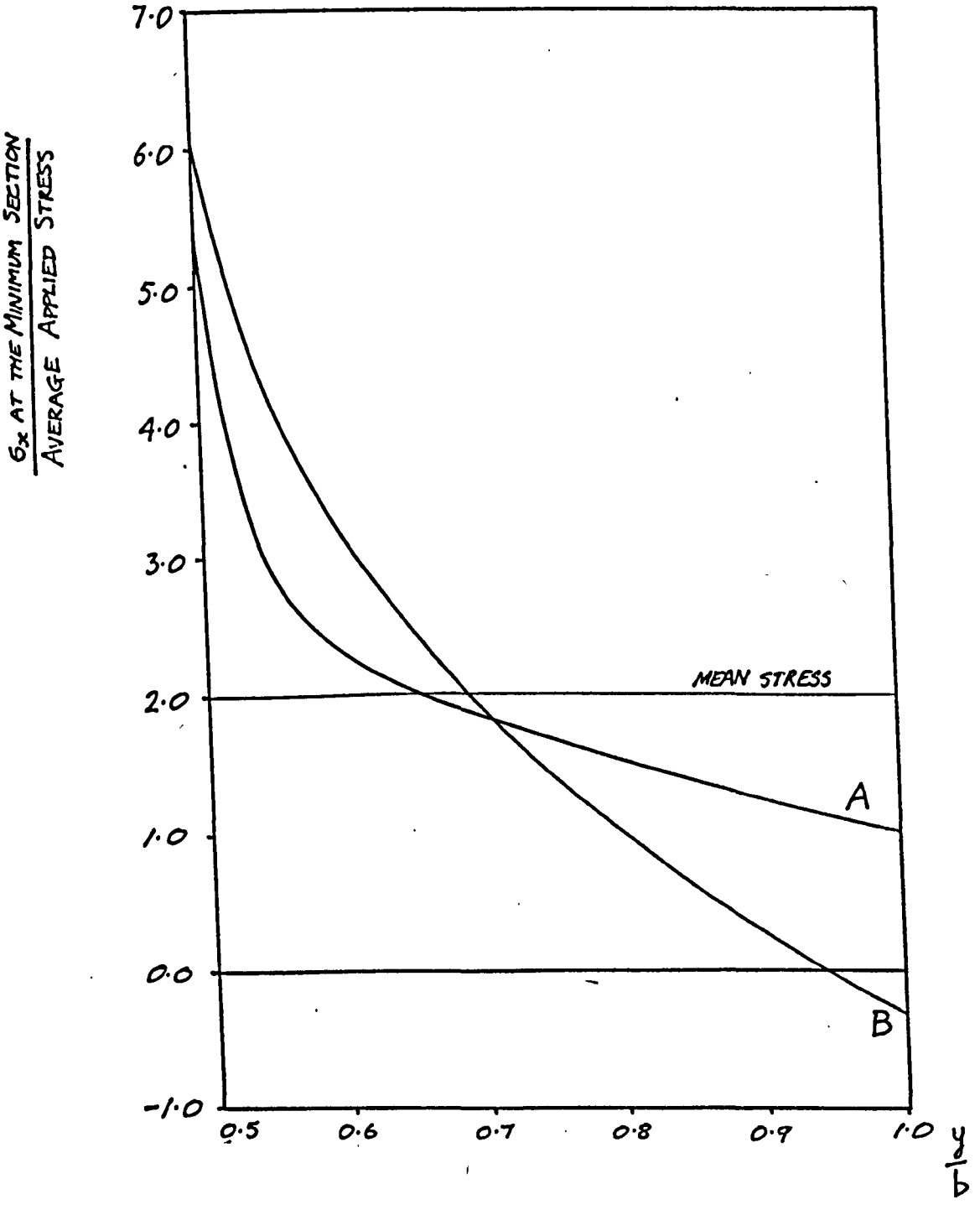

FIGURE 7.1 PRE-BUCKLING STRESS DISTRIBUTION IN A SQUARE PLATE WITH A HOLE OF RADIUS 0·5b

A - UNIFORM DISPLACEMENT LOADING

B - UNIFORM STRESS LOADING

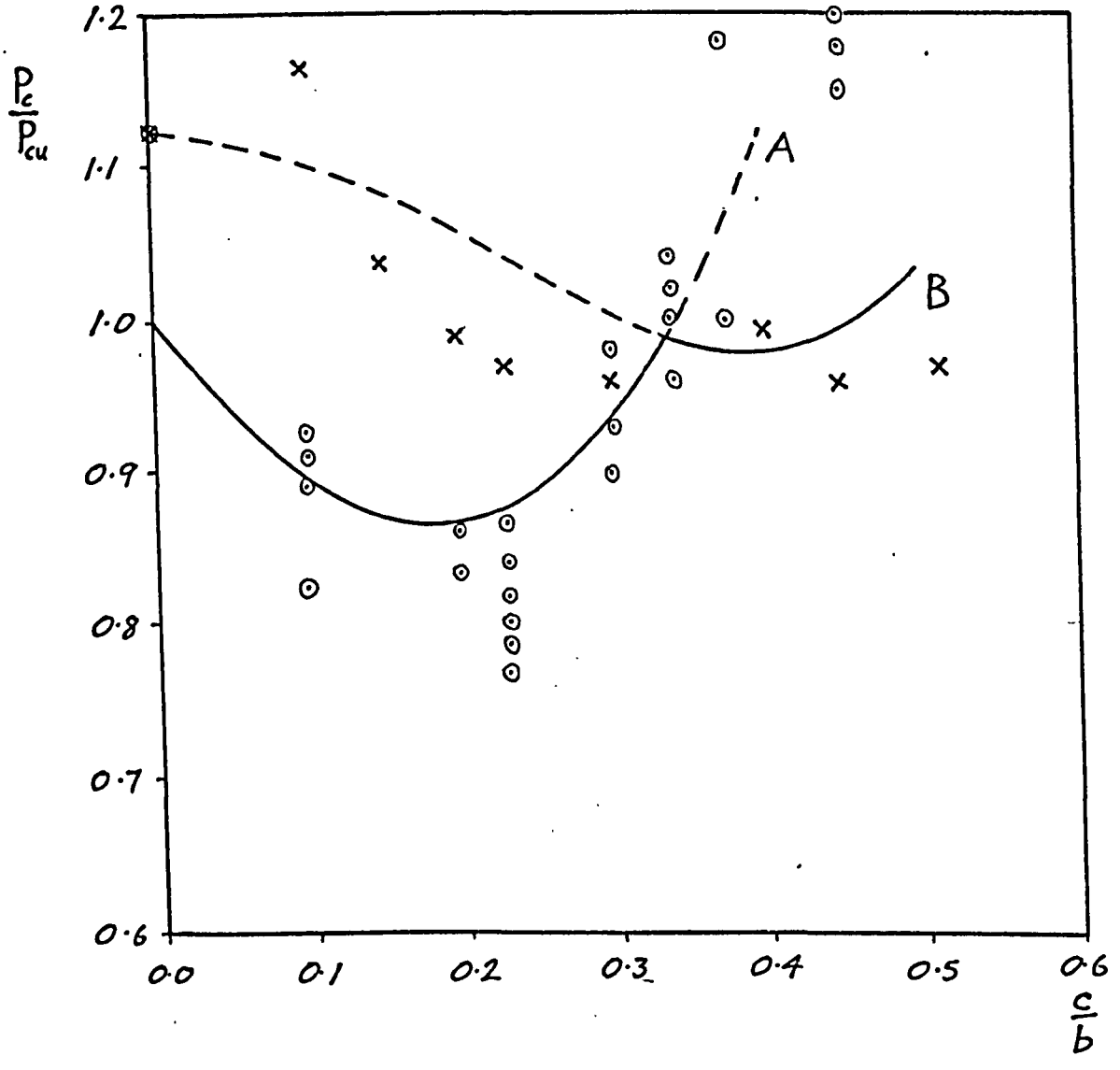

FIGURE 7.2 THEORETICAL AND EXPERIMENTAL VARIATION OF BUCKLING LOAD WITH HOLE RADIUS FOR CLAMPED SQUARE PLATES. DERIVED BY KUMAI (18).

⊙ A - FIRST MODE

× B - SECOND MODE

CHAPTER EIGHT

Conclusions and Suggestions for Future Work

The discussion of the theoretical analysis, and its comparison with the author's experimental results and the experimental results of previous investigators led to certain conclusions being drawn, and also suggested some areas and directions for future work.

8.1 Suggestions for Future Work

1. A thorough experimental examination of the post-buckling out-of-plane deflections for initial buckling modes and changes of buckling mode could be made.
2. The stability analysis could be applied to perforated compression flanges of typical cold formed sections.
3. The stability analysis of suggestion 2 could be extended to a post-buckling analysis, using a theoretical analysis such as that described in reference 35 as a basis for the post-buckling behaviour.
4. The collapse analysis could be extended to plates with different boundary conditions, and to the compression flanges of thin-walled beams and columns.

8.2 Conclusions

1. The theoretical buckling analysis was successful, in that it accurately predicted the results of tests conducted on square and rectangular plates described in this

thesis, and also predicted the experimental results of other investigators with improved accuracy over previous theoretical analyses.

2. The theoretical post-buckling analysis of out-of-plane deflections was most successful at predicting the experimentally observed out-of-plane deflections of the simply supported square and rectangular plates tested, for the range of hole diameters 0.0 to 0.3 times the plate width.

3. The experimentally measured post-buckling membrane stress distribution showed the redistribution of stresses in the post-buckling range of a plate with a centrally located circular hole to occur in a manner similar to that in a plate with no hole, in that the maximum stress in the direction of loading became concentrated close to the supported edge of the plate.

4. The theoretical analysis of post-buckling stresses successfully predicted the trends of post-buckling stress redistribution and showed good agreement with the experimentally measured stresses for plates with relatively small holes (diameters less than 0.3 times the plate width) for applied loading up to approximately twice the buckling load.

5. The experimentally measured collapse loads of the plates were not appreciably influenced by hole size until a hole diameter of approximately 0.3 times the plate width. Beyond this hole size the collapse loads decreased slightly with increasing hole diameter.

6. The collapse analysis accurately and conservatively agreed with the experimentally observed collapse loads.

BIBLIOGRAPHY

1. TIMOSHENKO, S.P. GERE J.M.
   Theory of Elastic Stability
   McGraw-Hill

2. BLEICH F
   Buckling Strength of Metal Structures
   McGraw-Hill

3. BULSON, P.
   The Stability of Flat Plates
   Chatto and Windus, 1970.

4. ODEN, J.T.
   Mechanics of Elastic Structures
   McGraw-Hill

5. ARGYRIS, J.H. KELSEY, S.
   Energy Theorems and Structural Analysis
   Butterworth

6. BUDIANSKY, B. HU, P.C.
   The Lagrangian Multiplier Method of Finding Upper and Lower Limits to Critical Stresses of Clamped Plates
   N.A.C.A. Report No. 848 1946

7. CONWAY, H.D., LEISSA, A.W.
   A Method for Investigating certain Eigenvalue Problems in the Buckling and Vibration of Plates
   Jour. Applied Mechanics v. 27 pp. 557-558 1960

8. ZIENKIEWICZ, O.C.
   The Finite Element Method in Engineering Science
   McGraw-Hill

9. ARGYRIS, J.H. , KELSEY, S., KAMEL, H.

Matrix Methods of Structural Analysis

AGARD-ograph 72, Pergamon Press

10. ROCKEY, K.C., ANDERSON, R.G., CHEUNG, Y.K.

The Behaviour of Square Shear Webs having a Circular Hole.

Thin Walled Steel Structures

Crosby and Lockwood.

11. TURNER, M.J., DILL, E.H., MARTIN, H.C., MELOSH, R.J.

Large Deflections of Structures Subjected to Heating and External Loads.

Jour. of Aeronautical Sciences v. 27, pp. 97-106 1960

12. BREBBIA, C., CONNOR, J.

Geometrically Non-Linear Finite Element Analysis

Proc. A.S.C.E. Jour. Engineering Mechanics Div. v. 95 EM2 April 1969

13. MURRAY, D.W. WILSON, E.L.

Finite Element Large Deflection Analysis of Plates

Proc. A.S.C.E. Jour. Engineering Mechanics Div. v. 94 EM1 1969

14. YETTRAM, A.L., AWADALLA, E.S.

A Direct Method for the Elastic Stability Analysis of Plates

Int. Jour. Mechanical Science v. 10 pp. 887-901 1968

15. WALKER, A.C.

Rayleigh-Ritz Method for Plate Flexure

Proc. A.S.C.E Jour. Engineering Mechanics Div. v. 93 EM6 1967

16. LEVY, S., WOOLLEY, R.M., KROLL, W.D.

Instability of a Simply Supported Square Plate with Reinforced Circular Hole in Edge Compression

Jour. Research National Bureau of Standards v. 39 pp. 571-577 December 1947

17. GURNEY, G.

An Analysis of the Stresses in a Flat Plate with a Reinforced Circular Hole under Edge Forces

Aero. Research Committee R and M No. 1834 1938

18. KUMAI, T.

Elastic Stability of the Square Plate with a Central Circular Hole under Edge Thrust

Reports of the Research Institute for Applied Mechanics (Japan) v. 1 No. 2 1952

19. SCHLACK, A.L.

Elastic Stability of Pierced Square Plates

Proc. Soc. Experimental Stress Analysis v. 21 pt. 1 pp. 167-172 1964

20. SCHLACK, A.L.

Experimental Critical Loads for Perforated Square Plates

Proc. Soc. Experimental Stress Analysis v. 25 pt. 1 pp. 69-74, 1968

21. COAN, J.M.

Large Deflection Theory for Plates with Small Initial Curvature Loaded in Edge Compression

Trans. A.S.M.E. Jour. Applied Mechanics v. 73 pp. 143-151 1951

22. YAMAKI, N.

Post-Buckling Behaviour of Rectangular Plates with Small Initial Curvature Loaded in Edge Compression

Jour. Applied Mechanics v. 26 pp. 407-414 1959
Jour. Applied Mechanics v. 27 pp. 335-342 1960

23. YOSHIKI, M. FUJITA, Y KAWAMURA, A ARAI, H.

Instability of Plates with Holes

Proc. Soc. Naval Architects Japan No. 122 Dec. 1967
N.L.L. Translation RTS 8008

24. KAWAI, T. OHTSUBO, H.

A Method of Solution for the Complicated Buckling Problems of Elastic Plates with Combined Use of Rayleigh-Ritz's Procedure in the Finite Element Method.

Proc. 2nd Air Force Conference on Matrix Methods in Structural Mechanics October 1968

25. TIMOSHENKO, S.P. WOINOWSKY-KRIEGER, S.

Theory of Plates and Shells

McGraw-Hill

26. WANG, C-T.

Non-Linear Large Deflection Boundary Value Problems of Rectangular Plates.

N.A.C.A. TN 1425 1968

27. COX, H.L.

The Buckling of Plates and Shells

Chapter 2

Pergamon Press

28. HOWLAND, R.C.J.

On the Stresses in the Neighbourhood of a Circular Hole in a Strip under Tension

Phil. Trans. of the Royal Society v. 229A, p. 49 1930

29. MARGUERRE, K.

The Apparent Width of the Plate in Compression

N.A.C.A. Tech. Memo. 833

30. RHODES, J. HARVEY, J.M.

Post-Buckling Behaviour of Thin Flat Plates in Compression with the Unloaded Edges Elastically Restrained against Rotation

Jour. Mech. Eng. Sciences v. 13 n. 2 1971

31. YU, W.W. DAVIS, C.S.

Cold Formed Steel Members with Perforated Elements

Proc. A.S.C.E. Jour. Structural Division v. 99 ST 10 p. 2061 1973

32. LEVY, S.

Bending of Rectangular Plates with Large Deflections

N.A.C.A. Report No. 737 1942

33. WINTER, G.

Commentary on the 1968 Edition of the Specification for the Design of Cold-Formed Steel Structural Members.

American Iron and Steel Institute 1970

34. VON KARMAN, T., SECHLER, E.E., DONNELL, L.H.

The Strength of Thin Plates in Compression

Trans. A.S.M.E. v. 54 1932

35.

35. RHODES, J.

The Non-Linear Behaviour of Thin-Walled Beams subjected to Pure Moment Loading

Ph.D. Thesis University of Strathclyde 1969

36. ALFUTOV, N.A., BALABUKH, L.I.

Energy Criterion of the Stability of Elastic Bodies which does not require the Determination of the Initial Stress-Strain State.

Prikladnaya Matematika I Mechanika. v. 32 p. 703 1968

37. KHAN, M.Z., WALKER, A.C.

Buckling of Plates subjected to Localised Edge Loading

The Structural Engineer v. 50 No. 6, pp. 225-232 June 1972

38. KREYSZIG, E.

Advanced Engineering Mathematics

Wiley 1968

39. FOK, W.C.

Post-Buckling Behaviour of Plates with Discontinuous Change of Thickness

Ph.D. Thesis University of Strathclyde 1975

Acknowledgements

The author wishes to thank Professor J.M. Harvey, Head of the Department of Mechanics of Materials, for the laboratory and workshop facilities placed at the author's disposal.

The author wishes to express his gratitude to Dr. J. Rhodes, Lecturer in the Department of Mechanics of Materials, for his advice and encouragement throughout the investigation.

The author also wishes to thank the technical staff of the Department of Mechanics of Materials, in particular Mr. A. Lambie and Mr. J. Thompson, for their assistance with the experimental investigation.

The author is indebted to the Science Research Council for the award of a Research Studentship for the years 1971 to 1973.

APPENDIX ONE

The Derivation of the Stiffness Matrix of a Constant Strain Triangular Finite Element.

The finite element calculations performed for the theoretical analysis described in Chapter Three used the constant strain triangular elements described in Chapter Four of reference 8. Briefly, the Finite Element method minimises the total potential energy of a structure expressed in terms of the loads and displacements at discrete points in the structure. These discrete points, or nodes, are on the boundaries of small regions, or finite elements, of the structure, over which the strain energy can be expressed in terms of the loads and displacements at these points or nodes. This allows the total strain energy of the structure to be expressed in terms of these nodal displacements. This is accomplished by writing a relationship for the loads and displacements of the nodes for each element such that

$$\{P\} = [k]\{\delta\} \qquad A1.1$$

where $\{P\}$ is the vector of the nodal loads and $\{\delta\}$ is the vector of the nodal displacements. $[k]$ is the stiffness matrix. The stiffness matrix should produce nodal loads which are in equilibrium, and which are zero for rigid body displacements or rotations.

The derivation of the stiffness matrix for the plane stress constant strain triangular element is simple, direct and rapid to calculate. Figure A1.1 shows a typical

triangular element with nodes numbered i = 1, 2 and 3. Each node has two degrees of freedom, the displacements u_i and v_i represented by the vector

$$\{\delta\} = \begin{Bmatrix} u_1 \\ v_1 \\ u_2 \\ v_2 \\ u_3 \\ v_3 \end{Bmatrix} \qquad \text{A1.2}$$

In order to define the displacements within the element by these six nodal displacements, $\{\delta\}$, it is necessary to represent the displacements by displacement functions with a total of six arbitrary coefficients. The simplest functions which fulfil this requirement are

$$u = U_1 + U_2 x + U_3 y \qquad \text{A1.3}$$

$$v = V_1 + V_2 x + V_3 y \qquad \text{A1.4}$$

The nodal values of the u displacement can be written using equation A1.3 as

$$\begin{aligned} u_1 &= U_1 + U_2 x_1 + U_3 y_1 \\ u_2 &= U_1 + U_2 x_2 + U_3 y_2 \\ u_3 &= U_1 + U_2 x_3 + U_3 y_3 \end{aligned} \qquad \text{A1.5}$$

i.e.

$$\{u\} = [G]\{U\}$$

where $\{u\} = \begin{Bmatrix} u_1 \\ u_2 \\ u_3 \end{Bmatrix}$ and $\{U\} = \begin{Bmatrix} U_1 \\ U_2 \\ U_3 \end{Bmatrix}$

Hence $$\{U\} = [G]^{-1}\{u\} \qquad \text{A1.6}$$

For such a small matrix, the inverse of $[G]$ can readily be found by substitution of variables i.e.

$$[G]^{-1} = \frac{1}{2\Delta}\begin{bmatrix} (x_2y_3 - x_3y_2) & (x_3y_1 - x_1y_3) & (x_1y_2 - x_2y_1) \\ (y_2 - y_3) & (y_3 - y_1) & (y_1 - y_2) \\ (x_3 - x_2) & (x_1 - x_3) & (x_1 - x_2) \end{bmatrix} \qquad \text{A1.7}$$

where Δ = area of the triangular element.

Thus the coefficients of equation A1.3 can be directly expressed in terms of the nodal displacements. A similar operation can be performed on equation A1.4 to produce the corresponding expression

$$\{V\} = [G]^{-1}\{v\} \qquad \text{A1.8}$$

The matrix $[G]^{-1}$ can be re-written as follows in order to allow the relationships described by equations A1.8 and A1.6 to be expressed as

$$\{U\} = [G_1]\{\delta\} \qquad \text{A1.9}$$

$$\{V\} = [G_1]\{\delta\} \qquad \text{A1.10}$$

where

$$[G_1] = [G]^{-1} \begin{bmatrix} 1 & 0 & 0 & 0 & 0 & 0 \\ 0 & 0 & 1 & 0 & 0 & 0 \\ 0 & 0 & 0 & 0 & 1 & 0 \end{bmatrix}$$

and

$$[G_2] = [G]^{-1} \begin{bmatrix} 0 & 1 & 0 & 0 & 0 & 0 \\ 0 & 0 & 0 & 1 & 0 & 0 \\ 0 & 0 & 0 & 0 & 0 & 1 \end{bmatrix}$$

The strain in each element can be written as follows

$$\{\varepsilon\} = \begin{Bmatrix} \varepsilon_x \\ \varepsilon_y \\ \gamma_{xy} \end{Bmatrix} = \begin{Bmatrix} \frac{\partial u}{\partial x} \\ \frac{\partial v}{\partial y} \\ \frac{\partial u}{\partial y} + \frac{\partial v}{\partial x} \end{Bmatrix}$$

This can be obtained from equations A1.3 and A1.4 as being

$$\{\varepsilon\} = \begin{Bmatrix} U_2 \\ V_3 \\ U_3 + V_2 \end{Bmatrix} \qquad \text{A1.11}$$

Expression A1.11 can be re-written using expressions A1.9 and A1.10

i.e.

$$\{\varepsilon\} = \begin{bmatrix} \{0 \ 1 \ 0\}[G_1] \\ \{0 \ 0 \ 1\}[G_2] \\ \{0 \ 0 \ 1\}[G_1] + \{0 \ 1 \ 0\}[G_2] \end{bmatrix} \qquad \text{A1.12}$$

This becomes, after substitution for $[G_1]$, $[G_2]$ etc.

$$\{\varepsilon\} = [H]\{\delta\} \qquad \text{A1.13}$$

where

$$[H] = \begin{bmatrix} (y_2 - y_3) & 0 & (y_3 - y_1) & 0 & (y_1 - y_2) & 0 \\ 0 & (x_3 - x_2) & 0 & (x_1 - x_3) & 0 & (x_2 - x_1) \\ (x_3 - x_2)(y_2 - y_3) & (x_1 - x_3)(y_3 - y_1) & (x_2 - x_1)(y_1 - y_2) \end{bmatrix} . \qquad \text{A1.14}$$

The stresses in each element can be written in terms of the strains for a plane stress relationship as follows

$$\sigma_x = \frac{E}{(1-\nu^2)} (\varepsilon_x + \nu \varepsilon_y)$$

$$\sigma_y = \frac{E}{(1-\nu^2)} (\varepsilon_y + \nu \varepsilon_x)$$

$$\tau_{xy} = \frac{E}{2(1+\nu)} \gamma_{xy}$$

The relationship between stress and strain can be written from this into a matrix formulation

$$\{\sigma\} = \begin{Bmatrix} \sigma_x \\ \sigma_y \\ \tau_{xy} \end{Bmatrix} = [D]\{\varepsilon\} \qquad \text{A1.15}$$

where

$$[D] = \begin{bmatrix} 1 & \nu & 0 \\ \nu & 1 & 0 \\ 0 & 0 & \frac{(1-\nu)}{2} \end{bmatrix}$$

The strain energy in an element is

$$U_e = \frac{1}{2} \int \{\varepsilon\}^T \{\sigma\} \, t \, dx \, dy \qquad \text{A1.16}$$

where the integration is over the surface of the element. U_e can be re-written by the substitution of equations A1.15 and A1.13 into A1.16 to give

$$U_e = \frac{1}{2}\int \{\delta\}^T [H]^T [D][H]\{\delta\}\, t\, dx\, dy \qquad \text{A1.17}$$

The coefficients of the matrices in equation A1.17 are all independent of x and y. Therefore the integration of equation A1.17 becomes

$$U_e = \frac{1}{2}\Delta \{\delta\}^T [H]^T [D][H]\{\delta\}\, t \qquad \text{A1.18}$$

The total potential energy of the element is therefore

$$U_T = \{P\}\{\delta\}^T - U_e$$

where $\{P\}$ is the vector of the nodal loads i.e.

$$\{P\} = \begin{Bmatrix} P_{u1} \\ P_{v1} \\ P_{u2} \\ P_{v2} \\ P_{u3} \\ P_{v3} \end{Bmatrix}$$

i.e.

$$U_T = \{P\}\{\delta\}^T - \frac{1}{2}\Delta t \{\delta\}^T [H]^T [D][H]\{\delta\} \qquad \text{A1.19}$$

The equation for total potential energy is then minimised with respect to the nodal displacements, in order to produce an equilibrium relationship. This produces the following equation.

$$\frac{\partial U_T}{\partial \{\delta\}} = \{P\} - \Delta t\,[H]^T[D][H]\{\delta\} = 0$$

A1.20

Equation A1.20 can be arranged to give

$$\{P\} = \Delta t\,[H]^T[D][H]\{\delta\}$$

A1.21

Equation A1.21 is of the form of equation A1.1 where

$$[k] = \Delta t\,[H]^T[D][H]$$

A1.22

The stiffness matrix is therefore the product of only two matrices which can be directly written without any previous matrix inversion or numerical integration.

As no finite element programs of sufficient size were generally available within the University of Strathclyde at the start of this investigation, the author wrote a simple plane stress or plane strain two dimensional finite element program, using constant strain triangular elements. The program could accept either prescribed load or prescribed displacement boundary conditions, and was written for the IBM 370/155 computer which had become available to the University of Strathclyde at that time.

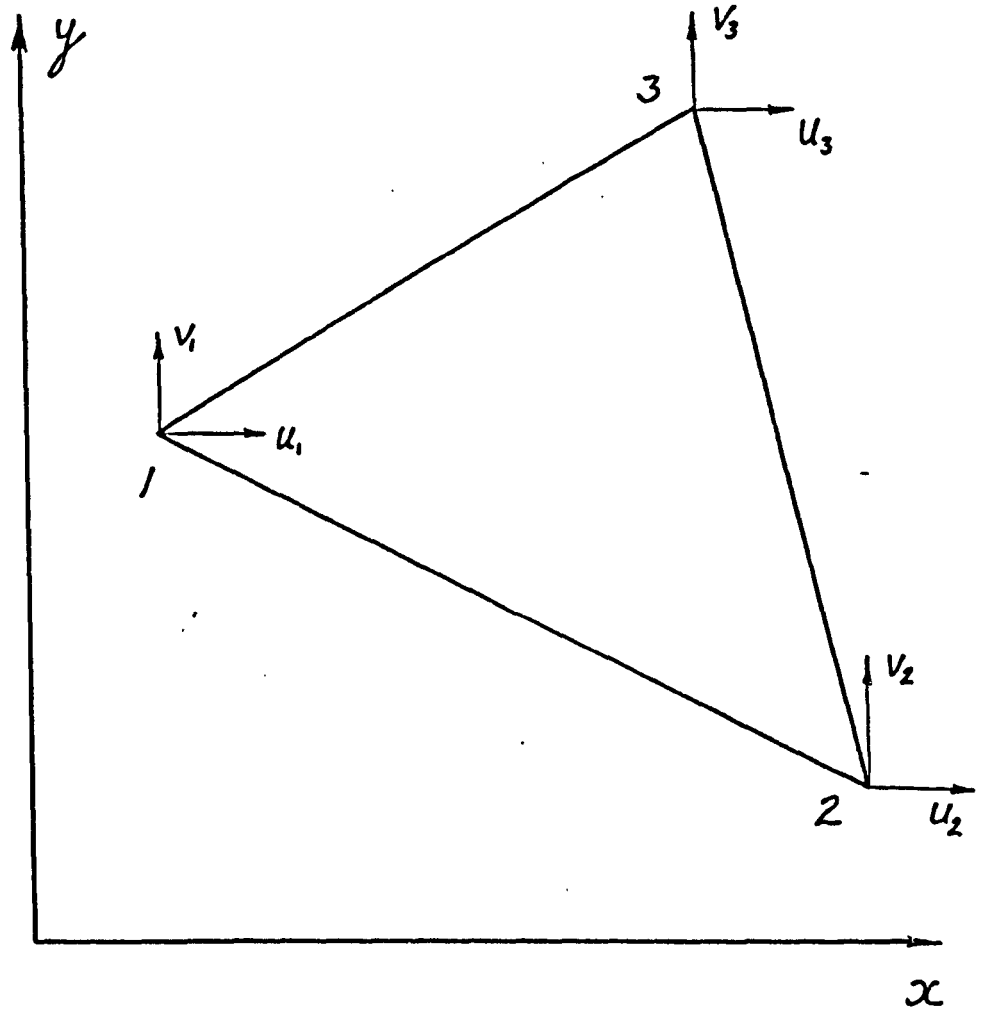

FIGURE A1.1 DIAGRAM OF A TRIANGULAR FINITE ELEMENT

APPENDIX TWO

Calculation of the Minimum Eigenvalues

The calculation of the smallest eigenvalue of equation 3.13 was performed by a simple iterative method. The method is described in reference 38. However, its application to the eigenvalue problem specified by equation 3.13 is described as follows.

Equation 3.13 is written in the following manner:-

$$\left[[K_{1nm}] + \phi [K_{3nm}] \right] \{A\} = 0 \qquad \text{A2.1}$$

This equation can be re-written as

$$[K_{1nm}]\{A\} = -\phi [K_{3nm}]\{A\}$$

i.e.

$$\frac{1}{\phi} \{A\} = -[K_{1nm}]^{-1}[K_{3nm}]\{A\} \qquad \text{A2.2}$$

or

$$\lambda \{A\} = [C_{nm}]\{A\} \qquad \text{A2.3}$$

where $\lambda = \frac{1}{\phi}$ and $[C_{nm}] = -[K_{1nm}]^{-1}[K_{3nm}]$

A2.4

The iterative method of solution was commenced by taking an arbitrary real vector $\{A\}_0$ and calculating an approximate value of $\lambda\{A\}$ from equation A2.3

i.e.

$$\lambda_1 \{A\}_1 = [C_{nm}]\{A\}_0$$

The first approximation for the eigenvalue of equation A2.3, λ_1, is the largest term in the product $[C_{nm}]\{A\}_0$, and the eigenvector $\{A\}_1$ is this product normalised with respect to

the largest term. The iteration was continued by repeating the calculation in order to obtain the second approximation from the first approximation, until the r th approximation is

$$\lambda_r \{A\}_r = [C_{nm}]\{A\}_{(r-1)}$$

At some point in this calculation, the eigenvalue converged to within suitable limits of accuracy to give the largest eigenvalue λ_r of equation A2.3, which is therefore the smallest eigenvalue, ϕ , of equation A2.1. In practice, the eigenvector takes longer to converge than the eigenvalue. However, convergence was assisted by choosing a suitable initial approximation for $\{A\}_0$. In practice this was found to be a zero vector with a unit value in the location corresponding to the row containing the largest absolute term on the leading diagonal of the matrix $[C_{nm}]$. Convergence to within 0.1% of the eigenvalue was taken as the point at which the iterations were stopped. However, as this was found to occur within twenty iterations, a standard number of thirty iterations was adopted to simplify programming, as the additional computing time was negligible for 3 x 3 matrices.

APPENDIX THREE

The Material Properties

The material properties of the plates were established as part of the experimental investigation. These properties were measured from standard tensile test specimens made to B.S. 485 from unused plate specimens. The tensile test specimens were taken from both directions of the plating.

The Tinius Olsen machine was used to test the specimens in tension. An extensometer was attached to each specimen, which allowed a continuous recording of the load-extension behaviour of each specimen to be obtained from the machine. These recordings were used to calculate the Young's Modulus and yield stress of the material. A few tensile test specimens were strain gauged both in the axial direction and across it, and were used to estimate Poisson's ratio.

The average material properties were found to be

$$E = 30{\cdot}2 \cdot 10^{6}\ \text{lbf.ins}^{-2} \quad (208{\cdot}0 \cdot 10^{3}\ \text{MN.m}^{-2})$$

$$\sigma_Y = 43100\ \text{lbf ins}^{-2} \quad (297\ \text{MN.m}^{-2})$$

$$\nu = 0{\cdot}3$$

The scatter on the results for the Young's Modulus was slight. However, the scatter on the values for the yield stress were relatively large, ranging between +9% and -7% on the mean value. The mean values of the material properties were used in all calculations.